



HAL
open science

Modular variables in quantum information

Andreas Ketterer

► **To cite this version:**

Andreas Ketterer. Modular variables in quantum information. Quantum Physics [quant-ph]. Université Paris 7, Sorbonne Paris Cité, 2016. English. NNT: . tel-01502539

HAL Id: tel-01502539

<https://theses.hal.science/tel-01502539>

Submitted on 5 Apr 2017

HAL is a multi-disciplinary open access archive for the deposit and dissemination of scientific research documents, whether they are published or not. The documents may come from teaching and research institutions in France or abroad, or from public or private research centers.

L'archive ouverte pluridisciplinaire **HAL**, est destinée au dépôt et à la diffusion de documents scientifiques de niveau recherche, publiés ou non, émanant des établissements d'enseignement et de recherche français ou étrangers, des laboratoires publics ou privés.

Laboratoire Matériaux et Phénomènes Quantiques

École doctorale: Physique en Ile-de-France

Doctorat

Physique

Andreas Ketterer

Modular variables in quantum information

Variables modulaires en information quantique

Thèse dirigée par Thomas Coudreau et Pérola Milman

Soutenue le 14 octobre 2016

Jury

M.	Thomas Coudreau	Directeur de thèse
M.	Philippe Grangier	Rapporteur
M.	Otfried Gühne	Examineur
Mme.	Pérola Milman	Co-directrice de thèse
M.	Peter Rabl	Rapporteur
M.	Sébastien Tanzilli	Président du jury

Abstract

Quantum information can be processed in two fundamentally different ways, using either discrete or continuous variable implementations. Each one of them provides different practical advantages and drawbacks. In this thesis we study theoretical means allowing to implement quantum information protocols originally formulated for discrete quantum systems in physical objects characterized by continuous variables. At the heart of our considerations is the use of modular variables as helpful technique to reveal discrete structure in continuous-variable states, operations and observables. The present work is strongly guided by the experimental applicability of our ideas in quantum optics experiments, with a particular focus on the transverse degrees of freedom of single photons.

One of the main themes of this thesis is the formulation of a framework for quantum information processing in phase-space based on the use of modular variables. The term modular variables refers to a specific class of observables that are periodic with respect to some pair of conjugate variables. In our framework we use these periodic observables in order to encode discrete quantum information in Hilbert spaces of infinite dimension. In particular, we consider protocols that involve measurements of judiciously chosen logical observables enabling the readout of the encoded discrete quantum information from the corresponding logical states. Using this framework we show how to perform tests of fundamental properties of quantum mechanics, such as entanglement, Bell nonlocality and contextuality, in Hilbert spaces of various dimensions. Particularly, we generalize known tests of each of these properties, that were originally formulated for measurements with discrete outcomes, to more general measurement contexts comprising the case of bounded continuous outcomes.

Concerning experimental implementations of the presented theoretical elaborations we discuss the transverse degrees of freedom of single photons as a natural platform to manipulate and measure modular variables. In particular, we demonstrate how to process discrete quantum information encoded in the spatial distribution of single photons via the optical Talbot effect - a near-field interference effect. Finally, we show how to produce d -dimensional entangled Talbot photon pairs without post-selection, using spontaneous parametric down-conversion and linear optical elements only.

As last topic we explore the nonlocal properties of a specific class of hybrid entanglement between particle-like and wave-like optical qubits. Using a hybrid measurement scheme of Pauli and displaced parity measurements we show that, even after including realistic experimental losses, a violation of local-realism is theoretically possible.

Résumé

L'information quantique peut être traitée de deux manières fondamentalement différentes: à l'aide de variables discrètes ou continues. Dans cette thèse, nous étudions de manière théorique la réalisation de protocoles d'information quantique dans les systèmes caractérisés par des variables continues. Pour ce faire, nous utilisons les variables modulaires comme outil permettant de révéler des structures discrètes dans les états, opérations et observables. Le présent travail est fortement motivé par l'applicabilité expérimentale de nos idées dans des expériences d'optique quantique.

Le thème principal de cette thèse est la formulation d'un cadre pour le traitement quantique de l'information dans l'espace des phases grâce aux variables modulaires. Les variables modulaires se réfèrent à une famille spécifique d'observables qui sont périodiques par rapport à une certaine paire de variables conjuguées. L'usage des variables modulaires permet d'encoder des états logiques dans des espaces de Hilbert de dimension infinie et de définir des opérations qui permettent de les manipuler. En particulier, nous considérons des protocoles qui impliquent des mesures de variables modulaires qui permettent la lecture d'information discrète codée dans des variables continues. Grâce à ce formalisme, nous montrons comment il est possible de réaliser des tests des propriétés fondamentales de la mécanique quantique comme l'intrication, la non-localité ou la contextualité dans des espaces de Hilbert de dimensions finie ou infinie.

Ensuite, nous discutons pourquoi les degrés de liberté transverse des photons sont des candidats naturels pour l'implémentation expérimentale des variables modulaires. À cet effet, nous démontrons comment il est possible d'utiliser l'effet Talbot - un effet d'interférence en champ proche - afin d'encoder de l'information discrète dans la distribution spatiales des photons. Finalement, nous montrons comment produire des photons Talbot intriqués de dimension arbitraire en utilisant la conversion paramétrique et des éléments d'optique linéaire.

En dernier lieu, nous explorons les propriétés non-locales d'une classe spécifique d'états hybrides intriqués entre degrés de liberté discrets et continus. En utilisant une mesure hybride composée par les matrices de Pauli et de la parité déplacée, on montre qu'il est possible de violer le principe de localité. De plus, on montre que cette violation est robuste aux pertes.

Acknowledgements

At this point I would like to take the opportunity to thank everyone who contributed to the creation of this thesis.

First of all I would like to thank Philippe Grangier, Peter Rabl, Otfried Gühne and Sébastien Tanzilli for evaluating my thesis and for being part of the jury of my thesis defense. I am very thankful to them for the time and energy they devoted to read the manuscript and for their fruitful comments and questions regarding my work.

Next, I want to thank Pérola and Thomas who gave me the opportunity to do the PhD in their group. I enjoyed very much working with them which is in great part due to the fact that they are two very nice bosses that always supported me during the last three years. From the beginning they gave me the feeling of being an equal part of the group and they were always ready to help me with bigger and smaller questions concerning science, bureaucracy or life. I thank them also for having introduced me to the world of modular variables which we tried to unravel during the last three years... with certain success. :-) Sometimes this was a somehow troublesome endeavour but finally it allowed me to learn many theoretical concepts of quantum information theory and, importantly, how to apply them in quantum optics experiments. Thereby, Pérola's persistence in believing in theoretical conjectures and Thomas' insistence on their experimental viability were indispensable qualities which formed me a lot. I thank you both for this great time and I hope we will keep in contact not only for further scientific discussions but also for the one or the other happy hour.

Further on, I want to thank Arne who contributed a lot to the development of my work. He was always open for discussions about scientific problems and he gave me many advises and suggestions about how to present my work in a pedagogically sound way. I wish you all the best and I hope we will meet often again when I come back to visit Paris.

I also want to thank Stephen (a.k.a. Steve) for a very fruitful collaboration on many modular variables related issues. I especially enjoyed working together with him during my two months internship in Rio de Janeiro which allowed me to learn more about experimental realizations of theoretical concepts that I studied throughout my PhD. At this point, I also want to thank Fernando for hosting me at the Centro Brasileiro de Pesquisas Físicas (CBPF) where I carried out much of the work during my time in Rio. Thanks also to Osvaldo, Leandro, Daniel and all the other guys who helped me to enjoy Rio even more. I want to thank here also Pérola again for having welcomed me so warmly in Rio where I was allowed to spend a really nice time with her family and friends.

Next, I want to thank Tom who started and (almost) finished the PhD at the same time as I. He was a very good friend during these last years and I thank him for hundreds of amusing coffee breaks and many other small discussions about physical problems. I also thank him for his incredible patience with me and my slow pace at which I was learning french. ;-) Je te souhaite tout le meilleur pour ton postdoc et pour l'avenir!

Further on, I want to thank Adrien who arrived shortly after I started the PhD and accompanied me in the above mentioned modular variables endeavor. Having been able to discuss with him about all sorts of nonlocality and contextuality related topics was a

great pleasure and helped me to understand some tricky concepts faster and even better. And, apart from all the physics stuff, he taught me how to speak real french without ever loosing the patience. ;-) I also thank Saulo for all the coffees we were taking together à la machine au troisième étage. It was always a great occasion to distract myself from work and to laugh and discuss about some (non)physical topics. Finally, I also thank Jared for accompanying me on the first floor at the very beginning of my PhD and for some great beers, parties and discussions about all sorts of topics of life. Mecs... profitez bien de la dernière année au labo, bonne courage pour la rédaction de la thèse et bonne chance pour tout ce qui va venir!

Now, let me also thank all the other members of my team. Thanks Sergueï for many discussions about series and movies. Even though we had not always the same opinion. ;-) Thanks Aurianne for making me laugh in many occasions. Thanks Simone for acknowledging my ability to express very modest opinions. Thanks Ibrahim for many interesting discussions about physics and life. Thanks Louis for appreciating german coffee and thanks Guillaume for understanding my french also after some beers at Caminito. I also want to thank all the past members of my group. Thanks Alexandre for sharing my excitement about the world cup and some nice discussions about physics. Thanks Cleidson for sharing with me the office on the first floor during the first months. Thanks Romeu for interesting discussions about the issue of compulsory voting in democracies. And, of course, thank you Giulia for many joyful lunches and discussions about continuous variables.

Let me thank now all the other people that I was allowed to work with during the last three years. First of all thanks to all the people of the thesarium: Romain, Dimitri, Pierre, Charlotte, Bastien, Remeu, Helene, Elisa, Jan, Adrian and Cynthia. Then, some guys from other offices: Fabricio, Florent, Riccardo, Nicola, Wim, Kaushik, Dong, Claire and Mizio. I also thank Anne, Jocelyne, Sandrine and Joelle for all the organizational help. And finally to all ancient members of MPQ: JB, Guillaume, Constance, Jonathan, Juan, Alexandre (1), Alexandre (2), Siham. And, of course, everyone I have forgotten.... sorry for that! ;-)

I also thank all my friends outside of the lab that helped me to enjoy the time that was not dedicated to physics. Thank you Ale, Anna, Giulia, Ale, Luisa, Elisa, Ludo, Micol, Simone, Lorenzo, Edgar, Marjorie, Thomas, Olga and Alessia. I thank Fred for being a great friend that had always an open ear for my problems and for many hilarious voice messages. And let me thank also everyone else in Freiburg (physicists or non-physicists) for all the great time we spent together when I came to visit you.

Finally, I want to thank my family for having given me the opportunity to study physics and for supporting me in doing this PhD. I especially thank my mother Annette and Gottfried for helping me so much to prepare the pot at the day of my defense. I thank my brother Chris for many skype calls and visits in Paris and for hosting me in Freiburg and Bonn. It was always a great occasion to get the necessary distraction from physics. I also want to thank Alessandra, Enzo and Marco for their support and many beautiful moments in Italy. But finally, and most importantly, I want to thank Vale for all her help and support during the last three years! Thank you for your humor and your joy that made us laugh in many unforgettable moments! And thank you for your love which is the best thing that ever happened to me!

Contents

I	Introduction	13
II	Theoretical and experimental foundations	19
II.1	Basic elements of quantum information theory	19
II.1.1	Quantum bits (qubits)	19
II.1.2	Quantum d -dimensional systems (qudits)	23
II.1.3	Continuous-variable (CV) systems	25
II.1.4	Theory of measurements	29
II.1.5	Bloch vector representation	32
II.1.6	Wigner function representation	35
II.2	Quantum theory of light	38
II.2.1	Quantization of the electromagnetic field	39
II.2.2	Mode representations	42
II.2.3	Transverse spatial modes	43
II.2.4	Relevant quantum states of light	45
II.2.4.1	Fock states	45
II.2.4.2	Coherent states	46
II.2.4.3	Squeezed states	47
II.2.4.4	Thermal states	49
II.2.4.5	Cat states	50
II.3	Experimental realizations	51
II.3.1	Spatial distribution of single photons	51
II.3.1.1	Manipulation of the spatial single photon field	52
II.3.1.2	Two-photon gates	56
II.3.1.3	Spatial correlations from parametric down-conversion	57
II.3.2	Single-mode multi-photon field	58
II.3.2.1	From linear optical operations.	58
II.3.2.2	. . . to Gaussian quantum computation	59
II.3.2.3	Homodyne detection	61
II.4	Summary	63
III	Quantum information processing with modular variables	65
III.1	Modular variables formalism	65
III.1.1	Periodic observables or modular variables	65
III.1.2	Modular variables and the characteristic function	68
III.1.3	Modular position and momentum	69
III.1.4	The modular representation	72
III.1.5	Examples of states in the modular representation	76

III.2	Dichotomizing the Hilbert space	80
III.2.1	Identifying qubits in the modular variables representation	81
III.2.2	Single and two qubit logical operations	85
III.2.2.1	Logical Pauli operations	85
III.2.2.2	Logical Clifford operations	87
III.3	State readout with modular variables	88
III.3.1	Definition of modular readout observables	88
III.3.2	Rotations of the logical basis	92
III.3.3	Phase space representation of modular readout observables	92
III.3.3.1	$\hat{\Gamma}_z$ -operator	93
III.3.3.2	$\hat{\Gamma}_x$ -operator	95
III.3.3.3	$\hat{\Gamma}_y$ -operator	96
III.3.3.4	Commutation relations	97
III.4	Experimental proposal using the spatial distribution of single photons	98
III.4.1	Creation of single photon states with periodic wave function	98
III.4.2	Logical operations realized by linear optical elements	101
III.4.2.1	Controlled two photon gate	103
III.4.3	Measuring the readout observables $\hat{\Gamma}_\beta$	103
III.4.3.1	Direct measurement	103
III.4.3.2	Indirect measurement	105
III.5	Discussion	106
IV	Tests of fundamental properties of quantum mechanics	109
IV.1	Entanglement	109
IV.1.1	Some basics about entanglement	109
IV.1.1.1	Entanglement witnesses	110
IV.1.1.2	Entanglement measures	111
IV.1.2	Stabilizer formalism and entanglement detection	111
IV.1.3	Modular variables entanglement witnesses	113
IV.2	Nonlocality	118
IV.2.1	Mathematical characterization of correlations	118
IV.2.1.1	Entanglement vs. nonlocality	121
IV.2.2	Experimental demonstration of Bell nonlocality	122
IV.2.3	Bell inequalities for bounded observables	125
IV.2.3.1	Bounded discrete measurement outcomes	125
IV.2.3.2	Bounded continuous measurement outcomes	126
IV.2.3.3	Nonlocality test with modular variables	128
IV.2.4	Violation of local-realism with modular variables	129
IV.2.4.1	Approach 1: Using logical rotations	130
IV.2.4.2	Approach 2: Using the shear operation	133
IV.3	Contextuality	134
IV.3.1	Contextuality and the Peres-Mermin square	135
IV.3.2	Peres-Mermin square for arbitrary unitary operators	138
IV.3.3	Contextuality in finite dimensional Hilbert spaces	142
IV.3.4	Contextuality in infinite dimensional Hilbert spaces	143
IV.3.5	Contextuality with modular variables	143

IV.4 Discussion	144
V Quantum information processing by means of the Talbot-Effect	147
V.1 Near-field interference behind diffraction gratings	147
V.2 Processing information by weaving Talbot carpets	150
V.2.1 Definition of logical states	150
V.2.2 Logical operations	151
V.2.2.1 The Talbot gate	151
V.2.2.2 Diagonal gates	152
V.2.2.3 The Talbot qubit	153
V.2.3 Spatially Dependent Beam Splitter	154
V.3 Creation of entangled Talbot carpets	156
V.3.1 Talbot carpet synthesizer	156
V.3.2 Entangled Talbot qudits	159
V.4 Nonlocality test with entangled Talbot carpets	162
V.4.1 CHSH scenario	162
V.4.2 Measurements with more outcomes	163
V.4.3 Perspectives: Bell test with material particles and matter waves .	165
V.5 Discussion	166
VI Nonlocality of hybrid entangled states	167
VI.1 Hybrid entanglement	167
VI.1.1 Hybrid entanglement between particle- and wave-like states . . .	167
VI.1.2 Experimental production of hybrid entangled states	169
VI.1.3 Measurement and experimental losses	171
VI.2 Qubit, parity and hybrid CHSH inequality	172
VI.3 Nonlocality of hybrid entanglement	174
VI.3.1 Theoretical violation of the CHSH inequality	174
VI.3.2 Nonlocality under the influence of losses	177
VI.4 Discussion	180
VII Summary and conclusions	183
A Laguerre- and Hermite polynomials	187
A.1 Laguerre polynomials	187
A.2 Hermite polynomials	188
B Modular variables: explicit calculations	189
B.1 Commutators of modular and integer operators	189
B.2 Bound on expectation values of readout observables	191
Bibliography	193

I Introduction

The field of quantum information science focused originally on the study of finite dimensional quantum systems used to encode and process information based on the fundamental laws of quantum mechanics [Nielsen and Chuang, 2000]. This led to the formulation of a plethora of quantum information protocols which exploit fundamental properties of quantum mechanics as a resource and often outperform their classical counterparts. In recent years, a novel way of processing quantum information, in terms of infinite dimensional continuous-variable systems, has been developed, providing several practical advantages and drawbacks compared to the finite dimensional case. In the present dissertation we will combine benefits of both routes and study strategies that allow to implement tasks originally formulated for discrete quantum systems in continuous-variable setups.

Historically, Einstein, Podolsky, and Rosen were among the first ones to explore the foundations of quantum mechanics trying to find a reasonable explanation for what we call entanglement today [Einstein et al., 1935]. However, a breakthrough for the understanding of entanglement was made about 30 years later by John S. Bell who showed that the predictions of quantum mechanics are in conflict with those of classical physics [Bell, 1964, 1966]. Practically, Bell provided an inequality which allows to test correlations for their compatibility with predictions made by classical local hidden variable theories and thus characterizes entanglement indirectly as a fundamental property of quantum mechanics. As a result of Bell’s work, and its experimental demonstration about 20 years later [Freedman and Clauser, 1972; Aspect et al., 1981, 1982b], the research exploring nonlocal aspects of quantum mechanics grew immensely over the last decades. On the one hand, the fundamental understanding of various types of nonlocal correlations, such as Bell nonlocality [Brunner et al., 2014], entanglement [Gühne and Tóth, 2009; Horodecki et al., 2009] or EPR steering [Reid et al., 2009; Cavalcanti and Skrzypczyk, 2016], has been improved. On the other hand, their important role as resources for applications in different areas of quantum information, such as quantum cryptography [Ekert, 1991; Scarani et al., 2009] or communication complexity [Buhrman et al., 2010; Brukner et al., 2004], has been established. One of the most recent highlights were the first loophole-free violations of Bell inequalities in quantum optics experiments [Hensen et al., 2015; Shalm et al., 2015; Giustina et al., 2015].

Another important fundamental property of quantum mechanics can be attributed to the non-commutativity of measurements of certain observables, commonly referred to as contextuality. Specifically, quantum mechanics is said to be a contextual theory because it cannot be reproduced by noncontextual hidden variable theories, as proven by S. Kochen and E. P. Specker in [Kochen and Specker, 1967]. An important distinction between the previously discussed nonlocal properties and contextuality is that the latter can occur in a state-independent fashion [Cabello, 2008; Badziąg et al., 2009]. Experimental demonstrations of state-independent contextuality have been re-

ported with single photons, trapped ions and with nuclear spins [Amselem et al., 2009; Kirchmair et al., 2009; Moussa et al., 2010]. Similar to nonlocality, also contextuality can be employed as a resource in quantum information applications. For instance, in [Horodecki et al., 2010] a device-independent quantum key distribution protocol, or in [Gühne et al., 2014] state-independent dimension witnesses, based on non-contextuality tests have been established. Moreover, contextuality has recently been identified as a resource that supplies the power for qudit quantum computations [Raussendorf, 2013; Howard et al., 2014; Delfosse et al., 2015; Raussendorf et al., 2015].

At this point we note that most of the aforementioned tests and protocols were first formulated for measurements with finitely many outcomes described by operators on finite dimensional Hilbert spaces, even though, EPR originally concentrated their elaborations on systems that are characterized by continuous degrees of freedom (*e.g.* the position of a particle) and thus are performed on infinite dimensional Hilbert spaces. Nevertheless, the latter regained again of popularity at the beginning of the 1990s due to increasing experimental abilities allowing for the efficient preparation, manipulation and measurement of the quadratures of the electromagnetic field [Leonhardt, 1997]. Consequently, a number of entanglement and nonlocality test for continuous variable measurements have been derived [Eisert and Plenio, 2003; Braunstein and van Loock, 2005; Cavalcanti et al., 2007]. Among the most important advances in the field of continuous variable quantum information are the realization of quantum teleportation [Braunstein and Kimble, 1998; Furusawa et al., 1998], as well as quantum cryptography protocols [Grosshans and Grangier, 2002; Grosshans et al., 2003]. Universality for manipulation of continuous variables quantum states was defined in [Lloyd and Braunstein, 1999], and subsequently measurement based quantum computation was generalized from the discrete to the continuous realm [Gu et al., 2009; Menicucci et al., 2006].

Today, the use of continuous variable degrees of freedom is by no means restricted to the description of optical quadrature amplitudes. The emergence of novel technologies in the fields of superconducting as well as semiconductor physics have brought into reach also other frequency domains, such as the microwave and infrared [Blais et al., 2004; Gunter et al., 2009; Devoret and Schoelkopf, 2013]. Furthermore, spatial degrees of freedom also often require a treatment in a continuous variable setup. A prominent example is that of the spatial multi-mode field of a single photon whose transverse position and momentum can be handled in analogy to a single mode of the electromagnetic field [Walborn et al., 2010; Tasca et al., 2011]. Apart from the description of electromagnetic waves, continuous variables appear also when studying vibrational degrees of freedom of trapped ions and atoms, or micro- and nano-mechanical oscillators [Monroe et al., 1996; Leibfried et al., 2003; Rabl et al., 2009]. Each of the mentioned platforms provides several experimental advantages and drawbacks in the creation, manipulation and measurement of states defined in a continuous-variable representation. A promising strategy is therefore to use so-called hybrid systems which combine, on the one hand, various experimental techniques (see above) but, on the other hand, also benefit from different theoretical strategies, *i.e.* discrete- and continuous-variable quantum information processing schemes.

In quantum information, hybrid systems are studied with the goal to combine the most attractive capabilities of different quantum optical, mechanical and solid state systems in order to improve the performance of quantum information protocols [Kim-

ble, 2008; Kurizki et al., 2015]. Each of these physical setups offers advantages in tasks as efficient storage, processing, transmission or readout of quantum information. Part of the development of such hybrid strategies is concerned with the combination of approaches that apply different, discrete- or continuous-variable, quantum encodings [van Loock, 2011]. This comprises, for instance, the creation of hybrid entanglement among particle-like (discrete) and wave-like (continuous) states [Morin et al., 2014]. Thereby, particle-like states refer to states that have a discrete character, such as single photon states. The latter can be used to encode a two dimensional quantum system through the presence and absence of the photon [Knill et al., 2001; Morin et al., 2013]. Alternatively, wave-like states usually contain a large number of photons whose discrete character is rather inaccessible. Examples are coherent states with opposite phases, or cat states with different parity [Lund et al., 2008; Vlastakis et al., 2013; Albert et al., 2016]. Hybrid entanglement between two such types of states might offer advantages for teleportation or communication protocols [Rigas et al., 2006; Lee and Jeong, 2013].

Other hybrid strategies make use of the possibility to exploit more than one degree of freedom of a single quantum system. Important examples are the time bin encoding for single photons or the use of the transverse degrees of freedom aside the usual polarization degree of freedom [de Riedmatten et al., 2004; Ali-Khan et al., 2007]. There have been several experiments reporting the creation of hybrid entanglement between the photon's polarization and either its orbital angular momentum (OAM) modes [Nagali et al., 2009; Karimi et al., 2010; Erhard et al., 2015], or its transverse momentum [Neves et al., 2005, 2009]. A novel way to encode d -dimensional quantum systems in the transverse distribution of single photons is by taking advantage of the optical Talbot effect [Farias et al., 2015]. The latter, historically first discovered by H. F. Talbot and later on theoretically described by L. Rayleigh [Rayleigh, 1881], is a near field interference effect that occurs when plane waves are refracted by periodic grating structures [Case et al., 2009].

Finally, we want to mention one more technique that will be important for our studies of the relationship between discrete- and continuous-variable quantum systems and has recently attracted some attention, the technique of modular variables. Modular variables are classes of observables that are periodic with respect to some pair of canonically conjugate variables. Among the first ones to use this technique was Y. Aharonov and co-workers in 1969, who studied signatures of quantum interference in the Aharonov-Bohm effect [Aharonov et al., 1969]. After Aharonov's work modular variables were not used much until about 40 years later when J. Tollaksen and co-workers explored new aspects of the relation between modular variables and weak measurements [Tollaksen et al., 2010]. Moreover, the usefulness of modular variables in quantum information related tasks was discovered. Notably, using the modular variables formalism, a novel criteria allowing to detect entanglement in spatial interference patterns of particle pairs was developed [Gneiting and Hornberger, 2011, 2013] and shortly after experimentally implemented [Carvalho et al., 2012]. Later on, modular variables have also been used in other areas of quantum information to propose test of the Clauser-Horne-Shimony-Holt (CHSH) [Ketterer et al., 2015; Arora and Asadian, 2015], the Leggett-Garg [Asadian et al., 2014; Moreira et al., 2015] and noncontextuality inequalities [Plastino and Cabello, 2010; Asadian et al., 2015; Laversanne-Finot et al., 2015]. Finally, modular variables played a crucial role in the demonstration that fault-tolerant quantum computation

with continuous-variable cluster states is possible [Menicucci, 2014].

In this manuscript we seek to employ methods from both the fields of discrete- and continuous-variable quantum information so as to investigate means that allow to process discrete quantum information encoded in infinite dimensional Hilbert spaces. To do so, we will pursue three main strategies, the first of which aims at devising a framework for quantum information processing in phase space based on the use of modular variables [Vernaz-Gris et al., 2014; Ketterer et al., 2016]. Following this framework, we will discuss methods to perform tests of fundamental properties of quantum mechanics, such as entanglement, nonlocality and contextuality, using measurements of modular variables [Ketterer et al., 2015; Laversanne-Finot et al., 2015; Laversanne-Finot et al., 2016]. Further on, we will exploit the optical Talbot effect to encode and manipulate finite dimensional quantum states using the transverse degrees of freedom of single photons [Barros et al., 2016]. And last, in a third study, we will analyse the entanglement and nonlocality of a particular class of hybrid entangled states consisting of mixtures of single-photon and cat-state encodings. Our results are, on the one hand, conceptually interesting because they explore the boundary between the two regimes of continuous-variable and discrete-variable quantum information. On the other hand, they might prove beneficial for the realization of hybrid quantum devices, since they provide alternative ways to process discrete quantum information in systems characterized by continuous degrees of freedom.

Outline of this thesis

After the above introductory words, we start in Chapter II to provide basic theoretical and experimental concepts that are important for subsequent considerations throughout this thesis. First, we discuss two main strategies used to process information in quantum mechanics in terms of finite and infinite dimensional Hilbert spaces. For each of these strategies we introduce the basic theoretical tools to process, measure, and represent the corresponding quantum states. We then move on and show how to describe quantum-mechanically the electromagnetic radiation field and review different mode representations as well as typical quantum states of light. Finally, two experimental platforms allowing to process continuous degrees of freedom, the transverse degrees of freedom of a single photon and a single mode of a multi-photon field, are discussed.

In Chapter III, we devise a framework for quantum information processing in phase space using the formalism of modular variables. We thus give first a detailed introduction to the topic of modular variables including their general definition, a discussion of the modular position and momentum as one particular example of modular variables, and an introduction to the modular representation defined through the common eigenstates of the modular position and momentum operator. Further on, we use the modular representation to dichotomize the Hilbert space with respect to the modular position and define appropriate logical states and operations allowing to process discrete quantum information encoded in an infinite dimensional Hilbert space. Moreover, we define a set of appropriate modular variables that enable the readout of the discrete

quantum information by measurements of observables which have a continuous spectrum. Finally, we focus on an experimental proposal of these ideas using the transverse degrees of freedom of single photons.

Chapter IV is devoted to a study of fundamental properties of quantum mechanics, namely entanglement, Bell nonlocality and contextuality. After introducing conceptually each of these fundamental properties and known methods for their detection in finite dimensional Hilbert spaces, we show how to generalize these methods to more general cases involving infinite dimensional Hilbert spaces and measurements with continuous outcomes. In particular, we derive entanglement witnesses and nonlocality tests that involve measurements of bounded observables. In both cases we discuss modular variables as an example and provide applications of the modular variables phase space framework devised in Chapter III. Finally, we turn to contextuality and generalize known methods for its detection in terms of measurements with discrete outcomes to more general measurement settings. Also here we discuss several examples including the use of modular variables for the state-independent detection of contextuality.

The topic of Chapter V is once again the processing of discrete quantum information encoded in continuous variables. This time, however, we focus from the beginning on a specific experimental platform, the transverse degrees of freedom of single photons. Specifically, we show how to manipulate d -dimensional quantum states encoded in the spatial distribution of single photons via the optical Talbot effect. Furthermore, we design a method that allows us to produce deterministically d -dimensional entangled photon pairs from spontaneous parametric down-conversion and the application of linear optical elements only. Finally, we show how to use these entangled photon pairs to violate discrete-variable Bell inequalities and give a perspective on possible realizations of such nonlocality test with material particles.

Chapter VI contains a study of the nonlocal properties of a particular class of hybrid entangled states involving particle-like and wave-like optical qubits. We thus review some known methods for the detection of nonlocality in terms of photon number parity measurements and then discuss a hybrid approach that involves both Pauli-like and parity measurements. We find that the hybrid approach leads to a slightly improved violation of local-realism compared to a pure parity measurement setup. This holds even after the inclusion of a reasonable rate of experimental imperfections in the theoretical evaluation the signal.

The last Chapter VII contains a summary of this thesis and a brief outlook.

II Theoretical and experimental foundations

In this second chapter, we provide several theoretical and experimental quantum mechanical concepts that build the foundation of the work developed in subsequent chapters of this dissertation. Thereby, we do not aim at giving a comprehensive introduction to quantum mechanics but rather provide a brief summary of the most important concepts needed later on. At the same time we use this opportunity to establish the nomenclature that will be used throughout the remainder of this manuscript. We start by introducing basic elements of quantum information theory such as states and operations in Hilbert spaces of different dimensions, including a discussion of the theory of measurements in quantum mechanics and different state representations. Further on, we review the quantization of the electromagnetic field in order to have the necessary tools to describe quantum states of light in different experimental contexts. Finally, the transverse degrees of single photons and the quadratures of a single mode of the electromagnetic field are discussed as possible experimental platforms for the realization of quantum information processing tasks.

II.1 Basic elements of quantum information theory

II.1.1 Quantum bits (qubits)

One of the most important constituents of quantum information theory is the *qubit* which represents the quantum mechanical analog of the classical information unit *bit* [Nielsen and Chuang, 2000]. In classical information theory a bit refers to a binary variable that always takes one of two determined outcomes, usually denoted as 0 and 1, such as the result of a coin toss or an electric voltage taking two distinct values. However, in quantum information theory a qubit is associated with a two dimensional Hilbert space structure that leads to the possibility of preparing a qubit in a superposition of the states 0 and 1. It is this structure which leads in general to probabilistic outcomes of qubit measurements. Examples of qubits are the polarization state of a photon (*e.g.* horizontal and vertical polarization) or two isolated energy levels of an atom, ion, or molecule. Information processing in terms of qubits can lead to surprising advantages as compared to what is possible with classical bits, such as exponential speedups in certain computation algorithms, and therefore reflect some of the exciting properties of quantum mechanics. In the following, we will introduce the basic notions of qubits and show how to manipulate them.

The pure state of a qubit is described by a unit vector belonging to a two-dimensional complex Hilbert space $\mathcal{H}^{(2)}$ which is spanned by two orthonormal basis vectors, usually denoted by *kets* as $|0\rangle$ and $|1\rangle$, and referred to as the computational basis. An arbitrary qubit state in this space, denoted by the ket $|\Psi\rangle$, can be written as a linear combination

$|\Psi\rangle = \alpha|0\rangle + \beta|1\rangle$, with $\alpha, \beta \in \mathbb{C}$, fulfilling the normalization condition $\sqrt{|\alpha|^2 + |\beta|^2} = 1$. If we further disregard any global phase, involved in $|\Psi\rangle$, we find the following representation of an arbitrary qubit state:

$$|\Psi\rangle = \cos\left(\frac{\theta}{2}\right)|0\rangle + \sin\left(\frac{\theta}{2}\right)e^{i\phi}|1\rangle, \quad (\text{II.1})$$

determined by the two parameters $\theta \in [0, \pi[$ and $\phi \in [0, 2\pi[$. The inner (scalar-)product between two arbitrary qubit states, $|\Psi\rangle$ and $|\Phi\rangle$, is given by $\langle\Psi|\Phi\rangle = \cos\left(\frac{\theta}{2}\right)\cos\left(\frac{\theta'}{2}\right) + \sin\left(\frac{\theta}{2}\right)\sin\left(\frac{\theta'}{2}\right)e^{i(\phi-\phi')}$, confirming the unit length of the state vector (II.1) through $||\Psi\rangle|^2 = \langle\Psi|\Psi\rangle = 1$. In the course of this thesis we will often consider composite quantum systems consisting of two or more qubits which live on a composite Hilbert space $\mathcal{H} = \bigotimes_{k=1}^n \mathcal{H}_k^{(2)} = \mathcal{H}_1^{(2)} \otimes \dots \otimes \mathcal{H}_n^{(2)}$, which is spanned by the basis of all products of single qubit basis states and whose overall dimension is 2^n . For instance, the two-qubit Hilbert space $\mathcal{H}_1^{(2)} \otimes \mathcal{H}_2^{(2)}$ is spanned by the basis $\{|i\rangle \otimes |j\rangle | i, j = 0, 1\}$. For brevity we will denote tensor products of states also by the following shorthand notations $|\psi\rangle \otimes |\phi\rangle = |\psi\rangle|\phi\rangle = |\psi\phi\rangle$.

The dynamical evolution of an isolated quantum system is described by a unitary transformation which maps a state $|\Psi(t_0)\rangle$, given at an initial time t_0 , to a future state $|\Psi(t_1)\rangle = \hat{U}(t_0, t_1)|\Psi(t_0)\rangle$, at the time t_1 , via the unitary operator $\hat{U}(t_0, t_1)$ [Cohen-Tannoudji et al., 1998]. Alternatively, we know that the evolution of a quantum state is determined by the *Schrödinger equation* $i\hbar \frac{d}{dt}|\Psi\rangle = \hat{H}|\Psi\rangle$, with the Hermitian Hamilton operator \hat{H} and the *Planck constant* $\hbar = h/2\pi$. Combining these two views by solving the *Schrödinger equation* with the Ansatz $|\Psi(t_1)\rangle = \hat{U}(t_0, t_1)|\Psi(t_0)\rangle$ leads to the definition of the quantum time evolution operator:

$$\hat{U}(t_0, t_1) = \exp(-i\hat{H}(t_1 - t_0)/\hbar). \quad (\text{II.2})$$

In this thesis we will mostly consider time evolutions in terms of the application of unitary gates each of which represent the dynamics of an underlying physical process described by a Hamiltonian \hat{H} and the duration of the evolution $\Delta t = t_1 - t_0$.

The most famous examples of single qubit gates are the *Pauli operators*:

$$\hat{\sigma}_x = |0\rangle\langle 1| + |1\rangle\langle 0|, \quad (\text{II.3})$$

$$\hat{\sigma}_y = i|1\rangle\langle 0| - i|0\rangle\langle 1|, \quad (\text{II.4})$$

$$\hat{\sigma}_z = |0\rangle\langle 0| - |1\rangle\langle 1|, \quad (\text{II.5})$$

which fulfil the relation

$$\hat{\sigma}_\alpha \hat{\sigma}_\beta = \mathbb{1} \delta_{\alpha,\beta} + i \sum_{\gamma=x,y,z} \epsilon_{\alpha\beta\gamma} \hat{\sigma}_\gamma, \quad \alpha, \beta = x, y, z, \quad (\text{II.6})$$

and in their matrix representation $(\hat{\sigma}_\alpha)_{k,l} = \langle k|\hat{\sigma}_\alpha|l\rangle$, with $k, l = 0, 1$, can be written as:

$$\hat{\sigma}_x = \begin{pmatrix} 0 & 1 \\ 1 & 0 \end{pmatrix}, \quad \hat{\sigma}_y = \begin{pmatrix} 0 & -i \\ i & 0 \end{pmatrix}, \quad \hat{\sigma}_z = \begin{pmatrix} 1 & 0 \\ 0 & -1 \end{pmatrix}. \quad (\text{II.7})$$

When applied to a single qubit state the Pauli operators (II.3) or (II.5) implement a

NOT or a PHASE gate: $\hat{\sigma}_x|0/1\rangle = |1/0\rangle$ and $\hat{\sigma}_z|0/1\rangle = \pm|0/1\rangle$, respectively. Further on, the Pauli matrices (II.7) are a basis of the Lie-Algebra $su(2)$ which exponentiates to the *Special Unitary Group* $SU(2)$, *i.e.* the group of all unitary 2×2 -matrices with determinant 1, through:

$$\hat{R}_{\mathbf{n}}(\phi) = \exp\left(-i\frac{\phi}{2}(\mathbf{n} \cdot \hat{\boldsymbol{\sigma}})\right) = \cos\left(\frac{\phi}{2}\right)\mathbb{1} + i\sin\left(\frac{\phi}{2}\right)(\mathbf{n} \cdot \hat{\boldsymbol{\sigma}}), \quad (\text{II.8})$$

parametrised by the rotation angle ϕ and the rotation axis defined by the unit vector $\mathbf{n} = (n_x, n_y, n_z)^T$, and the Pauli spin operator $\hat{\boldsymbol{\sigma}} = (\hat{\sigma}_x, \hat{\sigma}_y, \hat{\sigma}_z)^T$. Including an extra phase γ into (II.8) thus allows to implement arbitrary single qubit unitary operations $\hat{U} = e^{i\gamma}\hat{U}_{\mathbf{n}}(\phi)$, leading to the definition of another important unitary operator, the *Hadamard gate*:

$$\begin{aligned} \hat{H} &= e^{i\frac{\pi}{2}} \left[\cos\left(\frac{\pi}{2}\right)\mathbb{1} + \frac{i}{\sqrt{2}}\sin\left(\frac{\pi}{2}\right)(\hat{\sigma}_x + \hat{\sigma}_y) \right] \\ &= \frac{1}{\sqrt{2}} \begin{pmatrix} 1 & 1 \\ 1 & -1 \end{pmatrix}, \end{aligned} \quad (\text{II.9})$$

where we set $\gamma = \pi/2$, $\phi = \pi$ and $\mathbf{n} = (1/\sqrt{2}, 0, 1/\sqrt{2})^T$. The Hadamard gate takes computational basis states into equal superpositions and vice versa: $\hat{H}|0(1)\rangle = \frac{1}{\sqrt{2}}(|0\rangle \pm |1\rangle) \equiv |\pm\rangle$ or $\hat{H}|\pm\rangle = \frac{1}{\sqrt{2}}(|+\rangle \pm |-\rangle) = |0(1)\rangle$. At this point we note that it is possible to approximate any single qubit unitary operation \hat{U} to arbitrary accuracy using only two gates, the Hadamard gate \hat{H} and a rotation by $\pi/4$ around $\hat{\sigma}_z$, $\hat{T} = \hat{R}_z(\pi/4) = e^{-i\frac{\pi}{8}\hat{\sigma}_z}$. The latter is often referred to as $\pi/8$ -gate because up to a global phase it can be expressed as:

$$\hat{T} = \begin{pmatrix} e^{-i\frac{\pi}{8}} & 0 \\ 0 & e^{i\frac{\pi}{8}} \end{pmatrix}. \quad (\text{II.10})$$

The square of the $\pi/8$ -gate \hat{T} leads to the simple phase gate \hat{S} , which in its matrix representation reads:

$$\hat{S} = \begin{pmatrix} 1 & 0 \\ 0 & i \end{pmatrix}. \quad (\text{II.11})$$

Next, we introduce two important two-qubit gates, the controlled-NOT and the controlled-PHASE gates, which in their matrix representation in the computational basis $\{|00\rangle, |01\rangle, |10\rangle, |11\rangle\}$, read:

$$\hat{C}_X = \begin{pmatrix} 1 & 0 & 0 & 0 \\ 0 & 1 & 0 & 0 \\ 0 & 0 & 0 & 1 \\ 0 & 0 & 1 & 0 \end{pmatrix}, \quad \hat{C}_Z = \begin{pmatrix} 1 & 0 & 0 & 0 \\ 0 & 1 & 0 & 0 \\ 0 & 0 & 1 & 0 \\ 0 & 0 & 0 & -1 \end{pmatrix}, \quad (\text{II.12})$$

and are related through a unitary transformation $\hat{C}_X = (\mathbb{1} \otimes \hat{H})\hat{C}_Z(\mathbb{1} \otimes \hat{H})$. From the matrix Eqs. (II.12) it is apparent that \hat{C}_X and \hat{C}_Z perform either a NOT or a PHASE operation on the second (target) qubit depending on the state of the first (control)

qubit and thus fixes the assignment *control* \otimes *target*. Having available either one of the two-qubit gates (II.12) together with the possibility to perform arbitrary single-qubit rotations (II.8), allows one to implement exactly any n -qubit unitary transformation \hat{U} , *i.e.* $|\Psi\rangle = \hat{U}|\Phi\rangle$, for all $|\Psi\rangle$ and $|\Phi\rangle$ being arbitrary n -qubit states, by concatenation of the respective gates. In this sense, we call a set of unitary gates *universal* for quantum computation [Nielsen and Chuang, 2000]. However, since this notion of universality can lead in general to infinitely long runtimes in order to implement a given unitary we relax it slightly and allow for an approximate definition of universality, stating that a set of unitary gates is *approximately universal* if it allows to approximate any n -qubit unitary transformation to arbitrary precision. The advantage of approximate universality is that it can be achieved already through application of gates contained in the finite set: $\{\hat{H}, \hat{S}, \hat{T}, \hat{C}_X\}$.

Fault-tolerant implementations of approximately universal sets are possible using quantum error correcting codes [Nielsen and Chuang, 2000; Gottesman, 1997]. The latter are closely related to the *Clifford group* which contains all n -qubit unitaries \hat{G} that fulfill $\hat{P}\hat{G}\hat{P} = \hat{P}'$, where \hat{P} and \hat{P}' are products of operators contained in the Pauli group, that is, all Pauli operators together with the identity operator $\mathbb{1}$ and multiplications by $x \in \{\pm 1, \pm i\}$. More precisely, Clifford group is generated by the set $\{\hat{H}, \hat{S}, \hat{C}_X\}$, and computations containing solely Clifford operations can be efficiently simulated on a classical computer according to the *Gottesman-Knill theorem* [Nielsen and Chuang, 2000]. For fault-tolerance it is required that the error rate per gate application is below a certain *fault-tolerance threshold* guaranteeing that attempts to detect and correct errors will not introduce more errors than they correct for.

Finally, we want to mention the possibility of representing pure states $|\Psi\rangle$ in a density matrix representation $\hat{\rho} = |\Psi\rangle\langle\Psi|$. More generally, this representation allows us not only to express every pure state as a matrix but also classical mixtures of different qubit states $|\Psi_\alpha\rangle$ according to some probability distribution $\{p_\alpha\}$ by:

$$\hat{\rho} = \sum_{\alpha} p_{\alpha} |\Psi_{\alpha}\rangle\langle\Psi_{\alpha}|, \quad (\text{II.13})$$

with the normalization condition $\text{tr}\hat{\rho} = \sum_{\alpha} p_{\alpha} = 1$, where $\text{tr}(\cdot)$ denotes the trace operation. Equation (II.13) implies that all density matrices are positive $\hat{\rho} \geq 0$.¹ The analog of the Schrödinger equation in the density matrix formalism reads:

$$i\hbar \frac{d}{dt} \hat{\rho}(t) = [\hat{H}, \hat{\rho}(t)], \quad (\text{II.14})$$

thus leading to the unitary time evolution $\hat{\rho}(t) = \hat{U}(t_0, t_1) \hat{\rho}_0 \hat{U}^\dagger(t_0, t_1)$ of an initial density matrix $\hat{\rho}_0$. The density matrix formulation becomes especially useful if one deals with open quantum systems that account for the additional interaction with an environment leading to decoherence or dephasing processes. The latter correspond in general to nonunitary time evolutions and thus cannot be described solely Schrödinger dynamics of pure quantum states [Nielsen and Chuang, 2000; Breuer and Petruccione, 2007]. For an arbitrary multi-partite density matrix $\hat{\rho}$ one can calculate its reduced density matrices (*marginals*) through the partial trace operation. For instance, given

¹We will refer to a positive semi-definit operator usually as positive.

a bipartite density matrix $\hat{\rho}$ that acts on the Hilbert space $\mathcal{H}_A \otimes \mathcal{H}_B$, we get for the marginal corresponding to the first subsystem

$$\hat{\rho}_A = \text{tr}_B \hat{\rho} = \sum_i (\mathbb{1} \otimes \langle i|_B) \hat{\rho} (\mathbb{1} \otimes |i\rangle_B), \quad (\text{II.15})$$

with an arbitrary basis $\{|i\rangle_B\}$ of subsystem B . The marginal $\hat{\rho}_B$ follows equivalently by tracing over the subsystem A .

Having recalled the most basics of qubits and their manipulation in terms of sets of gates we want to move on now and generalize those concepts to higher but finite dimensional quantum systems.

II.1.2 Quantum d -dimensional systems (qudits)

The concept of a qubit can be generalized to higher dimensional quantum systems which, in general, are described by a d -dimensional Hilbert space \mathcal{H}_d and referred to as *qudits*. A general qudit state, expressed in terms of its computational basis $\{|j_d\rangle | j = 0, \dots, d-1\}$, then reads $|\Psi\rangle = \sum_j \alpha_j |j_d\rangle$, with the normalization condition $\sum_j |\alpha_j|^2 = 1$. Qudits can be experimentally realized, for instance, with spin- S particles leading to a $d = 2S + 1$ dimensional Hilbert space or by exploiting the orbital angular momentum of single photons [Allen et al., 2003].

A general pure qudit state (compare with Eq. (II.1)) can be written in the following way

$$\begin{aligned} |\Psi\rangle &= \cos\left(\frac{\theta_1}{2}\right) \cos\left(\frac{\theta_2}{2}\right) \dots \cos\left(\frac{\theta_{d-1}}{2}\right) |(0)_d\rangle \\ &+ \cos\left(\frac{\theta_1}{2}\right) \dots \cos\left(\frac{\theta_{d-2}}{2}\right) \sin\left(\frac{\theta_{d-1}}{2}\right) e^{i\phi_{d-1}} |(1)_d\rangle \\ &+ \dots \\ &+ \cos\left(\frac{\theta_1}{2}\right) \sin\left(\frac{\theta_2}{2}\right) e^{i\phi_2} |(d-2)_d\rangle \\ &+ \sin\left(\frac{\theta_1}{2}\right) e^{i\phi_1} |(d-1)_d\rangle \end{aligned} \quad (\text{II.16})$$

with $2(d-1)$ parameters $\theta_j \in [0, \pi[$ and $\phi_j \in [0, 2\pi[$, where $j = 0, \dots, d-1$. Pure qubit and qudit states, such as (II.1) and (II.16), can be represented as points on a unit sphere in a $d^2 - 1$ -dimensional *Euclidean* space. More details about the geometric representation of qubits and qudits will be discussed in Sec. II.1.5.

A generalization of the Pauli operations (II.3) and (II.5) for qudits can be defined in the following way:

$$\hat{\sigma}_x^{(d)} = \sum_{j=0}^{d-1} |(j+1)_d\rangle \langle (j)_d| \quad (\text{II.17})$$

$$\hat{\sigma}_z^{(d)} = \sum_{j=0}^{d-1} \omega^j |(j)_d\rangle \langle (j)_d| \quad (\text{II.18})$$

with $\omega = e^{2\pi i/d}$. Upon application on a computational basis state, Eq. (II.17) performs a unit shift modulo d , leading to an arbitrary shift of k units by $(\hat{\sigma}_x^{(d)})^k$ and $(\hat{\sigma}_x^{(d)})^d = \mathbb{1}$. Similarly, Eq. (II.18) applies a unit phase of ω^j to each computational basis state. Thus, the generalized Pauli operations (II.17) and (II.18), or often referred to as *Heisenberg-Weyl operators*, generate the Pauli, or Heisenberg-Weyl, group for qudits through multiplications and are important constituents in quantum error correction protocols for qudits. As we will see in Sec. II.1.3, an analog of the Heisenberg-Weyl operators for continuous-variables quantum systems follows in the limit $d \rightarrow \infty$. Further on, we introduce the Fourier transform operator:

$$\hat{F} = \sum_{j,k=0}^{d-1} \omega^{jk} |j\rangle_d \langle k|_d, \quad (\text{II.19})$$

which in analogy to the Hadamard gate takes states of the computational basis into uniform superpositions with the phases ω^{jk} , respectively. Using (II.19) we can define the Fourier basis $\{|j\rangle_d^* = \hat{F}|j\rangle_d |j = 0, \dots, d-1\}$ which is the generalization of the basis $|\pm\rangle = \hat{H}|0/1\rangle$ introduced in Sec. II.1.1. Expressed in the Fourier basis the Pauli operations, (II.17) and (II.18), read:

$$\hat{\sigma}_x^{(d)} = \sum_{j=0}^{d-1} \omega^{-j} |j\rangle_d^* \langle j|_d^*, \quad (\text{II.20})$$

$$\hat{\sigma}_z^{(d)} = \sum_{j=0}^{d-1} |(j+1)_d\rangle^* \langle j|_d^*, \quad (\text{II.21})$$

showing that in the Fourier space the Pauli operators, $\hat{\sigma}_x^{(d)}$ and $\hat{\sigma}_z^{(d)}$, act inversely as phase and shift gates, respectively. However, compared to the set of Pauli operators (II.3-II.5) these unitary operations are in general not Hermitian. Rotations similar to Eq. (II.8) have to be defined in terms of the corresponding spin- $\frac{(d-1)}{2}$ vector whose components in the qudit basis $\{|i\rangle_d\}$ read:

$$(\hat{S}_x)_{j,k} = \frac{\hbar}{2} \sqrt{jk(d+1)(i+j-1)/2} (\delta_{j,k+1} + \delta_{j+1,k}), \quad (\text{II.22})$$

$$(\hat{S}_y)_{j,k} = \frac{\hbar}{2} \sqrt{jk(d+1)(i+j-1)/2} (\delta_{j,k+1} - \delta_{j+1,k}), \quad (\text{II.23})$$

$$(\hat{S}_z)_{j,k} = \frac{\hbar}{2} (d+1-2j) \delta_{j,k}, \quad (\text{II.24})$$

with $0 \leq j, k \leq d-1$. The operators (II.22)-(II.24) form a $su(2)$ algebra for higher dimensional spin systems and generate rotation around the respective axis in space. A similar expression to Eq. (II.8) for the total spin operator $\hat{\mathbf{S}}$ can be found in [Curtright et al., 2014] but will not be further discussed here.

Instead, we want to introduce a controlled unitary operations (compare with Eqs.

(II.12)) for qudits. For instance, the controlled NOT operation for qudits is defined by:

$$\begin{aligned}\hat{C}_X^{(d)} &= \sum_{j=0}^{d-1} |(j)_d\rangle\langle(j)_d| \otimes (\hat{\sigma}_x^{(d)})^j \\ &= \sum_{j,k=0}^{d-1} |(j)_d\rangle\langle(j)_d| \otimes |(k+j)_d\rangle\langle(k)_d|,\end{aligned}\tag{II.25}$$

and, equivalently, we introduce a controlled PHASE operation

$$\hat{C}_Z^{(d)} = \sum_{j=0}^{d-1} |(j)_d\rangle\langle(j)_d| \otimes (\hat{\sigma}_z^{(d)})^j\tag{II.26}$$

$$= \sum_{j=0}^{d-1} \omega^{jk} |(j)_d\rangle\langle(j)_d| \otimes |(k)_d\rangle\langle(k)_d|\tag{II.27}$$

$$= \sum_{k=0}^{d-1} (\hat{\sigma}_z^{(d)})^k \otimes |(k)_d\rangle\langle(k)_d|\tag{II.28}$$

which is acting symmetrically on the control and target qudits. As for qubits we can define the universality for qudits by the possibility to implement any desired single qudit operation plus an appropriate two-qudit operation, such as (II.25) or (II.25). Finite sets for universal quantum computation do also exist [Muthukrishnan and Stroud, 2000], as well as a generalized version of the Gottesman-Knill theorem [Gottesman, 1998].

In the following Section we will make the transition from finite dimensional quantum systems to infinite dimensional ones focusing, in particular, on systems that are described by continuous variables.

II.1.3 Continuous-variable (CV) systems

Coming from the d -dimensional case, treated in Sec. II.1.2, we can make the transition to infinite dimensions by taking the limit $d \rightarrow \infty$. Then, the analogs of the qudit basis states become infinitely localized eigenstates $|x'\rangle_x$, characterized by a continuous parameter x' , of an unbounded hermitian operator \hat{x} , fulfilling the eigenvalue relation $\hat{x}|x'\rangle_x = x'|x'\rangle_x$. It is most common to associate the operator \hat{x} with the position of a system, however, in general it can refer to any physical quantity that is described by an unbounded continuous variable, such as the quadratures of the electromagnetic field (see Sec. II.2). Similarly, the momentum eigenstates $|p'\rangle_p$ are eigenstates of the unbounded momentum operator \hat{p} , defined through $\hat{p}|p'\rangle_p = p'|p'\rangle_p$.² Together, the position and momentum operator fulfil the canonical commutation relation $[\hat{x}, \hat{p}] = i\hbar$. In the following and in the rest of the manuscript we will set \hbar equal to *one*.

²The subscript x and p of the basis kets refer to the fact that they are eigenstates of the position \hat{x} or momentum operator \hat{p} , respectively. This will be useful later on when we deal with basis states of arbitrary quadratures (see Eqs. (II.110) and (II.111)).

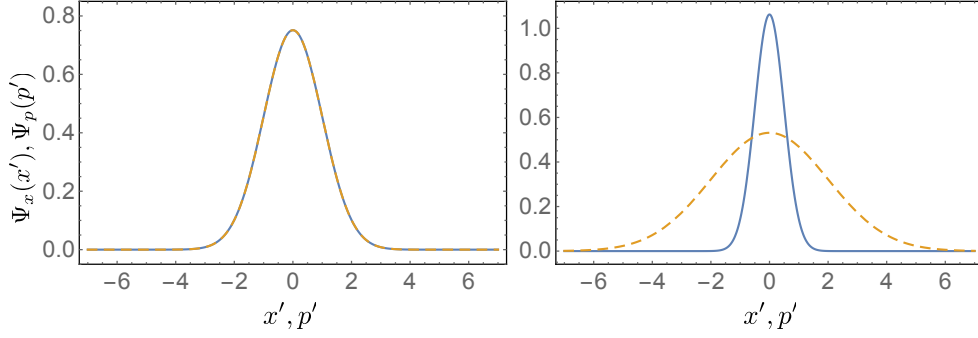


Figure II.1: (color online) Plots of the Gaussian real wave functions (II.31)

The position and momentum basis are orthogonal

$$\langle x|x' \rangle_x = \delta(x - x'), \quad \langle p|p' \rangle_p = \delta(p - p') \quad (\text{II.29})$$

and fulfil the completeness relation

$$\int_{-\infty}^{\infty} dx' |x' \rangle_x \langle x'|_x = \int_{-\infty}^{\infty} dp' |p' \rangle_p \langle p'|_p = \mathbb{1}. \quad (\text{II.30})$$

States can now be expressed in the position or momentum representation by expressing them as a continuous superposition of the position or momentum basis states, respectively:

$$|\Psi \rangle = \int_{-\infty}^{\infty} dx' \Psi_x(x') |x' \rangle_x = \int_{-\infty}^{\infty} dp' \Psi_p(p') |p' \rangle_p \quad (\text{II.31})$$

with square-integrable wave functions $\Psi_{x,p} : \mathbb{R} \rightarrow \mathbb{C}$, defined by $\Psi_x(x) = \langle x|x \Psi \rangle$ and $\Psi_p(p) = \langle p|p \Psi \rangle$. As simple example of such a wave functions we name here that of a Gaussian centered at the origin with width σ which, expressed in the position and momentum representation, respectively, read:

$$\Psi_x(x') = \frac{1}{\pi^{1/4} \sigma^{1/2}} e^{-\frac{x'^2}{2\sigma^2}}, \quad \text{and} \quad \Psi_p(p') = \frac{\sigma^{1/2}}{\pi^{1/4}} e^{-p'^2 \sigma^2 / 2}. \quad (\text{II.32})$$

The position and momentum uncertainty of this state can be easily calculated from the first and second moments of the position and momentum operator yielding the standard deviations: $\Delta x = \sqrt{\langle \hat{x}^2 \rangle - \langle \hat{x} \rangle^2} = \sigma / \sqrt{2}$ and $\Delta p = \sqrt{\langle \hat{p}^2 \rangle - \langle \hat{p} \rangle^2} = 1 / (\sqrt{2} \sigma)$. We thus find that the above Gaussian state saturates the *Heisenberg's uncertainty relation*: $\Delta x \Delta p \geq 1/2$. Furthermore, when setting $\sigma = 1$ we obtain a state with minimal uncertainty in position and momentum, whereas $\sigma < 1 (> 1)$ leads to a state with reduced uncertainty in position (momentum), and increased uncertainty in momentum (position).

As we were able to switch between the computational basis for qudits and its Fourier basis, we can switch between the position and momentum basis using the CV version

of the Fourier transform operator [Braunstein and van Loock, 2005]:

$$\hat{F} = e^{i\frac{\pi}{4}(\hat{x}^2 + \hat{p}^2)} = \frac{1}{\sqrt{2\pi}} \iint_{-\infty}^{\infty} ds ds' e^{iss'} |s\rangle_q \langle s'|_q, \quad (\text{II.33})$$

which acts as follows on the position and momentum eigenstates: $\hat{F}|s\rangle_x = |s\rangle_p$ and $\hat{F}^\dagger|s\rangle_p = |s\rangle_x$, and shows that $\langle x'|_x p'\rangle_p = e^{ix'p'}/\sqrt{2\pi}$. We further introduce the continuous analogs of the Pauli or Weyl-Heisenberg operators (II.17) and (II.18), being equal to the position and momentum displacement operators:

$$\hat{X}(s) = e^{-is\hat{p}} \quad \text{and} \quad \hat{Z}(s) = e^{is\hat{x}}, \quad (\text{II.34})$$

respectively, realizing the operations $\hat{X}(s)|s'\rangle_x = |s'+s\rangle_x$, $\hat{Z}(s)|s'\rangle_x = e^{iss'}|s'\rangle_x$, $\hat{X}(s)|s'\rangle_p = e^{iss'}|s'\rangle_p$ and $\hat{Z}(s)|s'\rangle_p = |s'+s\rangle_p$. As already indicated in the last section, the displacement operators (II.34) generate the continuous analog of the Weyl-Heisenberg group through multiplication.

Other CV gates are, for instance, the rotation operator $\hat{R}(\theta) = e^{i\theta(\hat{x}^2 + \hat{p}^2)/2}$, with angle θ , also referred to as fractional Fourier transform, which reproduces the Fourier transform \hat{F} for $\theta = \pi/2$, the squeezing operator $\hat{S}(r) = e^{ir(\hat{x}\hat{p} + \hat{p}\hat{x})/2}$, with $r \in \mathcal{R}$, which squeezes the position by a factor of e^r and stretches the momentum by e^{-r} accordingly, and the shear operator $\hat{N}(s) = e^{is\hat{x}^2}$, with $s \in \mathcal{R}$, which implements a shearing with respect to the position by a gradient s . Further on, CV gates acting on more than one system can be defined in analogy to the controlled qudit gates (II.25). For instance, a controlled version of the displacement operators (II.34) should perform controlled SHIFT and PHASE operations on the target subsystem depending on the position of the control subsystem, *i.e.* $\hat{C}_X|s_1\rangle_x|s_2\rangle_x = |s_1\rangle_x|s_1+s_2\rangle_x$ and $\hat{C}_Z|s_1\rangle_x|s_2\rangle_x = e^{is_1s_2}|s_1\rangle_x|s_2\rangle_x$, respectively. Such operations are generated by the operators $\hat{x} \otimes \hat{p}$ and $\hat{x} \otimes \hat{x}$, leading to the definition:

$$\hat{C}_X = e^{-i\hat{x} \otimes \hat{p}} \quad \text{and} \quad \hat{C}_Z = e^{i\hat{x} \otimes \hat{x}}. \quad (\text{II.35})$$

Another two-mode gate is the two-mode squeezing operation $\hat{S}_2(r) = e^{ir(\hat{x} \otimes \hat{p} + \hat{p} \otimes \hat{x})/2}$, which implements two controlled operations simultaneously with strength r . An experimental implementation of all these CV gates can be envisioned in different quantum optical setups such as the transverse degrees of freedom of single photons or the quadratures of the electromagnetic field. Both of these experimental platforms have advantages and disadvantages which we will discuss later on in this Chapter in Sec. II.3.1 and II.3.2.

Gates that are generated by Hamiltonians which are polynomials of maximal quadratic order in the position and momentum operators are called Gaussian operations and constitute the analogs of the Clifford operations in CV. They take their name from the fact that they map all states with a Gaussian Wigner function to other states having a Gaussian Wigner function as well [Weedbrook et al., 2012].³ In analogy to the Clifford group, Gaussian operations map the Heisenberg-Weyl group on itself and thus transform displacements into displacements. In other words, Gaussian operations act linearly on the Heisenberg-Weyl algebra, which consists of all linear combinations of the position and momentum operator, and therefore allows to write their action in the Heisenberg

³The Wigner function representation of CV quantum states will be discussed in Sec. II.1.6

representation as a linear transformation of the vector $\hat{\mathbf{v}} = (\hat{x}, \hat{p})^T$:

$$\hat{U}_G \hat{\mathbf{v}} \hat{U}_G^\dagger = \mathbf{M} \hat{\mathbf{v}} + \mathbf{c} \quad (\text{II.36})$$

where \hat{U}_G denotes an arbitrary Gaussian operation, \mathbf{M} is a symplectic 2×2 -matrix and the constant vector \mathbf{c} represents a displacement. Hence, the above introduced single system operations can be summarized by the following matrix equations:

$$\hat{\mathbf{v}} + \mathbf{c} = \begin{pmatrix} \hat{x} \\ \hat{p} \end{pmatrix} + \begin{pmatrix} s \\ t \end{pmatrix} = \begin{pmatrix} \hat{x} + s \\ \hat{p} + t \end{pmatrix}, \quad (\text{II.37})$$

$$\mathbf{M}_R(\theta) \hat{\mathbf{v}} = \begin{pmatrix} \cos \theta & -\sin \theta \\ \sin \theta & \cos \theta \end{pmatrix} \begin{pmatrix} \hat{x} \\ \hat{p} \end{pmatrix} = \begin{pmatrix} \cos \theta \hat{x} - \sin \theta \hat{p} \\ \sin \theta \hat{x} + \cos \theta \hat{p} \end{pmatrix}, \quad (\text{II.38})$$

$$\mathbf{M}_S(r) \hat{\mathbf{v}} = \begin{pmatrix} e^r & 0 \\ 0 & e^{-r} \end{pmatrix} \begin{pmatrix} \hat{x} \\ \hat{p} \end{pmatrix} = \begin{pmatrix} e^r \hat{x} \\ e^{-r} \hat{p} \end{pmatrix}, \quad (\text{II.39})$$

$$\mathbf{M}_N(s) \hat{\mathbf{v}} = \begin{pmatrix} 1 & 0 \\ s & 1 \end{pmatrix} \begin{pmatrix} \hat{x} \\ \hat{p} \end{pmatrix} = \begin{pmatrix} \hat{x} \\ s\hat{x} + \hat{p} \end{pmatrix}, \quad (\text{II.40})$$

where the vector $\mathbf{c} = (s, t)^T \in \mathbb{R}$ denotes a position and momentum displacements by s and t , and $\mathbf{M}_R(\theta)$, $\mathbf{M}_S(r)$ and $\mathbf{M}_N(s)$ are the corresponding symplectic transformations matrices of a rotation, a squeezing and a shear operation, respectively. Note, that any symplectic matrix can be decomposed into $\mathbf{M}_R(\theta)\mathbf{M}_S(r)\mathbf{M}_R(\phi)$, using singular-value decomposition, and thus any Gaussian unitary can be expressed as $\hat{U}_G = \hat{X}(s)\hat{Z}(t)\hat{R}(\theta)\hat{S}(r)\hat{R}(\phi)$ [Braunstein and van Loock, 2005].

In the same way we can express the action of the two-mode gates (II.35) by a linear transformation acting on a vector containing the position and momentum operator of both modes $\hat{\mathbf{v}} = (\hat{x}_1, \hat{p}_1, \hat{x}_2, \hat{p}_2)^T$. For \hat{C}_X we find, for instance:

$$\mathbf{M}_{C_X} \hat{\mathbf{v}} = \begin{pmatrix} 1 & 0 & 0 & 0 \\ 0 & 1 & 0 & -1 \\ 1 & 0 & 1 & 0 \\ 0 & 0 & 0 & 1 \end{pmatrix} \begin{pmatrix} \hat{x}_1 \\ \hat{p}_1 \\ \hat{x}_2 \\ \hat{p}_2 \end{pmatrix} = \begin{pmatrix} \hat{x}_1 \\ \hat{p}_1 - \hat{p}_2 \\ \hat{x}_1 + \hat{x}_2 \\ \hat{p}_2 \end{pmatrix}, \quad (\text{II.41})$$

where \hat{x}_1 (\hat{p}_1) and \hat{x}_2 (\hat{p}_2) have to be read as $\hat{x} \otimes \mathbb{1}$ ($\hat{p} \otimes \mathbb{1}$) and $\mathbb{1} \otimes \hat{x}$ ($\mathbb{1} \otimes \hat{p}$), respectively. Or the two-mode squeezing operation can be expressed as:

$$\mathbf{M}_{S_2} \hat{\mathbf{v}} = \begin{pmatrix} \cosh r & 0 & \sinh r & 0 \\ 0 & \cosh r & 0 & -\sinh r \\ \sinh r & 0 & \cosh r & 0 \\ 0 & -\sinh r & 0 & \cosh r \end{pmatrix} \begin{pmatrix} \hat{x}_1 \\ \hat{p}_1 \\ \hat{x}_2 \\ \hat{p}_2 \end{pmatrix} = \begin{pmatrix} \cosh r \hat{x}_1 + \sinh r \hat{x}_2 \\ \cosh r \hat{p}_1 - \sinh r \hat{p}_2 \\ \cosh r \hat{x}_1 + \cosh r \hat{x}_2 \\ \cosh r \hat{p}_2 - \sinh r \hat{p}_1 \end{pmatrix}. \quad (\text{II.42})$$

If we now define universality for CV quantum computation as in the finite dimensional case, by the ability to implement any desired unitary operation on a n -partite CV system, we can ask the natural question if the above introduced operations are already sufficient to achieve universality. The answer to this question is obviously *no*, since we

already mentioned that all so far introduced operations are Gaussian operations which are the analogs of the Clifford operations in finite dimensions. To understand this better we remind that all Gaussian operations are generated by Hamiltonians which are of maximal quadratic order in the position and momentum operators. Furthermore, combining gates generated by Hamiltonians $\{\pm\hat{H}_i\}$, leads to unitaries that are generated by linear combinations of the operators $\pm i[\hat{H}_i, \hat{H}_j]$, $\pm[\hat{H}_i, [\hat{H}_i, \hat{H}_j]]$, \dots , only [Lloyd and Braunstein, 1999; Lloyd, 1995]. Hence, concatenation of only Gaussian operations cannot lead to unitaries that are of higher than quadratic order in the position and momentum. In order to produce such higher order operations and thus to achieve universality for CV quantum computations, we need to introduce at least one gate that is of higher than quadratic order in position or momentum. A famous example of such is the cubic gate $\hat{V}(s) = e^{is\hat{x}^3}$, which is Non-Gaussian and therefore cannot be expressed as linear-symplectic transformation of the position and momentum operators.

Now, after having introduced the three of the most common ways to process information in quantum mechanics, we will discuss some convenient methods to represent quantum states. However, before doing so, we will recall some basic concepts about measurements in quantum mechanics.

II.1.4 Theory of measurements

If one opens a standard textbook of quantum mechanics one finds usually the following postulate [Cohen-Tannoudji et al., 1998; Messiah, 1991]:

In quantum mechanics all physical observables are represented by self-adjoint operators \hat{A} on a Hilbert space \mathcal{H} . The possible measurement outcomes of an observable are given by its eigenvalue spectrum and the expectation value of the distribution of the measurement outcomes with respect to a quantum state $|\Psi\rangle \in \mathcal{H}$ can be calculated through $\langle\hat{A}\rangle = \langle\Psi|\hat{A}|\Psi\rangle$.

Formulated in a slightly more mathematical way this means that every observable is given by a self-adjoint operator \hat{A} which admits a spectral decomposition in terms of projection operators $\hat{P}_i = \sum_k |\phi_{i,k}\rangle\langle\phi_{i,k}|$ leading to the diagonal representation:

$$\hat{A} = \sum_i a_i \hat{P}_i = \sum_{i,k} a_i |\phi_{i,k}\rangle\langle\phi_{i,k}| \quad (\text{II.43})$$

where a_i denote the eigenvalues of \hat{A} and k labels the degeneracy of each eigenvalue. The projectors \hat{P}_i form an orthogonal and hermitian set of operators, thus having the properties $\hat{P}_i \hat{P}_j = \delta_{i,j} \hat{P}_i$ and $\hat{P}_i = \hat{P}_i^\dagger = \hat{P}_i^2$. Further on, if a measurement of \hat{A} yields as outcome the eigenvalue a_i , the quantum state $|\Psi\rangle$ of the system is projected by \hat{P}_i onto the corresponding eigenspace \mathcal{H}_i spanned by the basis $\{|\phi_{i,k}\rangle | k = 1, \dots, \dim\mathcal{H}_i\}$. This process is called *projective measurement* and represents a particular case of a general measurement in quantum mechanics. Indeed, a projective measurement can be seen rather as an ideal measurement which will be difficult to realize in any realistic experimental situation.

In a general measurement theory we consider a set \mathcal{M} of measurement outcomes $m \in \mathcal{M}$ each associated with a measurement operator \hat{M}_m such that the probability for

obtaining an outcome m can be expressed as:

$$p_m = \langle \Psi | \hat{F}_m | \Psi \rangle = \langle \Psi | \hat{M}_m^\dagger \hat{M}_m | \Psi \rangle, \quad (\text{II.44})$$

where $\hat{F}_m = \hat{M}_m^\dagger \hat{M}_m$ is a positive operator, called *effect* [Breuer and Petruccione, 2007]. The difference to the postulate quoted above is that here we do not focus on a particular observable \hat{A} and its possible eigenvalues, but rather on all possible outcomes that might occur in an experiment when attempting to measure an observable. Furthermore, the measurement operators \hat{M}_m and thus the effects \hat{F}_m , which are both in general no projectors and \hat{M}_m not even hermitian, have to fulfil the completeness relation

$$\sum_m \hat{F}_m = \sum_m \hat{M}_m^\dagger \hat{M}_m = \mathbb{1}, \quad (\text{II.45})$$

reflecting the normalization of the probabilities p_m . After a general measurement the state reduces to the following post-measurement state:

$$|\Psi_m\rangle = \frac{1}{\sqrt{p_m}} \hat{M}_m |\Psi\rangle. \quad (\text{II.46})$$

Equivalently, one can express Eqs. (II.44) and (II.46) in the density matrix formalism as:

$$\hat{\rho}_m = \frac{1}{p_m} \hat{M}_m \hat{\rho} \hat{M}_m^\dagger \quad \text{with} \quad p_m = \text{tr} \left[\hat{M}_m \hat{\rho} \hat{M}_m^\dagger \right], \quad (\text{II.47})$$

which shows that the mapping $\hat{\rho} \rightarrow \hat{\rho}_m$ is the special case of a more general *Kraus map* $\hat{\rho}_m = \Phi_m(\hat{\rho}) = \sum_k \hat{\Omega}_{m,k} \hat{\rho} \hat{\Omega}_{m,k}^\dagger$ with $\sum_{m,k} \hat{\Omega}_{m,k}^\dagger \hat{\Omega}_{m,k} = \mathbb{1}$. Hence, the reduction of the quantum state due to a general measurement process is always described by a *completely-positive* and trace preserving map. Completely-positive means that not only the map Φ_m has to be positive but also its extension $\Phi_m \otimes \mathbb{1}$ for any dimension of the second subsystem. This is a reasonable assumption since the map $\Phi_m \otimes \mathbb{1}$ can describe a measurement on one of two separated subsystems which leaves the second subsystem untouched.⁴

Often when speaking about a generalized measurement one does not specify the measurement operators \hat{M}_m , but only introduces directly the set of positive operators (effects) \hat{F}_m and refers to them as a *positive operator valued measurement* (POVM). In this case, the exact shape of the operators \hat{M}_m and thus of the post-measurement state $|\Psi_m\rangle$ yet has to be specified, for instance as $\hat{M}_m = \sqrt{\hat{F}_m}$.

As example we treat the case of a two-valued POVM in terms of which one can measure the expectation value of an arbitrary bounded observable. For instance, consider an observable \hat{A} with bounded spectrum $a_{min} \leq \{|a_i|\} \leq a_{max}$, from which we can construct a two-valued POVM $\{\hat{E}_0, \hat{E}_1\}$ with corresponding measurement operators

⁴For more details about the general theory of measurements in quantum mechanics and about the complete positivity of Kraus operations we refer the reader to the book [Breuer and Petruccione, 2007].

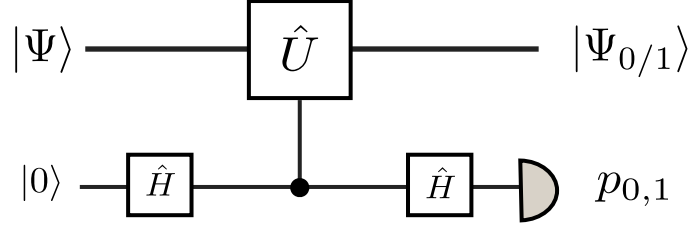


Figure II.2: (color online) Quantum circuit allowing for the measurement of the POVM $\hat{E}_{0/1}^{(a)}$. \hat{H} depict Hadamard gates, and a controlled unitary gate \hat{C}_U applies the unitary \hat{U} to the system if the ancilla is in the state $|0\rangle$ and does nothing otherwise. Measuring the ancilla in the computational basis yields the probability p_0 (p_1) of finding it in the state $|0\rangle$ ($|1\rangle$), and projects the system onto the states $|\Psi_0\rangle$ ($|\Psi_1\rangle$).

[Horodecki, 2003]:

$$\hat{M}_0 = \sqrt{(a_- \mathbb{1} + \hat{A})/a_+}, \quad (\text{II.48})$$

$$\hat{M}_1 = \sqrt{\mathbb{1} - \hat{M}_0^\dagger \hat{M}_0}, \quad (\text{II.49})$$

where $a_- = \max(0, -a_{\min})$ and $a_+ = a_- + a_{\max}$. Equations (II.48) and (II.49) fulfill the normalization condition $\hat{E}_0 + \hat{E}_1 = \hat{M}_0^\dagger \hat{M}_0 + \hat{M}_1^\dagger \hat{M}_1 = \mathbb{1}$ and allow to express the expectation value of \hat{A} as follows:

$$\langle \hat{A} \rangle = a_+ p_0 - a_-, \quad (\text{II.50})$$

where $p_0 = \langle \hat{E}_0 \rangle = \langle (a_- \mathbb{1} + \hat{A}) \rangle / a_+$. Hence, we have expressed the expectation value of an arbitrary bounded observable \hat{A} in terms of a single parameter p_0 that is measurable through the two-valued POVM $\{\hat{E}_{0/1}\}$.

The measurement of this POVM can be realized by coupling the system, on which \hat{A} is defined, to an ancilla qubit. To show this, let's consider the case where the spectrum of \hat{A} is bounded by $\pm a$ from above and below, respectively, thus yielding $a_- = a$ and $a_+ = 2a$. Then, the measurement operators (II.48) and (II.49) lead to the POVM $\hat{E}_{0/1}^{(a)} = \frac{1}{2}(\mathbb{1} \pm \hat{A}/a)$, in terms of the renormalized operator \hat{A}/a , which is bounded by ± 1 and can be expressed as the real part of an appropriate unitary operator \hat{U} . If we now realize the quantum circuit shown in Fig. II.2, which implements two Hadamard gates (see Eq. (II.9)) and a controlled unitary operation \hat{C}_U to the system plus ancilla, we are left with the state

$$|\Psi\rangle|0\rangle \rightarrow \frac{1}{2}(\mathbb{1} + \hat{U})|\Psi\rangle|0\rangle + \frac{1}{2}(\mathbb{1} - \hat{U})|\Psi\rangle|1\rangle. \quad (\text{II.51})$$

A measurement of the output ancilla state in the computational basis projects the output state with probability $p_{0/1} = \langle \Psi | \hat{E}_{0/1}^{(a)} | \Psi \rangle = \langle \Psi | \frac{1}{2}(\mathbb{1} \pm \text{Re}[\hat{U}]) | \Psi \rangle$ onto the state $|\Psi_{0/1}\rangle = \frac{1}{2\sqrt{p_{0/1}}}(\mathbb{1} \pm \hat{U})|\Psi\rangle$. This shows that the measurement of the ancilla implements

the POVM $\hat{E}_{0/1}^{(a)}$ with $\hat{A} = \text{Re}(\hat{U})$ and we have $a(p_0 - p_1) = a(2p_0 - 1) = \langle \hat{A} \rangle$. Experimental implementations of ancilla measurements, as shown in Fig. II.2, can be envisioned with different quantum optical platforms, for instance, the transverse degrees of freedom of single photons [Machado et al., 2013; Hor-Meyll et al., 2014; Ketterer et al., 2015] (see also Sec. II.3.1), in cavity QED [Haroche et al., 2007] or with micro-mechanical oscillators [Asadian et al., 2014].

II.1.5 Bloch vector representation

In this section, we introduce the Bloch vector representation of quantum states in finite dimensional Hilbert spaces. To do so, we first discuss some general properties of density matrices and introduce a general operator basis in which we can expand each of them.

The space of density matrices $\mathcal{L}_+(\mathcal{H}_d)$ over a d -dimensional Hilbert space \mathcal{H}_d is defined by:

$$\mathcal{L}_+(\mathcal{H}_d) = \{\hat{\rho} \in \mathcal{L}(\mathcal{H}_d) | \text{tr}\hat{\rho} = 1, \hat{\rho} \geq 0\}, \quad (\text{II.52})$$

where $\mathcal{L}(\mathcal{H}_d)$ denotes the space of all linear operators on \mathcal{H}_d . The positivity condition $\hat{\rho} \geq 0$ in Eq. (II.52) is equivalent to demanding hermiticity $\hat{\rho}^\dagger = \hat{\rho}$ and positivity of all eigenvalues $\rho_i \geq 0$ of $\hat{\rho}$. As inner product on such operator spaces we introduce the *Hilbert-Schmidt inner product*, which is defined through $(\hat{A}, \hat{B}) = \text{tr}[\hat{A}^\dagger \hat{B}]$.

Next, we introduce a complete set of orthonormal basis operators $\hat{\Lambda}_i \in \mathcal{L}(\mathcal{H}_d)$, with $i = 0, \dots, d^2 - 1$, such that $\text{tr}[\hat{\Lambda}_i^\dagger \hat{\Lambda}_j] = \delta_{i,j}$. If we take into account that all density matrices have trace equal to one, we can choose one element of the operator basis equal to the identity $\hat{\Lambda}_0 = \mathbb{1}/d$, such that all other basis operators will be traceless, *i.e.* $\text{tr}[\hat{\Lambda}_i] = 0$, for all $i = 1, \dots, d^2 - 1$. In terms of this basis we can express every density matrix as a linear combination

$$\hat{\rho} = \frac{1}{d}\mathbb{1} + \sum_{i=1}^{d^2-1} c_i \hat{\Lambda}_i, \quad (\text{II.53})$$

with $d^2 - 1$ complex coefficients $c_i = \text{tr}[\hat{\Lambda}_i^\dagger \hat{\rho}]$, which define a representation of the density matrix $\hat{\rho}$. In general, there exist many density matrix representation depending on the specific choice of the operator basis $\{\hat{\Lambda}_i\}_{i=1}^{d^2-1}$.

A famous example, for $d = 2$, are the Pauli matrices (II.7), which lead to the Bloch vector representation of a qubit $\hat{\rho} = \frac{1}{2}(\mathbb{1} + \mathbf{v} \cdot \hat{\boldsymbol{\sigma}})$, with the real Bloch vector $\mathbf{v} = (v_x, v_y, v_z)^\text{T} = 2(\langle \hat{\sigma}_x \rangle, \langle \hat{\sigma}_y \rangle, \langle \hat{\sigma}_z \rangle)^\text{T}$ and the Pauli spin operator $\hat{\boldsymbol{\sigma}} = (\hat{\sigma}_x, \hat{\sigma}_y, \hat{\sigma}_z)^\text{T}$. The advantage of using the Pauli matrices (II.7), which generate the *Special Unitary Group* $SU(2)$, as basis is that they are hermitian and thus allow for a representation in terms of the real Bloch vector \mathbf{v} that can be visualized in three-dimensional euclidian space. Before generalizing this representation to the d -dimensional case we want to discuss some of its properties. It is easy to see that the length of the Bloch vector is given by $|\mathbf{v}|^2 = 2\text{tr}\hat{\rho}^2 - 1$, which in the case of a pure state $\hat{\rho} = |\Psi\rangle\langle\Psi| = \hat{\rho}^2$ is equal to one $|\mathbf{v}| = 1$, but for a general mixed state $|\mathbf{v}| < 1$. Hence, all qubit states can be represented as a point inside a two-dimensional unit-sphere (see Fig. II.3), whereas all pure states lie on the surface of the sphere and mixed states inside of it with the maximally mixed state $\hat{\rho}_{\text{mm}} = \mathbb{1}/2$ at its origin. A parametrization of the pure qubits states on the surface

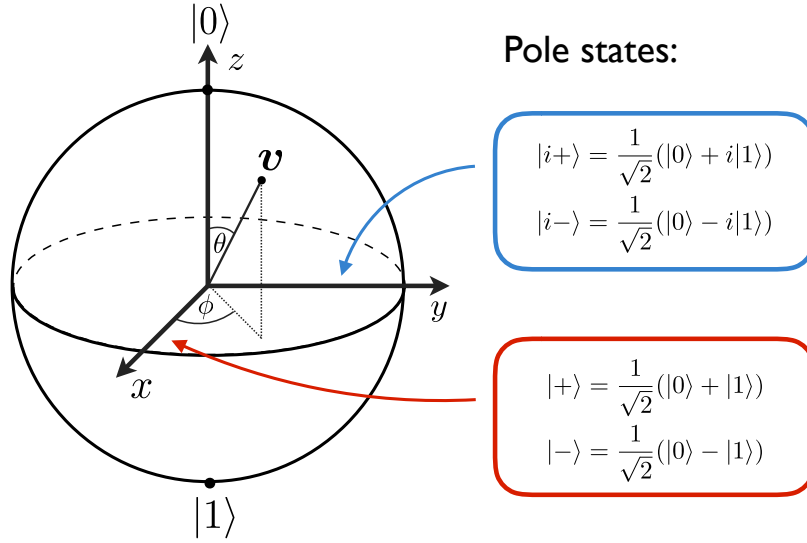


Figure II.3: (color online) Bloch sphere representation of the Bloch vector \mathbf{v} for qubits ($d = 2$). All pure states, which are represented by a Bloch vector \mathbf{v} of unit length, lie on the surface of the sphere characterized by the angles $\theta \in [0, \pi[$ and $\phi \in [0, 2\pi[$. States with Bloch vector $|\mathbf{v}| < 1$ are mixed states and the origin corresponds to the maximally mixed state $\hat{\rho} = \mathbb{1}_2/2$. While the poles of the Bloch sphere with respect to the z -axes (north and south pole) correspond to the computational basis states $|0\rangle$ and $|1\rangle$, the poles with respect to the y - and x -axes represent its mutually unbiased bases $|i\pm\rangle$ (blue) and $|\pm\rangle$ (red), respectively.

was given in Sec. II.1.1 by Eq. (II.1), what shows that the mapping from the qubit state space to the unit ball in three dimensions is not only one-to-one but also surjective, meaning that every point on or inside the sphere is associated to a qubit state.

In order to define the same Bloch vector representation for qudits we have to introduce the generators of the special unitary group in d dimensions $SU(d)$. As for the Pauli matrices (II.7), the generators of $SU(d)$ provide, together with the identity operator, a complete, orthogonal and hermitian operator basis that can be constructed systematically in the following way [Hioe and Eberly, 1981; Alicki and Lendi, 2007]:

$$\{\hat{\lambda}_i^{(d)}\}_{i=1,\dots,d^2-1} = \{\hat{u}_{j,k}, \hat{v}_{j,k}, \hat{w}_l\} \quad (\text{II.54})$$

where

$$\hat{u}_{j,k} = |j\rangle\langle k| + |k\rangle\langle j|, \quad \hat{v}_{j,k} = i(|k\rangle\langle j| - |j\rangle\langle k|), \quad (\text{II.55})$$

$$\hat{w}_l = \sqrt{\frac{1}{l(l+1)}} \sum_{j=1}^l (|j\rangle\langle j| - l|l+1\rangle\langle l+1|) \quad (\text{II.56})$$

with $1 \leq j \leq k \leq d$ and $1 \leq l \leq d-1$, and a orthonormal qudit basis $\{|m\rangle\}_{m=1}^d$ of \mathcal{H}_d . The $SU(d)$ generators $\hat{\lambda}_i^{(d)}$, defined by Eqs. (II.54)-(II.56), are characterized by their

commutation and anti-commutation relations, respectively:

$$[\hat{\lambda}_i^{(d)}, \hat{\lambda}_j^{(d)}] = 2if_{ijk}\hat{\lambda}_k^{(d)} \quad (\text{II.57})$$

$$\{\hat{\lambda}_i^{(d)}, \hat{\lambda}_j^{(d)}\} = \frac{4}{d}\delta_{i,j}\mathbb{1}_d + 2ig_{ijk}\hat{\lambda}_k^{(d)}, \quad (\text{II.58})$$

with the real structure constants g_{ijk} (f_{ijk}) which are completely (anti-)symmetric with respect to index permutations. Note that in Eqs. (II.57) and (II.58) repeated indices are summed from 1 to $d^2 - 1$. As a special case of the constructed $SU(d)$ generators we retrieve the Pauli matrices (II.7) for $d = 2$ with the commutation and anti-commutation relations, $[\hat{\sigma}_i, \hat{\sigma}_j] = 2i\varepsilon_{ijk}$ and $\{\hat{\sigma}_i, \hat{\sigma}_j\} = \delta_{i,j}\mathbb{1}$, whereas $f_{ijk} = \varepsilon_{ijk}$ and $g_{ijk} = 0$. For the case $d = 3$, we obtain the well-known Gell-Mann matrices $\{\hat{\lambda}_i^{(3)}\}_{i=1}^8$, defined as: $\hat{\lambda}_1 = \hat{u}_{12}$, $\hat{\lambda}_2 = \hat{v}_{12}$, $\hat{\lambda}_3 = \hat{w}_1$, $\hat{\lambda}_4 = \hat{u}_{13}$, $\hat{\lambda}_5 = \hat{v}_{13}$, $\hat{\lambda}_6 = \hat{u}_{23}$, $\hat{\lambda}_7 = \hat{v}_{23}$, $\hat{\lambda}_8 = \hat{w}_2$, or in matrix form by

$$\begin{aligned} \lambda_1 &= \begin{pmatrix} 0 & 1 & 0 \\ 1 & 0 & 0 \\ 0 & 0 & 0 \end{pmatrix} & \lambda_2 &= \begin{pmatrix} 0 & -i & 0 \\ i & 0 & 0 \\ 0 & 0 & 0 \end{pmatrix} & \lambda_3 &= \begin{pmatrix} 1 & 0 & 0 \\ 0 & -1 & 0 \\ 0 & 0 & 0 \end{pmatrix} \\ \lambda_4 &= \begin{pmatrix} 0 & 0 & 1 \\ 0 & 0 & 0 \\ 1 & 0 & 0 \end{pmatrix} & \lambda_5 &= \begin{pmatrix} 0 & 0 & -i \\ 0 & 0 & 0 \\ i & 0 & 0 \end{pmatrix} & \lambda_6 &= \begin{pmatrix} 0 & 0 & 0 \\ 0 & 0 & 1 \\ 0 & 1 & 0 \end{pmatrix} \\ \lambda_7 &= \begin{pmatrix} 0 & 0 & 0 \\ 0 & 0 & -i \\ 0 & i & 0 \end{pmatrix} & \lambda_8 &= \frac{1}{\sqrt{3}} \begin{pmatrix} 1 & 0 & 0 \\ 0 & 1 & 0 \\ 0 & 0 & -2 \end{pmatrix} \end{aligned} \quad (\text{II.59})$$

with structure constants:

$$\begin{aligned} f_{123} &= 1, \\ f_{458} &= f_{678} = \sqrt{3}/2, \\ f_{147} &= f_{246} = f_{257} = f_{345} = -f_{156} = -f_{367} = 1/2, \\ g_{118} &= g_{228} = g_{338} = -g_{888} = \sqrt{3}/3, \\ g_{448} &= g_{558} = g_{668} = g_{778} = -\sqrt{3}/6, \\ g_{146} &= g_{157} = g_{256} = g_{344} = g_{355} = -g_{247} = -g_{366} = -g_{377} = 1/2. \end{aligned} \quad (\text{II.60})$$

Having the generators of $SU(d)$ in hand we can express the density matrix of a general qudit state $\hat{\rho}^{(d)}$ in its Bloch vector representation, through:

$$\hat{\rho}^{(d)} = \frac{1}{d}\mathbb{1}_d + \frac{1}{2} \sum_{i=1}^{d^2-1} v_i^{(d)} \hat{\lambda}_i^{(d)}, \quad (\text{II.61})$$

with the generalized Bloch vector $\mathbf{v}^{(d)} = \{v_i^{(d)}\}_{i=1}^{d^2-1}$. From Eq. (II.61) we find that $\text{tr}\hat{\rho}^2 = \frac{1}{d} - \frac{1}{2}|\mathbf{v}^{(d)}|^2$, which shows that the length of the generalized Bloch vector for

pure qudit states ($\hat{\rho}^2 = \hat{\rho}$) is given by

$$|\mathbf{v}_{\text{pure}}^{(d)}| = \sqrt{2 \frac{d-1}{d}}. \quad (\text{II.62})$$

This confirms that for pure qubit states we get $\mathbf{v}_{\text{pure}}^{(2)} = 1$, but, for $d \geq 3$, pure states lie on the surface of a hyper-sphere with radius $\sqrt{2(d-1)/d}$ embedded in $(d^2 - 1)$ -dimensional *Euclidean* space. Also, in contrast to the qubit case, the mapping from the space of pure qudit states to the points on the generalized Bloch sphere is, in general, not surjective and thus not every point on the sphere corresponds to a pure qudit state. This becomes clear from Eq. (II.16), which shows that a general pure qudit state is characterized by $2(d-1)$ real parameters and therefore the set of pure qudit states forms a $2(d-1)$ -dimensional submanifold of the $(d^2 - 2)$ -dimensional generalized Bloch sphere. Similarly, not every point inside the generalized Bloch sphere will correspond to a mixed qudit state.

II.1.6 Wigner function representation

When dealing with continuous-variable degrees of freedom, as discussed in Sec. II.1.3, a Bloch vector representation, defined through a continuous set of basis operators spanning an infinite dimensional Hilbert space, is possible but often not as handy as in the finite dimensional case. The latter is more elegantly described by a phase space distribution $W(x, p)$ that is parametrized by the position and momentum variables. Ideally, such a phase space distribution would be given by a joint probability density $P(x, p)$ of position and momentum with the marginal probability densities, $P(x) = \langle x | \hat{\rho} | x \rangle$ and $P(p) = \langle p | \hat{\rho} | p \rangle$, respectively. However, a proper probability density $P(x, p)$ must be positive, for all x and p , and normalized to one. In the following, we will define such a phase space distribution and check if it fulfills the conditions of a proper probability density.

To begin, let us define the phase-space displacement operator:

$$\hat{D}(\nu, \mu) = e^{i\mu\hat{x} - i\nu\hat{p}} = e^{-i\mu\nu/2} e^{i\mu\hat{x}} e^{-i\nu\hat{p}}, \quad (\text{II.63})$$

that implements a displacement of the position and momentum by the values ν and μ , respectively. At the second equality of Eq. (II.63) we used the special case of the *Baker-Campbell-Hausdorff formula* $e^{\hat{A}+\hat{B}} = e^{\hat{A}} e^{\hat{B}} e^{-[\hat{A}, \hat{B}]/2} = e^{\hat{B}} e^{\hat{A}} e^{[\hat{A}, \hat{B}]/2}$, which holds if $[\hat{A}, [\hat{A}, \hat{B}]] = [\hat{B}, [\hat{A}, \hat{B}]] = 0$. The set of all displacement operators $\{\hat{D}(\mu, \nu) | (\mu, \nu) \in \mathbb{R}\}$ forms a non-hermitian operator basis fulfilling the orthogonality condition

$$\text{tr}[\hat{D}^\dagger(\nu, \mu) \hat{D}(\nu', \mu')] = 2\pi \delta(\mu' - \mu) \delta(\nu' - \nu). \quad (\text{II.64})$$

Therefore, an arbitrary quantum state can be expanded as

$$\hat{\rho} = \iint d\nu d\mu \chi_{\hat{\rho}}(\nu, \mu) \hat{D}(\nu, \mu) \quad (\text{II.65})$$

with the complex characteristic function

$$\chi_{\hat{\rho}}(\nu, \mu) = \frac{1}{2\pi} \text{tr}[\hat{\rho} \hat{D}^\dagger(\nu, \mu)]. \quad (\text{II.66})$$

By further evaluating Eq. (II.66) using Eq. (II.63) and by doing the substitution $x = x' + \nu/2$, we get:

$$\chi_{\hat{\rho}}(\nu, \mu) = \frac{1}{2\pi} \int_{-\infty}^{\infty} dx' e^{-i\nu\mu/2} \langle x' | \hat{\rho} e^{-i\mu\hat{x}} e^{i\nu\hat{p}} | x' \rangle \quad (\text{II.67})$$

$$= \frac{1}{2\pi} \int_{-\infty}^{\infty} dx e^{-i\mu x} \langle x + \frac{\nu}{2} | \hat{\rho} | x - \frac{\nu}{2} \rangle. \quad (\text{II.68})$$

Now, we define the phase space distribution $W_{\hat{\rho}}(x, p)$, also referred to as *Wigner Function*, as the inverse Fourier transform of the characteristic function (II.66):

$$W_{\hat{\rho}}(x, p) = \frac{1}{2\pi} \iint_{-\infty}^{\infty} d\mu d\nu e^{i\mu x - i\nu p} \chi_{\hat{\rho}}(\nu, \mu) \quad (\text{II.69})$$

$$= \frac{1}{(2\pi)^2} \iint_{-\infty}^{\infty} dx' d\nu e^{-i\nu p} \underbrace{\int_{-\infty}^{\infty} d\mu e^{i\mu(x-x')} \langle x' + \frac{\nu}{2} | \hat{\rho} | x' - \frac{\nu}{2} \rangle}_{=2\pi\delta(x-x')}, \quad (\text{II.70})$$

which leads to the final expression

$$W_{\hat{\rho}}(x, p) = \frac{1}{2\pi} \int_{-\infty}^{\infty} dx' e^{ix'p} \langle x - \frac{x'}{2} | \hat{\rho} | x + \frac{x'}{2} \rangle. \quad (\text{II.71})$$

The Wigner function has several useful properties that allows one ignore the quantum state or density matrix formalism and perform all calculations within phase space. For instance, the Wigner function is linear:

$$W_{p_1\hat{\rho}_1+p_2\hat{\rho}_2+\dots}(x, p) = p_1 W_{\hat{\rho}_1}(x, p) + p_2 W_{\hat{\rho}_2}(x, p) + \dots, \quad (\text{II.72})$$

we can use it to calculate the inner product between two operators $\hat{\rho}_1$ and $\hat{\rho}_2$ through the relation:

$$\text{tr}[\hat{\rho}_1 \hat{\rho}_2] = 2\pi \iint_{-\infty}^{\infty} dx dp W_{\hat{\rho}_1}(x, p) W_{\hat{\rho}_2}(x, p), \quad (\text{II.73})$$

and as we demanded above $W_{\hat{\rho}}(x, p)$ is a real and normalized distribution:

$$\iint_{-\infty}^{\infty} dx dp W_{\hat{\rho}}(x, p) = \int_{-\infty}^{\infty} dx \langle x | \hat{\rho} | x \rangle = 1 \quad (\text{II.74})$$

which yields the marginal probability densities:

$$P(x) = \langle x | \hat{\rho} | x \rangle = \int_{-\infty}^{\infty} dp W_{\hat{\rho}}(x, p), \quad (\text{II.75})$$

$$P(p) = \langle p | \hat{\rho} | p \rangle = \int_{-\infty}^{\infty} dx W_{\hat{\rho}}(x, p). \quad (\text{II.76})$$

Further on, using Eq. (II.73), we can calculate the expectation value of a quantum observable \hat{A} with respect to some quantum state $\hat{\rho}$ in the same fashion as we do for classical observables in probability theory:

$$\langle \hat{A} \rangle_{\hat{\rho}} = \iint_{-\infty}^{\infty} dx dp A(x, p) W_{\hat{\rho}}(x, p) \quad (\text{II.77})$$

where the quantity $A(x, p) = 2\pi W_{\hat{A}}(x, p)$ is proportional to the Wigner function of the observable \hat{A} . For instance, an arbitrary symmetrized observable

$$S(\hat{x}^n \hat{p}^m) = \frac{1}{2^n} \sum_{j=0}^n \binom{a}{b} \hat{p}^{n-j} \hat{x}^m \hat{p}^j \quad (\text{II.78})$$

yields with the so-called Weyl correspondence [Weyl, 1950]:

$$\langle S(\hat{x}^n \hat{p}^m) \rangle_{\hat{\rho}} = \iint_{-\infty}^{\infty} dx dp x^n p^m W_{\hat{\rho}}(x, p). \quad (\text{II.79})$$

And finally we note that the Wigner function is upper and lower bounded by $|W_{\hat{\rho}}(x, p)| \leq 1/\pi$.

However, the derived distribution $W_{\hat{\rho}}(x, p)$ is in general not strictly positive and thus cannot be associated with an ordinary joint probability density for the position and the momentum. It is only possible to define certain classes of quantum states which have a strictly positive Wigner function. For example, we can consider all states that have a Gaussian Wigner function:

$$W_{\text{Gauss}}(x, p) = \frac{1}{2\pi\sigma_x\sigma_p} e^{-\frac{(x-x_0)^2}{\sigma_x^2} - \frac{(p-p_0)^2}{\sigma_p^2}} \quad (\text{II.80})$$

with widths, σ_x and σ_p , and positions, x_0 and p_0 . More generally, we can express a Gaussian Wigner function as

$$W_{\text{Gauss}}(x, p) = \frac{1}{2\pi\sqrt{\det(\boldsymbol{\Sigma})}} e^{-\frac{1}{2}(\mathbf{v}-\mathbf{v}_0)^T \boldsymbol{\Sigma}^{-1}(\mathbf{v}-\mathbf{v}_0)}, \quad (\text{II.81})$$

in terms of the displacement vector $\bar{\mathbf{v}} = (\langle \hat{x} \rangle, \langle \hat{p} \rangle)^T$, the covariance matrix

$$\boldsymbol{\Sigma} = \begin{pmatrix} \langle \hat{x}^2 \rangle - \langle \hat{x} \rangle^2 & \langle \frac{1}{2} \{ \hat{x}, \hat{p} \} \rangle - \langle \hat{x} \rangle \langle \hat{p} \rangle \\ \langle \frac{1}{2} \{ \hat{x}, \hat{p} \} \rangle - \langle \hat{x} \rangle \langle \hat{p} \rangle & \langle \hat{p}^2 \rangle - \langle \hat{p} \rangle^2 \end{pmatrix} \quad (\text{II.82})$$

and the vector $\mathbf{v} = (x, p)^T$. One can transform Eq. (II.81) into Eq. (II.80) by diagonalizing the symmetric covariance matrix (II.82). Hence, all states with Gaussian Wigner

function, referred to as *Gaussian states*, are completely characterized by their covariance matrices and displacement vectors $(\Sigma, \bar{\mathbf{v}})$. For all other states, whose Wigner functions are not Gaussian, also higher order moments will be important. We have thus found a class of quantum states that have always a positive Wigner function $W_{\text{Gauss}}(x, p) \geq 0$, for all x and p .

Furthermore, for pure quantum states Gaussianity is a necessary and sufficient condition for the positivity of the corresponding Wigner function, as stated by the *Hudson-Piquet's theorem* [Hudson, 1974]: “A necessary and sufficient condition for the Wigner density $W_{\hat{\rho}}(x, p)$ corresponding to the Schrödinger state vector $|\Psi\rangle$ to be a true probability density is that $|\Psi\rangle$ be the exponential of quadratic polynomial.”. Or, formulated in other words, the Wigner function of a pure state $|\Psi\rangle$ is everywhere positive if and only if it is a Gaussian function. This allows us to classify all pure quantum states into two groups, called *Gaussian* and *Non-Gaussian* states, with positive and not strictly positive Wigner function, respectively. However, note that the above theorem is only valid for pure states and does not generalize to mixed states. For example, the classical mixture of two Gaussian states will, according to Eq. (II.72), also have a positive Wigner function which is in general not Gaussian. Examples of Gaussian and Non-Gaussian states of light will be discussed in Sec. II.2.4 after having introduced the quantum state and mode representation of the electromagnetic radiation field in Sec. II.2.1.

Last, we want to mention that the Wigner function (II.71) can also be generalized to N -partite systems, as follows:

$$W_{\hat{\rho}}(x_1, p_1; x_2, p_2; \dots; x_N, p_N) = \frac{1}{(2\pi)^N} \int_{-\infty}^{\infty} dx'_1 dx'_2 \dots dx'_N e^{ix'_1 p_1 + ix'_2 p_2 + \dots + ix'_N p_N} \times \langle x_1 - \frac{x'_1}{2} | \langle x_2 - \frac{x'_2}{2} | \dots \langle x_N - \frac{x'_N}{2} | \hat{\rho} | x_1 + \frac{x'_1}{2} \rangle | x_2 + \frac{x'_2}{2} \rangle \dots | x_N + \frac{x'_N}{2} \rangle. \quad (\text{II.83})$$

which will be of interest when studying nonlocality and entanglement in continuous-variable systems (see Chapter V).

II.2 Quantum theory of light

In this Section we will be mainly concerned with the formulation of the quantum theory of the electromagnetic field. The origins of this theory go back to the year 1900 when Planck derived, for the first time, the law which describes the amount of radiation emitted by a black body with temperature T at frequency ν , by assuming that the energy of the emitted radiation is proportional to the *Planck constant* h .⁵ Later on in 1905, it was Einstein who confirmed this *quantum hypothesis* in his work about the photoelectric effect, by postulating that light can only exchange quantized amounts of energy with matter because it occurs only in so-called energy quanta. While controversial at the beginning, the quantum hypothesis is today widely accepted and forms the foundation of a theoretical description of the electromagnetic field.

⁵The value of the Planck constant is $h = 6.626070040(81) \times 10^{-34} \text{Js}$ (see <http://physics.nist.gov/cuu/Constants/index.html>).

II.2.1 Quantization of the electromagnetic field

The electromagnetic field is a measurable quantity which in quantum mechanics is described by a self-adjoint operator. In order to derive this operator of the electromagnetic field we start from the classical theory of electromagnetism [Jackson, 1998]. According to the latter the classical electric and magnetic fields in vacuum, \mathbf{E} and \mathbf{B} , obey the free Maxwell equations:

$$\nabla \cdot \mathbf{E} = 0, \quad \nabla \times \mathbf{E} = -\frac{\partial \mathbf{B}}{\partial t}, \quad (\text{II.84})$$

$$\nabla \cdot \mathbf{B} = 0, \quad \nabla \times \mathbf{B} = \mu_0 \varepsilon_0 \frac{\partial \mathbf{E}}{\partial t}. \quad (\text{II.85})$$

It is often of advantage to express \mathbf{E} and \mathbf{B} in terms of a vector and a scalar potential:

$$\mathbf{B} = \nabla \times \mathbf{A}, \quad (\text{II.86})$$

$$\mathbf{E} = -\nabla \Phi - \frac{\partial \mathbf{A}}{\partial t}. \quad (\text{II.87})$$

which, by inserting Eq. (II.86) and (II.87) into Eq. (II.84) and (II.85), lead to the differential equations:

$$\nabla(\nabla \cdot \mathbf{A}) - \nabla^2 \mathbf{A} + \frac{1}{c^2} \frac{\partial}{\partial t} \nabla \Phi + \frac{1}{c^2} \frac{\partial^2 \mathbf{A}}{\partial t^2} = 0, \quad (\text{II.88})$$

$$-\nabla^2 \Phi - \nabla \cdot \frac{\partial \mathbf{A}}{\partial t} = 0. \quad (\text{II.89})$$

where we used the relation $c = 1/(\mu_0 \varepsilon_0)^{1/2}$, with the speed of light c . We can decouple Eqs. (II.88) and (II.89) by choosing the Coulomb gauge $\nabla \cdot \mathbf{A} = 0$ and by applying the Helmholtz' theorem⁶ to divide (II.88) and (II.89) into transversal and longitudinal parts, yielding the following equations for the vector and the scalar potential

$$\left(\frac{1}{c^2} \frac{\partial^2}{\partial t^2} - \nabla^2 \right) \mathbf{A} = 0, \quad (\text{II.90})$$

$$\nabla^2 \Phi = 0. \quad (\text{II.91})$$

The solution of Eq. (II.91) under the above conditions is given by $\Phi = 0$. Further on, by imposing periodic boundary conditions in a cubic volume with length L , we can write the solution of Eq. (II.90) as a superposition of plane transversal waves:

$$\mathbf{A}(\mathbf{r}, t) = \sum_{\mathbf{k}, \lambda} \mathcal{A}_k \boldsymbol{\varepsilon}_{\mathbf{k}, \lambda} \left[a_{\mathbf{k}, \lambda} e^{-i\omega_k t + i\mathbf{k} \cdot \mathbf{r}} + a_{\mathbf{k}, \lambda}^* e^{i\omega_k t - i\mathbf{k} \cdot \mathbf{r}} \right], \quad (\text{II.92})$$

⁶The Helmholtz' theorem states that any vector field can be represented as superposition of a divergence-free and a curl-free field component [Loudon, 2000].

with the wave vector $\mathbf{k} = (k_x, k_y, k_z)$, with $k_i = 2\pi n_i/L$ ($n_i \in \mathbb{Z} \setminus \{0\}$), and the polarization vector $\boldsymbol{\varepsilon}_\lambda(\mathbf{k})$, of the corresponding plane waves, which satisfy the conditions

$$\boldsymbol{\varepsilon}_{\mathbf{k},\lambda} \cdot \mathbf{k} = 0, \quad (\text{II.93})$$

$$\boldsymbol{\varepsilon}_{\mathbf{k},\lambda} \cdot \boldsymbol{\varepsilon}_{\mathbf{k},\lambda'} = \delta_{\lambda,\lambda'}. \quad (\text{II.94})$$

The quantities $a_{\mathbf{k},\lambda}$ and $a_{\mathbf{k},\lambda}^*$ in Eq. (II.92) represent the Fourier coefficients determining the particular shape of the solution (II.92), and \mathcal{A}_k is a constant. Substituting (II.92) into Eq. (II.86) and (II.87), one straightforwardly obtains the expressions for the classical magnetic and electric fields in free space with the energy

$$H_{em} = \frac{1}{2} \int_V dV [\varepsilon_0 \mathbf{E}^2(\mathbf{r}, t) + \mu_0^{-1} \mathbf{B}^2(\mathbf{r}, t)] = 2\varepsilon_0 V \sum_{\mathbf{k},\lambda} \mathcal{A}_k \omega_k^2 |a_{\mathbf{k},\lambda}|^2. \quad (\text{II.95})$$

To obtain a quantum mechanical description of the above equations, we have to incorporate the quantized nature of the electromagnetic field by a procedure referred to as canonical quantization [Loudon, 2000; Mandel and Wolf, 1995]. To do so, we express the coefficients $a_{\mathbf{k},\lambda}$ and $a_{\mathbf{k},\lambda}^*$ in terms of pairs of canonically conjugate observables, $X_{\mathbf{k},\lambda}$ and $P_{\mathbf{k},\lambda}$, as

$$a_{\mathbf{k},\lambda} = \frac{1}{\sqrt{2}} (X_{\mathbf{k},\lambda} + iP_{\mathbf{k},\lambda}) \quad X_{\mathbf{k},\lambda} = \frac{1}{\sqrt{2}} (a_{\mathbf{k},\lambda} + a_{\mathbf{k},\lambda}^*), \quad (\text{II.96})$$

$$a_{\mathbf{k},\lambda}^* = \frac{1}{\sqrt{2}} (X_{\mathbf{k},\lambda} - iP_{\mathbf{k},\lambda}) \quad P_{\mathbf{k},\lambda} = -\frac{i}{\sqrt{2}} (a_{\mathbf{k},\lambda} - a_{\mathbf{k},\lambda}^*), \quad (\text{II.97})$$

and quantize each in association to a quantum mechanical harmonic oscillator with the commutation relations (see Sec. II.1.3):

$$[\hat{X}_{\mathbf{k},\lambda}, \hat{X}_{\mathbf{k}',\lambda'}] = [\hat{P}_{\mathbf{k},\lambda}, \hat{P}_{\mathbf{k}',\lambda'}] = 0, \quad (\text{II.98})$$

$$[\hat{X}_{\mathbf{k},\lambda}, \hat{P}_{\mathbf{k}',\lambda'}] = i\hbar \delta_{\mathbf{k},\mathbf{k}'} \delta_{\lambda,\lambda'}. \quad (\text{II.99})$$

In this description the Fourier coefficients $a_{\mathbf{k},\lambda}$ and $a_{\mathbf{k},\lambda}^*$ (see (II.92)) become operators as well, $\hat{a}_{\mathbf{k},\lambda}$ and $\hat{a}_{\mathbf{k},\lambda}^\dagger$, which fulfil the bosonic commutation relations:

$$[\hat{a}_{\mathbf{k},\lambda}, \hat{a}_{\mathbf{k}',\lambda'}] = [\hat{a}_{\mathbf{k},\lambda}^\dagger, \hat{a}_{\mathbf{k}',\lambda'}^\dagger] = 0, \quad (\text{II.100})$$

$$[\hat{a}_{\mathbf{k},\lambda}, \hat{a}_{\mathbf{k}',\lambda'}^\dagger] = \delta_{\mathbf{k},\mathbf{k}'} \delta_{\lambda,\lambda'}. \quad (\text{II.101})$$

Note, that Eqs. (II.96) and (II.97) hold equivalently for the corresponding operators if one replaces the complex conjugation with the adjoint operations. In this case we find that the electromagnetic energy (II.95) is equal to the Hamilton operator of a infinite sum of independent harmonic oscillators:

$$\hat{H}_{em} = \frac{1}{2} \sum_{\mathbf{k},\lambda} \left(\hat{X}_{\mathbf{k},\lambda}^2 + \hat{P}_{\mathbf{k},\lambda}^2 \right) = \sum_{\mathbf{k},\lambda} \hbar \omega_k \left(\hat{a}_{\mathbf{k},\lambda} \hat{a}_{\mathbf{k},\lambda}^\dagger + \frac{1}{2} \right). \quad (\text{II.102})$$

where we chose $\mathcal{A}_k = \sqrt{\hbar/(\varepsilon_0 V 2\omega_k)}$.⁷ Let us remark that the ground state energy in (II.102) is an infinite sum of positive values, and is therefore divergent. However, the ground state energy does not influence the dynamics of the observables, and can be set to zero:

$$\hat{H}_{em} = \sum_{\mathbf{k}, \lambda} \hbar\omega_k \hat{a}_{\mathbf{k}, \lambda}^\dagger \hat{a}_{\mathbf{k}, \lambda}. \quad (\text{II.103})$$

The operators $\hat{a}_{\mathbf{k}, \lambda}$ ($\hat{a}_{\mathbf{k}, \lambda}^\dagger$) are to be interpreted as lowering (raising) operators, which annihilate (create) a photon in the mode $(\mathbf{k}, \varepsilon_\lambda(\mathbf{k}))$ of the field:

$$\hat{a}_{\mathbf{k}, \lambda} |\dots, n_{\mathbf{k}, \lambda}, \dots\rangle = \sqrt{n} |\dots, n_{\mathbf{k}, \lambda} - 1, \dots\rangle \quad (\text{II.104})$$

$$\hat{a}_{\mathbf{k}, \lambda}^\dagger |\dots, n_{\mathbf{k}, \lambda}, \dots\rangle = \sqrt{n+1} |\dots, n_{\mathbf{k}, \lambda} + 1, \dots\rangle. \quad (\text{II.105})$$

The eigenstates are called *Fock states* and the corresponding Hilbert space *Fock space*. The *Fock space* is spanned by the set of all Fock states, which are also eigenstates of the number operators $\hat{n}_{\mathbf{k}, \lambda} = \hat{a}_{\mathbf{k}, \lambda}^\dagger \hat{a}_{\mathbf{k}, \lambda}$, whose eigenvalues give the number of photons in each mode of the field, and thus of the Hamilton operator (II.103). After this quantization procedure, the vector potential and, hence, the electromagnetic field become operator valued functions

$$\hat{\mathbf{A}}(\mathbf{r}, t) = \sum_{\mathbf{k}, \lambda} \sqrt{\frac{\hbar}{\varepsilon_0 V 2\omega_k}} \varepsilon_{\mathbf{k}, \lambda} \left[\hat{a}_{\mathbf{k}, \lambda} e^{-i\omega_k t + i\mathbf{k} \cdot \mathbf{r}} + \hat{a}_{\mathbf{k}, \lambda}^\dagger e^{i\omega_k t - i\mathbf{k} \cdot \mathbf{r}} \right], \quad (\text{II.106})$$

$$\hat{\mathbf{E}}(\mathbf{r}, t) = i \sum_{\mathbf{k}, \lambda} \sqrt{\frac{\hbar\omega_k}{2\varepsilon_0 V}} \varepsilon_{\mathbf{k}, \lambda} \left[\hat{a}_{\mathbf{k}, \lambda} e^{-i\omega_k t + i\mathbf{k} \cdot \mathbf{r}} - \hat{a}_{\mathbf{k}, \lambda}^\dagger e^{i\omega_k t - i\mathbf{k} \cdot \mathbf{r}} \right], \quad (\text{II.107})$$

$$\hat{\mathbf{B}}(\mathbf{r}, t) = i \sum_{\mathbf{k}, \lambda} \sqrt{\frac{\hbar}{2\varepsilon_0 V \omega_k}} \mathbf{k} \times \varepsilon_{\mathbf{k}, \lambda} \left[\hat{a}_{\mathbf{k}, \lambda} e^{-i\omega_k t + i\mathbf{k} \cdot \mathbf{r}} - \hat{a}_{\mathbf{k}, \lambda}^\dagger e^{i\omega_k t - i\mathbf{k} \cdot \mathbf{r}} \right]. \quad (\text{II.108})$$

The choice of the annihilation and creation operators, $\hat{a}_{\mathbf{k}, \lambda}$ and $\hat{a}_{\mathbf{k}, \lambda}^\dagger$, in Eq. (II.92), and thus of the quadrature operators $\hat{X}_{\mathbf{k}, \lambda}$ and $\hat{P}_{\mathbf{k}, \lambda}$, is rather arbitrary. We can also define a rotated set of quadrature operators:

$$\begin{pmatrix} \hat{X}_{\mathbf{k}, \lambda}^{(\theta)} \\ \hat{P}_{\mathbf{k}, \lambda}^{(\theta)} \end{pmatrix} = \begin{pmatrix} \cos \theta & \sin \theta \\ -\sin \theta & \cos \theta \end{pmatrix} \begin{pmatrix} \hat{X}_{\mathbf{k}, \lambda} \\ \hat{P}_{\mathbf{k}, \lambda} \end{pmatrix} \quad (\text{II.109})$$

leading to

$$\hat{X}_{\mathbf{k}, \lambda}^{(\theta)} = \frac{1}{2} (\hat{a}_{\mathbf{k}, \lambda} e^{-i\theta} + \hat{a}_{\mathbf{k}, \lambda}^\dagger e^{i\theta}), \quad (\text{II.110})$$

$$\hat{P}_{\mathbf{k}, \lambda}^{(\theta)} = -\frac{i}{2} (\hat{a}_{\mathbf{k}, \lambda} e^{-i\theta} - \hat{a}_{\mathbf{k}, \lambda}^\dagger e^{i\theta}), \quad (\text{II.111})$$

⁷This convention allows us to deal with dimensionless quadrature operators, defined in Eqs. (II.96) and (II.96), which are related to the ordinary position and momentum operator through $\hat{X}_{\mathbf{k}, \lambda} = \sqrt{\frac{\omega_k}{\hbar}} \hat{x}_{\mathbf{k}, \lambda}$ and $\hat{P}_{\mathbf{k}, \lambda} = \sqrt{\frac{\hbar}{\omega_k}} \hat{p}_{\mathbf{k}, \lambda}$.

which fulfil also the commutation relations (II.98)-(II.101). The eigenstates of (II.110) and (II.111) form, as the position and momentum eigenstates discussed in Sec. II.1.3, two complete and conjugate bases, $|X_{\mathbf{k},\lambda}\rangle_\theta$ and $|P_{\mathbf{k},\lambda}\rangle_\theta$, which that obey the completeness relation:

$$\int_{-\infty}^{\infty} dX_{\mathbf{k},\lambda} |X_{\mathbf{k},\lambda}\rangle_\theta \langle X_{\mathbf{k},\lambda}|_\theta = \int_{-\infty}^{\infty} dP_{\mathbf{k},\lambda} |P_{\mathbf{k},\lambda}\rangle_\theta \langle P_{\mathbf{k},\lambda}|_\theta = \mathbb{1}. \quad (\text{II.112})$$

Using this quadrature basis we can represent quantum states of light in a phase space representation using the Wigner function, defined in Sec. II.1.6.

II.2.2 Mode representations

In Eq. (II.92) we expanded a general solution of the Maxwell equations in terms of transversal plane waves $\boldsymbol{\varepsilon}_{\mathbf{k},\lambda} e^{i\omega_{\mathbf{k}}t + i\mathbf{r}\cdot\mathbf{k}}$, with polarization λ , leading to the electromagnetic field vectors by virtue of Eqs. (II.86) and (II.87). This is by no means a unique strategy. Moreover, plane waves might not be considered as the physically most adapted choice. We can expand the solution (II.92) also in terms of another set of orthonormal functions $\boldsymbol{\varepsilon}_{\mathbf{k},\lambda} u_{\mathbf{k}}(\mathbf{r}, t)$, usually referred to as mode functions, corresponding to some degree of freedom of the electromagnetic field, such as the polarization, frequency, intensity or phase.

The generalized quantized version of the solution of Eq. (II.90) then reads:

$$\hat{\mathbf{A}}(\mathbf{r}, t) = \sum_{\mathbf{k},\lambda} \mathcal{A}_0 \boldsymbol{\varepsilon}_{\mathbf{k},\lambda} \left[\hat{a}_{\mathbf{k},\lambda} u_{\mathbf{k}}(\mathbf{r}, t) + \hat{a}_{\mathbf{k},\lambda}^\dagger u_{\mathbf{k}}^*(\mathbf{r}, t) \right], \quad (\text{II.113})$$

with the lowering and raising operators, $\hat{a}_{\mathbf{k},\lambda}$ and $\hat{a}_{\mathbf{k},\lambda}^\dagger$, that annihilate or create photons in modes (\mathbf{k}, λ) , each associated with one of the mode functions $\boldsymbol{\varepsilon}_{\mathbf{k},\lambda} u_{\mathbf{k}}(\mathbf{r}, t)$ which evolve according to the wave equation (II.90). Hence, each solution $\boldsymbol{\varepsilon}_{\mathbf{k},\lambda} u_{\mathbf{k}}(\mathbf{r}, t)$ corresponds to a Hilbert space $\mathcal{H}_{\mathbf{k},\lambda}$ spanned by the Fock basis $\{|n\rangle_{\mathbf{k},\lambda} | n = 1, 2, \dots\}$. The total Hilbert space of the quantum state of the light field is then given by a tensor product of the corresponding mode subspaces $\mathcal{H}_{\mathbf{k},\lambda}$, leading to:

$$\mathcal{H} = \bigotimes_{\mathbf{k},\lambda} \mathcal{H}_{\mathbf{k},\lambda}. \quad (\text{II.114})$$

When describing the light field one often focuses on a particular mode expansion given by the set of operators $\{\hat{a}_{\mathbf{k},\lambda}\}$. But this is not unique. We can create a new mode expansion $\{\hat{b}_{\mathbf{k},\lambda}\}$ by superposing other mode operators:

$$\hat{b}_{\mathbf{k},\lambda} = \sum_{\mathbf{k}',\lambda'} U_{\mathbf{k},\lambda;\mathbf{k}',\lambda'} \hat{a}_{\mathbf{k}',\lambda'} \quad (\text{II.115})$$

where $U_{\mathbf{k},\lambda;\mathbf{k}',\lambda'}$ must be such that the commutation relations (II.100) and (II.101) are preserved, meaning unitary:

$$\sum_{\mathbf{k}'',\lambda''} U_{\mathbf{k},\lambda;\mathbf{k}'',\lambda''}^\dagger U_{\mathbf{k}'',\lambda'';\mathbf{k}',\lambda'} = \delta_{\mathbf{k},\mathbf{k}'} \delta_{\lambda,\lambda'}. \quad (\text{II.116})$$

Note also that the index \mathbf{k} can in general refer to continuous variables, such as the frequency or spatial position variables. For instance, we can have an operator $\hat{a}_{\mathbf{r}}^\dagger$ creating a photon at position \mathbf{r} , or an operators $\hat{a}_{\mathbf{p}}^\dagger$ creating a photon with momentum \mathbf{p} , which are related by a Fourier transform:

$$\hat{a}_{\mathbf{r}} = \frac{1}{(2\pi)^{\frac{3}{2}}} \int d\mathbf{r}' e^{i\mathbf{r}\cdot\mathbf{p}} \hat{a}_{\mathbf{p}}. \quad (\text{II.117})$$

In practise, to keep things simple, we will often restrict ourselves to only one degree of freedom, thus a particular set of functions $\boldsymbol{\epsilon}_{\mathbf{k},\lambda} u_{\mathbf{k}}(\mathbf{r}, t)$, while keeping all other degrees of freedom unchanged. For instance, in Sec. II.2.3 we discuss the case where we keep temporal (frequency) modes fixed and focus only on spatial modes of the light field. Another example is the polarization degree of freedom of the electromagnetic field which, while keeping spatial and temporal/frequency modes fixed, leads to a decomposition of the Fock space into two parts $\mathcal{H}_H \otimes \mathcal{H}_V$, corresponding to the horizontal (H) and vertical (V) polarizations, respectively.

II.2.3 Transverse spatial modes

Now, we will consider the particular case of scalar monochromatic waves with harmonic time dependence $u_{\mathbf{k}}(\mathbf{r}, t) = u_{\mathbf{k}}(\mathbf{r}) e^{i\omega_{\mathbf{k}} t}$, thus focusing on the set of complex functions $\{u_{\mathbf{k}}(\mathbf{r})\}$ while keeping the polarization and temporal modes fixed. According to the above introduced quantum theory of light, the mode functions $u_{\mathbf{k}}(\mathbf{r}, t)$ have to fulfill Eq. (II.90) which in this case reduces to the Helmholtz equation:

$$(\nabla^2 + k^2) u_{\mathbf{k}}(\mathbf{r}) = 0, \quad (\text{II.118})$$

where $k = |\mathbf{k}|$. Further on, we want to consider paraxial light beams that propagate mainly in the z direction with transverse wave vector components $\mathbf{q} = (k_x, k_y)^\top$. The z -component of the total wave vector \mathbf{k} can then be written in the *Fresnel* or *paraxial approximation*:

$$k_z = \sqrt{k^2 - q^2} \approx k \left(1 - \frac{q^2}{2k^2} \right), \quad (\text{II.119})$$

if $q^2 \ll k^2$, where $q = |\mathbf{q}|$. The Fresnel or paraxial approximation is also known as small angle approximation because, in geometric optics where light is represented by rays, paraxial rays are those rays which lie at small angles to the propagation axis of the considered optical system. In this approximation we can write $u_{\mathbf{k}}(\mathbf{r}) = \mathcal{U}_{\mathbf{k}}(\mathbf{r}) e^{ikz}$, with a slowly varying function $\mathcal{U}_{\mathbf{k}}(\mathbf{r})$, such that $u(\mathbf{r})$ keeps a plane wave structure for small propagation distances. Then, Eq. (II.118) becomes

$$\left(\frac{\partial^2}{\partial x^2} + \frac{\partial^2}{\partial y^2} + 2ik \frac{\partial}{\partial z} \right) \mathcal{U}_{\mathbf{k}}(\mathbf{r}) = 0. \quad (\text{II.120})$$

where we have also used that $\partial^2 \mathcal{U}_{\mathbf{k}}(\mathbf{r}) / \partial z^2 \ll k \partial \mathcal{U}_{\mathbf{k}}(\mathbf{r}) / \partial z$ [Walborn et al., 2010]. Equation (II.120) is called *paraxial Helmholtz equation* and has the well-known *Laguerre*- and *Hermite-Gaussian* modes as solutions. The Laguerre-Gaussian modes, expressed

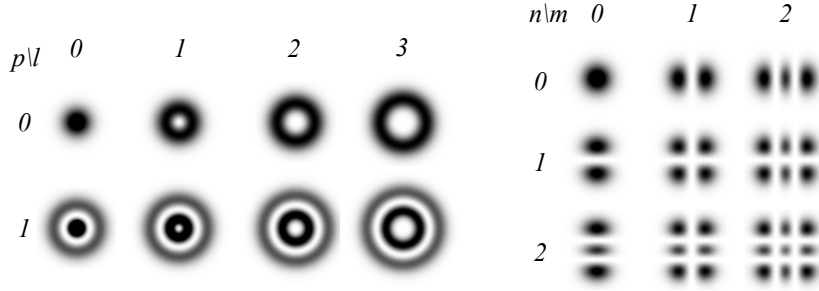


Figure II.4: Plots of the Laguerre- (left) and Hermite-Gaussian (right) modes for various values of their indices (ℓ, p) and (n, m) , respectively. Figure taken from [Walborn et al., 2010].

in cylindrical coordinates (ρ, ϕ, z) , are given by

$$\mathcal{U}_p^\ell(\rho, \phi, z) = D_p^\ell \frac{1}{w(z)} \left(\frac{\sqrt{2}\rho}{w(z)} \right)^\ell L_p^\ell \left(\frac{2\rho^2}{w(z)^2} \right) \exp \left(-\frac{\rho^2}{w(z)^2} \right) \exp \left\{ -i \left[\frac{k\rho^2}{2R} - (n+m+1)\gamma(z) \right] - (p-\ell)\phi \right\}, \quad (\text{II.121})$$

where ℓ and p denote the azimuthal and radial indices, respectively, D_p^ℓ is a constant, L_p^ℓ denote the associated Laguerre polynomials (see Appendix A for a definition of $L_p^\ell(x)$), z is the longitudinal propagation direction, $R(z)$ is the radius of curvature, $w(z)$ is the beam waist, $\gamma(z)$ is the phase retardation or *Gouy phase*, and the parameter z_R is the *Rayleigh range*. The order of the *LG* beam is defined as $\mathcal{N} = |\ell| + 2p$. In Fig. II.4 we present examples of Eq. (II.121) for the values $p = 0, 1$ and $\ell = 0, 1, 2, 3$. Other solutions of Eq. (II.120) are the so-called Hermite-Gaussian modes which, expressed in euclidian coordinates, read:

$$\mathcal{U}_{nm}^{HG}(x, y, z) = C_{nm} \frac{1}{w(z)} H_n \left(\frac{\sqrt{2}x}{w(z)} \right) H_m \left(\frac{\sqrt{2}y}{w(z)} \right) \exp \left(-\frac{x^2 + y^2}{w(z)^2} \right) \exp \left\{ -i \left[\frac{k(x^2 + y^2)}{2R(z)} - (n+m+1)\gamma(z) \right] \right\}. \quad (\text{II.122})$$

where C_{nm} are constants, $H_n(x)$ denotes the n^{th} -order Hermite polynomial (see Appendix A for a definition of $H_n(x)$). The Hermite polynomials $H_n(x)$ are even or odd functions of x depending if n is even or odd, respectively. The *order* of the beam is given by $\mathcal{N} = m + n$. Examples of Eq. (II.122) are presented in Fig. II.4. Both, the Laguerre- and Hermit-Gaussian modes, reduce in zeroth-order (\mathcal{U}_0^0 and \mathcal{U}_{00}^{HG}) to a simple Gaussian beam profile.

In Sec. II.3.1, we will be concerned with a special case of such spatial optical modes, namely those containing solely single photons. As we will see, in this case, we can consider the transverse field distribution of the single photon as a wave function of a

single particle in first quantization formalism.

II.2.4 Relevant quantum states of light

In this Section we discuss some important quantum states of light that will be relevant for the further reading of this manuscript. At the same time, we take this opportunity to show further examples of the Wigner function phase space representation introduced in Sec. II.1.6. In the following, we will restrict ourselves to a single mode of the electromagnetic field spanned by the set of Fock states $\{|n\rangle|n = 1, 2, \dots\}$.

II.2.4.1 Fock states

Before turning to more particular states let us discuss some properties of the Fock basis itself. We start with the vacuum state $|vac\rangle = |0\rangle$, which is defined by the fact that it vanishes after an application of the annihilation operator \hat{a} , *i.e.* $\hat{a}|0\rangle = 0$. Higher order Fock states $|n\rangle$, with $n > 0$, can then be formed by repeated application of the creation operator \hat{a}^\dagger on the vacuum state $|0\rangle$, leading to

$$|n\rangle = \frac{(\hat{a}^\dagger)^n}{\sqrt{n!}}|0\rangle, \quad (\text{II.123})$$

where the factor $1/\sqrt{n!}$ follows from the definition of \hat{a}^\dagger in Eq. (II.105). As mentioned in the previous Section the Fock states form a complete and orthonormal basis fulfilling $\sum_n |n\rangle\langle n| = \mathbb{1}$ and $\langle n|m\rangle = \delta_{n,m}$, respectively, and thus allow to express every quantum states of a single mode as:

$$|\Psi\rangle = \sum_{n=0}^{\infty} c_n |n\rangle, \quad (\text{II.124})$$

with $c_n = \langle n|\Psi\rangle$. The wave function of a Fock state $|n\rangle$ is exactly the n th order Harmonic oscillator eigenfunction[Mandel and Wolf, 1995]:

$$\langle x|n\rangle = \frac{1}{\sqrt{\sqrt{\pi}2^n n!}} H_n(x) e^{-x^2/2}, \quad (\text{II.125})$$

where $H_n(x)$ are the Hermite polynomials (see Appendix A), leading to the corresponding Wigner function (II.71):

$$W_{|n\rangle\langle n|}(x, p) = \frac{(-1)^n}{\pi} e^{-(x^2+p^2)} L_n(2(x^2 + p^2)), \quad (\text{II.126})$$

where L_n denote the n th order Laguerre polynomials (see Appendix A). In Fig. II.5 we present plots of the Wigner function of the four lowest order Fock states with $n = 0, 1, 2, 3$. We can even calculate the Wigner function of an arbitrary Fock state projector $|n\rangle\langle m|$:

$$W_{|n\rangle\langle m|}(x, p) = \frac{(-1)^n}{\pi} \sqrt{\frac{m!}{n!}} \left(\sqrt{2}(x - ip)\right)^{n-m} e^{-(x^2+p^2)} L_m^{n-m}(2(x^2 + p^2)), \quad (\text{II.127})$$

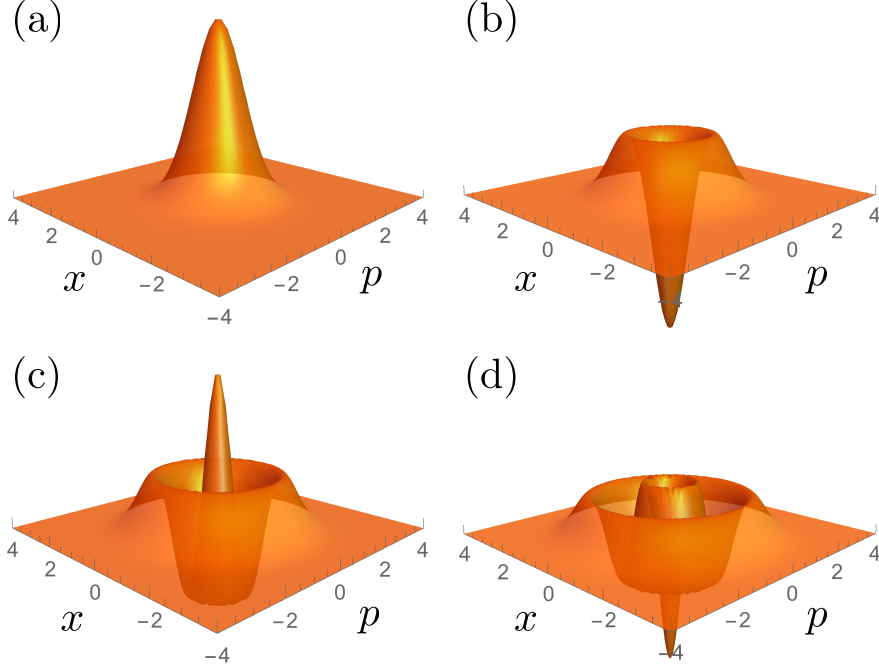


Figure II.5: Plots of the Wigner function (II.126) of the four Fock states $|0\rangle$ (a), $|1\rangle$ (b), $|2\rangle$ (c) and $|3\rangle$ (d).

which leads to a convenient way to express the Wigner function of an arbitrary density matrix $\hat{\rho}$ in terms of its matrix elements $\rho_{n,m} = \langle n|\hat{\rho}|m\rangle$:

$$W_{\hat{\rho}}(x, p) = \sum_{n,m} \hat{\rho}_{n,m} W_{|n\rangle\langle m|}(x, p). \quad (\text{II.128})$$

II.2.4.2 Coherent states

Coherent states $|\alpha\rangle$ are introduced as eigenstates of the photon annihilation operator \hat{a} with complex eigenvalues α , fulfilling the eigenvalue relation [Mandel and Wolf, 1995]:

$$\hat{a}|\alpha\rangle = \alpha|\alpha\rangle, \quad (\text{II.129})$$

or equivalently the conjugate relation

$$\langle\alpha|\hat{a}^\dagger = \alpha^*\langle\alpha|, \quad (\text{II.130})$$

The expression of the coherent state $|\alpha\rangle$ in terms of Fock states can be determined by inserting a general expansion (II.124) with $|\Psi\rangle = |\alpha\rangle$ into Eq. (II.129) which leads to a recursion formula for the coefficients c_n . Solving the latter with the additional

normalization condition $\langle \alpha | \alpha \rangle = 1$ yields:

$$|\alpha\rangle = e^{-\frac{|\alpha|^2}{2}} \sum_{n=0}^{\infty} \frac{\alpha^n}{\sqrt{n!}} |n\rangle, \quad (\text{II.131})$$

which reduces to the vacuum state if $\alpha = 0$. When measuring a coherent state (II.131) in the Fock basis $|n\rangle$, we see that the probability that n photons will be found is given by a Poisson distribution:

$$p(n) = |\langle n | \alpha \rangle|^2 = \frac{|\alpha|^{2n}}{n!} e^{-|\alpha|^2}. \quad (\text{II.132})$$

where $|\alpha|^2$ is a variable parameter. The mean number of photons present in a coherent state is thus given by $\langle \hat{n} \rangle_{|\alpha\rangle} = |\alpha|^2$. The scalar product of two coherent states is given by

$$\langle \alpha | \beta \rangle = e^{-|\alpha-\beta|^2/2} e^{(\alpha^*\beta - \alpha\beta^*)/2}, \quad (\text{II.133})$$

which shows that coherent states are never orthogonal, but they fulfill the over-completeness relation [Mandel and Wolf, 1995]

$$\frac{1}{\pi} \int d\alpha |\alpha\rangle \langle \alpha| = \mathbb{1}, \quad (\text{II.134})$$

thus allowing us to express every state in terms of an integral over the complex plane as

$$|\Psi\rangle = \frac{1}{\pi} \int d\alpha \langle \alpha | \Psi \rangle |\alpha\rangle. \quad (\text{II.135})$$

We can define the coherent state $|\alpha\rangle$ also through a displacement of the vacuum state $|0\rangle$, as:

$$|\alpha\rangle = \hat{D}(\alpha)|0\rangle = e^{\alpha\hat{a}^\dagger - \alpha^*\hat{a}}|0\rangle = e^{-|\alpha|^2/2} e^{\alpha\hat{a}^\dagger} e^{-\alpha^*\hat{a}}|0\rangle = e^{-|\alpha|^2/2} e^{\alpha\hat{a}^\dagger}|0\rangle \quad (\text{II.136})$$

where we used Eqs. (II.96) and (II.97) to express the displacement operator (II.63) in terms of the annihilation and creation operators, \hat{a} and \hat{a}^\dagger , with $\alpha = (\nu + i\mu)/\sqrt{2}$. The Wigner function of a coherent state is the same as of the vacuum state (see Fig. II.5 (a)) displaced to the position (ν, μ) in phase space:

$$W_{|\alpha\rangle\langle\alpha|}(x, p) = \frac{1}{\pi} e^{-(x-\nu)^2 - (p-\mu)^2}. \quad (\text{II.137})$$

II.2.4.3 Squeezed states

The coherent states $|\alpha\rangle$ have a Gaussian Wigner function (II.137) that is symmetric in x and p , leading to the minimal position and momentum uncertainty $\Delta x \Delta p = 1/2$. As already mentioned in Sec. II.1.3, we can reduce the uncertainty in the position or momentum variables with the cost of increasing the other one, respectively, but still fulfilling the relation $\Delta x \Delta p = 1/2$. Such states are called squeezed states (see Fig. II.1

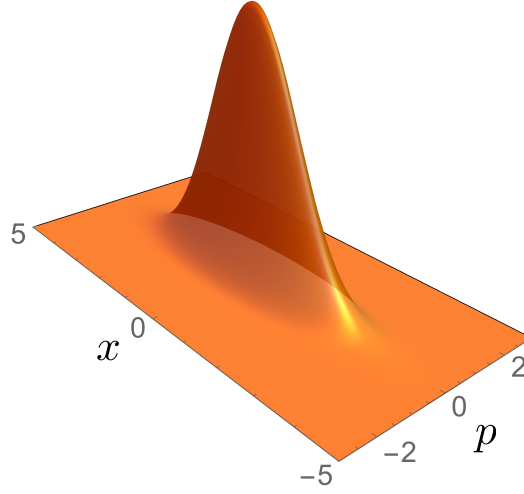


Figure II.6: Plot of the Wigner function (II.126) of a squeezed vacuum states $|0, r\rangle$ with 5dD of squeezing ($r \approx 0.57$).

for the plot of a squeezed wave function) and can be generated through the application of the squeezing operator $\hat{S}(r)$ (see Sec. II.1.3). For instance, for the squeezed vacuum we obtain:

$$|0, r\rangle = \hat{S}(r)|0\rangle = e^{\frac{r}{2}(\hat{a}^2 - \hat{a}^{\dagger 2})}|0\rangle = \frac{1}{\cosh r} \sum_{n=0}^{\infty} \frac{\sqrt{(2n)!}}{2^n n!} \tanh r^n |2n\rangle, \quad (\text{II.138})$$

and all other minimal uncertainty states can be reached by displacing the squeezed vacuum:

$$|\alpha, r\rangle = \hat{D}(\alpha)|0, r\rangle = \hat{D}(\alpha)\hat{S}(r)|0\rangle, \quad (\text{II.139})$$

with mean photon number $\langle \hat{n} \rangle_{|\alpha, r\rangle} = |\alpha|^2 + \sinh^2 r$. The wave function of the displaced squeezed vacuum state then reads:

$$\langle x|\alpha, r\rangle = \frac{1}{\pi^{1/4} e^{-r/2}} e^{-(x-\nu)^2/(2e^{2r}) - i\mu x + i\mu\nu}, \quad (\text{II.140})$$

and the corresponding Wigner function

$$W_{|\alpha, r\rangle\langle\alpha, r|}(x, p) = \frac{1}{\pi} e^{-(x-\nu)^2/e^{-2r} - (p-\mu)^2/e^{2r}}. \quad (\text{II.141})$$

The amount of squeezing can also be quantified in terms of the squeezing factor s which is defined as the variance of the squeezed state Δx^2 normalized to the shot noise limit given by the variance of the vacuum state Δx_0^2 , yielding $s = \Delta x^2/\Delta x_0^2 = e^{-2r}$. In experiments the squeezing factor is often given dB scale:

$$s_{\text{dB}} = 10 \log_{10} s. \quad (\text{II.142})$$

One can also generate two-mode squeezed states through application of the two-mode squeezing operator $\hat{S}_2(r)$ (see Sec. II.1.3) on a bipartite system. In analogy to Eq. (II.138), we define the two-mode squeezed vacuum (TMSV) state as:

$$\begin{aligned} |r\rangle_{\text{TMSV}} &= \hat{S}_2(r)|0\rangle_a|0\rangle_b = e^{\frac{r}{2}(\hat{a}\otimes\hat{a}-\hat{a}^\dagger\otimes\hat{a}^\dagger)}|0\rangle_a|0\rangle_b \\ &= \sqrt{1-\lambda^2} \sum_{n=0}^{\infty} (-\lambda)^n |n\rangle_a |n\rangle_b, \end{aligned} \quad (\text{II.143})$$

where a and b refer to the two modes of the bipartite system and $\lambda = \tanh r \in [0, 1]$. The Wigner function of the TMSV state reads:

$$W_{\text{TMSV}}(x_a, p_a; x_b, p_b) = \frac{1}{\pi^2} e^{-\frac{(x_a-x_b)^2}{2e^{-2r}} - \frac{(x_a+x_b)^2}{2e^{2r}} - \frac{(p_a-p_b)^2}{2e^{2r}} - \frac{(p_a+p_b)^2}{2e^{-2r}}}. \quad (\text{II.144})$$

The TMSV state (II.143) is also known as Einstein-Podolski-Rosen (EPR) state because, in the limit $r \rightarrow \infty$, Eq. (II.144) becomes

$$W_{\text{TMSV}}(x_a, p_a; x_b, p_b) = \frac{1}{\pi^2} \delta(x_a - x_b) \delta(p_a + p_b), \quad (\text{II.145})$$

which is the Wigner function of the famous EPR state:

$$|\text{EPR}\rangle = \int_{-\infty}^{\infty} dx |x\rangle_a |x\rangle_b = \int_{-\infty}^{\infty} dp |p\rangle_p | -p\rangle_b \quad (\text{II.146})$$

II.2.4.4 Thermal states

Instead of coherent superpositions of Fock states we can also consider incoherent mixtures with a fixed average photon number \bar{n} , so-called thermal states:

$$\hat{\rho}_{\text{th}} = \sum_{n=0}^{\infty} \frac{\bar{n}^n}{(\bar{n}+1)^{n+1}} |n\rangle\langle n|, \quad (\text{II.147})$$

with the Wigner function:

$$W_{\text{th}}(x, p) = \frac{1}{\pi(2\bar{n}+1)} e^{-(x^2+p^2)/(2\bar{n}+1)}. \quad (\text{II.148})$$

At this point we note that any single-mode Gaussian state can be generated by the application of a single-mode Gaussian unitary \hat{U}_G on a thermal state (II.147). Furthermore, as we learned in Sec. II.1.3, any single-mode Gaussian unitary operation can be decomposed into rotations, squeezings and displacements, yielding the most general Gaussian state:

$$\hat{\rho}_{\text{Gauss}} = \hat{D}(\alpha) \hat{R}(\theta) \hat{S}(r) \hat{R}(\phi) \hat{\rho}_{\text{th}} \hat{R}(\phi)^\dagger \hat{S}(r)^\dagger \hat{R}(\theta)^\dagger \hat{D}(\alpha)^\dagger \quad (\text{II.149})$$

whose Wigner function was introduced in Eq. (II.81). And by setting the average photon number of the thermal state equal to zero we obtain the most general single-mode pure Gaussian state through $|\alpha, \theta, r\rangle = \hat{D}(\alpha) \hat{R}(\theta) \hat{S}(r) |0\rangle$.

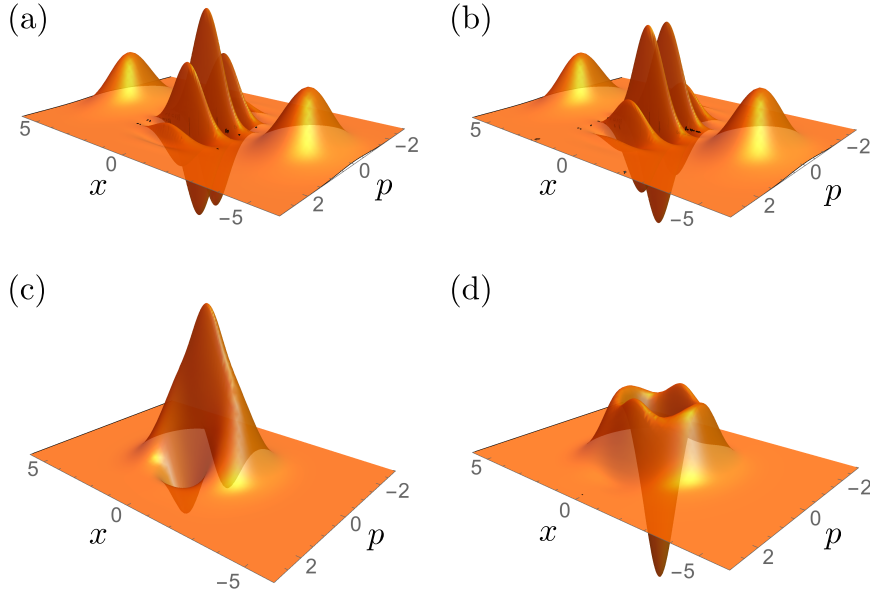


Figure II.7: Plot of the Wigner function (II.126) of the even (left) and odd (b,right) cat states $|\text{cat}^\pm\rangle$ with cat state amplitudes $\alpha = 1$ (bottom) and $\alpha = 3$ (top).

II.2.4.5 Cat states

Up to now we have, apart from the Fock basis states (see Sec. II.2.4.1), only considered Gaussian states. Now, we want to discuss an example of Non-Gaussian states that can be produced by superposing coherent states with different amplitudes, referred to as *Schrödinger-Cat states*. Even and odd Schrödinger-Cat states are defined as follows:

$$|\text{cat}^\pm\rangle = \frac{1}{\mathcal{N}_{\alpha,\pm}} (|\alpha\rangle \pm |-\alpha\rangle), \quad (\text{II.150})$$

with the normalization factor $\mathcal{N}_{\alpha,\pm} = \sqrt{2(1 \pm e^{-2|\alpha|^2})}$. In the Fock basis representation the even and odd cat states read:

$$|\text{cat}^+\rangle = \frac{2}{\mathcal{N}_{\alpha,+}} e^{-|\alpha|^2/2} \sum_{n=0}^{\infty} \frac{\alpha^{2n}}{\sqrt{(2n)!}} |2n\rangle \quad (\text{II.151})$$

and

$$|\text{cat}^-\rangle = \frac{2}{\mathcal{N}_{\alpha,-}} e^{-|\alpha|^2/2} \sum_{n=0}^{\infty} \frac{\alpha^{2n+1}}{\sqrt{(2n+1)!}} |2n+1\rangle, \quad (\text{II.152})$$

respectively. The Wigner function of $|\text{cat}^\pm\rangle$ with $\alpha = (\nu + i\mu)/\sqrt{2}$ can be expressed in terms of the Wigner function of two coherent states and the vacuum states (see

Eq. (II.137)), yielding:

$$W_{\text{cat}\pm}(x, p) = \frac{1}{\mathcal{N}_{\alpha, \pm}^2} [W_{|\alpha\rangle\langle\alpha|}(x, p) + W_{|-\alpha\rangle\langle-\alpha|}(x, p) \pm W_{|0\rangle\langle 0|}(x, p) 2 \cos(2x\mu - 2\nu y)]. \quad (\text{II.153})$$

In Fig. II.7 we present plots of the Wigner function of the even and odd cat states with different cat state amplitudes α . For a larger cat state amplitude it is apparent that the two Gaussian features in the Wigner functions are due to the first two terms in Eq. (II.153), while the interference fringes at the origin correspond to a vacuum state Wigner function modulated by a cosine. The even and odd cat state Wigner functions differ solely by the fact that the interference fringes at the origin are phase shifted by a factor of π . For smaller cat state amplitudes ($\alpha \simeq 1$) such a decomposition is not as obvious anymore. In fact, for $|\alpha| \rightarrow 0$ the even cat state becomes a vacuum state, while the Wigner function of an odd cat state tends towards that of a single photon state (compare with Fig. II.5(b)).

II.3 Experimental realizations

Since in the remainder of this thesis we will mainly be concerned with the implementation of discrete quantum information processing tasks in systems described by continuous variables, we discuss here two quantum optical systems that can be used as a platform to create and manipulate continuous-variable quantum states in a coherent fashion. Thereby, we will focus on two fundamentally different ways to process continuous-variable degrees of freedom with optical fields. On the one hand, we consider systems of single photons whose spatial distribution can be regarded as a single particle wave function that can be manipulated with linear optical elements. On the other hand, we discuss the electromagnetic field quadratures of some fixed spatial and temporal mode consisting in general of larger numbers of photons. These two approaches are fundamentally different since we deal, in the first case, with the Hilbert space of the spatial multi-mode field of a single photon, and, in the second case, with the multi-photon Fock space of a single mode of the electromagnetic field. Both approaches have advantages and disadvantages in the production of states, their manipulation and measurement, respectively, which we discuss in the following.

II.3.1 Spatial distribution of single photons

The spatial degrees of freedom of single photons can be described by the electromagnetic field composed of spatial optical modes (see also the discussion in Sec. II.2.3) in the paraxial approximation (II.119) evolving according to the paraxial Helmholtz equation (II.120). In the single photon regime this spatial multi-mode field can be regarded as a single particle wave function representing the probability amplitude for the detection of the photon in the transverse plane [Lvovsky and Raymer, 2009; Tasca et al., 2009, 2011]. The general situation is depicted in Fig. II.8. We assume that the coordinates x and p refer to the transverse position and momentum (or the wave-vector) of a single photon. These variables are related to the source (position plane) and Fourier plane

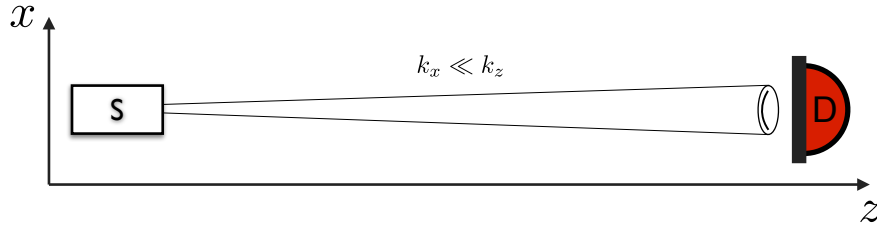


Figure II.8: Schematic representation of a single photon with spatial profile along the x -axis propagating in z -direction that has been produced in a source (S). The transverse spread of the photon is assumed to be small in the paraxial approximation ($k_x \ll k_z$). Finally, the spatial distribution of the photon is measured in using an appropriate detector (D), *e.g.* a position resolving CCD camera.

(momentum plane) of the single-photon field. Also, we restrict ourselves to the one dimensional case because the Hilbert space associated to the two-dimensional spatial photon field is a tensor product of the Hilbert spaces associated with the two orthogonal transverse directions of the photon (see Eq. (II.114)).

II.3.1.1 Manipulation of the spatial single photon field

Implementing single-mode continuous-variable gates (see Sec. II.1.3) on the transverse degrees of freedom of single photons can be achieved by using linear optical elements only. Yet, we have to account for the free evolution of the single-photon wave function $\mathcal{U}(x)$ before and after the application of such optical elements. As mentioned in Sec. II.2.3, this evolution is determined by the paraxial Helmholtz equation:

$$\left(\frac{\partial^2}{\partial x^2} + 2ik \frac{\partial}{\partial z} \right) \mathcal{U}(x, z) = 0, \quad (\text{II.154})$$

with $k = 2\pi/\lambda$, where λ is the corresponding wave length. Equation (II.154) is a Schrödinger type wave equation with fictitious time coordinate z . To see this more clearly, we rewrite (II.154) in terms of an appropriate operator formalism in which the transverse position of the photon is described by the position operator \hat{x} and the differential operator $-i\partial/\partial x$ refers to the momentum operator \hat{p} , fulfilling the usual commutation relation $[\hat{x}, \hat{p}] = i$. Now, we can express Eq. (II.154) in bracket notation with $\mathcal{U}(x, z) = \langle x | \mathcal{U}(z) \rangle$, as:

$$i \frac{\partial}{\partial z} | \mathcal{U}(z) \rangle = \frac{\hat{p}^2}{2k} | \mathcal{U}(z) \rangle, \quad (\text{II.155})$$

yielding the general solution

$$| \mathcal{U}(z) \rangle = e^{-iz\hat{p}^2/(2k)} | \mathcal{U}(0) \rangle. \quad (\text{II.156})$$

In Eq. II.155 we identify the free-space propagation operator

$$\hat{P}_z = e^{-iz\hat{p}^2/(2k)}, \quad (\text{II.157})$$

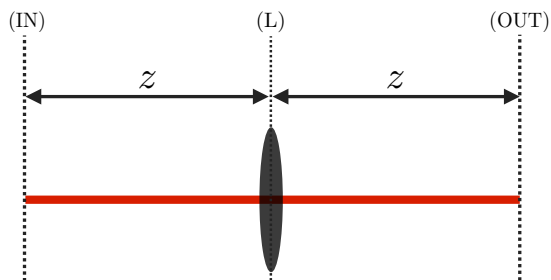


Figure II.9: Schematic representation of the optical setup of a single-lens system. The optical field (red line) is entering through the input plane (IN), propagates freely for a distance z , passes through a lens (L) with focal length f , propagates again freely for a distance z and exits the setup through the output plane (OUT).

which implements the propagation of the transverse single photon wave function $\mathcal{U}(x)$ from the origin to a distance z . Hence, by simply evolving the single photon through space we are able to implement a momentum-shear operation with variable parameter z . The latter is related to the normal shear operation by the application of the Fourier transform operator (see Sec. II.1.3).

Other continuous-variable unitary operations can be implemented by placing optical elements in the path of the freely propagating photon. For instance, an ordinary shear operation (see Eq. (II.40)) can be implemented directly using a single lens [Stoler, 1981; Tasca et al., 2011]:

$$\hat{\mathcal{L}}_f = e^{-ik\hat{x}^2/(2f)}, \quad (\text{II.158})$$

with the focal length of the lens f . We can use the operations (II.157) and (II.158) to create other continuous-variable gates by concatenation. However, note that finite size effects of the photon's transverse wave function, as appearing in every realistic experimental situation, lead to coarse grained resolution in terms of the corresponding conjugate variables. This has the consequence that only a finite amount of information can be encoded in the spatial distribution of a single photon. In what follows we will neglect such finite size effects that might also lead to diffraction effects at the edges of the implemented lenses. Furthermore, we consider only perfect lenses free of any aberration effects.

Combining the single lens operation (II.158) with the free-propagation (II.157) we can realize a single lens system, shown in Fig. II.9, that implements the operation:

$$\hat{\mathcal{U}}_{\text{SL}}(z, f) = \hat{\mathcal{P}}_z \hat{\mathcal{L}}_f \hat{\mathcal{P}}_z, \quad (\text{II.159})$$

which transforms the position and momentum operators as follows:

$$\hat{\mathcal{U}}_{\text{SL}}^\dagger(z, f) \hat{x} \hat{\mathcal{U}}_{\text{SL}}(z, f) = \left(1 - \frac{z}{f}\right) \hat{x} + \frac{z}{k} \left(2 - \frac{z}{f}\right) \hat{p}, \quad (\text{II.160})$$

$$\hat{\mathcal{U}}_{\text{SL}}^\dagger(z, f) \hat{p} \hat{\mathcal{U}}_{\text{SL}}(z, f) = \left(1 - \frac{z}{f}\right) \hat{p} + \frac{z}{f} \hat{x}. \quad (\text{II.161})$$

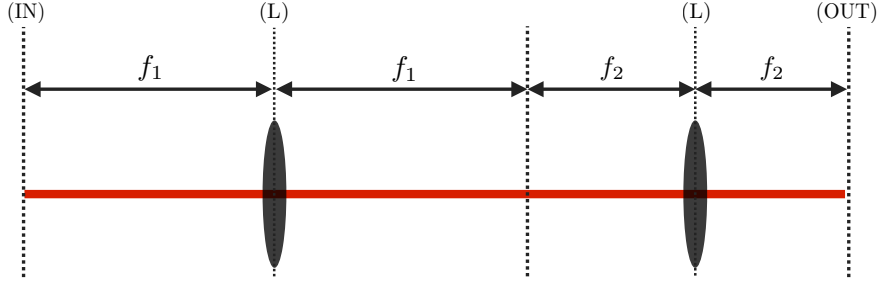


Figure II.10: Schematic representation of the optical setup of a two-lenses system implementing two consecutive Fourier transforms with different focal lengths, f_1 and f_2 .

The single lens system operation (II.159) is a Gaussian operation which acts linearly on the position and momentum operator, as discussed in Sec. II.1.3. Equations (II.160) and (II.161) seem familiar to the Gaussian quadrature rotation (II.38), and indeed for $z = 2f \sin^2 \theta/2$ and $f = f'/\sin \theta$ we get:

$$\hat{\mathcal{F}}_{d,\theta}^\dagger \hat{x} \hat{\mathcal{F}}_{d,\theta} = \cos \theta \hat{x} + \sin \theta d_\theta^2 \hat{p} \quad (\text{II.162})$$

$$\hat{\mathcal{F}}_{d,\theta}^\dagger \hat{p} \hat{\mathcal{F}}_{d,\theta} = -\frac{\sin \theta}{d_\theta^2} \hat{x} + \cos \theta \hat{p}, \quad (\text{II.163})$$

where $d_\theta = \sqrt{f' \sin \theta/k}$ and $\hat{\mathcal{F}}_{d,\theta} = e^{i\frac{\theta}{2}(\hat{x}^2/d_\theta^2 + d_\theta^2 \hat{p}^2)}$ denotes the operator of a rescaled *fractional Fourier transform*, which becomes a rescaled Fourier transform $\hat{\mathcal{F}}_d = e^{i\frac{\pi}{4}(\hat{x}^2/d^2 + d^2 \hat{p}^2)}$ for $\theta = \pi/2$:

$$\hat{\mathcal{F}}_d^\dagger \hat{x} \hat{\mathcal{F}}_d = d^2 \hat{p}, \quad (\text{II.164})$$

$$\hat{\mathcal{F}}_d^\dagger \hat{p} \hat{\mathcal{F}}_d = -\frac{1}{d^2} \hat{x}, \quad (\text{II.165})$$

with $d = d_{\pi/2} = \sqrt{f/k}$. Note, that above introduced rescaled transformation differ from the ordinary operations, introduced in Sec. II.1.3, solely by a scaling factor d_θ which can always be accounted for by defining new rescaled position and momentum variables $\hat{x}' = \hat{x}/d_\theta$ and $\hat{p}' = d_\theta \hat{p}$ [Tasca et al., 2011]. Yielding $\hat{\mathcal{F}}_\theta = e^{i\frac{\theta}{2}(\hat{x}'^2 + \hat{p}'^2)}$ with

$$\hat{\mathcal{F}}_\theta^\dagger \hat{x}' \hat{\mathcal{F}}_\theta = \cos \theta \hat{x}' + \sin \theta \hat{p}' \quad (\text{II.166})$$

$$\hat{\mathcal{F}}_\theta^\dagger \hat{p}' \hat{\mathcal{F}}_\theta = -\sin \theta \hat{x}' + \cos \theta \hat{p}', \quad (\text{II.167})$$

and $\hat{\mathcal{F}} = e^{i\frac{\pi}{4}(\hat{x}'^2 + \hat{p}'^2)}$ with

$$\hat{\mathcal{F}}^\dagger \hat{x}' \hat{\mathcal{F}} = \hat{p}' \quad (\text{II.168})$$

$$\hat{\mathcal{F}}^\dagger \hat{p}' \hat{\mathcal{F}} = -\hat{x}', \quad (\text{II.169})$$

as familiar from Sec. II.1.3.

Using a two-lens system, as depicted in Fig. II.10, we can also implement more com-

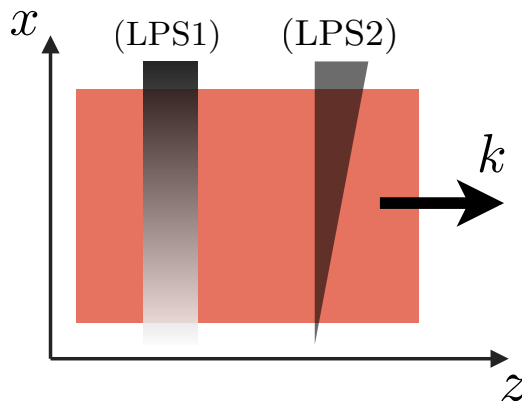


Figure II.11: Schematic representation of two possible realizations of a linear phase shifter. LPS1: Transparent plate with linearly varying refractive index $n(x) = n_0x$. LPS2: Transparent wedge shaped plate. The red area indicates the profile of the optical beam with wave vector k passing through the phase-shifters while propagating in z -direction.

plicated operations. For instance, consider a combination of two one-lens system (see Fig. II.9), each implementing a Fourier transform $\hat{\mathcal{F}}_d$, with focal lengths f and f' , respectively. Together they realize the operation:

$$\hat{\mathcal{F}}_{d_2}^\dagger \hat{\mathcal{F}}_{d_1}^\dagger \hat{x} \hat{\mathcal{F}}_{d_1} \hat{\mathcal{F}}_{d_2} = -\frac{d_1^2}{d_2^2} \hat{x} = -\frac{f_1}{f_2} \hat{x}, \quad (\text{II.170})$$

$$\hat{\mathcal{F}}_{d_2}^\dagger \hat{\mathcal{F}}_{d_1}^\dagger \hat{p} \hat{\mathcal{F}}_{d_1} \hat{\mathcal{F}}_{d_2} = -\frac{d_2^2}{d_1^2} \hat{p} = -\frac{f_2}{f_1} \hat{p}, \quad (\text{II.171})$$

which is nothing but a single-mode squeezing operation (see Eq. (II.39)) with the squeezing parameter r defined as $r = \ln(f_1/f_2)$. Hence, we can define an optical squeezing gate as $\hat{S}_r = \hat{\mathcal{F}}_{d_1} \hat{\mathcal{F}}_{d_2} = \hat{U}_{\text{SL}}(f_1, f_1) \hat{U}_{\text{SL}}(f_2, f_2)$. Note, that this transformation does not depend on the definition of the above rescaled coordinates \hat{x}' and \hat{p}' .

In order to complete the set of single-mode Gaussian operations on the transverse single photon field we have to find an optical realization of the displacement operations (II.34). To do so, we use that a displacement in the position or momentum variables corresponds to the linear phase shift in its conjugate (momentum or position) variables. In position we can implement such a phase shift using a *linear position phase-shifter*, realized, for instance, by a transparent plate of length l with a linear transverse modulation of its refractive index $n(x) = n_0x$ (see Fig. II.11(LPS1)), yielding a displacement by ln_0 in momentum space. Another way to implement such a position phase shift is by using a transparent wedge shaped plate with constant refractive index (see Fig. II.11(LPS2)). Displacements in position space can be realized with the same linear phase-shifters sandwiched between two Fourier transforms.

Finally, we introduce a very powerful optical element that allows us to implement all the so far introduced operations with a single device, a so-called spatial light modulator (SLM). A SLM works in a similar manner as an ordinary computer screen, consist-

ing of a transparent or reflective liquid crystal display divided into a certain number (depending on the resolution of the SLM) of pixels whose refractive index can be adjusted individually through the application of some voltage controlled by a computer. In general, this enables one to apply arbitrary phases and amplitude modulation to the spatial profile of an incident light beam. We will focus on the possibility to implement arbitrary phase modulations yielding the operation:

$$U_{\text{SLM}} = e^{if(\hat{x})}, \quad (\text{II.172})$$

where $f(x)$ is an arbitrary user-defined function. Similarly, one can implement phase modulations in momentum space by combining a SLM with the Fourier transform $\hat{\mathcal{F}}$.

II.3.1.2 Two-photon gates

The experimental implementation of the above introduced single-photon gates in terms of linear optical elements is relatively simple. For two-photon gates the situation changes since one needs to realize more challenging non-linear optical processes in order to generate photon-photon interactions. In [Tasca et al., 2011] a proof-of-principle was given how a non-linear 4-wave-mixing interaction can be used to entangle the spatial variables of two initially separable photons $|x_1\rangle|x_2\rangle$, yielding an EPR state:

$$|\Psi\rangle = \int dx |x_1 + x_2 - x\rangle_1 |x\rangle_2. \quad (\text{II.173})$$

The non-linearity problem occurs also in other quantum optical frameworks for quantum information processing. For instance, one needs non-linear optical elements to implement controlled logic gates on single-mode photonic qubits [Milburn, 1989]. To overcome these difficulties Knill, Laflamme and Milburn (KLM) proposed a method based on gate teleportation [Gottesman and Chuang, 1999] that allows to realize universal quantum logic gates with photonic qubits using only linear optical elements and post-selection [Knill et al., 2001]. Following the work by KLM several experimental realizations of probabilistic multi-photon logic gates have been reported [O'Brien et al., 2003; Langford et al., 2005; Kiesel et al., 2005; Okamoto et al., 2005; Lanyon et al., 2009]. However, this proposals do not focus on the transverse degrees of freedom of the photons as platform to process information. In Sec. V.2.3, we will propose one more such multi-photon logic gate allowing for the implementation of controlled logical gates of qudits encoded in the transverse degrees of freedom of the photons.

Another way to avoid the problem of implementing non-linear gate operations is to use off-line⁸ entanglement generation which then can be used as a resource for further computations. Such a procedure is very close to the model of measurement-based quantum computation in which one performs coordinated measurements with feed-forward on parts of a large entangled resource state in order to yield the desired computation at some output mode [Raussendorf and Briegel, 2001; Menicucci et al., 2006]. At this point we will not further go into details of this quantum computation model and focus

⁸*Off-line* entanglement or squeezing generation refers to the possibility of entangling or squeezing known quantum states. If the entangling or squeezing is applied to an unknown state we call it *on-line*.

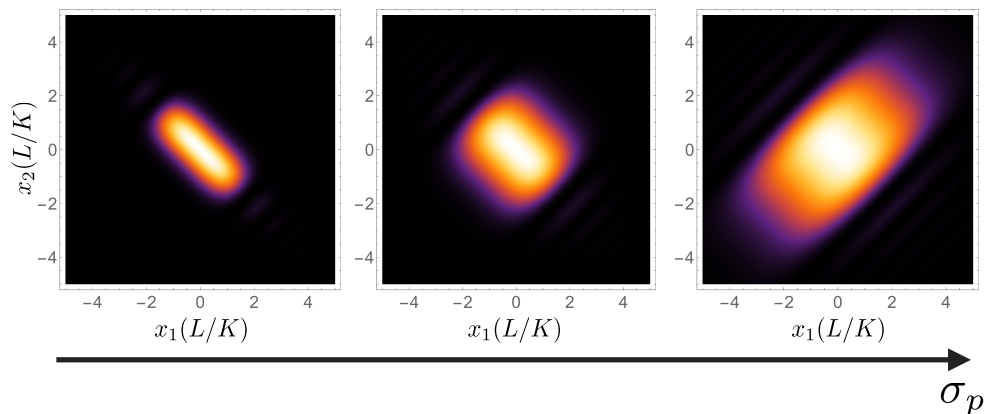


Figure II.12: Density plot of the joint-probability densities of the state (II.174) in units of the parameter L/K for different widths of the pump beam profile $\sigma_p = L/K, 2L/K, 4L/K$ (from left to right).

on the generation of bi-partite entangled state which will be important later on in this thesis.

II.3.1.3 Spatial correlations from parametric down-conversion

An efficient way to generate pairs of entangled photons is by using spontaneous parametric down-conversion. Therein, a non-linear birefringent crystal is pumped by an intense pump laser field with frequency ω_L and produces in a down-conversion process pairs of entangled signal and idler photons with frequency ω_s and ω_i , respectively. These photon pairs can be entangled in the polarization, spatial or temporal degrees of freedom. For the sake of clarity let's disregard here the polarization and temporal degrees of freedom and we focus on the spatial entanglement properties of the photons. In particular, SPDC generates photon pairs whose spatial distribution is described by states of the form:

$$|\Psi\rangle = \iint dx dx' \vartheta(x+x') \gamma(x-x') |x\rangle_s |x'\rangle_i, \quad (\text{II.174})$$

where $|x\rangle_s$ and $|x\rangle_i$ are single photon Fock state of a spatial mode with position x and x' , respectively, the function $\vartheta(x+x')$ is determined by the pump field profile and $\gamma(x-x') = \sqrt{2L/(\pi^2 K)} \text{sinc}(Lx^2/K)$, with the pump beam wave number K and the crystal thickness L , reflects the properties of the considered SPDC process.

In Fig. II.12 we present a plot of the probability density of a typical entangled biphoton wave function produced in SPDC with a pump beam profile given by $\vartheta(x) \propto e^{-x^2/2\sigma_p^2}$. By changing the width of the pump beam σ_p we can continuously scan between the creation of correlated, non-correlated and anti-correlated photon pairs. In order to assert the production of entanglement one has to apply an appropriate continuous-variable entanglement criteria. For instance, the Mancini–Giovannetti–Vitali–Tombesi

(MGVT) criteria [Mancini et al., 2002]:

$$\langle \Delta^2 \hat{X}_\pm \rangle \langle \Delta^2 \hat{P}_\mp \rangle \geq 1 \quad (\text{II.175})$$

where we introduced the global operators $X_\pm = \hat{x}_1 \pm \hat{x}_2$ and $\hat{P}_\mp = \hat{p}_1 \mp \hat{p}_2$. Inequality (II.175) can be violated by sufficiently correlated or anti-correlated states and thus allows to detect entanglement in the spatial degrees of freedom of the photons. Note that, even though Fig. II.12(b) shows almost no correlations, the underlying state is not separable because the spatial correlations have been transferred to the phase of the bi-photon state [Walborn et al., 2010].

There exist many other entanglement criteria for continuous-variable measurements [Duan et al., 2000; Simon, 2000; Braunstein and van Loock, 2005; Adesso and Illuminati, 2007] which have also been violated in experiments using spatially correlated photons [Gomes et al., 2009; D’Angelo et al., 2004]. EPR correlations, which are stronger than entanglement but weaker than Bell nonlocality, have been observed as well using spatially entangled photons [Howell et al., 2004; Walborn et al., 2011]. The demonstration of Bell nonlocality proved to be more difficult because of the need of either non-Gaussian states or measurements in order to violate a Bell inequality, but was finally achieved using measurements of the spatial parity of the single transverse wave function [Abouraddy et al., 2012, 2007].

In Sec. V.3 we will discuss how to use create specific types of spatially entangled photon states consisting of spatially encoded qudits.

II.3.2 Single-mode multi-photon field

Quantum states of a single mode of the electromagnetic field living in a single-mode Fock space (see Sec. II.2.1) are fundamentally different from those describing the spatial degrees of freedom of single photons. While in the latter case, linear optical elements allowed us to implement all single mode operations (Gaussian and non-Gaussian), we will now see that for the manipulation of the quadratures of the electromagnetic field this is no longer the case. In fact, as the name suggests, with linear optical elements we can only implement operations which act linearly on the quadrature operators. In this Section we will discuss how to realize some of the most important CV gates using linear optical elements and explain how non-linear processes can be used to produce non-classical states of light, *e.g.* squeezed states. Finally, we discuss the detection procedure of for the electromagnetic field quadratures.

II.3.2.1 From linear optical operations. . .

In order to perform operations on the quadratures of a single mode of the electromagnetic field one has to be able to manipulate, for instance, its phase. Theoretically, the phase rotation of the quadrature operators was introduced in Eq. (II.38), allowing to transform back and forth between different quadrature operators \hat{X}_θ and $\hat{X}_{\theta'}$ (see also Eqs. (II.110) and (II.111)). However, note that, in practice, the phase implemented by such a rotation has to be seen as relative to some mode-matched reference field, sometimes also referred to as local oscillator. Hence, in order to implement such a phase shift experimentally we simply have to increase the optical path length of the considered

light beam with respect to the local oscillator by inserting a transparent material with higher refractive index than vacuum.

Another very useful linear optical device is a four-port beam splitter (BS) which is acting on two modes (1 and 2) of the electromagnetic field according to the operator:

$$\hat{B}(\theta) = e^{\theta(\hat{a}_1^\dagger \hat{a}_2 - \hat{a}_1 \hat{a}_2^\dagger)} = e^{i\theta(\hat{X}_1 \hat{P}_2 - \hat{X}_2 \hat{P}_1)}, \quad (\text{II.176})$$

where \hat{a}_1 (\hat{a}_1^\dagger) and \hat{a}_2 (\hat{a}_2^\dagger) are the annihilation (creation) operators of mode one and two, respectively. In the Heisenberg picture Eq. (II.176) realizes the transformations:

$$\hat{B}^\dagger \hat{a}_1 \hat{B} = \sqrt{\tau} \hat{a}_1 + \sqrt{1-\tau} \hat{a}_2, \quad \hat{B}^\dagger \hat{a}_1^\dagger \hat{B} = \sqrt{\tau} \hat{a}_1^\dagger + \sqrt{1-\tau} \hat{a}_2^\dagger, \quad (\text{II.177})$$

$$\hat{B}^\dagger \hat{a}_2 \hat{B} = \sqrt{\tau} \hat{a}_2 - \sqrt{1-\tau} \hat{a}_1, \quad \hat{B}^\dagger \hat{a}_2^\dagger \hat{B} = \sqrt{\tau} \hat{a}_2^\dagger - \sqrt{1-\tau} \hat{a}_1^\dagger, \quad (\text{II.178})$$

where $\tau = \cos^2 \theta \in [0, 1]$ represents the transmissivity of the beam splitter. Equivalently, the beam splitter operation can be expressed as a transformation of the mode vector $\hat{\mathbf{v}} = (\hat{X}_1, \hat{P}_1, \hat{X}_2, \hat{P}_2)^T$ in terms of the symplectic matrix

$$\mathbf{M}_{\text{BS}}(\tau) = \begin{pmatrix} & \sqrt{\tau} \mathbb{1}_2 & & \\ -\sqrt{1-\tau} \mathbb{1}_2 & & \sqrt{1-\tau} \mathbb{1}_2 & \\ & & & \\ \sqrt{\tau} \mathbb{1}_2 & & & \end{pmatrix}. \quad (\text{II.179})$$

With the help of the beam splitter operation (II.176) we are able to implement some important CV gates. For instance, we can realize a phase-space displacement $\hat{D}(\alpha)$ by superposing the considered light beam with an intense coherent state $|\alpha\rangle$ on a highly transmissive ($\tau \rightarrow 1$) beam splitter [Paris, 1996]. Furthermore, using two beam splitter operations and two squeezing operations (II.39) we can implement the controlled phase gate \hat{C}_Z (II.35). This decomposition is possible due to the *Bloch-Messiah decomposition* which allows to split up any Gaussian transformation into a combination of linear optical elements (phase shifters and beam splitter), single-mode squeezing operations and phase-space displacements [Braunstein, 2005]. Thus, in order to implement universal Gaussian computations we need to complement the above linear optical operations with an appropriate single-mode squeezing operations. In the next section, we will discuss a commonly used method that permits the creation of squeezed vacuum states of light using a non-linear interaction. In this case one speaks also of off-line squeezing because it cannot be applied as gate operation to an arbitrary unknown input state.

II.3.2.2 ... to Gaussian quantum computation

One way to produce squeezed states of light is by using an *optical parametric oscillator* (OPO). Therefore, we pump a Fabry Perot cavity containing a dielectric crystal with a non-zero non-linear susceptibility $\chi^{(2)}$ with a strong laser beam which can lead to a down-conversion of the pump photons with frequency ω_p into pairs of photons with lower energy. Not taking into account the cavity, this process has to fulfil the energy conservation, $\omega_p = \omega_s + \omega_i$, and phase matching (momentum conservation) condition $\mathbf{k}_p = \mathbf{k}_s + \mathbf{k}_i$. The second condition can be fulfilled due to the birefringence of the optical medium which has different refraction indices for different polarizations leading to two types of possible phase matching conditions, referred to as type I and type II

(see below). This down-conversion process can be described through the Hamiltonian:

$$\hat{H}_{DC} = i\frac{g}{2} \left[\hat{a}_p \hat{a}_s^\dagger \hat{a}_i^\dagger + \hat{a}_p^\dagger \hat{a}_s \hat{a}_i \right] \quad (\text{II.180})$$

where g is related to the strength of the non-linear process. If we now assume that the two down-converted beams are degenerate in polarization ($\hat{a}_i = \hat{a}_s$) while the pump beam has a different polarization (type I phase matching) and that the pump field is in a strong coherent state $|\alpha\rangle$, we can solve the corresponding Heisenberg equations of motion, yielding:

$$\hat{a}(t) = \hat{a}(0)\cosh(\alpha gt) - \hat{a}^\dagger(0)\sinh(\alpha gt). \quad (\text{II.181})$$

The corresponding time evolution operation of this process is

$$\hat{U}_I(t) = e^{\frac{\alpha g}{2}(\hat{a}^2 - \hat{a}^{\dagger 2})t}, \quad (\text{II.182})$$

which is just the single-mode squeezing operator with squeezing factor $r = \alpha gt$ (see Sec. II.1.3 or II.2.4.3). In the case of type II phase matching the two generated photons are not polarization entangled but one of them has the same polarization as the pump beam, leading to a two-mode squeezing evolution:

$$\hat{U}_{II}(t) = e^{\frac{\alpha g}{2}(\hat{a}_s \hat{a}_i - \hat{a}_s^\dagger \hat{a}_i^\dagger)t}. \quad (\text{II.183})$$

The above explained down-conversion process is very weak which has to be compensated by increasing the pump power or the interaction time t_{int} in order to achieve a considerable amount of squeezing. In practice, this is usually done by placing the non-linear crystal inside an optical cavity because the crystal size is finite and the pump power of a continuous-wave (cw) laser field cannot be increased arbitrarily. However, the cavity will alter the dynamics of the field operators \hat{a}_i (\hat{a}_s) and thus has to be included in the theoretical description of the down-conversion process. However, such a description goes beyond the scope of this thesis and will not be further discussed here.

Hence, now we have the ability to create squeezed vacuum states by pumping an OPO which can be further processed using linear optical elements. This is a progress but still not enough to implement any Gaussian unitary operation for which in-line squeezing would be necessary. For this reason, the most common quantum computation model that uses the quadratures of the optical fields is measurement-based quantum computation [Raussendorf and Briegel, 2001; Menicucci et al., 2006]. Therein, as briefly mentioned in the last section, judiciously chosen measurements on an initially produced resource state yield the desired computation on some output mode of the resource state. Such resource states are, for instance, Gaussian cluster states which can be produced through application of \hat{C}_Z -gates on independently momentum squeezed modes [Zhang and Braunstein, 2006]:

$$|\Psi_{\text{Cluster}}\rangle = \prod_{(i,j) \in \Gamma} (\hat{C}_Z)_{i,j} |0\rangle_p^{\otimes N} \quad (\text{II.184})$$

where Γ is the set of all adjacent modes (i, j) of the cluster state and $|0\rangle_p^{\otimes N}$ denotes

a collection of infinitely momentum squeezed modes. Experimentally, such states can be produced by applying a linear optics setup to a collection of independently squeezed vacuum modes and are thus within reach of the previously introduced methods [van Loock et al., 2007].

Note that in an actual experiment the degree of squeezing of the produced cluster states (II.184) is restricted by the amount of squeezing of the initially squeezed vacuum states. Therefore, one deals in general with finite squeezing noise which leads to errors in the implemented computation [Gu et al., 2009]. To overcome this problem one has to apply an appropriate error correction procedure which counteracts the errors induced by finite squeezing [Gottesman et al., 2001]. This leads to a minimum squeezing threshold of the finitely squeezed cluster states in order to render the implemented CV quantum computation fault-tolerant [Menicucci, 2014].

Finally, having in hand a quantum computer that is able implement all Gaussian operations fault-tolerantly, we have to accompany it with at least one non-Gaussian gate in order to achieve universal quantum computations (see Sec. II.1.3). Such a non-Gaussian gate can be any unitary operation that is of order three or higher in its generating Hamiltonian [Lloyd and Braunstein, 1999]. There exist some proposals for experimental implementations of such a non-Gaussian gate [Gottesman et al., 2001; Gu et al., 2009; Marshall et al., 2015], however, they are in general very challenging because they require some non-Gaussian resource. That is, either non-Gaussian measurements, such as photon counting, on a Gaussian cluster state or the production of non-Gaussian states which can then be used as resource states in a gate teleportation process [Gottesman et al., 2001; Menicucci, 2014].

II.3.2.3 Homodyne detection

In the last Section we mentioned the term Gaussian measurements without giving a detailed explanation of it. Here we want to catch up with this and define a measurement as being Gaussian if it yields Gaussian distributed outcomes when applied to Gaussian states (see Sec. II.1.6 for the definition of Gaussian states) [Weedbrook et al., 2012]. The most prevalent Gaussian measurement used in continuous-variable quantum computation is homodyne detection which theoretically corresponds to a projective measurements of one of the quadratures \hat{X}_θ of a mode of the electromagnetic field. The outcome X_θ of this measurement yields a probability density $P(X_\theta)$ which is one of the marginals of the corresponding Wigner function $W(X_\theta, X_{\theta+\frac{\pi}{2}})$.

Experimentally a homodyne measurement can be realized by combining the target mode with an intense local oscillator $|\alpha_{\text{LO}}\rangle$ at a beam splitter with equal reflectivity and transmissivity, and measuring the intensity of the two outgoing modes, respectively [Braunstein and van Loock, 2005]. If we approximate the local oscillator as classical field with amplitude $\alpha_{\text{LO}} = |\alpha|e^{i\theta}$, we obtain for the output modes of the beam splitter:

$$\hat{a}_1 = \frac{1}{\sqrt{2}}(\alpha_{\text{LO}} + \hat{a}_{\text{in}}), \quad (\text{II.185})$$

$$\hat{a}_2 = \frac{1}{\sqrt{2}}(\alpha_{\text{LO}} - \hat{a}_{\text{in}}). \quad (\text{II.186})$$

Next, we measure the intensity of the field $\hat{i}_1 = q\hat{a}_1^\dagger\hat{a}_1$ ($\hat{i}_2 = q\hat{a}_2^\dagger\hat{a}_2$) in output mode one

(two) and take the difference:

$$\hat{i}_1 - \hat{i}_2 = q(\alpha_{\text{LO}}^* \hat{a}_{\text{in}} + \alpha_{\text{LO}} \hat{a}_{\text{in}}^\dagger) = q|\alpha_{\text{LO}}|(e^{-i\theta} \hat{a}_{\text{in}} + e^{i\theta} \hat{a}_{\text{in}}^\dagger), \quad (\text{II.187})$$

where q is a constant. Hence, the difference of the two photo currents (II.187) at the output of the beam splitter yield, up to a multiplicative constant, directly the value of the corresponding field quadrature X_θ , where θ can be adjusted through the phase of the local oscillator field α_{LO} .

II.4 Summary

In this Chapter we have built the theoretical and experimental foundations for the topics that will be discussed in the remainder of this manuscript.

We started by introducing basic elements of quantum information theory. Motivated by the classical concept of a bit we defined its quantum mechanical analog, the qubit (II.1), and showed how systems of qubits states can be manipulated in terms of unitary gate sets. We further discussed the properties of some important gate sets, *e.g.* Clifford gates, and introduced briefly the concept of mixed states and the density matrix formalism (II.13). Then, after having generalized the theory of qubits to d -dimensional (qudits) and continuous-variable (CV) quantum systems, we presented several popular ways to represent states of finite and infinite dimensional quantum systems. This included the Bloch vector (II.53) representation for finite dimensional systems and the Wigner function (II.71) representation for systems that are described by continuous variables. We took this possibility to say some words about the theory of measurements (see Sec. II.1.4) in quantum mechanics and to define Gaussian states (II.81). We closed the Section about basics of quantum information theory with a discussion about entanglement, its detection and relation to nonlocality (see Sec. IV.1).

Since a large part of this thesis will be concerned with applications in quantum optics experiments we introduced in Sec. II.2 the main concepts of the quantum theory of light. Thereby, we first discussed the quantization of the free radiation field and then turned to explain its representation in terms of different spatial or temporal modes (see Sec. II.2.2). We also presented examples of quantum states belonging to the single mode Fock space, *e.g.* coherent, squeezed, thermal or cat states. They will become important in subsequent Chapters which are dedicated to the search of nonlocality in quantum optical systems.

Finally, we introduced two experimental platforms that allow to experimentally process quantum information in terms of continuous variables. They are, on the one hand, the spatial degrees of freedom of a single photon (see Sec. II.3.1) and, on the other hand, the quadratures of a single mode of the electromagnetic field (see Sec. II.3.2). We summarized the most important features of both systems and discussed their advantages and disadvantages in terms of state production, manipulation and measurements. While the former platform will be mainly used in Chapter III and IV, the latter will concern us more in Chapter V.

III Quantum information processing with modular variables

We devise a theoretical framework with the aim to adapt known quantum information protocols, originally formulated for discrete systems, to a phase space formulation comprising the case of continuous-variables. The framework is based on the formalism of modular variables which provides a convenient way to encode and process discrete quantum information in phase space in terms of a particular class of periodic states and operators. It turns out that the most convenient way to express those logical components is in terms of the so-called modular representation that can be associated with the common eigenbasis of the modular position and momentum operators. To demonstrate our framework we show, on the one hand, its application to tests of fundamental properties of quantum mechanics, such as Bell nonlocality and contextuality, involving measurements of modular variables. On the other hand, the role of modular variables as an inevitable tool in continuous-variable quantum computations is discussed. Finally, we elaborate on experimental implementations of our ideas within different important quantum optical platforms.

III.1 Modular variables formalism

The term modular variables dates back to the year 1969 when Aharonov and co-workers studied the *conspicuous* aspects of non-local interactions in quantum mechanics [Aharonov et al., 1969]. This Section is devoted to a general introduction of the formalism of modular variables. We start with an elaboration of mathematical peculiarities of modular variables and specifically discuss the role of the modular position and momentum as pair of commuting observables. This brings us to the definition of the modular representation being the natural choice when dealing with periodic states and/or observables.

III.1.1 Periodic observables or modular variables

When we speak about modular variables we refer to a class of observables whose elements are defined by being periodic functions of a pair of canonically conjugate observables. Therefore, we recall that, given an arbitrary self-adjoint operator \hat{A} with continuous and non-degenerate spectrum $\{a \in \mathbb{R}\}$, an operator function is defined as

$$F(\hat{A}) = \int_{-\infty}^{\infty} da F(a) |a\rangle\langle a| \quad (\text{III.1})$$

where $|a\rangle\langle a|$ is the projector on the eigenspace of the corresponding eigenvalue a and $F : \mathbb{R} \rightarrow \mathbb{R}$ is an arbitrary real function. Since \hat{A} is an arbitrary self-adjoint operator

with continuous spectrum we can associate it with a dimensionless position operator \hat{x} , as introduced in Sec. II.1.3. Furthermore, the position operator \hat{x} is related to the momentum operator \hat{p} through the Fourier transform operator (II.33), making them a pair of conjugate observables. Now, we are in the position to define a periodic observable $f(\hat{x})$ as a Fourier series of the position operator:

$$f(\hat{x}) = \sum_{n \in \mathbb{Z}} f_n e^{2\pi i n \hat{x} / x_0} \quad (\text{III.2})$$

where f_n denotes the Fourier coefficients of the function $f(x)$ and x_0 the period of the function f . Equivalently, we can define a periodic operator $g(\hat{p})$ in terms of the momentum operator:

$$g(\hat{p}) = \sum_{n \in \mathbb{Z}} g_n e^{2\pi i n \hat{p} / p_0} \quad (\text{III.3})$$

with Fourier coefficients g_n and period p_0 . Periodic observables, as (III.2) and (III.3), are often referred to as *modular variables*¹ because their expectation values are determined solely by the corresponding modular operators $\hat{\hat{x}} = \hat{x} \bmod x_0$ and $\hat{\hat{p}} = \hat{p} \bmod p_0$, respectively. Indeed we have that $f(\hat{x}) = f(\hat{\hat{x}})$ and $g(\hat{p}) = g(\hat{\hat{p}})$. Modular variables have some interesting properties that we are going to discover in the subsequent sections.

A somehow unusual but crucial property of such periodic observables, as defined in Eq. (III.2) and (III.3), is their commutativity for a specific choice of the periods x_0 and p_0 . To see this, let us consider the commutator of Eq. (III.2) and (III.3):

$$\begin{aligned} [f(\hat{x}), g(\hat{p})] &= \sum_{n \in \mathbb{Z}} g_n [f(\hat{x}), e^{2\pi i n \hat{p} / p_0}] \\ &= \sum_{n \in \mathbb{Z}} g_n \left(f(\hat{x}) e^{2\pi i n \hat{p} / p_0} - e^{2\pi i n \hat{p} / p_0} f(\hat{x}) \right) \\ &= \sum_{n \in \mathbb{Z}} g_n e^{2\pi i n \hat{p} / p_0} \left(e^{-2\pi i n \hat{p} / p_0} f(\hat{x}) e^{2\pi i n \hat{p} / p_0} - f(\hat{x}) \right) \\ &= \sum_{n \in \mathbb{Z}} g_n e^{2\pi i n \hat{p} / p_0} (f(\hat{x} + 2\pi n / p_0) - f(\hat{x})), \end{aligned} \quad (\text{III.4})$$

where we used at the last equality that the operator $e^{-2\pi i n \hat{p} / p_0}$ implements a displacement in position by $2\pi n / p_0$. Equation (III.4) thus shows that $f(\hat{x})$ and $g(\hat{p})$ commute if the product of their periodicities is $x_0 p_0 = 2\pi$. One can even show that (III.2) and (III.3), with $x_0 p_0 = 2\pi$, are the only non-trivial solutions of the equation $[f(\hat{x}), g(\hat{p})] = 0$. Indeed, in [Busch and Lahti, 1986; Busch et al., 1987] it was demonstrated that $[f(\hat{x}), g(\hat{p})] = 0$ if and only if $f(\hat{x})$ and $g(\hat{p})$ are periodic and $x_0 p_0 = 2\pi k$, with $k \in \mathbb{Z}$. This commutativity can be used to define a set of eigenstates of two such periodic observables and consequently a new representation. In Sec. III.1.4 we will define such a modular representation in terms of the common eigenbasis of the modular position and momentum operators.

The observables (III.2) and (III.3) can also be represented by their corresponding

¹In the following, with the term modular variables we usually refer to the corresponding operator.

Wigner functions (see Sec. II.1.6), which read:

$$W_{f(\hat{x})}(x, p) = \frac{1}{2\pi} f(x), \quad (\text{III.5})$$

$$W_{g(\hat{p})}(x, p) = \frac{1}{2\pi} g(p). \quad (\text{III.6})$$

Motivated by Eqs. (III.5) and (III.6) we can also introduce more general types of periodic observables which are non-diagonal in the position and momentum basis. For instance, let's define an observable \hat{F} with a Wigner function representation proportional to a two-dimensional Fourier series $F(x, p)$:

$$W_{\hat{F}}(x, p) = \frac{1}{2\pi} \sum_{n \in \mathbb{Z}} d_{n,m} e^{2\pi i n x / x_0 - 2\pi i m p / p_0}, \quad (\text{III.7})$$

where $d_{n,m}$ denote the Fourier coefficients defining the precise shape of the function and, x_0 and p_0 , the periodicities in x and p , respectively. From the discussion in Sec. II.1.6 we know that the Wigner function is defined as the inverse Fourier transform of the characteristic function (II.66), yielding:

$$\begin{aligned} \chi_{\hat{F}}(\nu, \mu) &= \frac{1}{2\pi} \iint_{-\infty}^{\infty} dx dp e^{-i\mu x + i\nu p} W_{\hat{F}}(x, p) \\ &= \frac{1}{(2\pi)^2} \sum_{n \in \mathbb{Z}} d_{n,m} \int_{-\infty}^{\infty} dx e^{ix(2\pi n/x_0 - \mu)} \int_{-\infty}^{\infty} dp e^{ip(\nu - 2\pi m/p_0)}, \\ &= \sum_{n \in \mathbb{Z}} d_{n,m} \delta(2\pi n/x_0 - \mu) \delta(\nu - 2\pi m/p_0), \end{aligned} \quad (\text{III.8})$$

which, according to Eq. (II.65), can be used to express the operator \hat{F} as

$$\begin{aligned} \hat{F} &= \iint_{-\infty}^{\infty} d\nu d\mu \chi_{\hat{F}}(\nu, \mu) \hat{D}(\nu, \mu) \\ &= \sum_{n \in \mathbb{Z}} d_{n,m} \iint_{-\infty}^{\infty} d\nu d\mu \delta(2\pi n/x_0 - \mu) \delta(\nu - 2\pi m/p_0) \hat{D}(\nu, \mu) \\ &= \sum_{n \in \mathbb{Z}} d_{n,m} \underbrace{e^{2\pi i n \hat{x} / x_0 - 2\pi i m \hat{p} / p_0}}_{=\hat{D}(2\pi m/p_0, 2\pi n/x_0)}. \end{aligned} \quad (\text{III.9})$$

being a sum of displacements by integer multiples of $2\pi/p_0$ and $2\pi/x_0$ in position and momentum, respectively. Later on, we will denote \hat{F} always as $F(\hat{x}, \hat{p})$ emphasizing its structure as a function of the position and momentum operators, defined through Eq. (III.9).

Next, we discuss a specific example of modular variables that will be important for applications later on in this Section.

III.1.2 Modular variables and the characteristic function

An important set of modular variables is given by the hermitian components of the displacement operator $\hat{D}(\nu, \mu) = e^{i\mu\hat{x} - i\nu\hat{p}}$, which are defined as:

$$\text{Re}(\hat{D}(\nu, \mu)) = \frac{1}{2}(\hat{D}(\nu, \mu) + \hat{D}^\dagger(\nu, \mu)) = \cos(\mu\hat{x} - \nu\hat{p}), \quad (\text{III.10})$$

$$\text{Im}(\hat{D}(\nu, \mu)) = \frac{1}{2i}(\hat{D}(\nu, \mu) - \hat{D}^\dagger(\nu, \mu)) = \sin(\mu\hat{x} - \nu\hat{p}), \quad (\text{III.11})$$

and thus yield $\hat{D}(\nu, \mu) = \cos(\mu\hat{x} - \nu\hat{p}) + i \sin(\mu\hat{x} - \nu\hat{p})$. The observables (III.10) and (III.11) can be seen as special cases of the more general modular variable:

$$\hat{Q}_\varphi(\nu, \mu) = \frac{1}{2} \left[e^{i\varphi} \hat{D}(\nu, \mu) + e^{-i\varphi} \hat{D}^\dagger(\nu, \mu) \right] = \cos(\varphi + \mu\hat{x} - \nu\hat{p}), \quad (\text{III.12})$$

with $\phi = 0$ and $\varphi = -\pi/2$, respectively. An important properties of the expectation value of (III.12) is:

$$\langle \hat{Q}_\varphi(\nu, \mu) \rangle = \langle \cos(\varphi + \mu\hat{x} - \nu\hat{p}) \rangle \leq 1, \quad (\text{III.13})$$

for all values of ν , μ and φ . The boundedness of the modular variables (III.12) is crucial for the formulation of nonlocality or contextuality tests, as we will see later on in Sec. IV.2.

Further on, we want to comment on the possibility to determine the characteristic function $\chi_{\hat{\rho}}(\nu, \mu) = \frac{1}{2\pi} \text{tr}[\hat{\rho} \hat{D}^\dagger(\nu, \mu)]$ (see also Eq. (II.66)) by measuring the modular variables (III.12). Since the characteristic function $\chi_{\hat{\rho}}(\nu, \mu)$ is proportional to the expectation value of the adjoint displacement operator $\langle \hat{D}^\dagger(\nu, \mu) \rangle$, we can write

$$\chi_{\hat{\rho}}(\nu, \mu) = \langle \hat{Q}_0(\nu, \mu) \rangle + i \langle \hat{Q}_{\frac{\pi}{2}}(\nu, \mu) \rangle, \quad (\text{III.14})$$

thus allowing us to determine the complex characteristic function solely through measurements of modular variables. Furthermore, as we have seen in Sec. II.1.6, the Wigner function follows from Eq. (III.14) via an inverse Fourier transform:

$$W_{\hat{\rho}}(x, p) = \frac{1}{2\pi} \iint_{-\infty}^{\infty} d\mu d\nu e^{i\mu x - i\nu p} \chi_{\hat{\rho}}(\nu, \mu). \quad (\text{III.15})$$

Hence, measurements of the modular variables $Q_0(\nu, \mu)$ and $Q_{\frac{\pi}{2}}(\nu, \mu)$ for an appropriately large set of values (ν, μ) , one is able to reconstruct the Wigner function of the state the state $\hat{\rho}$. With respect to this, note that, as discussed in Sec. II.1.4, the expectation value the bounded observables (III.12) can be measured in terms of a two-valued POVM, thus by coupling ancilla atom to the CV system under consideration. This state tomography in terms of ancilla measurements can be of great advantage in optical [Machado et al., 2013; Hor-Meyll et al., 2014] but also in optomechanical systems [Gittsovich et al., 2015].

In the next Section we will continue the discussion about modular variables using the example of the modular position and momentum operators.

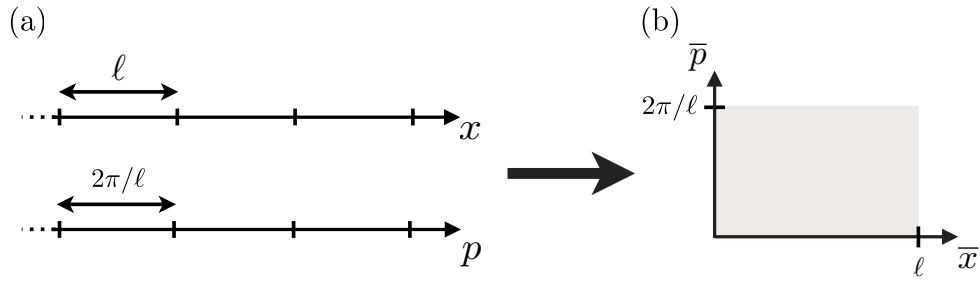


Figure III.1: (a) Schematic representation of the spectra of the position and momentum operator divided into boxes of length ℓ and $2\pi/\ell$, respectively, and (b) of the bounded spectra of the modular position and momentum operator.

III.1.3 Modular position and momentum

Let us consider the dimensionless position \hat{x} and momentum \hat{p} momentum operators in one dimension fulfilling the canonical commutation relation $[\hat{x}, \hat{p}] = i$, as defined in Sec. II.1.3. Each of these two conjugate operators has a unbounded continuous spectrum whose eigenvalues are denoted as x and p , and corresponding eigenstates $|x\rangle_x$ and $|p\rangle_p$, which define the position and momentum representation, respectively.

In the following, we seek a different representation in terms of two commuting modular variables (see Sec. III.1.1), called the modular position and momentum. To derive this representation we divide the spectrum of \hat{x} and \hat{p} into boxes of lengths ℓ , where ℓ is a dimensionless scaling factor, and $2\pi/\ell$, respectively, and redefine them, as:

$$\hat{x} = \ell \hat{N} + \hat{\bar{x}}, \quad (\text{III.16})$$

$$\hat{p} = \frac{2\pi}{\ell} \hat{M} + \hat{\bar{p}}. \quad (\text{III.17})$$

where we introduced the two discrete operators \hat{N} and \hat{M} , which have integer eigenvalues, and the modular position and momentum operators, $\hat{\bar{x}} = (\hat{x} - x_\ell) \bmod \ell + x_\ell$ and $\hat{\bar{p}} = (\hat{p} - p_\ell) \bmod 2\pi/\ell + p_\ell$, with bounded spectra given by the intervals $[x_\ell, x_\ell + \ell]$ and $[p_\ell, p_\ell + 2\pi/\ell]$, respectively. The variables x_ℓ and p_ℓ define the starting points of the bounded spectra of the two modular operators which can be set at will. In the following, we will use the convention $x_\ell = -\ell/2$ and $p_\ell = -\pi/\ell$.

In Fig. III.2(a) we plot the eigenvalues of both modular operators as a function of the position and momentum, respectively, showing that they are periodic while the product of their periods is equal to 2π . Hence, we can conclude, taking into account the discussion about the commutativity of periodic observables in Sec. III.1.1, that the modular position and momentum operators, $\hat{\bar{x}}$ and $\hat{\bar{p}}$, commute. In the next Section, we will make use of this commutativity to construct an alternate representation in terms of the common eigenstates $|\bar{x}, \bar{p}\rangle$ of the modular position $\hat{\bar{x}}$ and momentum $\hat{\bar{p}}$ operators. But, before we proceed with the derivation of this eigenbasis, let's discuss some qualitative consequences of the commutativity of the modular position and momentum operators. We will see that in order to get a complete picture we also have to take into account the commutators between the modular variables and their discrete counterparts, \hat{N} and \hat{M} .

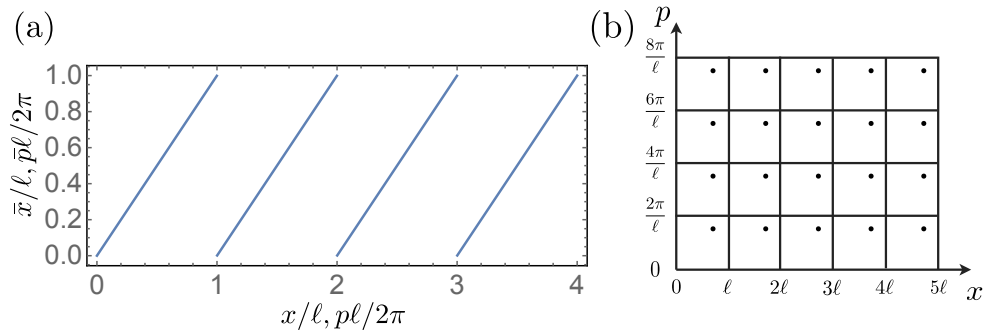


Figure III.2: Plot of the eigenvalues of the modular position and momentum operators, \hat{x} and \hat{p} , as a function of the eigenvalues of the position and momentum, \hat{x} and p , respectively.

It is well known that from a classical point of view quantum mechanics limits the information that an observer can extract from a physical system due to the non-commutativity of pairs of certain observables. In the case of the position and momentum operator this non-commutativity manifests itself in the Heisenberg uncertainty relation $\Delta x \Delta p \geq 1/2$ (remember that in Sec. II.1.3 we have set $\hbar = 1$), making it impossible to measure at the same time the position and momentum with arbitrary precision. In contrast, the modular position and momentum are two observables that give only partial information about the position and momentum of a particle which is reflected by their commutativity. Hence, we can simultaneously determine their precise values without violating the Heisenberg uncertainty principle. This is illustrated in Fig. III.2(b), where we schematically plot the result of a simultaneous modular position and momentum measurement in a phase space representation. While the modular variables can be determined exactly, a full information about the position and momentum would require also the corresponding values of the integer position and momentum observables \hat{N} and \hat{M} . The latter, however, have non-zero commutation relations with the modular position and momentum.

The remaining uncertainty between position and momentum, that cannot be revealed by a measurement of the corresponding modular values alone, is reflected by the commutator relations among the modular and integer operators in Eqs. (III.16) and (III.17), respectively. For instance, for the modular position and its discrete momentum counterpart, we find

$$[\hat{x}, \hat{M}] = i \frac{\ell}{2\pi} \left(\mathbb{1} - \ell \int_{-\pi/\ell}^{\pi/\ell} d\bar{p} |\ell/2, \bar{p}\rangle \langle \ell/2, \bar{p}| \right), \quad (\text{III.18})$$

where the second term on the right-hand side consists of a sum of projectors on modular eigenstates (see Sec. III.1.4) that is due to the boundedness of the domain of \bar{x} . Equivalently, the commutator relation between the modular momentum and its discrete

position counterpart, reads:

$$[\hat{N}, \hat{p}] = \frac{i}{\ell} \left(\mathbb{1} - \frac{2\pi}{\ell} \int_{-\ell/2}^{\ell/2} d\bar{x} |\bar{x}, \pi/\ell\rangle \langle \bar{x}, \pi/\ell| \right), \quad (\text{III.19})$$

with a similar projector on the right-hand side of the equation. For a mathematical derivation of these modular-integer commutation relations we refer the reader to Appendix B. For completeness, the commutator of the two integer operators, \hat{N} and \hat{M} , can be calculated using the relation

$$[\hat{N}, \hat{M}] = \frac{i}{2\pi} \mathbb{1} - \frac{1}{\ell} [\hat{x}, \hat{M}] - \frac{\ell}{2\pi} [\hat{N}, \hat{p}], \quad (\text{III.20})$$

which follows directly from Eqs. (III.18) and (III.19), and the commutators $[\hat{x}, \hat{p}] = i$ and $[\hat{x}, \hat{p}] = 0$.

Having available the commutators (III.18) and (III.19), we are also able to derive uncertainty relations for the corresponding observables using the *Robertson uncertainty relation*, which for two arbitrary observables \hat{A} and \hat{B} , reads:

$$\Delta A \Delta B \geq \frac{1}{2} \left| \langle [\hat{A}, \hat{B}] \rangle \right| \quad (\text{III.21})$$

where ΔA (ΔB) denotes the standard deviation of \hat{A} (\hat{B}). When applied to the commutators (III.18) and (III.19), Equation (III.21) becomes:

$$\Delta \bar{x} \Delta M \geq \frac{\ell}{4\pi} (1 - \ell P_1(\Psi)), \quad (\text{III.22})$$

$$\Delta N \Delta \bar{p} \geq \frac{1}{2\ell} (1 - \frac{2\pi}{\ell} P_2(\Psi)), \quad (\text{III.23})$$

with state dependent terms $P_1(\Psi)$ and $P_2(\Psi)$. Hence, for states which yield $P_1(\Psi) = P_2(\Psi) = 0$, we recover the canonical form of the position and momentum uncertainty relations, but in the general case, the value of minimal uncertainty depends on the state under consideration and thus on the experimental context.

To demonstrate the behaviour of the uncertainty relations (III.22) and (III.23) we consider the following example: a superposition of \mathcal{N} distinct wave packets $\Psi(x) = \sum_{n=0}^{\mathcal{N}-1} \psi(x - nL)$, with separation L . For the following discussion the choice of the exact shape of the wave packets $\psi(x)$ is rather flexible, as long as their width σ_x is small compared to their separation L . For instance, we can choose them to be Gaussian wave functions, as discussed in Sec. II.1.3. Then, we find for the state-dependent term on the right-hand side of Eq. (III.23), $P_2(\Psi) = (1 + (-1)^{\mathcal{N}+1})/2$, where we set $\ell = L$ and assumed $\sigma_x \ll L$. Hence, we see that, in the case of a single localized wave packet ($\mathcal{N} = 1$), we have $P_2(\Psi) = 1$ and thus $\Delta N \Delta \bar{p} \geq 0$, showing that one can always determine the exact values of the integer position N and the modular momentum \bar{p} . In contrast, for a superposition of many wave packets ($\mathcal{N} \rightarrow \infty$) we recover the canonical form of the uncertainty relation $\Delta N \Delta \bar{p} \geq 1/(2\ell)$, showing that N_x and \bar{p} cannot be resolved to arbitrary precision.

III.1.4 The modular representation

In this Section we derive the analytical expressions of the common eigenstates of the modular position and momentum operator. As mentioned in the last section such a set of eigenstates is characterized by the bounded values of the modular position and momentum, \bar{x} and \bar{p} , and thus can be expressed as $\{|\bar{x}, \bar{p}\rangle | \bar{x} \in [-\ell/2, \ell/2], \bar{p} \in [-\pi/\ell, \pi/\ell]\}$. In the following, we will introduce the modular eigenstates as superpositions of position or momentum eigenstates, $|x\rangle$ and $|p\rangle$, respectively.

Let's start by noting that the common basis $\{|\bar{x}, \bar{p}\rangle | \bar{x} \in [-\ell/2, \ell/2], \bar{p} \in [-\pi/\ell, \pi/\ell]\}$ is defined such that:

$$e^{i\hat{p}\mu\ell}|\bar{x}, \bar{p}\rangle = e^{i\bar{p}\mu\ell}|\bar{x}, \bar{p}\rangle \quad (\text{III.24})$$

$$e^{i2\pi\hat{x}\nu/\ell}|\bar{x}, \bar{p}\rangle = e^{i2\pi\bar{x}\nu/\ell}|\bar{x}, \bar{p}\rangle. \quad (\text{III.25})$$

Further on, for position and momentum displacements by $n\ell$ and $m2\pi/\ell$, respectively, we have that $e^{i\hat{p}r\ell/\hbar} = e^{i\bar{p}r\ell/\hbar}$ and $e^{i2\pi\hat{x}s/\ell} = e^{i2\pi\bar{x}s/\ell}$, with $r, s \in \mathbb{Z}$, yielding

$$\langle x'|e^{i2\pi\hat{x}s/\ell}e^{i\hat{p}r\ell}|\bar{x}, \bar{p}\rangle = e^{i2\pi s\bar{x}/\ell}e^{i\bar{p}r\ell}\langle x'|\bar{x}, \bar{p}\rangle, \quad (\text{III.26})$$

when acting on the ket $|\bar{x}, \bar{p}\rangle$, and

$$\langle x'|e^{i2\pi\hat{x}s/\ell}e^{i\hat{p}r\ell}|\bar{x}, \bar{p}\rangle = e^{i2\pi s\bar{x}'/\ell}\langle x' + r\ell|\bar{x}, \bar{p}\rangle, \quad (\text{III.27})$$

when acting on the bra $\langle x'|$. By combining Eqs. (III.26) and (III.27) we obtain the equation:

$$e^{i2\pi s\bar{x}/\ell}e^{i\bar{p}r\ell}\langle x'|\bar{x}, \bar{p}\rangle = e^{i2\pi s\bar{x}'/\ell}\langle x' + r\ell|\bar{x}, \bar{p}\rangle \quad (\text{III.28})$$

which, for $r = 0$, yields the solution $\langle x'|\bar{x}, \bar{p}\rangle = A\delta(\bar{x} - \bar{x}')$, with an arbitrary constant A that will be defined later on. Using this solution in Eq. (III.28), we find:

$$\langle x' + r\ell|\bar{x}, \bar{p}\rangle = e^{i\bar{p}r\ell}A\delta(\bar{x} - \bar{x}'), \quad (\text{III.29})$$

what allows us to express an arbitrary modular eigenstate as

$$\begin{aligned} |\bar{x}, \bar{p}\rangle &= \int_{-\infty}^{+\infty} dx' \langle x'|\bar{x}, \bar{p}\rangle |x'\rangle = \int_{-\ell/2}^{\ell/2} d\bar{x}' \sum_{r=-\infty}^{+\infty} \langle x' + r\ell|\bar{x}, \bar{p}\rangle |x' + r\ell\rangle \\ &= \int_{-\ell/2}^{\ell/2} d\bar{x}' \sum_{r=-\infty}^{+\infty} e^{i\bar{p}r\ell} A\delta(\bar{x} - \bar{x}') |x' + r\ell\rangle = A \sum_{r=-\infty}^{+\infty} e^{i\bar{p}r\ell} |\bar{x} + \mu\ell\rangle. \end{aligned} \quad (\text{III.30})$$

where we used the resolution of the identity (II.30). Alternatively, by inserting $|x\rangle = \int dp \langle p|x\rangle |p\rangle$, we can turn Eq. (III.30) into an expression that involves momentum eigen-

states:

$$\begin{aligned}
|\bar{x}, \bar{p}\rangle &= \frac{A}{\sqrt{2\pi\hbar}} \sum_{r=-\infty}^{+\infty} e^{i\bar{p}r\ell/\hbar} \int_{-\infty}^{+\infty} e^{-ip'(\bar{x}+r\ell)/\hbar} |p'\rangle dp' \\
&= \frac{A}{\sqrt{2\pi}} \sum_{s=-\infty}^{+\infty} e^{-i2\pi s\bar{x}/\ell} \int_{-\pi/\ell}^{\pi/\ell} d\bar{p}' \left(\sum_{r=-\infty}^{+\infty} e^{i(\bar{p}-\bar{p}')r\ell} \right) e^{-i\bar{p}'\bar{x}} |\bar{p}' + s\hbar/\ell\rangle, \\
&= \frac{A\sqrt{2\pi}}{\ell} e^{-i\bar{p}\bar{x}} \sum_{s=-\infty}^{+\infty} e^{-i2\pi s\bar{x}/\ell} |\bar{p} + s2\pi/\ell\rangle. \tag{III.31}
\end{aligned}$$

where we used that $\frac{2\pi}{\ell} \delta(2\pi/\ell)(\bar{p} - \bar{p}') = \sum_{r=-\infty}^{+\infty} e^{i(\bar{p}-\bar{p}')r\ell}$, where $\delta(2\pi/\ell)(\bar{p} - \bar{p}')$ is a comb of delta functions with period $2\pi/\ell$. In the following, we will often use the shorthand notation $\delta(\bar{x} - \bar{x}')$ and $\delta(\bar{p} - \bar{p}')$ to refer to combs of delta functions with period ℓ and $2\pi/\ell$, respectively. Next, we check the orthogonality of the modular basis:

$$\begin{aligned}
\langle \bar{x}', \bar{p}' | \bar{x}, \bar{p} \rangle &= |A|^2 \sum_{r,s=-\infty}^{+\infty} e^{-i\bar{p}'s\ell} e^{i\bar{p}r\ell} \langle \bar{x}' + s\ell | \bar{x} + r\ell \rangle \\
&= |A|^2 \delta(\bar{x}' - \bar{x}) \sum_{s=-\infty}^{+\infty} e^{i(\bar{p}-\bar{p}')s\ell/\hbar} = \frac{2\pi|A|^2}{\ell} \delta(\bar{x}' - \bar{x}) \delta(\bar{p}' - \bar{p}) \tag{III.32}
\end{aligned}$$

deducing the normalization factor $A = e^{i\varphi} \sqrt{\ell/(2\pi)}$, with an arbitrary phase φ . From now on we will omit the phase factor $e^{i\varphi}$ because it amounts to an unimportant global phase. To summarize, we found that the modular eigenstates can be expressed in terms of position and momentum eigenstates as

$$|\{\bar{x}, \bar{p}\}\rangle = \sqrt{\frac{\ell}{2\pi}} \sum_{n=-\infty}^{+\infty} e^{i\bar{p}n\ell} |\bar{x} + n\ell\rangle_x, \tag{III.33}$$

$$= \sqrt{\frac{1}{\ell}} e^{-i\bar{p}\bar{x}} \sum_{m=-\infty}^{+\infty} e^{-i2\pi m\bar{x}/\ell} |\bar{p} + m2\pi/\ell\rangle_p. \tag{III.34}$$

fulfilling the completeness relation:

$$\begin{aligned}
\int_{-\ell/2}^{\ell/2} d\bar{x} \int_{-\pi/\ell}^{\pi/\ell} d\bar{p} |\bar{x}, \bar{p}\rangle \langle \bar{x}, \bar{p}| &= \frac{\ell}{\hbar} \int_0^\ell d\bar{x} \sum_{r,s=-\infty}^{+\infty} \underbrace{\left(\int_{-\pi/\ell}^{\pi/\ell} d\bar{p} e^{i\bar{p}(r-s)\ell} \right)}_{\frac{2\pi}{\ell} \delta_{r,s}} |\bar{x} + r\ell\rangle \langle \bar{x} + s\ell| \\
&= \int_{-\ell/2}^{\ell/2} d\bar{x} \sum_{r=-\infty}^{+\infty} |\bar{x} + r\ell\rangle \langle \bar{x} + r\ell| = \int_{-\infty}^{\infty} dx |\bar{x}\rangle \langle \bar{x}| = \mathbb{1}. \tag{III.35}
\end{aligned}$$

Inversely, we can define the position and momentum eigenstates in terms of the modular

eigenstates, as:

$$|x\rangle_x = |\bar{x} + n\ell\rangle_x = \sqrt{\frac{\ell}{2\pi}} \int_{\pi/\ell}^{\pi/\ell} d\bar{p} e^{-i\bar{p}n\ell} |\bar{x}, \bar{p}\rangle \quad (\text{III.36})$$

$$|p\rangle_p = |\bar{p} + m\frac{2\pi}{\ell}\rangle_p = \sqrt{\frac{1}{\ell}} \int_{-\ell/2}^{\ell/2} d\bar{x} e^{i\bar{x}\bar{p}} e^{i2\pi m\bar{x}/\ell} |\bar{x}, \bar{p}\rangle. \quad (\text{III.37})$$

Hence, having derived all the symbolic expression of the modular eigenstates, we can now express arbitrary quantum states, such as $|\Psi\rangle = \int dx \Psi_x(x)|x\rangle$, in the modular representation:

$$|\Psi\rangle = \int_{-\ell/2}^{\ell/2} \int_{-\pi/\ell}^{\pi/\ell} d\bar{x} d\bar{p} \Psi(\bar{x}, \bar{p}) |\bar{x}, \bar{p}\rangle, \quad (\text{III.38})$$

with the *modular wave function* $\psi(\bar{x}, \bar{p})$, defined through

$$\Psi(\bar{x}, \bar{p}) = \sqrt{\frac{\ell}{2\pi}} \sum_{n=-\infty}^{\infty} \Psi_x(n\ell + \bar{x}) e^{-in\bar{p}\ell}, \quad (\text{III.39})$$

or for a state with the wave function $\Psi_p(p)$ defined in the momentum representation, we get

$$\Psi(\bar{x}, \bar{p}) = \sqrt{\frac{1}{\ell}} e^{i\bar{x}\bar{p}} \sum_{m=-\infty}^{\infty} \Psi_p(m2\pi/\ell + \bar{p}) e^{2\pi im\bar{x}/\ell}. \quad (\text{III.40})$$

The same representation was introduced by J. Zak in 1967 under the term *k, q-representation* [Zak, 1967]. The modular wave function, $\Psi(\bar{x}, \bar{p})$ is normalised as follows

$$1 = \langle \psi | \psi \rangle = \int_{-\ell/2}^{\ell/2} d\bar{x} \int_{-\pi/2}^{\pi/2} d\bar{p} |\Psi(\bar{x}, \bar{p})|^2. \quad (\text{III.41})$$

The above introduced representation can be seen as a mapping from the Hilbert space of square integrable functions on \mathbb{R} (position or momentum) onto the Hilbert space of square integrable functions on a bounded domain of \mathbb{R}^2 , defined by the product of the intervals $[-\ell/2, \ell/2[$ and $[-\pi/\ell, \pi/\ell[$ of the modular position and momentum, \bar{x} and \bar{p} , respectively. The resulting representation is characterized by the quasi-periodicity relations:

$$\Psi(\bar{x} + \ell, \bar{p}) = e^{i\bar{p}\ell} \Psi(\bar{x}, \bar{p}), \quad (\text{III.42})$$

$$\Psi(\bar{x}, \bar{p} + \frac{2\pi}{\ell}) = \Psi(\bar{x}, \bar{p}), \quad (\text{III.43})$$

through which the defined representation can be extended also to values outside of the domain $[-\ell/2, \ell/2[\times [-\pi/\ell, \pi/\ell[$. This is important, for instance, if one wants to calculate the inverse transform and recover the position or momentum representation from the modular one. Issues concerning the (quasi-)periodicity of the modular basis were discussed in more detail in [Englert et al., 2006].

Equivalently, in a bipartite system, states in the modular representation read:

$$\begin{aligned} |\psi\rangle &= \int_{-\infty}^{+\infty} dx_1 \int_{-\infty}^{+\infty} dx_2 \Psi(x_1, x_2) |x_1\rangle |x_2\rangle \\ &= \int_{-\ell/2}^{\ell/2} d\bar{x}_{1/2} \int_{-\pi/\ell}^{\pi/\ell} d\bar{p}_{1/2} \Psi(\bar{x}_1, \bar{p}_1, \bar{x}_2, \bar{p}_2) |\bar{x}_1, \bar{p}_1\rangle |\bar{x}_2, \bar{p}_2\rangle. \end{aligned} \quad (\text{III.44})$$

with the bipartite modular wave function

$$\Psi(\bar{x}_1, \bar{p}_1, \bar{x}_2, \bar{p}_2) = \frac{\ell}{2\pi} \sum_{n_{1/2}=-\infty}^{+\infty} \Psi(\bar{x}_1 + n_1\ell, \bar{x}_2 + n_2\ell) e^{-i\bar{p}_1 n_1\ell} e^{-i\bar{p}_2 n_2\ell}. \quad (\text{III.45})$$

Or we can define the modular representation of an arbitrary operator \hat{A} , as follows:

$$\hat{A} = \iint_{-\ell/2}^{\ell/2} d\bar{x} d\bar{x}' \iint_{-\pi/\ell}^{\pi/\ell} d\bar{p} d\bar{p}' \underbrace{\langle \bar{x}, \bar{p} | \hat{A} | \bar{x}', \bar{p}' \rangle}_{=A(\bar{x}, \bar{p}; \bar{x}', \bar{p}')} |\bar{x}, \bar{p}\rangle \langle \bar{x}', \bar{p}'|. \quad (\text{III.46})$$

with the matrix elements $A(\bar{x}, \bar{p}; \bar{x}', \bar{p}')$, which, by using the definition of the modular eigenstates in Eq. (III.34), can be expressed as

$$A(\bar{x}, \bar{p}; \bar{x}', \bar{p}') = \frac{\ell}{2\pi} \sum_{r,s=-\infty}^{\infty} e^{i(\bar{p}'r - \bar{p}s)\ell} \langle \bar{x} + s\ell | \hat{A} | \bar{x}' + r\ell \rangle. \quad (\text{III.47})$$

As an example, we use Eqs. (III.46) and (III.47) to derive the modular representation of the operator \hat{N}_x and \hat{N}_p . To this end, let's first calculate the matrix elements of the momentum operator which, according to Eq. (III.47), read

$$p(\bar{x}, \bar{p}; \bar{x}', \bar{p}') = \int_{-\infty}^{\infty} dp p \langle \bar{x}, \bar{p} | p | \bar{x}', \bar{p}' \rangle \quad (\text{III.48})$$

and by using the definition of the modular eigenstates (III.34) can be brought into the form

$$p(\bar{x}, \bar{p}; \bar{x}', \bar{p}') = \ell \delta(\bar{x} - \bar{x}') \delta(\bar{p} - \bar{p}') + i \left(e^{i\bar{p}(\bar{x} - \bar{x}')} \frac{\partial}{\partial \bar{x}'} \left[\delta(\bar{x} - \bar{x}') \right] \delta(\bar{p} - \bar{p}') \right). \quad (\text{III.49})$$

where the first term simply represents the modular position operator \hat{p} with diagonal matrix elements in the modular basis. In order to further simplify the second term in Eq. (III.49) we calculate its action on an arbitrary state expressed in the modular representation and after some algebra (see Appendix B for details of the calculation), we find

$$\hat{N}_p \Psi(\bar{x}, \bar{p}) = \frac{i\ell}{2\pi} \frac{\partial}{\partial \bar{x}} \Psi(\bar{x}, \bar{p}) - \frac{\ell}{2\pi} \bar{p} \Psi(\bar{x}, \bar{p}), \quad (\text{III.50})$$

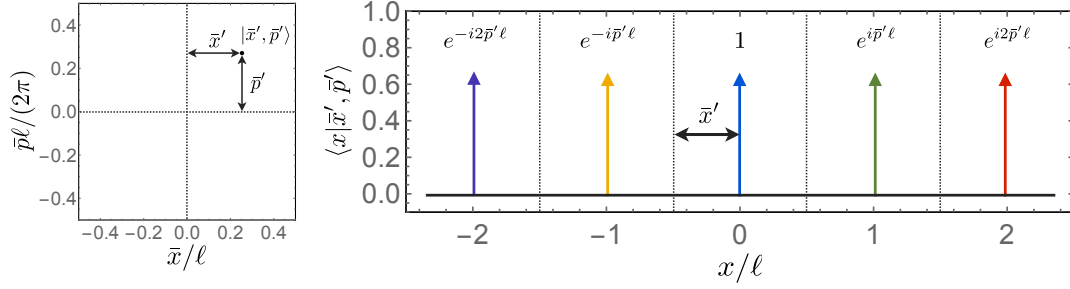


Figure III.3: Schematic plot of the modular (left) and the position (right) wave function of a modular eigenstates $|\bar{x}', \bar{p}'\rangle$. While the modular wave function consists of a single delta peak (black dot) in the bounded domain $[-\ell/2, \ell/2] \times [-\pi/\ell, \pi/\ell]$, the position wave function is given by a comb of delta functions (colored arrows) over the real line each multiplied by a phase factor $e^{i\bar{p}'n\ell}$. Different colors indicate different phase factors.

thus showing that in the modular representation we have

$$\hat{N}_p = \frac{\ell}{2\pi} \left(i \frac{\partial}{\partial \bar{x}} - \hat{p} \right). \quad (\text{III.51})$$

where the first terms on the right-hand side corresponds to the momentum operator $\hat{p} = i\partial/\partial \bar{x}$. In the same way one can derive the symbolic expressions of the position \hat{x} and integer position \hat{N}_x operator in the modular representation.

III.1.5 Examples of states in the modular representation

In this Section we will present several important examples of states expressed in the modular representation. Thereby, in order to improve our intuition, we will first discuss the position and momentum representation of the modular eigenstates $|\bar{x}, \bar{p}\rangle$ itself. Let's start with the most simple case $|\bar{x} = 0, \bar{p} = 0\rangle = \sqrt{\frac{\ell}{2\pi}} \sum_{n=-\infty}^{+\infty} |\ell n\rangle_x$, which in the modular domain consists of a single delta peak at the origin and in the position representation of a comb of equally separated delta functions with distance ℓ . Modular eigenstates with nonzero values of the modular position and momentum, such as $|\bar{x}', \bar{p}'\rangle$, then lead to a shift of this delta comb by \bar{x}' and to phase factors $e^{i\bar{p}'m\ell}$ multiplied with each peak in this comb, as illustrated in Fig. III.3. A similarly picture holds in the momentum representation, where a modular eigenstate consists of a comb of delta functions with separation $2\pi/\ell$, shifted by \bar{p}' from the origin and multiplied with phase factors $e^{2\pi n\bar{x}'/\ell}$.

As being infinite superpositions of position or momentum eigenstates, the modular eigenstates are nonphysical in a twofold sense. On the one hand, each position or momentum eigenstate is infinitely localized in phase space and thus by itself not normalizable. On the other hand, the infinite superposition which defines the modular eigenstate reflects a complete delocalization in position and momentum space. In order to construct physically sound states we need to consider continuous superpositions of

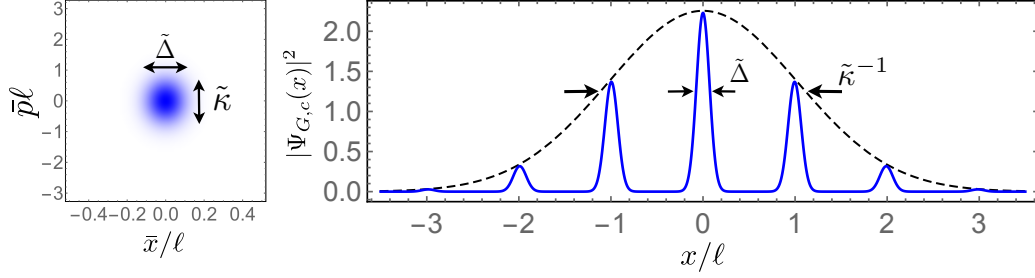


Figure III.4: Plots of the probability density of the state $|\Psi_{G,c}\rangle$ in the modular (left) and position (right) representation. For the modular probability density the full widths at half maximum (FWHM) in the modular position and momentum are given by $\tilde{\Delta} = 2\sqrt{\ln 2}\Delta$ and $\tilde{\kappa} = 2\sqrt{\ln 2}\kappa$, respectively, where $\Delta = 0.06\ell$ and $\kappa = 0.06/\ell$ are the standard deviations that define the corresponding modular wave function (III.53). In the position representation $\tilde{\Delta}$ denotes the FWHM of to the individual Gaussian spikes, and $\tilde{\kappa}$ is the inverse of the FWHM of the Gaussian envelope, provided $\Delta/\ell \ll 1$ and $\kappa\ell \ll 1$ hold. In the momentum representation one would obtain the a similar function with the roles of $\tilde{\Delta}$ and $\tilde{\kappa}$ exchanged.

modular eigenstates in terms of a normalizable wave function, as discussed in the las Section. For instance, we can replace each delta function in Fig. III.3) by a finitely squeezed Gaussian spike with width Δ and multiply them with a Gaussian envelope of width $1/\kappa$. The resulting wave function in the position representation then reads:

$$\Psi_{G,c}(x) = \frac{N}{(\pi\Delta^2)^{\frac{1}{4}}} e^{-(x\kappa)^2/2} \sum_{n=-\infty}^{\infty} e^{-(x-nL)^2/2\Delta^2}, \quad (\text{III.52})$$

with a normalization factor N . In the limit $\Delta/L \ll 1$ and $\kappa L \ll 1$, of a large envelope and sufficiently thin spikes, respectively, the latter can be approximated by $N \approx \sqrt{L\kappa}/\sqrt{\pi}$. Then, transforming Eq. (III.52) to the modular representation with the help of Eq. (III.34), yields:

$$\Psi_{G,c}(\bar{x}, \bar{p}) = T(\bar{x})C(\bar{p}), \quad (\text{III.53})$$

where

$$T(\bar{x}) = \frac{1}{(\pi\Delta^2)^{\frac{1}{4}}} \sum_{n=-\infty}^{\infty} e^{-(\bar{x}-n\ell)^2/2\Delta^2}, \quad (\text{III.54})$$

$$C(\bar{p}) = \frac{1}{(\pi\kappa^2)^{\frac{1}{4}}} \sum_{m=-\infty}^{\infty} e^{-(\bar{p}-m2\pi/\ell)^2/2\kappa^2}. \quad (\text{III.55})$$

To obtain the above result we used that according to the Poisson sum formula we have $\sqrt{a} \sum_m e^{-\pi a(m-b)^2} = \sum_n e^{2\pi i n b} e^{-\pi n^2/a}$, and that in the limit of large Gaussian envelopes we can approximate $e^{-x\kappa^2/2} \approx e^{-(nL\kappa)^2/2}$. Hence, the corresponding modular wave function $\langle \bar{x}, \bar{p} | \Psi_{G,c} \rangle$ is given by a Gaussian function with standard deviations Δ and

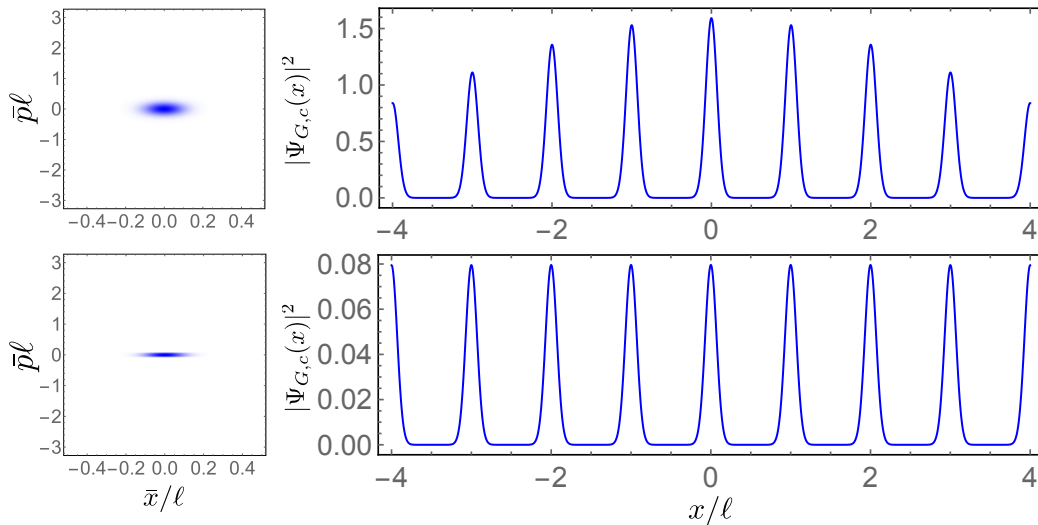


Figure III.5: Plots of the probability density of the state $|\Psi_{G,c}\rangle$ in the modular (left) and position (right) representation, for two sets of parameters: $\Delta = 0.1\ell$, $\kappa = 0.2/\ell$ (top) and $\Delta = 0.1\ell$, $\kappa = 0.01/\ell$ (bottom).

κ in the modular position and momentum variables, respectively, that is normalized and has quasi-periodic boundary conditions (see Eqs. (III.42) and (III.43)) on the domain $[-\ell/2, \ell/2] \times [-\pi/\ell, \pi/\ell]$. In Fig. III.4 we present plots of the probability density of the position wave function (III.52), as well as of its modular counterpart (III.53).

With smaller and smaller values of κ , while keeping Δ constant, the modular wave function becomes squeezed in the modular momentum compared to the modular position. This manifests itself in the position representation by an increasing width of the Gaussian that envelopes the Gaussian spikes with individual widths Δ (see Fig. III.4). Taking the limit $\kappa \rightarrow 0$ thus yields $C(\bar{p}) = \sum_m \delta(\bar{p} - m2\pi/\ell)$ in Eq. (III.55), and leaves us with a modular wave function that is infinitely squeezed in the modular position:

$$\Psi_{G,c}(\bar{x}, \bar{p}) \rightarrow T(\bar{x})\delta(\bar{p}). \quad (\text{III.56})$$

The wave function (III.56) is nonnormalizable and thus to some extent nonphysical even though it corresponds to a superposition of finitely squeezed Gaussian spikes in the position representation. Nevertheless, in limiting physical situation, such nonnormalizable wave functions can be used to make valid predictions. For instance, Eq. (III.56) can describe the wave front of a plane wave after it has passed through an infinitely extended diffraction grating. This scattering scenario will be the main subject of Chapter IV.

Up to now we have seen that states which are periodic in position or momentum space can be expressed nicely in the modular representation if the modular parameter ℓ is chosen equal to the corresponding period of the wave function (see Fig. III.4 and III.5). However, we can also express any other state in the modular representation. For instance, let's consider the state $|\Psi_{\text{Gauss}}\rangle$ with arbitrary Gaussian position wave

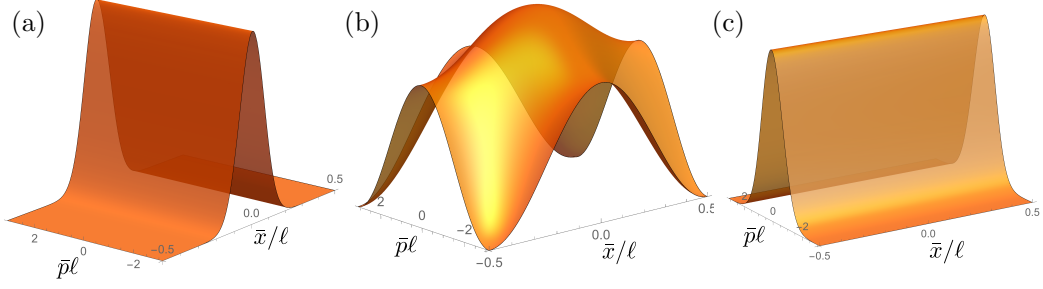


Figure III.6: Plots of the probability density of the Gaussian state $|\Psi_{\text{Gauss}}\rangle$ in the modular representation located at the origin, $x_0 = 0$ and $p_0 = 0$, for the widths: (a) $\sigma = 0.1\ell$, (b) $\sigma = 0.4\ell$ and (c) $\sigma = \ell$.

function (see also Eq. (II.32) and Fig. II.1 in Sec. II.1.3):

$$\Psi_{\text{Gauss}}(x) = \frac{1}{\pi^{1/4}\sigma^{1/2}} e^{-\frac{(x-x_0)^2}{2\sigma^2} + ip_0x - ix_0p_0} \quad (\text{III.57})$$

where x_0 and p_0 are the position and momentum offsets, respectively, and σ denotes the width of the Gaussian in position. Note that, up to a phase space rotation (II.38), Eq. (III.57) is the wave function of a general Gaussian state (see Eq. (II.80) and (II.81) in Sec. II.1.6). Transformed to the modular representation, with the help of Eq. (III.39), the wave function (III.57) reads:

$$\begin{aligned} \Psi_{\text{Gauss}}(\bar{x}, \bar{p}) &= \sqrt{\frac{\ell}{2\pi}} \sum_{n=-\infty}^{+\infty} \frac{e^{-i\bar{p}n\ell}}{\pi^{1/4}\sigma^{1/2}} e^{-\frac{(\bar{x}+n\ell-x_0)^2}{2\sigma^2} + i(\bar{x}+n\ell)p_0 - ix_0p_0} \\ &= \sqrt{\frac{\ell}{2\pi}} \frac{e^{-\frac{(\bar{x}-x_0)^2}{2\sigma^2} + i\bar{x}p_0 - ix_0p_0}}{\pi^{1/4}\sigma^{1/2}} \sum_{n=-\infty}^{+\infty} e^{-2in\left(\frac{\ell(\bar{p}-p_0)}{2} - i\frac{\ell(\bar{x}-x_0)}{2\sigma^2}\right)} e^{n^2 \ln\left[\exp\left(-\frac{\ell^2}{2\sigma^2}\right)\right]} \\ &= \sqrt{\frac{\ell}{2\pi}} \Psi_G(\bar{x}) \Theta_3\left(\frac{\ell(\bar{p}-p_0)}{2} - i\frac{\ell(\bar{x}-x_0)}{2\sigma^2}, \exp\left(-\frac{\ell^2}{2\sigma^2}\right)\right) \end{aligned} \quad (\text{III.58})$$

with the third elliptic theta-function

$$\Theta_3(u, q) = \sum_{n=-\infty}^{+\infty} q^{n^2} e^{-2inu} = 1 + 2 \sum_{n=1}^{\infty} q^{n^2} \cos(2nu). \quad (\text{III.59})$$

Hence, we see that the modular wave function (III.58) is given by a product of itself, restricted to the bounded modular position domain $[-\ell/2, \ell/2[$, and of a more complicated part which is defined in terms of the elliptic theta function (III.59). In Fig. III.6 we present three plots of the probability density of the modular wave function (III.58) for different widths σ of the Gaussian (III.57). We see that for small and large values of σ , compared to the length scale ℓ , the modular wave function becomes constant in the modular momentum and position coordinate, respectively, while the other coordinate displays the Gaussian profile corresponding to the position and momentum representa-

tion of $|\Psi_{\text{Gauss}}\rangle$. This can also be seen analytically by taking the limit $\ell/\sigma \rightarrow \infty$, for which $\exp(-\frac{\ell^2}{2\sigma^2}) \rightarrow 0$, and Eq. (III.58) becomes

$$\Psi_{\text{Gauss}}(\bar{x}, \bar{p}) \rightarrow \sqrt{\frac{\ell}{2\pi}} \Psi_{\text{Gauss}}(\bar{x}), \quad (\text{III.60})$$

where we used that $\Theta_3(u, q) \rightarrow 1$ for $q \rightarrow 0$. A similar argument holds for the reverse limit $\ell/\sigma \rightarrow 0$, because then the width of the wave function in momentum space becomes small compared to the length of the modular momentum interval $[-\pi/\ell, \pi/\ell]$. In an intermediate regime, as presented in Fig. III.6(b), the modular wave functions exhibits features of both the position and momentum wave functions.

As last example of states in the modular representation we want to mention an entangled two-mode state. The ideal nonnormalizable EPR state $|\Psi_{\text{EPR}}\rangle = \int dx |x\rangle |x+q\rangle$ has the position wave function

$$\Psi_{\text{EPR}}(x) = \delta(x_1 - x_2 + q). \quad (\text{III.61})$$

Transformed to the modular representation it becomes:

$$\begin{aligned} \Psi_{\text{EPR}}(\bar{x}_1, \bar{p}_1; \bar{x}_2, \bar{p}_2) &= \frac{\ell}{2\pi} \sum_{n_{1/2}=-\infty}^{+\infty} \delta(x_1 + q - x_2) e^{-i\bar{p}_1 n_1 \ell} e^{-i\bar{p}_2 n_2 \ell} \\ &= e^{-i\bar{p}_2(\bar{x}_1 + q - \bar{x}_1 + q)\ell} \delta(\bar{x}_1 + q - \bar{x}_2) \delta(\bar{p}_1 + \bar{p}_2), \end{aligned} \quad (\text{III.62})$$

where we used $\sum_{n_1=-\infty}^{+\infty} e^{-i(\bar{p}_1 + \bar{p}_2)n_1 \ell} = \frac{2\pi}{\ell} \delta(\bar{p}_1 + \bar{p}_2)$. If we also set $q = 0$, we arrive at:

$$\Psi_{\text{EPR}}^{q=0}(\bar{x}_1, \bar{p}_1; \bar{x}_2, \bar{p}_2) = \delta(\bar{x}_1 - \bar{x}_2) \delta(\bar{p}_1 + \bar{p}_2), \quad (\text{III.63})$$

or

$$|\Psi_{\text{EPR}}^{q=0}\rangle = \int_{-\ell/2}^{\ell/2} d\bar{x} \int_{-\pi/\ell}^{\pi/\ell} d\bar{p} |\bar{x}, -\bar{p}\rangle |\bar{x}, \bar{p}\rangle. \quad (\text{III.64})$$

With that we finish the general discussion about modular variables and their properties. In particular, we have seen that the commutativity of the modular position and momentum yields an alternative representation of the Hilbert space allowing to express CV quantum states in terms of a basis that is characterized by two bounded modular values. Finally, we presented several important examples of states expressed in the modular representation.

III.2 Dichotomizing the Hilbert space

In this Section we will show how the Hilbert space of a continuous-variable system can be divided in two or more equally sized parts in order to encode discrete quantum information in continuous-variable logical states. Doing so in the modular representation yields logical qubit states that are periodic with respect to the position and momentum. Further on, we introduce appropriate phase-space logical operations that allow to

manipulate the logical qubit states and thus the encoded discrete quantum information.

III.2.1 Identifying qubits in the modular variables representation

In the following, we will introduce logical qubit states by dichotomizing the Hilbert space with respect to the modular position \bar{x} . Therefore, let's start by recognizing that every state $|\Psi\rangle$, expressed in the modular representation (III.38), can be rewritten in a qubit-like fashion. From now on we will use a slightly more convenient definition of the modular position operator \hat{x} in Eq. (III.16) by setting $x_\ell = -\ell/4$, such that $\bar{x} \in [-\ell/4, 3\ell/4[$. Then, we split the domain of the integration over \bar{x} , in Eq. (III.38), into two equally sized domains. Such a splitting can be done in infinitely many ways, and in order to illustrate the principles of our ideas we discuss in detail the splitting into two subintervals, $[-\ell/4, \ell/4[$ and $[\ell/4, 3\ell/4[$, that yields:

$$|\Psi\rangle = \int_{-\ell/4}^{\ell/4} d\bar{x} \int_{-\pi/\ell}^{\pi/\ell} d\bar{p} \Psi(\bar{x}, \bar{p}) |\{\bar{x}, \bar{p}\}\rangle + \psi(\bar{x} + \ell/2, \bar{p}) |\{\bar{x} + \ell/2, \bar{p}\}\rangle. \quad (\text{III.65})$$

Further on, we redefine the complex modular wave function $\Psi(\bar{x}, \bar{p}) = |\Psi(\bar{x}, \bar{p})| e^{i\varphi(\bar{x}, \bar{p})}$ as:

$$\Psi(\bar{x}, \bar{p}) := f(\bar{x}, \bar{p}) \cos(\theta(\bar{x}, \bar{p})/2), \quad (\text{III.66})$$

$$\Psi(\bar{x} + \ell/2, \bar{p}) := f(\bar{x}, \bar{p}) e^{i\phi(\bar{x}, \bar{p})} \sin(\theta(\bar{x}, \bar{p})/2). \quad (\text{III.67})$$

where $f(\bar{x}, \bar{p}) = |f(\bar{x}, \bar{p})| e^{i\epsilon(\bar{x}, \bar{p})}$ is a complex function with $\int_{-\ell/4}^{\ell/4} d\bar{x} \int_{-\pi/\ell}^{\pi/\ell} d\bar{p} |f(\bar{x}, \bar{p})|^2 = 1$, and $\epsilon(\bar{x}, \bar{p})$, $\theta(\bar{x}, \bar{p})$ and $\phi(\bar{x}, \bar{p})$ are real functions, all defined on the domain $[-\ell/4, \ell/4[\times [-\pi/\ell, \pi/\ell[$. Inversely, they are related to the modular wave function $\Psi(\bar{x}, \bar{p})$ through:

$$|f(\bar{x}, \bar{p})| = \sqrt{|\Psi(\bar{x}, \bar{p})|^2 + |\Psi(\bar{x} + \ell/2, \bar{p})|^2}, \quad (\text{III.68})$$

$$\epsilon(\bar{x}, \bar{p}) = \varphi(\bar{x}, \bar{p}), \quad (\text{III.69})$$

and

$$\theta(\bar{x}, \bar{p}) = 2 \operatorname{arccot} \left| \frac{\Psi(\bar{x}, \bar{p})}{\Psi(\bar{x} + \ell/2, \bar{p})} \right|, \quad (\text{III.70})$$

$$\phi(\bar{x}, \bar{p}) = \varphi(\bar{x} + \ell/2, \bar{p}) - \varphi(\bar{x}, \bar{p}). \quad (\text{III.71})$$

Hence, we can express every state as:

$$|\Psi\rangle = \int_{-\ell/4}^{\ell/4} d\bar{x} \int_{-\pi/\ell}^{\pi/\ell} d\bar{p} f(\bar{x}, \bar{p}) |\tilde{\Psi}(\bar{x}, \bar{p})\rangle, \quad (\text{III.72})$$

where

$$|\tilde{\Psi}(\bar{x}, \bar{p})\rangle = \cos\left(\frac{\theta(\bar{x}, \bar{p})}{2}\right) |\bar{x}, \bar{p}\rangle + \sin\left(\frac{\theta(\bar{x}, \bar{p})}{2}\right) e^{i\phi(\bar{x}, \bar{p})} |\bar{x} + \ell/2, \bar{p}\rangle. \quad (\text{III.73})$$

(compare with Eq. (II.1) in Sec. II.1.1). Since Eq. (III.73) defines a continuum of two-level systems $\{|\bar{x}, \bar{p}\rangle, |\bar{x} + \ell/2, \bar{p}\rangle\}$ labeled by the pairs (\bar{x}, \bar{p}) , we can interpret Eq. (III.72)

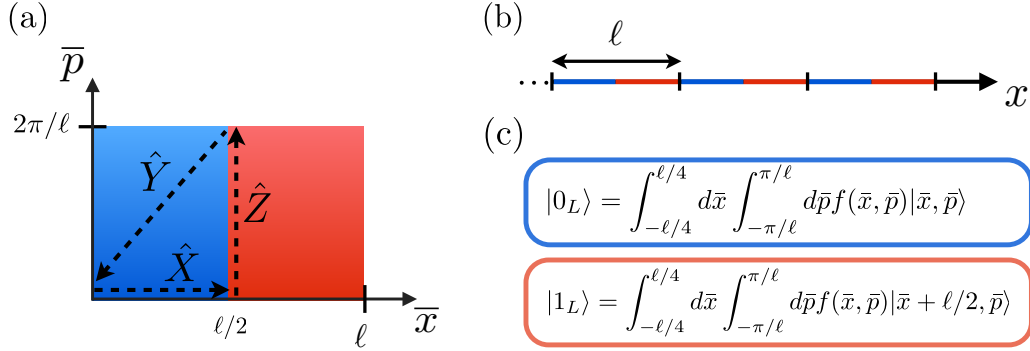


Figure III.7: (a) Schematic representation of the modular position and momentum domain split into two equal parts with respect to the modular position \bar{x} , and (b) the same splitting in the position domain. (c) The corresponding logical qubit states defined on the blue and red domains, respectively. The arrows in (a) illustrate the displacements implementing the three logical Pauli operation \hat{X} , \hat{Y} and \hat{Z} , as introduced in Sec. III.2.2.

as a continuous superposition of qubit states weighted by the complex factors $f(\bar{x}, \bar{p})$. We emphasize that, so far, no approximation or dichotomization has been performed and Eq. (III.72) provides simply an alternative way of writing an arbitrary state in the modular representation. Note that the choice of ℓ is also arbitrary, and modifying it for a given state modifies the definition of the functions (III.68)-(III.71) [Vernaz-Gris et al., 2014; Ketterer et al., 2016].

Equivalently, it is possible to define such a qubit structure in terms of the modular momentum \bar{p} . In this case, one splits the integration over \bar{p} , in Eq. (III.65), into two parts and obtains a similar result to Eqs. (III.72) and (III.73), now with

$$|\tilde{\Psi}_p(\bar{x}, \bar{p})\rangle = \cos\left(\frac{\theta_p(\bar{x}, \bar{p})}{2}\right)|\bar{x}, \bar{p}\rangle + \sin\left(\frac{\theta_p(\bar{x}, \bar{p})}{2}\right)e^{i\phi_p(\bar{x}, \bar{p})}|\bar{x}, \bar{p} + \pi/\ell\rangle. \quad (\text{III.74})$$

The p -subscripts in Eq. (III.74) emphasizes that the splitting was performed with respect to \bar{p} , and the corresponding relations for changing the representation are equivalent to Eqs. (III.68)-(III.71). In the remainder we omit this subscript because, if not indicated differently, we restrict ourselves to splittings with respect to \bar{x} . A generalization of the above equations to the case of qudit systems, by splitting the integration in Eq. (III.65) into d -parts instead of two, is possible and will be provided later on.

In the following, in order to encode discrete quantum information in CV states, we assume that $\theta(\bar{x}, \bar{p}) = \theta$ and $\phi(\bar{x}, \bar{p}) = \phi$ are constant functions such that Eq. (III.72) becomes $|\Psi\rangle = \cos(\theta/2)|0_L\rangle + \sin(\theta/2)e^{i\phi}|1_L\rangle$ with logical qubit states, defined as:

$$|0_L\rangle = \int_{-\ell/4}^{\ell/4} d\bar{x} \int_{-\pi/\ell}^{\pi/\ell} d\bar{p} f(\bar{x}, \bar{p}) |\bar{x}, \bar{p}\rangle, \quad (\text{III.75})$$

$$|1_L\rangle = \int_{-\ell/4}^{\ell/4} d\bar{x} \int_{-\pi/\ell}^{\pi/\ell} d\bar{p} f(\bar{x}, \bar{p}) |\bar{x} + \ell/2, \bar{p}\rangle, \quad (\text{III.76})$$

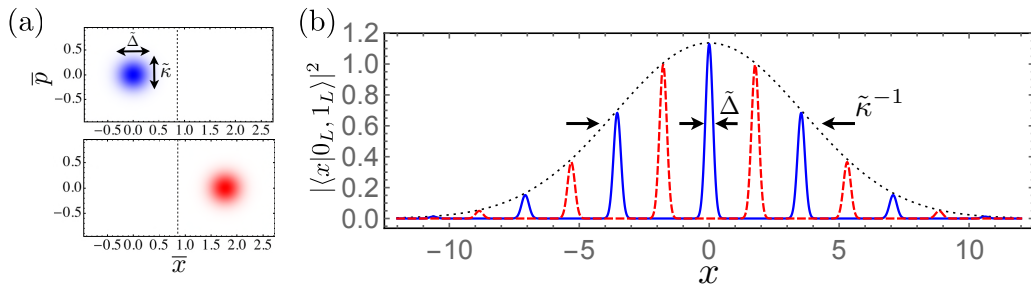


Figure III.8: Plots of the probability densities of the logical states $|0_L\rangle$ and $|1_L\rangle$ in the modular (left) and position (right) representation. For the modular probability density the full widths at half maximum (FWHM) in the modular position and momentum are given by $\tilde{\Delta} = 2\sqrt{\ln 2}\Delta$ and $\tilde{\kappa} = 2\sqrt{\ln 2}\kappa$, respectively, where $\Delta = 0.1\ell$ and $\kappa = 0.1(2\pi/\ell)$ are the standard deviations that define the corresponding modular wave function (III.53). The distance between the Gaussian spikes of each state $|0_L\rangle$ and $|1_L\rangle$, respectively, are chosen to be $\ell = 2\sqrt{\pi}$.

These logical qubit states (Eqs. (III.75) and (III.76)) reflect a dichotomization of the Hilbert space with respect to the modular position \bar{x} , as illustrated in Fig. III.7. The exact choice of $f(\bar{x}, \bar{p})$ is arbitrary as long as it emerges from a properly defined modular wave function $\Psi(\bar{x}, \bar{p})$ (see Sec. III.1.4). In this respect, Eqs. (III.42)-(III.43) and (III.68)-(III.71) imply that $f(\bar{x}, \bar{p})$ fulfills the periodicity conditions, $f(\bar{x} + \ell/2, \bar{p}) = f(\bar{x}, \bar{p})e^{i\phi}$ and $f(\bar{x}, \bar{p} + 2\pi/\ell) = f(\bar{x}, \bar{p})$.

For instance, we can choose $f(\bar{x}, \bar{p})$ as being a two dimensional Gaussian function centered at the origin with widths Δ and κ in the modular position and momentum variables, respectively. In position space these states belong to two combs of Gaussian spikes with width Δ and a Gaussian envelope of width κ^{-1} that are shifted with respect to each other by $\ell/2$, in accordance with the discussion in Sec. III.1.5. In Fig. III.8, we present the plots of the probability densities of this type of logical states in the modular and position representation, respectively. Note, that this correspondence between modular and position wave functions is true if $\Delta/\ell \ll 1$ and $\kappa\ell \ll 1$, as discussed in Sec. III.1.4. It ensures also that the corresponding modular wave functions vanish on the boundaries of their domains such that the above periodicity conditions for $f(\bar{x}, \bar{p})$ hold.

Finally, we want to discuss a special case of the logical states $|0_L\rangle$ and $|1_L\rangle$. If, in the above example, we take the limit $\Delta, \kappa \rightarrow 0$, that is of vanishing width of the two-dimensional Gaussian $f(\bar{x}, \bar{p})$, we arrive at the following logical states:

$$|0_{\text{GKP}}\rangle = |\bar{x} = 0, \bar{p} = 0\rangle = \sum_n |\ell(2n)/2\rangle_x, \quad (\text{III.77})$$

$$|1_{\text{GKP}}\rangle = |\bar{x} = \frac{\ell}{2}, \bar{p} = 0\rangle = \sum_n |\ell(2n+1)/2\rangle_x. \quad (\text{III.78})$$

This particular case of the logical states (III.75) and (III.76) is known by a previous work of Gottesman, Kitaev and Preskill (GKP), who studied how to encode a qubit in

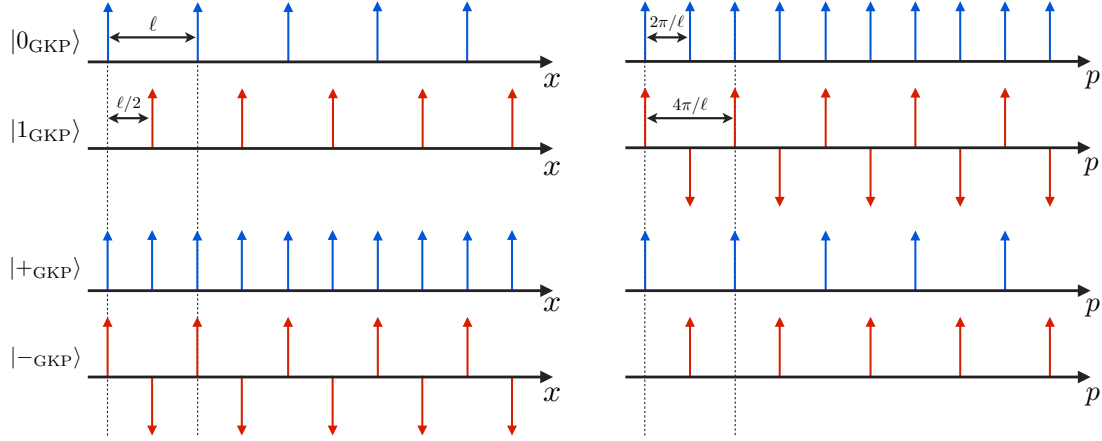


Figure III.9: Schematic plots of the wave functions of the GKP logical states $|0_{\text{GKP}}\rangle$ and $|1_{\text{GKP}}\rangle$ in the position (left) and momentum (right) representation, respectively. The arrows represent combs of delta function shifted by $\ell/2$ with respect to each other. The lower two plots depict the the logical states of the alternative basis $|\pm_{\text{GKP}}\rangle = (|0_{\text{GKP}}\rangle \pm |1_{\text{GKP}}\rangle)/\sqrt{2}$. If one chooses $\ell = 2\sqrt{\pi}$ the the two logical bases $|(0/1)_{\text{GKP}}\rangle$ and $|\pm_{\text{GKP}}\rangle$ have a symmetric structure because they are shifted by the same amount in the position and momentum representation, respectively.

an oscillator [Gottesman et al., 2001]. In the particular case $\ell = 2\sqrt{\pi}$, the states (III.77) and (III.78) become symmetric in the position and momentum space ($2\pi/\ell = \sqrt{\pi}$), as illustrated in Fig. III.9.

This encoding, in the following referred to as GKP encoding, has several useful properties, some of which will come back later on in the course of this thesis. However, its drawback is that the logical states $|0_{\text{GKP}}\rangle$ and $|1_{\text{GKP}}\rangle$ are modular eigenstates, *i.e.* infinite superpositions of position eigenstates, and thus unphysical. GKP deal with this problem by using imperfect logical states, similar to those shown in Fig. III.8, that are close to the real logical states (III.77) and (III.78), but introduce errors when used in actual computations. In turn this problem can be solved by applying an appropriate error correction protocol that allows to counteract the errors induced by imperfect logical states [Gottesman et al., 2001; Glancy and Knill, 2006]. Even though this might be the right strategy to follow if one wants to implement full-fledged fault-tolerant quantum computer operating on a CV system, for realizations of more modest quantum information protocols, involving a small number of logical qubits and gates, it is a rather excessive endeavor. That is why here we focus on the more general definitions (III.75) and (III.76), allowing for a freedom of choice of the wave function $f(\bar{x}, \bar{p})$. In the following we will show how to manipulate these logical states with appropriately defined logical operations.

III.2.2 Single and two qubit logical operations

III.2.2.1 Logical Pauli operations

In this section, we will continue by introducing logical operations that allow for a manipulation of the logical qubit states introduced in the last Section. One of the most basic set of single qubit operations is that of the single qubit Pauli operations (II.3), (II.4) and (II.5). In order to find such logical Pauli operations implemented by unitary phase space operations, we start by expressing the single mode phase space displacement operator (II.63) in the modular representation. Calculating its action on a modular eigenstate (III.34), yields

$$\hat{D}(\nu, \mu)|\bar{x}, \bar{p}\rangle = e^{-i\frac{\nu\mu}{2}} \frac{e^{-i\bar{p}\bar{x}}}{\sqrt{\ell}} \sum_{m=-\infty}^{+\infty} e^{-i(\bar{p}+m\frac{2\pi}{\ell})\nu} e^{-i2\pi m\bar{x}/\ell} |\bar{p} + m\hbar/\ell + \mu\rangle, \quad (\text{III.79})$$

and, together with (III.37) and $\sum_{m=-\infty}^{+\infty} e^{i2\pi m(\bar{x}' - \bar{x} - \nu)/\ell} = \ell \sum_{n=-\infty}^{+\infty} \delta(\bar{x}' - \bar{x} - \nu - n\ell)$, becomes

$$\hat{D}(\nu, \mu)|\bar{x}, \bar{p}\rangle = e^{-i\frac{\nu\mu}{2}} e^{i(\bar{p}+\mu)(\overline{\bar{x}+\nu})} e^{-i\bar{p}(\overline{\bar{x}+\nu})} |\overline{\bar{x} + \nu}, \overline{\bar{p} + \mu}\rangle. \quad (\text{III.80})$$

Hence, we find that

$$\hat{D}(\nu, \mu) = e^{-i\frac{\nu\mu}{2}} \int_{-\ell/4}^{3\ell/4} d\bar{x} \int_{-\pi/\ell}^{\pi/\ell} d\bar{p} e^{i(\bar{p}+\mu)(\overline{\bar{x}+\nu})} e^{-i\bar{p}(\overline{\bar{x}+\nu})} |\overline{\bar{x} + \nu}, \overline{\bar{p} + \mu}\rangle \langle \bar{x}, \bar{p}|. \quad (\text{III.81})$$

where overlined values denote the corresponding modular parts of position and momentum, respectively. Equation (III.81) shows that a phase space displacement by (ν, μ) leads to a displacement of the corresponding modular position and momentum accompanied by the generation of additional relative phases. The latter encode information about the change of the discrete position and momentum values, $\ell\hat{N}_x$ and $2\pi/\ell\hat{N}_p$, induced by displacements in position or momentum that are large then ℓ or $2\pi/\ell$, respectively.

It is the displacement operator (III.81) that we exploit to define logical Pauli operations. For instance, by setting the displacements (ν, μ) equal $(0, 2\pi/\ell)$ or $(\ell/2, 0)$, respectively, and by splitting the integration over \bar{x} in two parts, as in Eq. (III.65) in the last Section, we reveal the operators:

$$\hat{Z} = e^{2\pi i\hat{x}/\ell} = \int_{-\ell/4}^{\ell/4} d\bar{x} \int_{-\pi/\ell}^{\pi/\ell} d\bar{p} e^{2\pi i\bar{x}/\ell} \hat{\sigma}_z(\bar{x}, \bar{p}), \quad (\text{III.82})$$

$$\hat{X} = e^{-i\hat{p}\ell/2} = \int_{-\ell/4}^{\ell/4} d\bar{x} \int_{-\pi/\ell}^{\pi/\ell} d\bar{p} e^{-i\bar{p}\ell/2} \hat{\sigma}_x(\bar{x}, \bar{p}), \quad (\text{III.83})$$

where we introduced the (\bar{x}, \bar{p}) -dependent Pauli matrices

$$\hat{\sigma}_z(\bar{x}, \bar{p}) = \|\bar{x}, \bar{p}\rangle \langle \bar{x}, \bar{p}| - \|\bar{x} + \ell/2, \bar{p}\rangle \langle \bar{x} + \ell/2, \bar{p}|, \quad (\text{III.84})$$

$$\hat{\sigma}_x(\bar{x}, \bar{p}) = \|\bar{x}, \bar{p}\rangle \langle \bar{x} + \ell/2, \bar{p}| + \|\bar{x} + \ell/2, \bar{p}\rangle \langle \bar{x}, \bar{p}|, \quad (\text{III.85})$$

with $||\bar{x}, \bar{p}\rangle = e^{-i\bar{p}\ell/4}|\bar{x}, \bar{p}\rangle$ and $||\bar{x} + \ell/2, \bar{p}\rangle = e^{i\bar{p}\ell/4}|\bar{x} + \ell/2, \bar{p}\rangle$. Equations (III.82) and (III.83) thus provide analogs of the Pauli operators $\hat{\sigma}_z$ and $\hat{\sigma}_x$ acting on the logical qubit states (III.75) and (III.76). The analog of the third Pauli operator $\hat{\sigma}_y$ can be obtained from the product of the former two $\hat{Y} = i\hat{X}^\dagger\hat{Z}^\dagger$, yielding:

$$\hat{Y} = \int_{-\ell/4}^{\ell/4} d\bar{x} \int_{-\pi/\ell}^{\pi/\ell} d\bar{p} e^{i\bar{p}\ell/2 - 2\pi i\bar{x}/\ell} \hat{\sigma}_y(\bar{x}, \bar{p}), \quad (\text{III.86})$$

with

$$\hat{\sigma}_y(\bar{x}, \bar{p}) = i(|\bar{x} + \ell/2, \bar{p}\rangle\langle\bar{x}, \bar{p}| - |\bar{x}, \bar{p}\rangle\langle\bar{x} + \ell/2, \bar{p}|). \quad (\text{III.87})$$

On the other hand, using the commutator rules for the phase space displacement operator, we find that $\hat{X}^\dagger\hat{Z}^\dagger = -i\hat{D}^\dagger(\ell/2, 2\pi/\ell)$, yielding $\hat{Y} = \hat{D}^\dagger(\ell/2, 2\pi/\ell)$. Thus, as illustrated in Fig. III.7(a), the three displacements implementing the logical Pauli operations \hat{X} , \hat{Y} and \hat{Z} , form a triangular in phase space that encloses an area of $\pi/2$. The latter is closely related to the fact that the anti-commutators between the displacements (III.83), (III.82) and (III.86), vanish [Asadian et al., 2015], yielding the anti-commutation relations of our logical Pauli operators:

$$\{\hat{Z}, \hat{X}\} = \{\hat{Z}, \hat{Y}\} = \{\hat{X}, \hat{Y}\} = 0, \quad (\text{III.88})$$

as expected from the algebra of Pauli matrices.

However, despite the similarities, the above defined logical operations are not completely equivalent to a Pauli algebra in the general case. This becomes apparent from their commutation relations which are found to be $[\hat{X}, \hat{Y}] = 2i\hat{Z}^\dagger$, $[\hat{Z}, \hat{X}] = 2i\hat{Y}^\dagger$ and $[\hat{Y}, \hat{Z}] = 2i\hat{X}^\dagger$. They resemble those of the Pauli matrices (compare with Eq. (II.6)), but since the operators \hat{X} , \hat{Y} and \hat{Z} are not hermitian, deviate in the fact that the commutator between each of them yields the adjoint of the third one. Hence, the above introduced logical Pauli operations do not form a Pauli algebra (see Sec. II.1.1) but, as we will see in the remainder of this Chapter, they are still useful with respect to the implementation of certain quantum information protocols. We further note that, in the specific case when applying \hat{X} , \hat{Y} and \hat{Z} to perfect GKP states, *i.e.* those logical states (III.75) and (III.76) which are equal to modular eigenstates, they operate as usual Pauli matrices. Restricted to this subspace, our logical Pauli operations act as Hermitian operators ($\hat{X} = \hat{X}^\dagger$, $\hat{Y} = \hat{Y}^\dagger$ and $\hat{Z} = \hat{Z}^\dagger$), and the above commutation relations become those of a perfect Pauli algebra.

The fact that we are dealing with a nonperfect Pauli algebra has some consequences. For instance, if we calculate the square of one of the logical Pauli operators we get:

$$\hat{Z}^2 = e^{4\pi i\hat{x}/\ell} = \int_{-\ell/4}^{\ell/4} d\bar{x} \int_{-\pi/\ell}^{\pi/\ell} d\bar{p} e^{4\pi i\bar{x}/\ell} \mathbb{1}(\bar{x}, \bar{p}), \quad (\text{III.89})$$

with $\mathbb{1}(\bar{x}, \bar{p}) = ||\bar{x}, \bar{p}\rangle\langle\bar{x}, \bar{p}| + ||\bar{x} + \ell/2, \bar{p}\rangle\langle\bar{x} + \ell/2, \bar{p}|$, which differs from an identity through the appearance of a \bar{x} dependent phase factor under the integral. Similarly, such phase factors also appear when manipulating the states $|0_L\rangle$ and $|1_L\rangle$ with one of the logical operations (III.82), (III.83) or (III.86). We will see later on that these phase factors become redundant if one considers only protocols involving a specific class of

modular variables as readout observables. In the light of the definition of these readout observables, which will be given in Sec. III.3, we will also introduce appropriate rotation operators allowing to perform measurements according to different mutually unbiased bases of the logical space (see Sec. III.3.2). Consequently, the above defined logical states and Pauli operations, together with the modular readout observables and the corresponding rotations (see Sec. III.3), establish a solid framework to handle CV quantum information from a quantum measurement point of view. In particular, this renders the formulation of test of fundamental properties of quantum mechanics possible, as presented in Chapter IV.

III.2.2.2 Logical Clifford operations

Further on, before proceeding with the definition of the above mentioned modular readout observables and the corresponding rotation operations in Sec. III.3, we want to review some other single and two qubit logical operations, which have been introduced also by GKP [Gottesman et al., 2001].

Let's start with the single qubit phase gate \hat{S} (see Eq. (II.11)) which can be realized by the CV shear operation $\hat{N}(s) = e^{is\hat{x}^2}$ (see Sec. II.1.3), with $s = 1/(2d^2)$ and $d = \ell/(2\sqrt{\pi})$. It transforms the logical Pauli operators, (III.82) and (III.83), as:

$$\hat{X} \rightarrow \int_{-\ell/4}^{\ell/4} d\bar{x} \int_{-\pi/\ell}^{\pi/\ell} d\bar{p} e^{2\pi i \bar{x}/\ell - i\bar{p}\ell/2} \hat{\sigma}_y(\bar{x}, \bar{p}) = i\hat{X}^\dagger \hat{Z}^\dagger = \hat{Y}, \quad (\text{III.90})$$

and $\hat{Z} \rightarrow Z$. In this case, the shear implements a rotation of \hat{X} around the z-axis of the Bloch sphere. Further on, the Hadamard gate \hat{H} can be directly realised using a rescaled Fourier transform $\hat{\mathcal{F}}_d = e^{i\frac{\pi}{4}(\hat{x}^2/d^2 + \hat{p}^2 d^2)}$ (compare with the optical Fourier transform introduced in Sec. II.3.1), with d chosen as above, which transforms the logical Pauli operators as $\hat{X} \rightarrow \hat{Z}$ and $\hat{Z} \rightarrow \hat{X}^{-1}$. In combination with the above defined logical phase-gate, we can define the Fourier transformed shear $e^{i\hat{p}^2 d^2/2}$, which implements a $\pi/2$ -rotation of \hat{Z} around the x-axis, namely $\hat{Z} \rightarrow \hat{Y}$ and $\hat{X} \rightarrow -\hat{Y}$. This gate will play an important role in the next Chapter IV, where we will introduce a framework to process quantum information based on the near-field interference of the spatial distribution of single photons (see Sec. II.3.1). Finally, the two-qubit Clifford operator \hat{C}_{NOT} can be realized by the two-mode Gaussian unitary $e^{-i\hat{x}_a \otimes \hat{p}_b}$ which implements the operations $\hat{X}^a \otimes \hat{X}^b \rightarrow \hat{X}^a \otimes \hat{X}^{b-a}$ and $\hat{Z}^a \otimes \hat{Z}^b \rightarrow \hat{X}^{a+b} \otimes \hat{Z}^b$, with $a, b = 0, 1$. Note, that the logical controlled-phase gate \hat{C}_Z follows from \hat{C}_{NOT} by an additional application of $\hat{\mathcal{F}}$ on the second mode.

Note that the above logical operations implement the desired Clifford group operation only if applied to perfect GKP logical states $|0_{\text{GKP}}\rangle = |0, 0\rangle$ and $|1_{\text{GKP}}\rangle = |\ell/2, 0\rangle$. This can be seen more clearly when calculating the action of the corresponding operations on modular eigenstates $|\bar{x}, \bar{p}\rangle$. For the shear this yields, for instance:

$$e^{i\hat{x}^2/(2d^2)} |\bar{x}, \bar{p}\rangle = e^{i\bar{x}^2/(2d^2)} |\bar{x}, \overline{\bar{p} + 2\bar{x}/d^2}\rangle. \quad (\text{III.91})$$

thus showing that, if we restrict ourselves to the subspace spanned by $|0, 0\rangle$ and $|\ell/2, 0\rangle$, we recover the single qubit phase operation. Similarly, the action of the Fourier trans-

form $\hat{\mathcal{F}}$ and of the two-mode \hat{C}_X operator, on a modular eigenstate (III.34), yield:

$$\hat{\mathcal{F}}|\bar{x}, \bar{p}\rangle = \frac{1}{d\sqrt{2}} e^{-i\bar{x}\bar{p}} \left[|\bar{p}d^2, -\bar{x}/d^2\rangle + e^{-i2\pi\bar{x}/\ell} |\bar{p}d^2 + \ell/2, -\bar{x}/d^2\rangle \right], \quad (\text{III.92})$$

and

$$e^{i\hat{x}_a \otimes \hat{x}_b / d^2} |\bar{x}_a, \bar{p}_a\rangle |\bar{x}_b, \bar{p}_b\rangle = e^{i\bar{x}\bar{x}'/d^2} |\bar{x}, \bar{p} + \bar{x}'/d^2\rangle |\bar{x}', \bar{p}' + \bar{x}/d^2\rangle, \quad (\text{III.93})$$

respectively. As for the shear, when restricted to the GKP subspace, Eq. (III.92) and (III.93) perfectly implement the qubit gates \hat{H} and \hat{C}_{NOT} .

This shows that, as discussed at the end of Sec. III.2.1, finite squeezing of the logical states $|0_L\rangle$ and $|1_L\rangle$ (see Fig. III.8) leads to a faulty implementation of the above defined logical Clifford operations. Faulty means here that, after several gate operations, the signal will blur out and a distinction of $|0_L\rangle$ and $|1_L\rangle$ is not possible anymore. To circumvent such errors one has to apply an error correction protocol, consisting of syndrome measurements and correction operations, in order to keep the squeezing on a tolerable level [Gottesman et al., 2001; Glancy and Knill, 2006; Menicucci, 2014].

Finally, even though this is beyond the scope of this thesis, we want to mention the possibility to render the above operations universal by supplementing them with one single qubit non-Clifford operation, such as the $\pi/8$ -gate (see Eq. II.10). In [Gottesman et al., 2001], it was shown that such a logical non-Clifford operation can be realized on GKP states with the unitary $\hat{U} = \exp \left[i\frac{\pi}{4} (2(\hat{x}2/\ell)^3 + (\hat{x}2/\ell)^2 - 2(\hat{x}2/\ell)) \right]$, which is equal to a product of Gaussian and one non-Gaussian operations. As already discussed in Sec. II.3.1 and II.3.2, an implementation of such a unitary is straightforward when exploiting the spatial degrees of freedom of single photons as CV system, but rather challenging in terms of the quadratures of a single mode of the electromagnetic field. Alternatively, the $\pi/8$ -gate can be realized by gate teleportation of so-called magic states [Gottesman et al., 2001].

We finish here our deliberations about different logical operations and turn to the question of how to readout the encoded discrete quantum information from our CV logical states in terms of measurements of modular variables.

III.3 State readout with modular variables

In this Section, we will discuss how the discrete quantum information that is encoded in the above introduced logical states can be readout through measurements of judiciously chosen modular variables. In this respect, we start first by introducing an abstract set of observables whose expectation values are related to the Bloch vector of the encoded qubit state and discuss some of their properties. Later on, we will relate these observables to specific classes of modular variables revealing their role as proper phase space observables.

III.3.1 Definition of modular readout observables

The readout of discrete quantum information that is encoded with respect to the logical states (III.75) and (III.76) can be performed using a specific set of hermitian operators,

to which we refer to as *modular readout observables*. In analogy to the logical Pauli operations, introduced in Sec. III.2.2, we define such set of readout observables as:

$$\hat{\Gamma}_\beta = \int_{-\ell/4}^{\ell/4} d\bar{x} \int_{-\pi/\ell}^{\pi/\ell} d\bar{p} \zeta_\beta(\bar{x}, \bar{p}) \hat{\sigma}_\beta(\bar{x}, \bar{p}), \quad \beta = x, y, z \quad (\text{III.94})$$

where $\zeta_\beta(\bar{x}, \bar{p})$ are arbitrary real functions with domain $[-\ell/4, \ell/4] \times [-\pi/\ell, \pi/\ell]$, and the operators $\hat{\sigma}_\beta(\bar{x}, \bar{p})$ are defined as in Eqs. (III.84), (III.85) and (III.87). In Sec. III.3.3 we will show which class of general phase space operators $F(\hat{x}, \hat{p})$ obey such a representation, however, for the moment we take their form as granted in order to discuss several important properties. We note first that the operators (III.84), (III.85) and (III.87) behave as Pauli operators in each of the subspaces defined by the tuples (\bar{x}, \bar{p}) , as reflected by the relation:

$$\hat{\sigma}_\alpha(\bar{x}, \bar{p}) \hat{\sigma}_\beta(\bar{x}', \bar{p}') = \delta(\bar{x}' - \bar{x}) \delta(\bar{p}' - \bar{p}) \left[i \sum_{\gamma=x,y,z} \varepsilon_{\alpha\beta\gamma} \hat{\sigma}_\gamma(\bar{x}, \bar{p}) + \delta_{\alpha,\beta} \mathbb{1}(\bar{x}, \bar{p}) \right] \quad (\text{III.95})$$

where $\alpha, \beta = x, y, z$ and $\mathbb{1}(\bar{x}, \bar{p}) = \|\bar{x}, \bar{p}\rangle \langle \bar{x}, \bar{p}| + \|\bar{x} + \ell/2, \bar{p}\rangle \langle \bar{x} + \ell/2, \bar{p}|$. The relation (III.95) resembles the one of a real Pauli algebra, which was given in Eq. (II.6), with additional delta functions ensuring that the products of Pauli operators corresponding to different subspaces, labeled by (\bar{x}, \bar{p}) and (\bar{x}', \bar{p}') , respectively, vanish. Furthermore, the matrix elements of these (\bar{x}, \bar{p}) -dependent Pauli matrices in the modular basis read:

$$\begin{aligned} \langle \bar{x}', \bar{p}' | \hat{\sigma}_z(\bar{x}_0, \bar{p}_0) | \bar{x}, \bar{p} \rangle &= \delta(\bar{p} - \bar{p}_0) \delta(\bar{p}' - \bar{p}_0) \\ &\times \left[\delta(\bar{x} - \bar{x}_0) \delta(\bar{x}' - \bar{x}_0) \pm \delta(\bar{x} - \frac{\ell}{2} - \bar{x}_0) \delta(\bar{x}' - \frac{\ell}{2} - \bar{x}_0) \right], \end{aligned} \quad (\text{III.96})$$

$$\begin{aligned} \langle \bar{x}', \bar{p}' | \hat{\sigma}_x(\bar{x}_0, \bar{p}_0) | \bar{x}, \bar{p} \rangle &= \delta(\bar{p} - \bar{p}_0) \delta(\bar{p}' - \bar{p}_0) \\ &\times \left[\delta(\bar{x}' - \bar{x}_0) \delta(\bar{x} - \frac{\ell}{2} - \bar{x}_0) e^{-i\bar{p}\ell/2} + \delta(\bar{x}' - \frac{\ell}{2} - \bar{x}_0) \delta(\bar{x} - \bar{x}_0) e^{i\bar{p}\ell/2} \right], \end{aligned} \quad (\text{III.97})$$

$$\begin{aligned} \langle \bar{x}', \bar{p}' | \hat{\sigma}_y(\bar{x}_0, \bar{p}_0) | \bar{x}, \bar{p} \rangle &= -i \delta(\bar{p} - \bar{p}_0) \delta(\bar{p}' - \bar{p}_0) \\ &\times \left[\delta(\bar{x}' - \bar{x}_0) \delta(\bar{x} - \frac{\ell}{2} - \bar{x}_0) e^{-i\bar{p}\ell/2} - \delta(\bar{x}' - \frac{\ell}{2} - \bar{x}_0) \delta(\bar{x} - \bar{x}_0) e^{i\bar{p}\ell/2} \right]. \end{aligned} \quad (\text{III.98})$$

Using Eqs. (III.95)-(III.98), we can calculate the expectation value of the observables (III.94) with respect to an arbitrary CV state expressed in the modular representation (III.72), yielding:

$$\langle \hat{\Gamma}_x \rangle = \int_{-\ell/4}^{\ell/4} d\bar{x} \int_{-\pi/\ell}^{\pi/\ell} d\bar{p} \zeta_x(\bar{x}, \bar{p}) |f(\bar{x}, \bar{p})|^2 \sin(\theta(\bar{x}, \bar{p})) \cos(\phi(\bar{x}, \bar{p})), \quad (\text{III.99})$$

$$\langle \hat{\Gamma}_y \rangle = \int_{-\ell/4}^{\ell/4} d\bar{x} \int_{-\pi/\ell}^{\pi/\ell} d\bar{p} \zeta_y(\bar{x}, \bar{p}) |f(\bar{x}, \bar{p})|^2 \sin(\theta(\bar{x}, \bar{p})) \sin(\phi(\bar{x}, \bar{p})), \quad (\text{III.100})$$

$$\langle \hat{\Gamma}_z \rangle = \int_{-\ell/4}^{\ell/4} d\bar{x} \int_{-\pi/\ell}^{\pi/\ell} d\bar{p} \zeta_z(\bar{x}, \bar{p}) |f(\bar{x}, \bar{p})|^2 \cos(\theta(\bar{x}, \bar{p})). \quad (\text{III.101})$$

For a more detailed calculation we refer to Appendix B.2. In a vector notation we can

express Eqs. (III.99)-(III.101) as

$$\langle \hat{\Gamma} \rangle = \int_{-\ell/4}^{\ell/4} d\bar{x} \int_{-\pi/\ell}^{\pi/\ell} d\bar{p} |f(\bar{x}, \bar{p})|^2 (\zeta(\bar{x}, \bar{p}) \cdot \mathbf{v}(\bar{x}, \bar{p})), \quad (\text{III.102})$$

where $\zeta(\bar{x}, \bar{p}) = (\zeta_x(\bar{x}, \bar{p}), \zeta_y(\bar{x}, \bar{p}), \zeta_z(\bar{x}, \bar{p}))^T$, and

$$\begin{aligned} \mathbf{v}(\bar{x}, \bar{p}) &= (v_x(\bar{x}, \bar{p}), v_y(\bar{x}, \bar{p}), v_z(\bar{x}, \bar{p}))^T \\ &= (\sin(\theta(\bar{x}, \bar{p})) \cos(\phi(\bar{x}, \bar{p})), \sin(\theta(\bar{x}, \bar{p})) \sin(\phi(\bar{x}, \bar{p})), \cos(\theta(\bar{x}, \bar{p})))^T. \end{aligned} \quad (\text{III.103})$$

Further on, we can show that the sum over the squares of the expectation values (III.99), (III.100) and (III.101) is bounded:

$$\langle \hat{\Gamma} \rangle^2 = \langle \hat{\Gamma}_x \rangle^2 + \langle \hat{\Gamma}_y \rangle^2 + \langle \hat{\Gamma}_z \rangle^2 \leq \left(\max_{\bar{x}, \bar{p}, \alpha} |\zeta_\beta(\bar{x}, \bar{p})| \right)^2, \quad (\text{III.104})$$

where we used that $(v_\beta(\bar{x}, \bar{p}) - v_\beta(\bar{x}', \bar{p}'))^2 \geq 0$, the triangle inequality and that the Bloch vector of a pure qubit state is normalized to 1 (see Appendix B for more details of this calculation). Hence, we found that the norm of the vector formed by the expectation values of the operators (III.94) with respect to an arbitrary state CV state $|\Psi\rangle$ is bounded by $\max_{\bar{x}, \bar{p}, \alpha} |\zeta_\beta(\bar{x}, \bar{p})|$. Furthermore, if we restrict ourselves to the case $\theta(\bar{x}, \bar{p}) = \theta$ and $\phi(\bar{x}, \bar{p}) = \phi$, and thus encode a single qubit state with Bloch vector $\mathbf{v} = (\sin \theta \cos \phi, \sin \theta \sin \phi, \cos \theta)^T$ into the CV state $|\Psi\rangle$ in terms of the logical states $|0_L\rangle$ and $|1_L\rangle$, we find that the expectation values (III.99), (III.100) and (III.101) become:

$$\langle \hat{\Gamma}_\beta \rangle_{|\Psi\rangle} = K_\beta v_\beta, \quad (\text{III.105})$$

where $\beta = x, y, z$, $K_\beta = \int_{-\ell/4}^{\ell/4} d\bar{x} \int_{-\pi/\ell}^{\pi/\ell} d\bar{p} \zeta_\beta(\bar{x}, \bar{p}) |f(\bar{x}, \bar{p})|^2$ and v_β are the Bloch vector components of the qubit state that has been encoded into the CV state $|\Psi\rangle$. Hence, we find that the expectation values of the observables (III.94) are proportional to the Bloch vector of the encoded qubit states, whereas the proportionality factors K_β are determined by the overlap of the modulus square of the logical wave function $f(\bar{x}, \bar{p})$ with the functions $\zeta_\beta(\bar{x}, \bar{p})$ that define the exact form of the observables (III.94). This allows one to draw conclusions about the state of the logical qubit through measurements of the expectation values $\langle \hat{\Gamma}_\beta \rangle$.

The form of the operators (III.94) is chosen so as to be operationally analogous to the logical Pauli operations, defined in Eqs. (III.82), (III.83) and (III.86). Interestingly, unwanted phase factors, appearing when manipulating the states $|0_L\rangle$ and $|1_L\rangle$ with some logical operation, disappear. For instance, if we consider the operator \hat{Z}^2 (see Eq. (III.89)) and apply it to an arbitrary state of the logical space $|\Psi\rangle = \cos \theta |0_L\rangle + \sin \theta e^{i\phi} |1_L\rangle$, we obtain $|\Psi'\rangle = \hat{Z}^2 |\Psi\rangle$, where $|\Psi'\rangle$ differs from $|\Psi\rangle$ by a modular position (momentum) dependent phase factor, but the expectation value (III.105) yields $\langle \hat{\Gamma}_\beta \rangle_{\Psi'} = \langle \hat{\Gamma}_\beta \rangle_{\Psi}$, for all $\beta = x, y, z$. Therefore, for implementations of protocols involving measurements of the expectation values $\langle \hat{\Gamma}_\beta \rangle_{|\psi\rangle}$, the \hat{Z}^2 operator acts as the identity. Similarly, phase factors that appear due to the application of the logical Pauli operations (III.82), (III.83) and (III.86) to a logical state $|\Psi\rangle$, are invisible

to measurements of the expectation values of (III.94). Consequently, as discussed at the end of Sec. III.2.2.1, this allows one to establish a solid framework for handling discrete quantum information encoded in the CV logical states $|0_L\rangle$ and $|1_L\rangle$.

Prominent examples of the observables (III.94) are the modular variables $\text{Re}(\hat{X})$, $\text{Re}(\hat{Y})$ and $\text{Re}(\hat{Z})$ (see also Sec. III.1.2), which can be expressed in the form of Eq. (III.94) with the functions $\zeta_x(\bar{x}, \bar{p}) = \cos(\bar{p}\ell/2)$, $\zeta_y(\bar{x}, \bar{p}) = \cos(2\pi\bar{x}/\ell - \bar{p}\ell/2)$ and $\zeta_z(\bar{x}, \bar{p}) = \cos(2\pi\bar{x}/\ell)$, respectively.² We note that these modular variables, as one would expect from a set of qubit readout observables, are noncommuting which is related to the fact that the product of their periods with respect to the position or momentum is not equal to 2π (see also Sec. III.1.1). This is in contrast to the case of the modular position or momentum operator where this is the case (see Sec. III.1.3). A more general discussion of the commutation relations of the observables (III.94) can be found in Sec. III.3.3.4.

Further on, we note that the general definition of the observables (III.94) leads only in the case $\zeta_\beta(\bar{x}, \bar{p}) = 1$, for all β , to a real set of Pauli operators. However, if one aims at an experimental implementation in terms of measurements of continuous variables, it is desirable to keep the freedom of choice of the functions $\zeta_\beta(\bar{x}, \bar{p})$ making (III.94), in general, an operator with a continuous spectrum. As compared to truly binary case ($\zeta_\beta(\bar{x}, \bar{p}) = 1$), such operators can be accessed via POVMs (see Sec. II.1.4) in a plethora of physical systems, such as the spatial degrees of freedom of photons [Machado et al., 2013; Hor-Meyll et al., 2014], vibrational modes of ions [Lake et al., 2015; Monroe et al., 1996] and mechanical oscillators [Rabl et al., 2009; Lambert et al., 2011; Gittsovich et al., 2015]. In Sec. III.4, we will go more into details of an experimental implementation of such measurements.

In Sec. III.3.3, we will discuss the conditions a general phase space observable $F(\hat{x}, \hat{p})$, where F is a real-valued symmetrized function, has to fulfill such that it can be written in the form (III.94). We emphasize that once the corresponding phase space representation of the observables (III.94) is known, their outcomes can be inferred from true phase-space measurements of the canonically conjugate quantities under consideration, *e.g.* the position and momentum. This is in crucial contrast to other dichotomic observables, such as the photon number parity $\hat{P} = \exp(i\pi\hat{n})$, which have an unbounded, possibly infinitely localized, phase-space distribution and resolve quantum properties that cannot be always accessed through phase space measurements alone. Hence, our modular readout observables (III.94) have a clear classical correspondence in terms of the Weyl correspondence principle (see also the discussion in Sec. II.1.6). The potential of such classical measurements for the implementation of a macroscopic test of Bell nonlocality was also discussed in [Arora and Asadian, 2015].

We can also define spatial and temporal correlations among the observables (III.94) which are important for the implementation of many quantum information protocols. For instance, for the detection of spatial correlations, such as entanglement or Bell nonlocality, one often has to measure correlation functions of the form:

$$C_{\beta_1, \beta_2, \dots, \beta_n} = \langle \hat{\Gamma}_{\beta_1}^{(1)} \otimes \hat{\Gamma}_{\beta_2}^{(2)} \otimes \dots \otimes \hat{\Gamma}_{\beta_n}^{(n)} \rangle \quad (\text{III.106})$$

where $\hat{\Gamma}_{\beta_k}^{(k)}$ acts on the k th subsystem, respectively, and $\beta_1, \dots, \beta_n = x, y, z$. On the other hand, for the realization of test of non-contextuality or Leggett-Garg inequalities

²Equivalently, one can consider the imaginary parts of \hat{X} , \hat{Y} and \hat{Z} .

one often has to measure temporal correlation functions, being defined as:

$$T_{\beta;t_1,t_2,\dots,t_n} = \langle \hat{\Gamma}_\beta(t_1) \hat{\Gamma}_\beta(t_2) \dots \hat{\Gamma}_\beta(t_n) \rangle \quad (\text{III.107})$$

where $\hat{\Gamma}_\beta(t) = \hat{U}(t) \hat{\Gamma}_\beta \hat{U}^\dagger(t)$, with a unitary evolution operator $\hat{U}(t)$ that can represent either the free evolution of the system or the application of some unitary gate before the measurement. Correlation functions involved in contextuality tests are special cases of Eq. (III.107), where the observables are pairwise commuting.

III.3.2 Rotations of the logical basis

In the last Section we have created the possibility to retrieve the discrete quantum information encoded in our CV logical states through measurements of appropriately chosen readout observables. Thereby, the three observables $\hat{\Gamma}_{\beta=x,y,z}$, defined in Eq. (III.94), correspond to measurements according to mutually unbiased bases of the logical space. For instance, the observables $\hat{\Gamma}_z$ and $\hat{\Gamma}_x$ reflect measurements of the mutually unbiased bases $\{|0_L\rangle, |1_L\rangle\}$ and $\{|\pm_L\rangle = (|0_L\rangle \pm |1_L\rangle)/\sqrt{2}\}$, respectively. However, many tests of fundamental properties of quantum mechanics require the possibility of performing measurements according to different sets of mutually unbiased bases which are related by a unitary transformation. Therefore, we devise a way that allows to scan continuously between different mutually unbiased bases in terms of logical qubit rotations.

In Sec. II.1.1, we have seen that single qubit rotations (II.8) can be generated by exponentiating the Pauli operators (II.7) with the proper multiplicative factors. Here, in order to define analogous rotations of our logical qubits, we would like to apply the same procedure to the logical Pauli operations \hat{X} , \hat{Y} and \hat{Z} , defined in Sec. III.2.2.1. This is, however, a priori not possible because these logical Pauli operations are not hermitian. Instead, we consider the hermitian operators (III.94) with the particular choice $\zeta_\beta(\bar{x}, \bar{p}) = 1$, for all \bar{x}, \bar{p} and β , which correspond to the case of binary projective measurements. To make this distinction clear, we will denote these observables in the following as $\hat{\Gamma}_\beta^{(1)}$.

Now we are in the position to define a unitary rotation operator in our logical space:

$$e^{i\frac{\phi}{2}(\hat{\Gamma}^1 \cdot \mathbf{n})} = \cos\left(\frac{\phi}{2}\right)\mathbb{1} + i \sin\left(\frac{\phi}{2}\right)(\hat{\Gamma}^1 \cdot \mathbf{n}), \quad (\text{III.108})$$

where $\hat{\Gamma}^{(1)} = (\hat{\Gamma}_x^{(1)}, \hat{\Gamma}_y^{(1)}, \hat{\Gamma}_z^{(1)})^T$ and $\mathbf{n} = (n_x, n_y, n_z)^T$ indicates the axis of rotation. Equation (III.108) allows to perform rotations of the general observables (III.94) without changing the function $\zeta_\beta(\bar{x}, \bar{p})$ and thus to implement measurements in different mutually unbiased bases of the logical space. Note that, in contrary to logical operations discussed in Sec. III.2.2.2, the operators (III.108) perform well not only on the subspace spanned by perfect GKP states but on the whole space spanned by the logical states $|0_L\rangle$ and $|1_L\rangle$. A proposal of an experimental implementation of these rotation operations using the spatial distribution of single photons is discussed in Sec. III.4.

III.3.3 Phase space representation of modular readout observables

After having discussed several important properties of the abstract readout observables (III.94) we proceed by studying their representation in phase space. In this respect,

we search for classes of phase space observables that admit the form (III.94) when transformed to the modular representation.

An arbitrary observable in phase space, *i.e.* a real and symmetric function of the position and momentum operator, represented in the modular basis, reads:

$$F(\hat{x}, \hat{p}) = \iint_0^\ell d\bar{x}d\bar{x}' \iint_0^{2\pi/\ell} d\bar{p}d\bar{p}' \underbrace{\langle \bar{x}, \bar{p} | F(\hat{x}, \hat{p}) | \bar{x}', \bar{p}' \rangle}_{\equiv F(\bar{x}, \bar{p}; \bar{x}', \bar{p}')}. \quad (\text{III.109})$$

with matrix elements $F(\bar{x}, \bar{p}; \bar{x}', \bar{p}')$. Using the definition of the modular eigenstates (III.34), we can express these matrix elements as:

$$F(\bar{x}, \bar{p}; \bar{x}', \bar{p}') = \frac{\ell}{2\pi} \sum_{r,s=-\infty}^{\infty} e^{i(\bar{p}'s - \bar{p}r)\ell} \langle \bar{x} + r\ell | F(\hat{x}, \hat{p}) | \bar{x}' + s\ell \rangle. \quad (\text{III.110})$$

Further on, if we assume that the function $F(\hat{x}, \hat{p})$ is periodic with respect to \hat{x} and \hat{p} with periods L and $2\pi/L'$, respectively, we can, according to the discussion in Sec. III.1.1, rewrite it as a superposition of displacement operators:

$$\begin{aligned} F(\hat{x}, \hat{p}) &= \sum_{n=-\infty}^{\infty} \sum_{m=-\infty}^{\infty} d_{n,m} \hat{D}(mL, 2\pi n/L'), \\ &= \sum_{n=-\infty}^{\infty} \sum_{m=-\infty}^{\infty} d_{n,m} e^{2\pi i n \hat{x}/L' - i L m \hat{p}}, \end{aligned} \quad (\text{III.111})$$

where the $d_{n,m}$'s are the complex Fourier coefficients of the Wigner function representation $W_{\hat{F}}(x, p)$ of (III.111) which is a two-dimensional Fourier series in x and p (see Eq. (III.7)). The coefficients $d_{n,m}$ obey the normalization condition $\sum_{n \in \mathbb{Z}} \sum_{m=-\infty}^{\infty} |d_{n,m}|^2 = 1$, and we have by definition: $W_{\hat{F}}(x + L, p + 2\pi/L') = W_{\hat{F}}(x, p)$. In the following, we discuss which classes of periodic observables (III.111) can be expressed in the form (III.94).

III.3.3.1 $\hat{\Gamma}_z$ -operator

To start, we review what are the matrix elements $F_z(\bar{x}, \bar{p}; \bar{x}', \bar{p}')$ of to the operator $\hat{\Gamma}_z$, and then compare them to the matrix elements of an arbitrary periodic observable (III.111). Since the observable $\hat{\Gamma}_z$ is diagonal in the modular basis its matrix elements read:

$$F_z(\bar{x}, \bar{p}; \bar{x}', \bar{p}') = \delta(\bar{x} - \bar{x}') \delta(\bar{p} - \bar{p}') \tilde{F}_z(\bar{x}, \bar{p}). \quad (\text{III.112})$$

In addition, they have to fulfil the periodicity condition $\tilde{F}_z(\bar{x}, \bar{p}) = -\tilde{F}_z(\bar{x} - \ell/2, \bar{p})$, yielding

$$\begin{aligned} F_z(\hat{x}, \hat{p}) &= \int_{-\ell/4}^{\ell/4} d\bar{x} \int_{-\pi/\ell}^{\pi/\ell} d\bar{p} \tilde{F}_z(\bar{x}, \bar{p}) \left(|\bar{x}, \bar{p}\rangle \langle \bar{x}, \bar{p}| - |\bar{x} + \frac{\ell}{2}, \bar{p}\rangle \langle \bar{x} + \frac{\ell}{2}, \bar{p}| \right) \\ &= \int_{-\ell/4}^{\ell/4} d\bar{x} \int_{-\pi/\ell}^{\pi/\ell} d\bar{p} \tilde{F}_z(\bar{x}, \bar{p}) \hat{\sigma}_z(\bar{x}, \bar{p}) \equiv \hat{\Gamma}_z. \end{aligned} \quad (\text{III.113})$$

where we defined

$$\hat{\sigma}_z(\bar{x}, \bar{p}) = e^{+i\theta_-} |\bar{x}, \bar{p}\rangle \langle \bar{x}, \bar{p}| e^{-i\theta_-} - e^{+i\theta_+} |\bar{x} + \frac{\ell}{2}, \bar{p}\rangle \langle \bar{x} + \frac{\ell}{2}, \bar{p}| e^{-i\theta_+}, \quad (\text{III.114})$$

for $-\ell/4 \leq \bar{x} < \ell/4$ and $-\pi/\ell \leq \bar{p} < \pi/\ell$, and with phases $\theta_{\pm} = \theta_{\pm}(\bar{x}, \bar{p})$ which, up to now, can assume any value.

Now, if we assume a phase space operator of the form (III.111), with $L = L' = \ell$, and use Eq. (III.110) we get

$$\begin{aligned} F_z(\bar{x}, \bar{p}; \bar{x}', \bar{p}') &= \frac{\ell}{2\pi} \sum_{r,s,n,m=-\infty}^{\infty} e^{i(\bar{p}'s - \bar{p}r)\ell} d_{n,m} \langle \bar{x} + r\ell | e^{2\pi i n \hat{x}/\ell - i \ell m \hat{p}} | \bar{x}' + s\ell \rangle \\ &= \frac{\ell}{2\pi} \sum_{r,s,n,m=-\infty}^{\infty} e^{i(\bar{p}'s - \bar{p}r)\ell} d_{n,m} e^{-i\pi n m} e^{2\pi i n \bar{x}'} \underbrace{e^{2\pi i n (s+m)}}_{=1} \delta(\bar{x} - \bar{x}') \delta_{r,s+m} \\ &= \frac{\ell}{2\pi} \sum_{n,m=-\infty}^{\infty} e^{-i\bar{p}m\ell} d_{n,m} e^{-i\pi n m} \underbrace{\sum_{s=-\infty}^{\infty} e^{i(\bar{p}' - \bar{p})s\ell} e^{2\pi i n \bar{x}'/\ell}}_{=\frac{2\pi}{\ell} \delta(\bar{p} - \bar{p}')} \delta(\bar{x} - \bar{x}') \\ &= \tilde{F}(\bar{x}, \bar{p}) \delta(\bar{x} - \bar{x}') \delta(\bar{p} - \bar{p}'). \end{aligned} \quad (\text{III.115})$$

We thus find that periodic phase space operators with periodicity ℓ and $2\pi/\ell$ in \hat{x} and \hat{p} , respectively, lead to diagonal operators in the modular representation with matrix elements $\tilde{F}(\bar{x}, \bar{p}) = \sum_{n,m=-\infty}^{\infty} d_{n,m} e^{2\pi i n \bar{x} - i \bar{p} m \ell} e^{-i\pi n m}$. Moreover, to obtain the operator $\hat{\Gamma}_z$, the condition $\tilde{F}(\bar{x} + \ell/2, \bar{p}) = -\tilde{F}(\bar{x}, \bar{p})$ needs to be enforced as well. The latter is true if $d_{n,m} = 0$, for all even n , leading to the following form of the diagonal elements in Eq. (III.112):

$$\tilde{F}_z(\bar{x}, \bar{p}) = \sum_{n',m=-\infty}^{\infty} d_{2n'+1,m} e^{2\pi i (2n'+1)\bar{x}'/\ell - i \bar{p} m \ell} e^{-i\pi m}. \quad (\text{III.116})$$

which correspond to the phase space observable:

$$F_z(\hat{x}, \hat{p}) = \sum_{n',m=-\infty}^{\infty} d_{2n'+1,m} \hat{D}(\ell m, 2\pi(2n'+1)/\ell), \quad (\text{III.117})$$

Hence, with Eq. (III.117) we provide a specific class of modular variables which in

the modular representation can be expressed in the form of $\hat{\Gamma}_z$, with $\zeta_z(\bar{x}, \bar{p})$ chosen according to Eq. (III.116). A particular example of the observable (III.117) is obtained by choosing only two nonzero coefficients $d_{+1,0} = 1/2$ and $d_{-1,0} = 1/2$, leading to $F_z(\hat{x}, \hat{p}) = \cos(2\pi\hat{x}/\ell) = \text{Re}(\hat{Z})$ and $F_z(\bar{x}, \bar{p}) = \cos(2\pi\bar{x}/\ell)$, as discussed in Sec. III.3.1.

III.3.3.2 $\hat{\Gamma}_x$ -operator

Next, we focus on the observable $\hat{\Gamma}_x$ whose matrix elements can be expressed as follows:

$$F_x(\bar{x}, \bar{p}; \bar{x}', \bar{p}') = \tilde{F}_x(\bar{x}, \bar{p})\delta(\bar{p} - \bar{p}') \\ \times \begin{cases} e^{+i\kappa_x(\bar{x}, \bar{p})} \delta(\bar{x} - (\bar{x}' + \ell/2)), & \text{for } -\ell/4 \leq \bar{x} \leq \ell/4 \\ e^{-i\kappa_x(\bar{x}, \bar{p})} \delta(\bar{x} - (\bar{x}' - \ell/2)), & \text{for } \ell/4 \leq \bar{x} \leq 3\ell/4 \end{cases}, \quad (\text{III.118})$$

with the periodicity properties $\tilde{F}_x(\bar{x} + \ell/2, \bar{p}) = \tilde{F}_x(\bar{x}, \bar{p})$ and $\kappa_x(\bar{x} + \ell/2, \bar{p}) = \kappa_x(\bar{x}, \bar{p})$, leading to

$$F_x(\hat{x}, \hat{p}) = \int_{-\ell/4}^{\ell/4} d\bar{x} \int_{-\pi/\ell}^{\pi/\ell} d\bar{p} \tilde{F}_x(\bar{x}, \bar{p}) \\ \times \left(e^{-i\kappa_x(\bar{x}, \bar{p})} |\bar{x}, \bar{p}\rangle \langle \bar{x} + \frac{\ell}{2}, \bar{p}| + e^{i\kappa_x(\bar{x}, \bar{p})} |\bar{x} + \frac{\ell}{2}, \bar{p}\rangle \langle \bar{x}, \bar{p}| \right) \\ = \int_{-\ell/4}^{\ell/4} d\bar{x} \int_{-\pi/\ell}^{\pi/\ell} d\bar{p} \tilde{F}_x(\bar{x}, \bar{p}) \hat{\sigma}_x(\bar{x}, \bar{p}) \equiv \hat{\Gamma}_x. \quad (\text{III.119})$$

where we defined

$$\hat{\sigma}_x(\bar{x}, \bar{p}) = e^{+i\theta_-} |\bar{x}, \bar{p}\rangle \langle \bar{x} + \frac{\ell}{2}, \bar{p}| e^{-i\theta_+} + e^{+i\theta_+} |\bar{x} + \frac{\ell}{2}, \bar{p}\rangle \langle \bar{x}, \bar{p}| e^{-i\theta_-}, \quad (\text{III.120})$$

with $\theta_+(\bar{x}, \bar{p}) - \theta_-(\bar{x}, \bar{p}) = \kappa_x(\bar{x}, \bar{p})$.

Further on, we want to find the conditions on the general periodic phase space observable (III.111), such that its matrix elements can be expressed as in Eq. (III.118). Therefore, we assume $L = L' = \ell/2$ and $d_{n,m} = 0$, for all even m , what yields:

$$F_x(\bar{x}, \bar{p}; \bar{x}', \bar{p}') = \frac{\ell}{2\pi} \sum_{r,s,n,m=-\infty}^{\infty} d_{n,2m+1} e^{i(\bar{p}'s - \bar{p}r)\ell} \langle \bar{x} + r\ell | e^{4\pi i n \hat{x}/\ell - i\ell(2m+1)\hat{p}/2} | \bar{x}' + s\ell \rangle \\ = \frac{\ell}{2\pi} \sum_{r,s,n,m=-\infty}^{\infty} d_{n,2m+1} e^{i(\bar{p}'s - \bar{p}r)\ell} e^{i\pi n} e^{4\pi i n \bar{x}'/\ell} \langle \bar{x} + r\ell | \bar{x}' + \frac{\ell}{2} + (s+m)\ell \rangle \\ = \frac{\ell}{2\pi} \sum_{r,s,n,m=-\infty}^{\infty} d_{n,2m+1} e^{i(\bar{p}'s - \bar{p}r)\ell} e^{i\pi n} e^{4\pi i n \bar{x}'/\ell} \\ \times \left[\langle \bar{x} + r\ell | \bar{x}' + \frac{\ell}{2} + (s+m)\ell \rangle \Theta_1(\bar{x}') \right. \\ \left. + \langle \bar{x} + r\ell | \bar{x}' - \frac{\ell}{2} + (s+m+1)\ell \rangle \Theta_2(\bar{x}') \right] \quad (\text{III.121})$$

where we split up the domain of \bar{x}' with the two rectangular functions $\Theta_1(\bar{x}) = \Theta(\bar{x} + \ell/4) - \Theta(\bar{x} - \ell/4)$ and $\Theta_2(\bar{x}) = \Theta(\bar{x} - \ell/4) - \Theta(\bar{x} - 3\ell/4)$, defined in terms of the

Heaviside stepfunction $\Theta(\bar{x}')$. With this, Eq. (III.121) becomes:

$$\begin{aligned}
F_x(\bar{x}, \bar{p}; \bar{x}', \bar{p}') &= \frac{\ell}{2\pi} \sum_{r,s,n,m=-\infty}^{\infty} d_{n,2m+1} e^{i(\bar{p}'s - \bar{p}r)\ell} e^{i\pi n} e^{4\pi i n \bar{x}'/\ell} \\
&\quad \times \left[\delta(\bar{x} - (\bar{x}' + \frac{\ell}{2})) \delta_{r,s+m} \Theta_1(\bar{x}') + \delta(\bar{x} - (\bar{x}' - \frac{\ell}{2})) \delta_{r,s+m+1} \Theta_2(\bar{x}') \right] \\
&= \delta(\bar{p}' - \bar{p}) \sum_{n,m=-\infty}^{\infty} d_{n,2m+1} e^{i\pi n} e^{4\pi i n \bar{x}'/\ell - i\ell m \hat{p}} \\
&\quad \left[\delta(\bar{x} - (\bar{x}' + \frac{\ell}{2})) \delta_{r,s+m} \Theta_1(\bar{x}') + e^{-i\bar{p}\ell} \delta(\bar{x} - (\bar{x}' - \frac{\ell}{2})) \delta_{r,s+m+1} \Theta_2(\bar{x}') \right] \\
&= \tilde{F}_x(\bar{x}, \bar{p}) \delta(\bar{p} - \bar{p}') \begin{cases} e^{+i\bar{p}\ell/2} \delta(\bar{x} - (\bar{x}' + \ell/2)), & \text{for } -\ell/4 \leq \bar{x} \leq \ell/4 \\ e^{-i\bar{p}\ell/2} \delta(\bar{x} - (\bar{x}' - \ell/2)), & \text{for } \ell/4 \leq \bar{x} \leq 3\ell/4 \end{cases} .
\end{aligned} \tag{III.122}$$

where

$$\tilde{F}_x(\bar{x}, \bar{p}) = \sum_{n,m=-\infty}^{\infty} d_{n,2m+1} e^{i\pi n} e^{4\pi i n \bar{x} - i\bar{p}\frac{\ell}{2}(2m+1)}. \tag{III.123}$$

We thus find that all operators of the form

$$F_x(\hat{x}, \hat{p}) = \sum_{n,m=-\infty}^{\infty} d_{n,2m+1} \hat{D}(\ell(2m+1)/2, 4\pi n/\ell), \tag{III.124}$$

where we set $L = L' = \ell/2$ and $d_{n,m} = 0$, for all even m , can be expressed as $\hat{\Gamma}_x$ with $\zeta_x(\bar{x}, \bar{p}) = \tilde{F}_x(\bar{x}, \bar{p})$ and $\kappa_x(\bar{x}, \bar{p}) = \bar{p}\ell/2$. An example of Eq. (III.124) is given by the operator $\text{Re}(\hat{X}) = \cos(\hat{p}\ell/2)$, where only $d_{0,1} = 1/2$ and $d_{0,-1} = 1/2$ are nonzero, which is equal to $\hat{\Gamma}_x$ with $\zeta_x(\bar{x}, \bar{p}) = F_x(\bar{x}, \bar{p}) = \cos(\bar{p}\ell/2)$.

III.3.3.3 $\hat{\Gamma}_y$ -operator

Finally, we consider the operator $\hat{\Gamma}_y$ which has matrix elements

$$\begin{aligned}
F_y(\bar{x}, \bar{p}; \bar{x}', \bar{p}') &= \tilde{F}_y(\bar{x}, \bar{p}) \delta(\bar{p} - \bar{p}') \\
&\quad \times \begin{cases} (+i) e^{+i\kappa_y(\bar{x}, \bar{p})} \delta(\bar{x} - (\bar{x}' + \ell/2)), & \text{for } -\ell/4 \leq \bar{x} \leq \ell/4 \\ (-i) e^{-i\kappa_y(\bar{x}, \bar{p})} \delta(\bar{x} - (\bar{x}' - \ell/2)), & \text{for } \ell/4 \leq \bar{x} \leq 3\ell/4 \end{cases} ,
\end{aligned} \tag{III.125}$$

that lead, together with the periodicity properties $\tilde{F}_y(\bar{x} + \ell/2, \bar{p}) = -\tilde{F}_y(\bar{x}, \bar{p})$ and $\kappa_y(\bar{x} + \ell/2, \bar{p}) = \kappa_y(\bar{x}, \bar{p})$, to the operator

$$\begin{aligned}
F_y(\hat{x}, \hat{p}) &= \int_{-\ell/4}^{\ell/4} d\bar{x} \int_{-\pi/\ell}^{\pi/\ell} d\bar{p} \tilde{F}_y(\bar{x}, \bar{p}) i (e^{i\kappa_x(\bar{x}, \bar{p})} |\bar{x} + \frac{\ell}{2}, \bar{p}\rangle \langle \bar{x}, \bar{p}| - e^{-i\kappa_x(\bar{x}, \bar{p})} |\bar{x}, \bar{p}\rangle \langle \bar{x} + \frac{\ell}{2}, \bar{p}|) \\
&= \int_{-\ell/4}^{\ell/4} d\bar{x} \int_{-\pi/\ell}^{\pi/\ell} d\bar{p} \tilde{F}_y(\bar{x}, \bar{p}) \hat{\sigma}_x(\bar{x}, \bar{p}) \equiv \hat{\Gamma}_y,
\end{aligned} \tag{III.126}$$

where we defined

$$\hat{\sigma}_y(\bar{x}, \bar{p}) = +e^{+i\theta_+} |\bar{x} + \frac{\ell}{2}, \bar{p}\rangle \langle \bar{x}, \bar{p}| e^{-i\theta_-} - ie^{+i\theta_-} |\bar{x}, \bar{p}\rangle \langle \bar{x} + \frac{\ell}{2}, \bar{p}| e^{-i\theta_+}, \quad (\text{III.127})$$

with $\theta_+(\bar{x}, \bar{p}) - \theta_-(\bar{x}, \bar{p}) = \kappa_y(\bar{x}, \bar{p})$.

Further on, we search again for the conditions on the general periodic phase space observable (III.111), such that its matrix elements can be expressed as in Eq. (III.125). The latter can be achieved with $L = \ell/2$ and $L' = \ell$, and $d_{n,m} = 0$ for all even n and m , yielding the matrix elements

$$\begin{aligned} F_y(\bar{x}, \bar{p}; \bar{x}', \bar{p}') &= \frac{\ell}{2\pi} \sum_{r,s,n,m=-\infty}^{\infty} e^{i(\bar{p}'s - \bar{p}r)\ell} d_{n,m} \langle \bar{x} + r\ell | e^{2\pi i n \hat{x}/\ell - i \ell m \hat{p}/2} | \bar{x}' + s\ell \rangle \\ &= \tilde{F}_y(\bar{x}, \bar{p}) \delta(\bar{p} - \bar{p}') \left[ie^{i\bar{p}\ell/2} \delta(\bar{x} - (\bar{x}' + \ell/2)) \Theta_1(\bar{x}) - ie^{-i\bar{p}\ell/2} \delta(\bar{x} - (\bar{x}' - \ell/2)) \Theta_2(\bar{x}) \right] \\ &= \tilde{F}_y(\bar{x}, \bar{p}) \delta(\bar{p} - \bar{p}') \begin{cases} (+i)e^{+i\bar{p}\ell/2} \delta(\bar{x} - (\bar{x}' + \ell/2)), & \text{for } -\ell/4 \leq \bar{x} \leq \ell/4 \\ (-i)e^{-i\bar{p}\ell/2} \delta(\bar{x} - (\bar{x}' - \ell/2)), & \text{for } \ell/4 \leq \bar{x} \leq 3\ell/4 \end{cases}, \end{aligned} \quad (\text{III.128})$$

with

$$\tilde{F}_y(\bar{x}, \bar{p}) = \sum_{n,m=-\infty}^{\infty} d_{2n+1, 2m+1} e^{i\pi(n+m)} e^{2\pi i(2n+1)\bar{x} - i\bar{p}(2m+1)\ell/2}. \quad (\text{III.129})$$

We thus find that all operators of the form

$$F_y(\hat{x}, \hat{p}) = \sum_{n,m=-\infty}^{\infty} d_{2n+1, 2m+1} \hat{D}(\ell(2m+1)/2, 2\pi(2n+1)/\ell), \quad (\text{III.130})$$

where we set $L = \ell/2$, $L' = \ell$ and $d_{n,m} = 0$, for all even n and m , can be expressed as $\hat{\Gamma}_y$ with $\zeta_y(\bar{x}, \bar{p}) = \tilde{F}_y(\bar{x}, \bar{p})$ and $\kappa_y(\bar{x}, \bar{p}) = \bar{p}\ell/2$. An example of Eq. (III.130) is given by $\text{Re}(\hat{Y}) = \cos(2\pi/\ell \hat{x} - \hat{p}\ell/2)$, corresponding to the case where only $d_{1,1} = 1/2$ and $d_{-1,-1} = -1/2$ are nonzero, which is equal to $\hat{\Gamma}_y$ with $\zeta_y(\bar{x}, \bar{p}) = F_y(\bar{x}, \bar{p}) = \cos(2\pi/\ell \bar{x} - \bar{p}\ell/2)$.

III.3.3.4 Commutation relations

Finally, we want to study shortly the commutation relations between the modular readout observables $\hat{\Gamma}_\beta$, with $\beta = x, y, z$. In particular, with the help of Eq. (III.95) we find

$$[\hat{\Gamma}_\alpha, \hat{\Gamma}_\beta] = \int_{-\ell/4}^{\ell/4} d\bar{x} \int_{-\pi/\ell}^{\pi/\ell} d\bar{p} \zeta_\alpha(\bar{x}, \bar{p}) \zeta_\beta(\bar{x}, \bar{p}) \hat{\sigma}_\gamma(\bar{x}, \bar{p}). \quad (\text{III.131})$$

The commutation relations thus differ from those of the logical Pauli operations introduced in Sec. III.2.2.1, which is due to the fact that here we are dealing with hermitian and in general nonunitary operators. As mentioned earlier, only in the particular case $\zeta_\beta(\bar{x}, \bar{p}) = 1$, for all β , we recover the binary case of hermitian and unitary Pauli opera-

tors. Now, one could ask the question why the observables $\hat{\Gamma}_x$ and $\hat{\Gamma}_z$, which according to our preceding elaborations are equal to specific sets of modular variables, are non-commuting and what makes them different from a commuting pair of modular variables, such as \hat{x} and \hat{p} . The answer to this question was given in Sec. III.1.1, where we showed that a pair of modular variables commutes if and only if the product of their periods is equal to 2π (see also Eqs. (III.2) and (III.3)). The latter is not the case for different pairs of the set of observables $\{\hat{\Gamma}_\beta | \beta = x, y, z\}$. For instance, in the case of the earlier discussed example, $\hat{\Gamma}_x = \cos(\hat{p}\ell/2)$ and $\hat{\Gamma}_y = \cos(2\pi/\ell\hat{x})$, we can easily verify that the products of the periods of the two cosine's is equal to π .

III.4 Experimental proposal using the spatial distribution of single photons

In this Section we outline a possible experimental implementation of our modular variables framework using the transverse degrees of freedom of single photons. Using this system, we will show how to create appropriate states with periodic wave functions, how to manipulate them using linear optical operations and finally how to perform a readout of the encoded discrete quantum information from the spatial field of the photons.

As outlined in Sec. II.3.1, we will assume in the following that the coordinates \hat{x} and \hat{p} refer to the transverse position and momentum of a single photon. If we remain in the paraxial approximation (see Eq. (II.119) and the discussion in the same Section) the wave function of this field can be seen as the wave function of a single point particle, here being the photon. A general quantum state of the transverse momentum (or position) of the photon can be written in the *modular basis*, as shown in (III.72).

III.4.1 Creation of single photon states with periodic wave function

One major advantage in using the transverse degrees of freedom of single photons is that we can very efficiently produce states with a periodic wave function, as those presented in Fig. III.4. To do so, we simply pass the photons through a periodic diffraction grating, as indicated in Fig. III.10. If the photon that is impinging on the grating has a Gaussian transverse wave function $f_G(x) \propto e^{-(x\kappa)^2/2}$, with width κ^{-1} , and the transmission function of the grating is given by $\sum_m a_m e^{imx2\pi/L}$, where $a_m = \exp(-\frac{1}{2}m^2(2\pi\Delta/L)^2)$ with slit width Δ and distance L , the resulting wave function of the diffracted photons has the form (III.53). Hence, by adjusting the slit widths and distances of the grating, we can produce the logical qubit states $|0\rangle_L$ and $|1\rangle_L$. In Fig. III.10, the photons are also sent through a lens system before the grating in order to prepare them in approximate plane waves. This allows us additionally to adjust the width κ^{-1} of the Gaussian envelope of the wave function (III.53), which corresponds to the quality of the prepared plane waves. Experimentally gratings are often realized using spatial light modulators (SLMs) (see discussions at the end of Sec. II.3.1.1).

Note that the propagation of the diffracted photons will lead to a blurring in the photon's transverse wave function. This is due to the fact that the photon field is initially in a Gaussian state and thus can cover only a finite number of slits in the grating. The dependency of this blurring on the number of irradiated slits is illustrated in Fig. III.11, where we present the fidelity of the initially prepared wave function

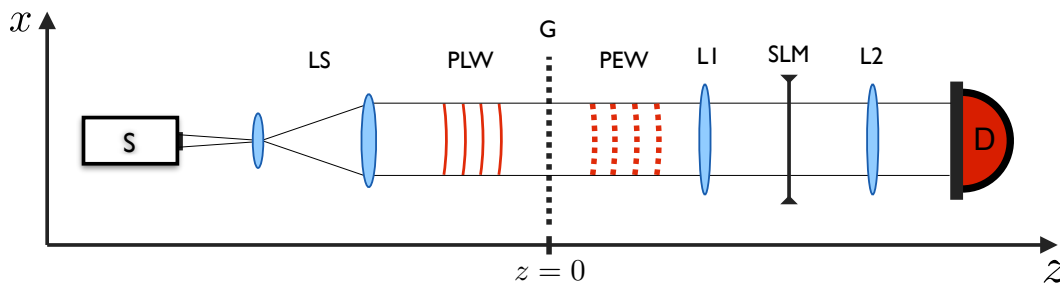


Figure III.10: (color online) Scheme showing the production, processing and detection of the transverse degrees of single photons. The photons are produced in a source (S) and then send through a lens systems (LS) in order to prepare them in approximate plane waves. Further on, a periodic refraction grating prepares the photon's transverse wave function in a periodic state. The photons can be manipulated using a spatial light modulator (SLM) implementing the unitary operation \hat{U}_{SLM} , or optionally $\hat{\mathcal{F}}\hat{U}_{\text{SLM}}\hat{\mathcal{F}}^\dagger$ if placing lenses (L1,L2) before and after the SLM. Finally, the photons are measured with a spatially resolving detector (D) or sent through an interferometric scheme, as presented in Sec. III.4.3.2.

with its revivals after specific propagation distances. These revivals are related to a near field interference effect, referred to as Talbot effect, which refers to the complex diffraction pattern of a wave that has passed through a periodic diffraction grating (see Sec. V.1 for a discussion of the Talbot effect). The Talbot effect can also be used to implement single qubit operations on qubits that are encoded in periodic wave functions and is thus closely related to the presently developed framework. In Chapter IV, we will independently introduce the Talbot effect and a quantum information processing framework based upon it. One finds that for currently available diffraction gratings a fidelity higher than 0.9 can be maintained for a propagation distance of about 10 times the Talbot distance. This might be enough to demonstrate the implementation of some single and two qubit gates, and their corresponding readout, but is of course not enough for a scalable implementation of our framework. For that, as discussed previously, it is inevitable to implement GKP error correction, as introduced in [Gottesman et al., 2001].

Once it is known how to prepare single photons in the corresponding logical states $|0_L\rangle$ and $|1_L\rangle$, we can try to entangle a pair of photons which then can be further used to demonstrate entanglement or nonlocal correlations, and to implement certain quantum information protocols. One possibility to do so is by producing polarization entangled states in a type-2 parametric down-conversion process [Walborn et al., 2010] and subsequently swapping the polarization entanglement to the spatial distribution of the photon pair, as suggested in [Ketterer et al., 2015]. Therefore, the photons are sent through a Mach-Zehnder interferometer made up of polarization dependent beam-splitters, half- and quarter-wave plates and diffraction gratings, similar as the one depicted in Fig. 3(c) of the main text. The output states of the interferometers will yield to 50% the desired spatially entangled photons, while the other half of the emerging photons has to be discarded.

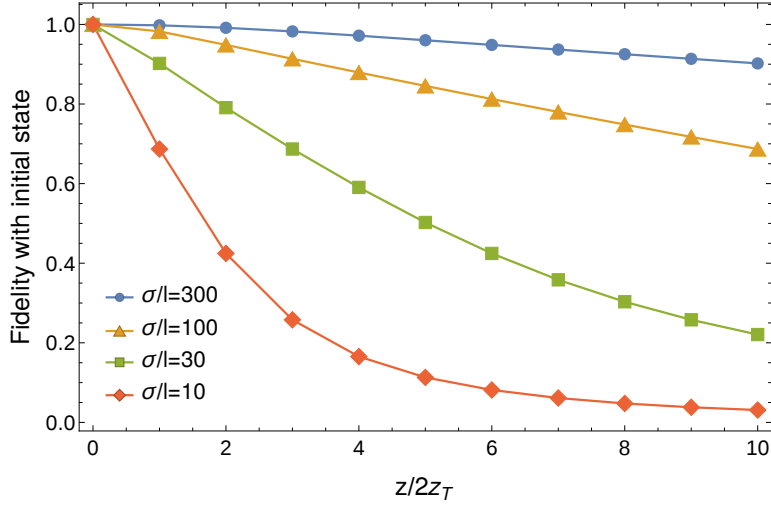


Figure III.11: Fidelity of an initial logical state $|0_L\rangle$ with respect to itself after the free-propagation of a distance $2mz_T$, with an integer m and the Talbot distance z_T (see Sec. V.1 for a precise definition of the Talbot distance), for different initial widths of the Gaussian envelope $\sigma = \kappa^{-1}$ and varying number of illuminated slits l . While this fidelity decays rapidly for small values of $\sigma = \kappa^{-1}$ it is well preserved for values of the order of 102 illuminated slits, as is the case in the experiment reported in [Case et al., 2009].

In more detail, the entangled state of the down-converted photons reads $\frac{1}{\sqrt{2}}(|H\rangle_a|H\rangle_b + |V\rangle_a|V\rangle_b)$, produced by pumping two adjacent nonlinear crystals (type I) with a laser beam polarized at 45° . Next, depending on what kind of spatially entangled state we want to produce, we have to apply local unitary transformations on each of the entangled photons, realized by a combination of half- and quarter-wave plates, as indicated in Fig. III.12. For instance, for the logical entangled state (IV.87) we need to transform the above down-converted state into the form:

$$|\psi_{pol}\rangle = \frac{1}{N_{\pm}} \left[|H\rangle_a|H\rangle_b + |V\rangle_a|V\rangle_b \pm i(\sqrt{2} \mp 1) (|H\rangle_a|V\rangle_b + |V\rangle_a|H\rangle_b) \right], \quad (\text{III.132})$$

where $N_{\pm} = 2\sqrt{2 - \sqrt{2}}$. Thereby, the transverse wave function of the two photons remains in the separable Gaussian state $|\psi_g\rangle_a|\psi_g\rangle_b$. Next, we have to swap the entanglement from the polarization to the transverse degrees of freedom of the photons according to $|H\rangle_{a/b}|\psi_G\rangle_{a/b} \rightarrow |H\rangle_{a/b}|f\rangle_{a/b}$ and $|V\rangle_{a/b}|\psi_G\rangle_{a/b} \rightarrow |V\rangle_{a/b}|\bar{f}\rangle_{a/b}$. This swapping is realized experimentally using an interferometer with polarizing beam-splitters (see Fig. III.12). The latter separates the photons with opposite polarization by sending them in different spatial modes (arms) of the interferometer and thus allows to apply polarization dependent operations to the transverse field of the photons. In this way we can realize the operations $|\psi_G\rangle \rightarrow |f\rangle$ and $|\psi_G\rangle \rightarrow |\bar{f}\rangle$, by placing diffraction gratings in each arm of the interferometer that are slightly displaced with respect to each other. In order to assure that H-polarized a -photons will go through the same arm of the interferometer as H-polarized b -photons, we have to apply an additional half-wave

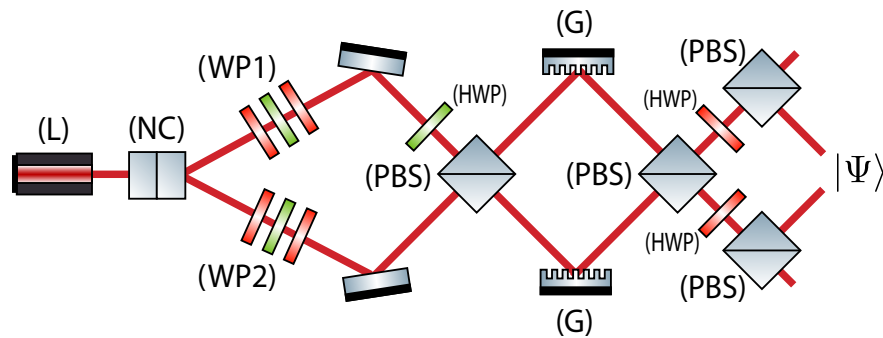


Figure III.12: Proposed experimental setup to create a spatially entangled two photon state $|\Psi\rangle$ of the form (IV.87). L: laser, NC: nonlinear crystals (type I), HWP: half-wave plate, WP1/WP2: combination of half- and quarter-wave plates, PBS: polarizing beam splitter, G: diffraction grating.

plate (HWP) to the photon in mode b before it enters into the polarizing beam-splitter. Finally, one uses half-wave plates oriented at the angle $\pi/8$ in the path of both photons and polarizing beam-splitters in order to factorize the polarization from the transverse degrees of freedom yielding a conditional preparation of the desired state (IV.87) with a 50% probability. Equivalently, we can produce the logical entangled state (IV.80) by applying another set of wave plates to each photon of the down-converted pair.

Another possibility to create the desired entangled states, that will be discussed in detailed in Sec. V.3 and published soon in [Barros et al., 2016], is to take directly advantage of the spatial correlations of photon pairs produced in spontaneous parametric down-conversion (see discussion in Sec. II.3.1.3). This method takes the transverse state of the two photons

$$|\psi\rangle_{12} = \iint dx_1 dx_2 \psi_{12}(x_1, x_2) |x_1\rangle |x_2\rangle, \quad (\text{III.133})$$

with the transverse wave function

$$\psi_{12}(x_1, x_2) = \vartheta(x_1 + x_2) \gamma(x_1 - x_2), \quad (\text{III.134})$$

and transforms it deterministically into the desired entangled state after applying a set of linear optical elements to each photon individually.

III.4.2 Logical operations realized by linear optical elements

Now, we will discuss how the logical qubit operations can be implemented using the transverse distribution of single photons. In the light of the discussion about experimental implementations of CV gate operations in this experimental platform (see Sec. II.3.1), a realization of single qubit Pauli or Clifford operations, as defined in Sec. III.2.2.1 and III.2.2.2, respectively, is straightforward. For this reason, we will focus here on the experimental implementation of the rotation operations, introduced in Sec. III.3.2. As explained previously, the latter form a particular group of operations because, in con-

trast to the Clifford operations, they perform exact operations not only on a subspace defined by modular eigenstates but on the whole logical space defined in Sec. III.2.1.

In order to implement the logical rotation operator

$$e^{i\frac{\phi}{2}(\hat{\mathbf{\Gamma}}^1 \cdot \mathbf{n})} = \cos\left(\frac{\phi}{2}\right)\mathbb{1} + i \sin\left(\frac{\phi}{2}\right)(\hat{\mathbf{\Gamma}}^1 \cdot \mathbf{n}), \quad (\text{III.135})$$

where $\hat{\mathbf{\Gamma}}^1 = (\hat{\Gamma}_x^1, \hat{\Gamma}_y^1, \hat{\Gamma}_z^1)$ and $\mathbf{n} = (n_x, n_y, n_z)$ is the rotation axis, we need to employ a spatial light modulator (see Sec. II.3.1). We focus on rotation around the two main axes of $\hat{\Gamma}_z$ and $\hat{\Gamma}_x$, which by composition allow to implement any desired single qubit rotation. Therefore, we remind the reader that

$$\begin{aligned} \hat{\Gamma}_z^1 &= \int_{-\ell/4}^{\ell/4} d\bar{x} \int_{-\pi/\ell}^{\pi/\ell} d\bar{p} \hat{\sigma}_z(\bar{x}, \bar{p}) \\ &= \int_{-\ell/4}^{3\ell/4} d\bar{x} \int_{-\pi/\ell}^{\pi/\ell} d\bar{p} s_z(\bar{x}) |\bar{x}, \bar{p}\rangle \langle \bar{x}, \bar{p}|, \end{aligned} \quad (\text{III.136})$$

with the step function $s_z(\bar{x})$ that takes the value +1 if $\bar{x} \in [-\ell/4, \ell/4[$ and -1 if $\bar{x} \in [\ell/4, 3\ell/4[$. By means of the discussion in Sec. III.3.3 we know that Eq. (III.136) reads in the position representation as follows:

$$\hat{\Gamma}_z^1 = \int_{-\infty}^{\infty} dx s_z(x) |x\rangle \langle x|, \quad (\text{III.137})$$

where $s(x)$ is a ℓ -periodic rectangular function taking the value +1 if $x \in [-(2n)\ell/4, (2n)\ell/4[$ and -1 if $x \in [(2n+1)\ell/4, (2n+1)3\ell/4[$, with integers n . Hence, the rotation operator (III.135) reads:

$$e^{i\frac{\phi}{2}\hat{\Gamma}_z^1} = \int_{-\infty}^{\infty} dx e^{i\frac{\phi}{2}s_z(x)} |x\rangle \langle x|, \quad (\text{III.138})$$

which is a simple position phase gate that can be implemented through the SLM operation \hat{U}_{SLM} with $f(x) = \frac{\phi}{2}s_z(x)$. For an introduction of the SLM operation see the discussion at the end of Sec. II.3.1.1.

Similarly, we can write

$$\begin{aligned} \hat{\Gamma}_x^1 &= \int_{-\ell/4}^{\ell/4} d\bar{x} \int_{-\pi/\ell}^{\pi/\ell} d\bar{p} \hat{\sigma}_x(\bar{x}, \bar{p}) \\ &= \int_{-\ell/4}^{3\ell/4} d\bar{x} \int_{-\pi/\ell}^{\pi/\ell} d\bar{p} s_x(\bar{x}, \bar{p}) |\bar{x}, \bar{p}\rangle \langle \bar{x}, \bar{p}|, \end{aligned} \quad (\text{III.139})$$

where $s_x(\bar{x}, \bar{p})$ that takes the value $e^{i\bar{p}\ell/2}$ if $\bar{x} \in [-\ell/4, \ell/4[$ or $e^{i\bar{p}\ell/2}$ if $\bar{x} \in [\ell/4, 3\ell/4[$. And again, by following the arguments in Sec. III.3.3, we find that Eq. (III.139) can be written in the momentum representation as

$$\hat{\Gamma}_x^1 = \int_{-\infty}^{\infty} dp s_x(p) |p\rangle \langle p|, \quad (\text{III.140})$$

where $s_x(p)$ is a $4\pi/\ell$ -periodic rectangular function which takes the value $+1$ if $p \in [-(2m)\pi/\ell, (2m)\pi\ell/4]$, and -1 if $p \in [(2m+1)\pi/\ell, (2m+1)3\pi/\ell]$, with integer values m . From Eq. (III.140) then follows directly

$$e^{i\frac{\phi}{2}\hat{\Gamma}_x^1} = \int_{-\infty}^{\infty} dp e^{i\frac{\phi}{2}s_x(p)} |p\rangle\langle p|, \quad (\text{III.141})$$

which is a momentum phase gate that can be implemented with a SLM operation programmed with the function $f(x) = \frac{\phi}{2}s_x(x)$, sandwiched between two Fourier transforms, as discussed previously. Figure III.10 depicts the sequence of optical elements allowing for an implementation of the rotations (III.138) and (III.141) on the transverse degrees of freedom of a single photon. The lenses (L1) and (L2) must be removed or inserted to perform either of the operations.

III.4.2.1 Controlled two photon gate

For the sake of completeness, we comment in here briefly on the possibility of implementing a two photon controlled phase gate in terms of a recently proposed device, called spatially dependent beam splitter (SPBS) [Farías et al., 2015]. For a more refined introduction to this device we refer the reader to Sec. V.2.3. A SPBS has, in contrast to an ordinary beam splitter with complex transmission and reflection coefficients t and r , such that $|t|^2 + |s|^2 = 1$, spatially dependent coefficients $t(x)$ and $s(x)$, where x denotes one of the transverse position coordinates of the incoming light field, such that $|t(x)|^2 + |s(x)|^2 = 1$ for all x . We can thus imagine a device applying different transmission and reflection coefficients to different regions of our logical states which in position space correspond to periodic wave functions with period ℓ (see Fig. (2) in the main text). By combining three such SDBC in a row one can realize probabilistically a controlled phase gate between two photonic logical qubits with a success probability of $1/9$. We do not comment further on this scheme because our main source of entangled photons is spontaneous parametric downconversion, however, for more details we refer the reader to the work [Farías et al., 2015].

III.4.3 Measuring the readout observables $\hat{\Gamma}_\beta$

Finally, we discuss two possible strategies for measurements of the modular readout observables $\hat{\Gamma}_\beta$, that have been introduced in Sec. III.3. The first possibility, hereafter referred to as direct measurement approach, consists in measuring first the position of the photon and then to calculate the expectation values of $\hat{\Gamma}_\beta$ by a post-processing of the measured data. The second one is to measure these expectation values indirectly by coupling the system to an additional ancilla state, and therefore referred to as the indirect measurement approach.

III.4.3.1 Direct measurement

We first remind that the observables $\hat{\Gamma}_\beta$, with $\beta = x, y, z$, correspond to phase space operators $F(\hat{x}, \hat{p})$ fulfilling certain periodicity constraints, as discussed in Sec. III.3.3. If we further consider only those readout observables which can be expressed as a function

of a general quadrature $\hat{x}_\phi = \sin(\phi)\hat{x} + \cos(\phi)\hat{p}$, we can write them in the corresponding diagonal form

$$F_\beta(\hat{x}_\phi) = \int_{-\infty}^{\infty} dx F_\beta(x) |x\rangle_\phi \langle x|_\phi \quad (\text{III.142})$$

where the subscripts ϕ of the bras and kets indicate the corresponding \hat{x}_ϕ -representation. Examples, as mentioned in Sec. III.3, are $\hat{\Gamma}_x = \cos(\hat{p}\ell/2)$, $\hat{\Gamma}_z = \cos(2\pi\hat{x}/\ell)$ and $\hat{\Gamma}_y = \cos(2\pi\hat{x}/\ell - \hat{p}\ell/2) = \cos(\frac{2\pi}{\ell}g(\sin(\phi')\hat{x} + \cos(\phi')\hat{p}))$, being functions of $\hat{x}_{\frac{\pi}{2}}$, \hat{x}_0 and $\hat{x}_{\phi'}$, where $g = \sqrt{1 + \ell^4/(4\pi)^2}$ and $\phi' = \arctan(-\ell^2/(4\pi))$. Accordingly, the expectation value of the operator (III.142) reads:

$$\langle F_\beta(\hat{x}_\phi) \rangle = \int_{-\infty}^{\infty} dx F_\beta(x) |\langle x|_\phi|\Psi\rangle|^2, \quad (\text{III.143})$$

which is solely determined by the probability density $p_\phi(x) = |\langle x|_\phi|\Psi\rangle|^2$. We can reproduce the same reasoning in a bipartite system where we get for a product of two readout observables $\hat{\Gamma}_\beta \otimes \hat{\Gamma}_{\beta'}$:

$$\begin{aligned} F_\beta(\hat{x}_{\phi_1}) \otimes F_{\beta'}(\hat{x}_{\phi_2}) &= \iint_{-\infty}^{\infty} dx_1 dx_2 F_\beta(x_2) F_{\beta'}(x_1) \\ &\quad \times |x_1\rangle_{\phi_1} \langle x_2|_{\phi_2} \langle x_1|_{\phi_1} \langle x_2|_{\phi_2} \end{aligned} \quad (\text{III.144})$$

and the corresponding expectation value:

$$\begin{aligned} \langle F_\beta(\hat{x}_{\phi_1}) \otimes F_{\beta'}(\hat{x}_{\phi_2}) \rangle &= \iint_{-\infty}^{\infty} dx_1 dx_2 F_\beta(x_2) F_{\beta'}(x_1) \\ &\quad \times |\langle x_1|_{\phi_1} \langle x_2|_{\phi_2}|\Psi\rangle|^2, \end{aligned} \quad (\text{III.145})$$

with the joint-probability density $p_{\phi_1, \phi_2}(x_1, x_2) = |\langle x_1|_{\phi_1} \langle x_2|_{\phi_2}|\Psi\rangle|^2$.

In an experimental setup with pairs of single photons we can determine the position or momentum probability densities $p_0(x)$ or $p_{\frac{\pi}{2}}(p)$, by detecting the position of the photons in the near- or far-field with respect to the output plane of the source of the photons. Position measurements of single photons can be performed either by scanning a single photon counter in the transverse plane of the photon or by using a single-photon sensitive camera [Moreau et al., 2014; Aspden et al., 2013]. Arbitrary quadratures \hat{x}_ϕ can be assessed via fractional Fourier transforms realized with lens systems [Ozaktas et al., 2001; Tasca et al., 2008], allowing to determine arbitrary distributions $p_\phi(x)$. Finally, we can use Eq. (III.143) to calculate expectation values of the desired readout observables $\hat{\Gamma}_\beta$.

The same measurement schemes can be applied to entangled pairs of photons (see Sec. III.4.1), using respectively two single photon counters or two single photon sensitive cameras, in order to determine the joint-probability distributions $p_{\phi_1, \phi_2}(x_1, x_2) = |\langle x_1|_{\phi_1} \langle x_2|_{\phi_2}|\Psi\rangle|^2$ and to calculate the expectation values of products of operators $\hat{\Gamma}_\beta$ through Eq. (III.145).

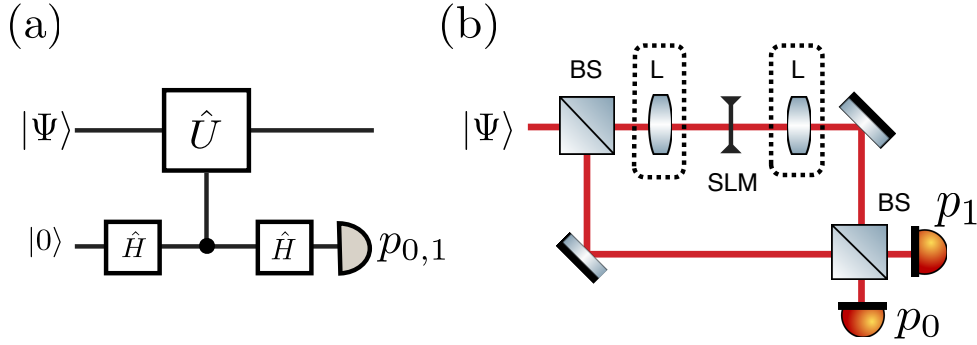


Figure III.13: (a) Quantum circuit allowing for the measurement of the observables (III.94). \hat{H} depict Hadamard gates and a controlled unitary gate \hat{U} is applied if the ancilla is in the state $|0\rangle$. The expectation value of (III.94) is given by $p_0 - p_1$, where p_0 (p_1) are the probabilities of detecting the ancilla in the state $|0\rangle$ ($|1\rangle$). In the case of the specific example mentioned in the text we choose $\hat{U} = \hat{X}, \hat{Y}, \hat{Z}$. (b) Proposal of an experimental implementation of circuit (a) using the spatial field of single photons passing through a Mach-Zehnder interferometer. Controlled unitaries are realized by linear optical transformations inserted in one arm of the interferometer. Unitaries of the form $e^{ih(\hat{x})}$ or $e^{ih(\hat{p})}$ can be implemented using a SLM and lenses (L) allowing to switch from the position to the momentum space.

III.4.3.2 Indirect measurement

In order to indirectly measure the expectation values of the observables $\hat{\Gamma}_\beta$, $\beta = x, y, z$, we first show that the latter can be obtained from measurements of positive operator valued measures (POVMs) which then can be realized by coupling the system to an ancilla qubit (see discussion in Sec. II.1.4). We assume in the following the the spectrum of the operators $\hat{\Gamma}_\beta$ is bounded by one. Let us define the following POVM elements:

$$\hat{E}_+ = \frac{1}{2}(\mathbb{1} + \hat{\Gamma}_\beta) \quad (\text{III.146})$$

$$\hat{E}_- = \frac{1}{2}(\mathbb{1} - \hat{\Gamma}_\beta) \quad (\text{III.147})$$

which satisfy the relation $\hat{E}_+ + \hat{E}_- = \mathbb{1}$. The probability to obtain the outcome $+$ or $-$ is thus given by $p_+ = \langle \hat{E}_+ \rangle$ or $p_- = \langle \hat{E}_- \rangle = 1 - p_+$, respectively, and we can calculate $\langle \hat{\Gamma}_\beta \rangle = \langle \hat{E}_+ - \hat{E}_- \rangle = p_+ - p_-$. Hence, the expectation value of every $\hat{\Gamma}_\beta$ can always be measured in terms of a two-valued POVM. More generally, if the spectrum of $\hat{\Gamma}_\beta$ is bounded between γ_- and γ_+ , one can simply rescale the spectrum of the corresponding POVM to reproduce the same argument [Horodecki, 2003].

Further on, we show how to implement a measurement of \hat{E}_\pm by coupling our CV system to an ancilla qubit. Consider the quantum circuit shown in Fig. III.13(a) of the main text which implements the operation

$$|\Psi\rangle|0\rangle \rightarrow \frac{1}{2}(\mathbb{1} + \hat{U})|\Psi\rangle|0\rangle + \frac{1}{2}(\mathbb{1} - \hat{U})|\Psi\rangle|1\rangle \quad (\text{III.148})$$

on the initial state $|\Psi\rangle|0\rangle$. Hence, by measuring the ancilla state in the basis $|0(1)\rangle$, we project the system state onto $|\Psi_{\pm}\rangle = \hat{D}_{\pm}|\Psi\rangle = \frac{1}{2}(\mathbb{1} \pm \hat{U})|\Psi\rangle$ with the probability $p_{0/1} = \langle\Psi_{\pm}|\Psi_{\pm}\rangle = \langle\Psi|\hat{D}_{\pm}^{\dagger}\hat{D}_{\pm}|\Psi\rangle = \langle\Psi|\hat{E}_{\pm}|\Psi\rangle$, which is equivalent to measuring the POVM \hat{E}_{\pm} with the corresponding measurement operators \hat{D}_{\pm} . With a general unitary operator $\hat{U} = e^{ig(\hat{x},\hat{p})}$, where $g(\hat{x},\hat{p})$ is a real and symmetric function of position and momentum operator, we can also write $\hat{E}_{\pm} = \frac{1}{2}[\mathbb{1} \pm \cos(g(\hat{x},\hat{p}))]$, leading to $p_+ - p_- = \langle\cos(f(\hat{x},\hat{p}))\rangle$. Now, in order to measure any of the observables $\hat{\Gamma}_{\beta}$, we define $g(\hat{x},\hat{p}) = \arccos(F(\hat{x},\hat{p}))$, with the corresponding phase-space operator $F_{\beta}(\hat{x},\hat{p})$ (see Sec. III.3.3), yielding $p_+ - p_- = \langle F_{\beta}(\hat{x},\hat{p})\rangle = \langle\hat{\Gamma}_{\beta}\rangle$.

The above measurement strategy can be straightforwardly implemented with single photons passing through balanced Mach-Zehnder interferometers, as depicted in Fig. III.13(b) of the main text. Therein, the spatial distribution of the single photons represent the CV system and the path of the interferometer the state of the ancilla. Controlled unitary operations are realized via linear optical elements placed in one of the arms of the interferometer, and measurements of the ancilla state by detecting photons that exit from one of the two output ports using single photon bucket detectors. In the most general case we use a SLM with the option of additionally placing it in the Fourier plane between to lenses allowing us to perform arbitrary position or momentum phase gates, $e^{if(\hat{x})}$ or $e^{if(\hat{p})}$, where $f(\cdot)$ is user defined on the SLM. As discussed previously x and p can be considered as the near- and far-field variables with respect to the output plane of the source. Phase gates $e^{if(\hat{x}_{\phi})}$ in terms of an arbitrary quadrature $\hat{x}_{\phi} = \sin(\phi)\hat{x} + \cos(\phi)\hat{p}$ can be realized through fractional Fourier transform before and after the SLM using lens systems [Ozaktas et al., 2001; Tasca et al., 2008]. Hence, we have the ability to implement a broad class of unitaries on the spatial distribution of the photons allowing us to measure expectation values through $p_+ - p_- = \langle\cos f(\hat{x}_{\phi})\rangle$, in order to measure $\langle\hat{\Gamma}_{\beta}\rangle$ as described above.

At this point we note that the indirect measurement of the observables $\hat{\Gamma}_{\beta}$, as described in this Section, is less expensive in terms of the number of measurements that need to be performed in order to determine the expectation values $\langle\hat{\Gamma}_{\beta}\rangle$, than the direct measurement strategy, introduced in the previous Section [Machado et al., 2013; Hor-Meyll et al., 2014]. Also, as already mentioned in Sec. II.1.4, the indirect measurement strategy can be realized in several other experimental platforms using, for instance, trapped ions, cold atoms or micro-mechanical oscillators. To do so, one has to couple the considered system to an additional physical ancilla atom in order to implement the interferometer operation (III.148). In this case, one refers to such measurement strategies usually as Ramsey correlation measurements [Asadian et al., 2014; Gittsovich et al., 2015; Asadian et al., 2015].

III.5 Discussion

We presented a general framework that allows to encode, manipulate and readout discrete quantum information in phase space in terms of continuous variables states. This was possible by using the modular variables formalism that naturally leads to an intuitive definition of a set of logical qubit states and the corresponding logical operations. We demonstrated its strong relationship with the GKP formalism and show that, as

far as one is interested in performing quantum protocols involving expectation values of bounded periodic observables, so called modular variables, it is possible to encode binary quantum information in more general states than the ones introduced by GKP. The development of the present framework was strongly guided by its promising experimental applicability in terms of the transverse degrees of freedom of single photons. Nevertheless, other experimental platforms, such as trapped ions or micro-/nano-mechanical oscillators, that might profit from our ideas were discussed, as well.

From a fundamental point of view, our framework shows how to reveal naturally discrete structures of states and operations written in a continuous variable representation. This partially answers to the long-standing question of what is the most adapted way to process discrete quantum information in terms of continuous-variable states. Here we showed that, what concerns protocols involving measurements according to different mutually unbiased bases, our framework yields advantages compared to previous approaches. We will further demonstrate this point in the next Chapter which is devoted to the study of tests of fundamental properties of quantum mechanics. Furthermore, our framework provides a unifying formalism that shows how measurements of modular variables can be employed in quantum information protocols. In particular, we established a relation between a certain class of modular variables and their corresponding logical states which is a connection that was not known in previous studies involving measurements of modular variables.

An application of our ideas in hybrid quantum systems, which use CV besides some discrete degree of freedom, as is the case for single photons, could be advantageous for future experimental implementations of quantum information protocols. Moreover, the role of modular variables as phase space observables with a clear classical correspondence could be advantageous in macroscopic implementations of test of fundamental properties of quantum mechanics. Finally, we note that a generalization of the presented framework to d -dimensional logical encodings is rather straightforward and will be concluded in future work [Vernaz-Gris et al., 2014].

IV Tests of fundamental properties of quantum mechanics

The topic of the present Chapter is the study of fundamental properties of quantum mechanics in Hilbert spaces of various dimensions. In particular, we will focus on three of them: entanglement, Bell nonlocality and contextuality. For each of these properties we will first discuss its basic definition and review some known tools for its detection in terms of measurements of observables with finitely many outcomes. Following these introductions we will, for each fundamental property, propose methods that allow for generalizations of known criteria to the case of measurements of observables with bounded continuous outcomes, acting on infinite dimensional Hilbert spaces. Specifically, we will show how to derive entanglement witnesses and how to test discrete variable Bell inequalities in terms of measurements of bounded observables. In the case of contextuality we elucidate the peculiar structure obeyed by the spectrum of observables leading to state-independent maximal violation of contextuality. Examples demonstrating our insights are discussed in each of the following Sections, respectively, whereas we put special emphasis on applications of the modular variables framework introduced in the previous Chapter.

IV.1 Entanglement

In this Section we will give first a definition of entanglement and discuss some basic methods for its detection in terms of entanglement witnesses. Further on, we show how the stabilizer formalism can be used to derive entanglement witnesses and discuss applications for measurements of modular variables.

IV.1.1 Some basics about entanglement

When entanglement was discussed by Einstein, Podolsky and Rosen in 1935 in their seminal paper “Can Quantum-Mechanical Description of Physical Reality Be Considered Complete?” it was not yet clear how great the impact of this seemingly weird property on modern quantum physics would become [Einstein et al., 1935]. While at that time the greatest motivation was to find a reasonable explanation of entanglement, nowadays no one is questioning its crucial role as resource for many quantum information protocols. In the following, we will remind the definition of entanglement and discuss some quantities that can be used to detect it.

In practice, the nonlocal nature of entanglement reveals itself as correlations between two or more parties that are imprinted in the multi-partite quantum mechanical state vector $|\Psi\rangle \in \mathcal{H}$. More precisely, we say that a quantum state $|\Psi\rangle$ is *entangled* if it is not *separable*, meaning that it cannot be written as a tensor product state of its individual

parties:

$$|\Psi\rangle = \bigotimes_{k=1}^n |\psi_k\rangle = |\psi_1\rangle \otimes |\psi_2\rangle \otimes \dots \otimes |\psi_n\rangle, \quad (\text{IV.1})$$

where $|\psi_k\rangle \in \mathcal{H}_k$ and $\mathcal{H} = \bigotimes_{k=1}^n \mathcal{H}_k$ [Nielsen and Chuang, 2000]. Famous examples of entangled qubits states are the *Bell states*:

$$|\Psi_{\pm}\rangle = \frac{1}{\sqrt{2}} [|01\rangle \pm |10\rangle] \quad \text{and} \quad |\Phi_{\pm}\rangle = \frac{1}{\sqrt{2}} [|00\rangle \pm |11\rangle]. \quad (\text{IV.2})$$

For mixed states entanglement is defined similarly. A density matrix $\hat{\rho}$ is called entangled if it cannot be written as a classical mixture of product state:

$$\hat{\rho} = \sum_{\lambda} p_{\lambda} \bigotimes_{k=1}^n \hat{\rho}_k^{(i)} = \sum_{\lambda} p_{\lambda} \hat{\rho}_1^{(\lambda)} \otimes \hat{\rho}_2^{(\lambda)} \otimes \dots \otimes \hat{\rho}_n^{(\lambda)}, \quad (\text{IV.3})$$

with a normalized probability distribution $\{p_i\}$. In the following, we will mostly focus on bipartite entanglement which, for the remainder of this thesis, is the most relevant one.

IV.1.1.1 Entanglement witnesses

In this Section we want to discuss some possibilities to detect and quantify entanglement in terms of entanglement witnesses and measures, respectively. Thereby, we will also compare the two seemingly similar concepts of entanglement witnesses, on the one hand, and Bell inequalities, on the other hand.

In general, entanglement witness are defined as hermitian operators \hat{W} which fulfil:

$$\langle \hat{W} \rangle_{\hat{\rho}_s} \geq 0 \quad (\text{IV.4})$$

for all separable states $\hat{\rho}_s$ [Terhal, 2002; Horodecki et al., 2009; Gühne and Tóth, 2009]. Hence, if one finds $\langle \hat{W} \rangle_{\hat{\rho}_e} < 0$ one can conclude that $\hat{\rho}_e$ is entangled. Entanglement witnesses have a clear geometrical interpretation, because the condition $\langle \hat{W} \rangle = 0$ defines a hyper-plane in the space of all quantum states dividing it into two parts. Namely, one part which contains the whole subspace of separable states, and a second part which contains the remaining entangled quantum states. The existence of entanglement witnesses is guaranteed by the convexity of the set of separable states. In principle, it is possible to find for each entangled state an appropriate entanglement witness that is capable of detecting it [Horodecki et al., 1996]. However, the construction of entanglement witnesses is a mathematically non-trivial task and, in general, one would require an infinite number of witnesses in order to completely characterize the set of separable states [Ioannou and Travaglione, 2006; Gühne and Tóth, 2009]. In Sec. IV.1.2, we will discuss a method to derive entanglement witnesses based on the stabilizer formalism.

IV.1.1.2 Entanglement measures

For completeness, we mention also one possible measure of entanglement, namely the *entanglement entropy*. This measure relies on the fact that the reduced subsystems of a pure entangled system will be in a mixed state. Hence, by measuring the mixedness of the reduced density matrices of an entangled state we can quantify its entanglement. In order to measure the mixedness of a quantum states $\hat{\rho}$ we introduce the *von Neumann entropy*:

$$S(\hat{\rho}) = -\text{tr}[\hat{\rho} \ln(\hat{\rho})] = -\sum_i \lambda_i \ln(\lambda_i), \quad (\text{IV.5})$$

where $\{\lambda_i\}$ denotes the set of eigenvalues of the density operator $\hat{\rho}$. It is easy to see that the von Neumann entropy is equal to zero if $\hat{\rho} = |\Psi\rangle\langle\Psi|$ is a pure state, because then $\hat{\rho}$ has only one non-zero eigenvalue $\lambda = 1$. Thus, for non-pure state we have $S(\hat{\rho}) > 0$, and for maximally mixed states ($\hat{\rho}_{\text{mm}} = \mathbb{1}/d$) we reach the maximal value $\ln(d)$ of Eq. (IV.5). Now, we can define the entanglement entropy of a pure state $\hat{\rho}_{AB} \in \mathcal{H}_A \otimes \mathcal{H}_B$ as the von Neumann entropy of any of the two reduced states, $\hat{\rho}_A = \text{tr}_B[\hat{\rho}]$ or $\hat{\rho}_B = \text{tr}_A[\hat{\rho}]$ [Nielsen and Chuang, 2000]:

$$E(\hat{\rho}_{AB}) := S(\hat{\rho}_A) = S(\hat{\rho}_B) \quad (\text{IV.6})$$

Hence, we have that $E(\hat{\rho}_{AB}) = 0$ if $\hat{\rho}_{AB}$ is in a product state and $E(\hat{\rho}_{AB}) > 0$ if $\hat{\rho}_{AB}$ is entangled. It is important to note that the entanglement entropy provides only for pure states a meaningful measure of entanglement in the above sense.

With this we close this short introduction to the detection and quantification of entanglement. Some of the above introduced concepts will appear again in subsequent sections of this manuscript.

IV.1.2 Stabilizer formalism and entanglement detection

In the following we will review how the stabilizer formalism can be employed to derive entanglement witnesses. In this respect we will give first a brief introduction to the stabilizer formalism and show how it can be used to characterize classes of entangled states by so called stabilizer operators. The latter are then used to derive entanglement witnesses for the respective stabilized entangled states.

The goal of the stabilizer theory is to describe a quantum state through a set of so-called stabilizer operators instead of using its state vector [Gottesman, 1996, 1997]. In particular, one says that $|\Psi\rangle$ is stabilized by the operator \hat{S}_k if $|\Psi\rangle$ is an eigenstate of \hat{S}_k with eigenvalue $+1$:

$$\hat{S}_k |\Psi\rangle = |\Psi\rangle. \quad (\text{IV.7})$$

From this condition follows immediately that if two operators \hat{S}_k and \hat{S}_l stabilize the same state $|\Psi\rangle$ then also their product $\hat{S}_k \hat{S}_l$ stabilizes the same state. Furthermore, different stabilizers commute and we have $\hat{S}_k^2 = \mathbb{1}$. From these observations it follows that the stabilizer operators form a commutative group, referred to as *stabilizer*, which is closed under multiplications. In particular, for an n -qubit quantum state the group

of stabilizer operators has 2^n elements, but is generated by only N group generators \hat{g}_k . Using the stabilizer operators we can write $|\Psi\rangle\langle\Psi| = 1/(2^n) \sum_{k=1}^{2^n} \hat{S}_k = \prod_{l=1}^n \hat{g}_l$.

An example of an entangled state that can be expressed through stabilizer operators is the n -qubit Greenberger-Horne-Zeillinger (GHZ) state:

$$|\text{GHZ}_n\rangle = \frac{1}{\sqrt{2}} (|0\rangle_1|0\rangle_2 \dots |0\rangle_n + |1\rangle_1|1\rangle_2 \dots |1\rangle_n), \quad (\text{IV.8})$$

which is stabilized by the operators:

$$\hat{S}_1^{(\text{GHZ}_n)} = \prod_{k=1}^n \hat{\sigma}_x^{(k)}, \quad (\text{IV.9})$$

$$\hat{S}_k^{(\text{GHZ}_n)} = \hat{\sigma}_z^{(k)} \hat{\sigma}_z^{(k-1)}, \quad (\text{IV.10})$$

for $k = 2, \dots, n$, and where $\sigma_\alpha^{(k)}$, with $\alpha = x, y, z$, denotes the three Pauli operators (see Sec. II.1.1) acting on the k th qubit. It is straightforward to check that the operators (IV.9) and (IV.10) stabilize the GHZ state (IV.8) uniquely and we thus have:

$$\hat{S}_k^{(\text{GHZ}_n)} |\text{GHZ}_n\rangle = |\text{GHZ}_n\rangle \quad (\text{IV.11})$$

for all $k = 1, \dots, n$. As mentioned previously the GHZ state is not only stabilized by the operators $\hat{S}_k^{(\text{GHZ}_n)}$ but also by their products which are part of the same stabilizer group denoted as $\mathcal{S}^{(\text{GHZ}_n)}$.

Using the stabilizer operators (IV.9) and (IV.10) we can derive entanglement witnesses detecting entanglement around the n -qubit GHZ states, which read:

$$\hat{W}^{(\text{GHZ}_n)} = c\mathbb{1} - \hat{S}_k^{(\text{GHZ}_n)} - \hat{S}_l^{(\text{GHZ}_n)}, \quad (\text{IV.12})$$

where

$$c = \max_{\hat{\rho} \in \mathcal{S}_{\text{sep}}} \langle \hat{S}_k^{(\text{GHZ}_n)} - \hat{S}_l^{(\text{GHZ}_n)} \rangle, \quad (\text{IV.13})$$

and \mathcal{S}_{sep} denotes the set of separable states. However, the witness (IV.12) is only capable of detecting entanglement if c is smaller than $\langle \hat{S}_k^{(\text{GHZ}_n)} + \hat{S}_l^{(\text{GHZ}_n)} \rangle$ for entangled states. Whether or not this is the case depends on the local commutativity of the stabilizer operators contained in (IV.12). In particular, $\hat{S}_k^{(\text{GHZ}_n)}$ and $\hat{S}_l^{(\text{GHZ}_n)}$ are called locally commuting if each of the local operators $\hat{\sigma}_\alpha^{(k)}$ and $\hat{\sigma}_{\alpha'}^{(l)}$ forming the tensor products (IV.9) and (IV.10) are commuting. In this case, they share a common eigenstate and we find that $\langle \hat{S}_k^{(\text{GHZ}_n)} + \hat{S}_l^{(\text{GHZ}_n)} \rangle = 2$ for separable and entangled states. Hence, to detect entanglement in terms of stabilizer operators we have to choose them to be locally non-commuting [Tóth and Gühne, 2005; Gühne and Tóth, 2009].

Once we accepted this, we can show that for product states we have:

$$\begin{aligned}
\langle \hat{S}_1^{(\text{GHZ}_n)} \rangle + \langle \hat{S}_k^{(\text{GHZ}_n)} \rangle &= \langle \hat{\sigma}_x^{(1)} \rangle \dots \langle \hat{\sigma}_x^{(n)} \rangle + \langle \hat{\sigma}_z^{(k-1)} \rangle \langle \hat{\sigma}_z^{(k)} \rangle \\
&\leq |\langle \hat{\sigma}_x^{(k-1)} \rangle| |\langle \hat{\sigma}_x^{(k)} \rangle| + |\langle \hat{\sigma}_z^{(k-1)} \rangle| |\langle \hat{\sigma}_z^{(k)} \rangle| \\
&\leq \sqrt{\langle \hat{\sigma}_x^{(k-1)} \rangle^2 + \langle \hat{\sigma}_z^{(k-1)} \rangle^2} + \sqrt{\langle \hat{\sigma}_x^{(k)} \rangle^2 + \langle \hat{\sigma}_z^{(k)} \rangle^2} \\
&\leq 1
\end{aligned} \tag{IV.14}$$

where we used the Cauchy-Schwarz inequality and the boundedness of the Bloch vector $\langle \hat{\sigma}_x^{(k)} \rangle^2 + \langle \hat{\sigma}_z^{(k)} \rangle^2 \leq \langle \hat{\sigma}_x^{(k)} \rangle^2 + \langle \hat{\sigma}_y^{(k)} \rangle^2 + \langle \hat{\sigma}_z^{(k)} \rangle^2 \leq 1$. Convexity, extends the bound in Eq. (IV.14) also to separable states. Hence, we find that $c = 1$ and the GHZ state witness reads:

$$\hat{W}^{(\text{GHZ}_n)} = \mathbb{1} - \hat{S}_1^{(\text{GHZ}_n)} - \hat{S}_k^{(\text{GHZ}_n)}, \tag{IV.15}$$

with $k = 2, \dots, n$. One can also construct witnesses involving more than two stabilizer operator, e.g. $\hat{W}^{(\text{GHZ}_n)} = \mathbb{1} - \hat{S}_1^{(\text{GHZ}_n)} - \hat{S}_k^{(\text{GHZ}_n)} - \hat{S}_1^{(\text{GHZ}_n)} \hat{S}_k^{(\text{GHZ}_n)}$, leading to a higher noise tolerance [Tóth and Gühne, 2005].

Similarly, we can construct entanglement witnesses also for other types of entangled states that can be uniquely described by a stabilizer. For instance, for cluster states $|C_n\rangle$ which are stabilized by the operators:

$$\hat{S}_1^{(C_n)} = \hat{\sigma}_x^{(1)} \hat{\sigma}_z^{(2)}, \tag{IV.16}$$

$$\hat{S}_k^{(C_n)} = \hat{\sigma}_z^{(k-1)} \hat{\sigma}_x^{(k)} \hat{\sigma}_z^{(k+1)}, \tag{IV.17}$$

$$\hat{S}_n^{(C_n)} = \hat{\sigma}_z^{(n-1)} \hat{\sigma}_x^{(n)}, \tag{IV.18}$$

with $k = 2, \dots, n-1$, or for general graph states $|G_n\rangle$ whose stabilizers read:

$$\hat{S}_k^{(G_n)} = \hat{\sigma}_x^{(k)} \prod_{l \neq k} (\hat{\sigma}_z^{(l)})^{\Omega_{kl}}, \tag{IV.19}$$

with the adjacency matrix Ω . A graph state is defined by a graph consisting of N vertices which are connected by edges according to the adjacency matrix Ω . Thus, we have $\Omega_{kl} = 1$ or 0 depending if two vertices are connected or not.

For more details about the entanglement detection in terms of stabilizer operators, for instance, for a generalization to multi-partite entanglement detection, we refer the reader to the literature [Tóth and Gühne, 2005; Gühne and Tóth, 2009]. Instead, in the following, we want to apply the above formalism to derive entanglement witnesses involving measurements of modular variables.

IV.1.3 Modular variables entanglement witnesses

Now we turn to the entanglement detection in phase space in terms of suitably designed entanglement witnesses involving measurements of modular variables. To do so we will first employ the above introduced stabilizer formalism to the case of continuous variables and show how to stabilize classes of entangled states in terms of unitary

phase space operations. These stabilizer operations then lead us to (novel) modular-variable entanglement witnesses detecting entanglement in the logical space introduced in Sec. III.2.1.

Let us recall that in Sec. III.2.1 we introduced logical states (III.75) and (III.76) by dichotomizing the Hilbert space with respect to the modular position \bar{x} (see Fig. III.7). In the same Section we also discussed the role of GKP states (III.77) and (III.78) as a nonphysical example of these logical states, since they consist of superpositions of infinitely squeezed position and momentum eigenstates. For convenience, we recall their definitions here:

$$|0_{\text{GKP}}\rangle = |\bar{x} = 0, \bar{p} = 0\rangle = \sum_n |\ell(2n)/2\rangle_x, \quad (\text{IV.20})$$

$$|1_{\text{GKP}}\rangle = |\bar{x} = \frac{\ell}{2}, \bar{p} = 0\rangle = \sum_n |\ell(2n+1)/2\rangle_x. \quad (\text{IV.21})$$

In [Gottesman et al., 2001], the author's particular interest in this set of states was motivated by the fact that they can be characterized by two unitary stabilizer operations:

$$\hat{S}_1^{(\text{GKP})} = e^{4\pi i \hat{x}/\ell}, \quad (\text{IV.22})$$

$$\hat{S}_2^{(\text{GKP})} = e^{i\hat{p}\ell}, \quad (\text{IV.23})$$

which yield some convenient error correction properties (see [Gottesman et al., 2001] for more details). Equivalently, the GKP stabilizer operations can be expressed through the logical Pauli operations (III.82) and (III.83) as: $\hat{S}_1^{(\text{GKP})} = \hat{Z}^2$ and $\hat{S}_2^{(\text{GKP})} = \hat{X}^2$, respectively.

Similarly to the discussion in the previous Section, we can now use the logical Pauli operations \hat{Z} and \hat{X} also to define stabilizer operations characterizing entangled states in the GKP logical basis $|0_{\text{GKP}}\rangle$ and $|1_{\text{GKP}}\rangle$. For instance, an n -mode GHZ state in the GKP basis:

$$|\text{GHZ}_{\text{GKP}}^{(n)}\rangle = \frac{1}{\sqrt{2}} (|0_{\text{GKP}}\rangle_1 |0_{\text{GKP}}\rangle_2 \dots |0_{\text{GKP}}\rangle_n + |1_{\text{GKP}}\rangle_1 |1_{\text{GKP}}\rangle_2 \dots |1_{\text{GKP}}\rangle_n), \quad (\text{IV.24})$$

is stabilized by the operations:

$$\hat{S}_1^{(\text{GHZ}_n)} = \prod_{k=1}^N \hat{X}^{(k)}, \quad (\text{IV.25})$$

$$\hat{S}_k^{(\text{GHZ}_n)} = \hat{Z}^{(k)} \hat{Z}^{(k-1)}. \quad (\text{IV.26})$$

with $k = 2, \dots, n$, where $\hat{Z}^{(k)}$ and $\hat{X}^{(k)}$ denote the logical operations (III.82) and (III.83) acting on mode k . At this point we emphasize that the stabilizer operations (IV.25) and (IV.26) can only characterize uniquely the non-physical GHZ state (IV.24). Nevertheless, in the following we would like to exploit them to construct entanglement witnesses capable of detecting physical continuous-variable GHZ states that are close to the nonphysical ones defined in Eq. (IV.24).

According to the remarks made in Sec. IV.1.2, it would be desirable to define such

entanglement witnesses as a straightforward generalization of the finite dimensional witness (IV.15), as

$$\hat{W}^{(\text{GHZ}_n)} = \mathbb{1} - \hat{S}_1^{(\text{GHZ}_n)} - \hat{S}_k^{(\text{GHZ}_n)}. \quad (\text{IV.27})$$

However, even though the stabilizer operations $\hat{S}_1^{(\text{GHZ}_n)}$ and $\hat{S}_k^{(\text{GHZ}_n)}$ are locally non-commuting (see commutation relations of the logical Pauli operations \hat{Z} and \hat{X} in Sec. III.2.2.1), they are defined as products of phase space displacements and thus nonphysical quantities. To define a measurable, thus hermitian, entanglement witness operator we have to consider quantities involving real (or imaginary) parts of the above stabilizer operations, for instance:

$$\hat{W}_R^{(\text{GHZ}_n)} = \mathbb{1} - \hat{R}_1^{(\text{GHZ}_n)} - \hat{R}_k^{(\text{GHZ}_n)}, \quad (\text{IV.28})$$

where

$$\hat{R}_1^{(\text{GHZ}_n)} = \prod_{k=1}^n \text{Re}[\hat{X}^{(k)}], \quad (\text{IV.29})$$

$$\hat{R}_k^{(\text{GHZ}_n)} = \text{Re}[\hat{Z}^{(k)}] \text{Re}[\hat{Z}^{(k-1)}], \quad (\text{IV.30})$$

with $k = 2, \dots, n$. Remember that the operators $\text{Re}[\hat{X}^{(k)}]$ and $\text{Re}[\hat{Z}^{(k)}]$ are examples of the modular variables discussed in Sec. III.1.2 and also particular cases of the general readout observables (III.94), introduced in Sec. III.3.1. Let us write $\hat{\Gamma}_x^{(k)} = \text{Re}[\hat{X}^{(k)}] = \cos(\hat{p}_k \ell/2)$ and $\hat{\Gamma}_z^{(k)} = \text{Re}[\hat{Z}^{(k)}] = \cos(\hat{x}_k 2\pi/\ell)$. We also note that, as previously discussed in Sec. III.3.3.4, the operators $\hat{\Gamma}_x^{(k)}$ and $\hat{\Gamma}_z^{(k)}$ are non-commuting due to the fact that the product of their periods is not equal to 2π . Hence, the correlation operators (IV.29) and (IV.30) do not commute locally and are thus good candidates for the detection of entangled states that are close to the logical GHZ state (IV.24).

Further on, with the help of the triangle and Cauchy-Schwarz inequalities we can show that for product states:

$$\begin{aligned} \langle \hat{R}_1^{(\text{GHZ}_n)} \rangle + \langle \hat{R}_k^{(\text{GHZ}_n)} \rangle &= \langle \hat{\Gamma}_x^{(1)} \rangle \dots \langle \hat{\Gamma}_x^{(n)} \rangle + \langle \hat{\Gamma}_z^{(k-1)} \rangle \langle \hat{\Gamma}_z^{(k)} \rangle \\ &\leq |\langle \hat{\Gamma}_x^{(k-1)} \rangle| |\langle \hat{\Gamma}_x^{(k)} \rangle| + |\langle \hat{\Gamma}_z^{(k-1)} \rangle| |\langle \hat{\Gamma}_z^{(k)} \rangle| \\ &\leq \sqrt{\langle \hat{\Gamma}_x^{(k-1)} \rangle^2 + \langle \hat{\Gamma}_z^{(k)} \rangle^2} \sqrt{\langle \hat{\Gamma}_x^{(k)} \rangle^2 + \langle \hat{\Gamma}_z^{(k-1)} \rangle^2} \\ &\leq 1 \end{aligned} \quad (\text{IV.31})$$

where the last inequality holds due the relation (III.104), namely that the sum of the modulus squares of the operators $\hat{\Gamma}_\beta^{(k)}$ is bounded by $(\max_{\bar{x}, \bar{p}, \alpha} |\zeta_\beta(\bar{x}, \bar{p})|)^2$. And, as discussed in Sec. III.3.1, in the particular case of the modular variables $\text{Re}[\hat{X}^{(k)}]$ and $\text{Re}[\hat{Z}^{(k)}]$ this bound is equal to *one*. On the other hand, if we consider the operator

$$\hat{R}_1^{(\text{GHZ}_n)} + \hat{R}_k^{(\text{GHZ}_n)} = \prod_{l=1}^n \hat{\Gamma}_x^{(l)} + \hat{\Gamma}_z^{(k-1)} \hat{\Gamma}_z^{(k)} \quad (\text{IV.32})$$

and evaluate its expectation value with respect to a physical GHZ state in the logical basis $\{|0_L\rangle, |1_L\rangle\}$:

$$|\text{GHZ}_L^{(n)}\rangle = \frac{1}{\sqrt{2}}(|0_L\rangle_1|0_L\rangle_2 \dots |0_L\rangle_n + |1_L\rangle_1|1_L\rangle_2 \dots |1_L\rangle_n), \quad (\text{IV.33})$$

we expect to violate the separability bound in Eq. (IV.31), for an appropriate choice of the logical state wave functions $f_k(\bar{x}^{(k)}, \bar{p}^{(k)})$. And indeed the expectation value of (IV.32) with respect to the state (IV.33) reads:

$$\begin{aligned} \langle \hat{R}_1^{(\text{GHZ}_n)} + \hat{R}_k^{(\text{GHZ}_n)} \rangle &= \prod_{l=1}^n \int_{-\frac{\ell}{4}}^{\frac{\ell}{4}} d\bar{x}^{(l)} \int_{-\frac{\pi}{\ell}}^{\frac{\pi}{\ell}} d\bar{p}^{(l)} \cos(\bar{p}^{(l)} \frac{\ell}{2}) |f_l(\bar{x}^{(l)}, \bar{p}^{(l)})|^2 \\ &+ \prod_{l=k-1}^k \int_{-\frac{\ell}{4}}^{\frac{\ell}{4}} d\bar{x}^{(l)} \int_{-\frac{\pi}{\ell}}^{\frac{\pi}{\ell}} d\bar{p}^{(l)} \cos(\bar{x}^{(l)} \frac{2\pi}{\ell}) |f_l(\bar{x}^{(l)}, \bar{p}^{(l)})|^2, \end{aligned} \quad (\text{IV.34})$$

which can be simplified by assuming that the wave functions $f_k(\bar{x}^{(k)}, \bar{p}^{(k)}) = f(\bar{x}^{(k)}, \bar{p}^{(k)})$ are equal for all k :

$$\langle \hat{R}_1^{(\text{GHZ}_n)} + \hat{R}_k^{(\text{GHZ}_n)} \rangle = K_x^n + K_z^2 \quad (\text{IV.35})$$

where

$$K_x = \int_{-\ell/4}^{\ell/4} d\bar{x} \int_{-\pi/\ell}^{\pi/\ell} d\bar{p} \cos(\bar{p} \frac{\ell}{2}) |f(\bar{x}, \bar{p})|^2, \quad (\text{IV.36})$$

$$K_z = \int_{-\ell/4}^{\ell/4} d\bar{x} \int_{-\pi/\ell}^{\pi/\ell} d\bar{p} \cos(\bar{x} \frac{2\pi}{\ell}) |f(\bar{x}, \bar{p})|^2. \quad (\text{IV.37})$$

Thus, the expectation value (IV.35) solely depends on the values K_x , K_z and the number of modes n .

To study a numerical example of the values K_x and K_z we choose $f(\bar{x}, \bar{p})$ to be a Gaussian with widths Δ and κ in the modular position and momentum, respectively, and with periodic boundary conditions on the domains $[-\ell/4, \ell/4] \times [-\pi/\ell, \pi/\ell]$. In particular, as studied in Sec. (III.1.5), we have $f(\bar{x}, \bar{p}) = \mathcal{N} T(\bar{x} - a_{\bar{x}}) C(\bar{p} - a_{\bar{p}})$ (see Eq. (III.53)), where $T(\bar{x} - a_{\bar{x}})$ and $C(\bar{p} - a_{\bar{p}})$ are defined according to Eqs. (III.54) and (III.55), respectively, and with $L = \ell/2$. The parameters $a_{\bar{x}}$ and $a_{\bar{p}}$ fix the location of the Gaussian inside the domain $[-\ell/4, \ell/4] \times [-\pi/\ell, \pi/\ell]$. Note that, if the limits $\Delta/L \ll 1$ and $\kappa L \ll 1$ hold, this modular wave function corresponds to a comb of Gaussian spikes with widths Δ , that are separated by the distance $\ell/2$ and enclosed by an envelope of width $1/\kappa$ (see Figs. III.4 and III.5 for examples). The constant \mathcal{N} ensures that the wave function $f(\bar{x}, \bar{p})$ is normalized on the domain $[-\ell/4, \ell/4] \times [-\pi/\ell, \pi/\ell]$. Accordingly, in the above limit we have $\mathcal{N} \approx 1$ reproducing Eq. (III.53).

Figure IV.1 shows a density plot of the modulus square of the Gaussian wave function $f(\bar{x}, \bar{p})$ and indicates the location $(a_{\bar{x}}, a_{\bar{p}})$ of the Gaussian in the modular domain $[-\ell/4, \ell/4] \times [-\pi/\ell, \pi/\ell]$. On the right-hand side of Fig. IV.1 we present a plot of the value K_x (K_z) as a function of $a_{\bar{p}}$ ($a_{\bar{x}}$), for different modular position and momentum widths, Δ and κ . Thereby, it is enough to plot K_x as a function of $a_{\bar{p}}$ and K_z as a

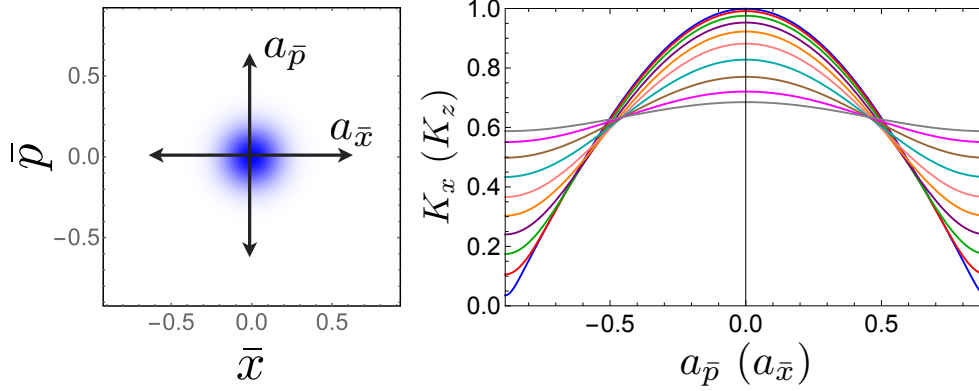


Figure IV.1: (Left) Density plot of the modulus square of the wave function $f(\bar{x}, \bar{p})$ in the case of a Gaussian with $\ell = 2\sqrt{\pi}$, as discussed in the text. The two double arrows indicate the position of the Gaussian $(a_{\bar{x}}, a_{\bar{p}})$ in the modular domain $[-\ell/4, \ell/4] \times [-\pi/\ell, \pi/\ell]$. (Right) Plot of the value K_x (K_z), in the case of the Gaussian wave function $f(\bar{x}, \bar{p})$, as a function of the position $a_{\bar{p}}$ ($a_{\bar{x}}$) of the Gaussian in the modular momentum (position) direction. Different curves correspond to different widths in the modular momentum: $\kappa = 0.02(2\pi/\ell)$ (blue), $\kappa = 0.06(2\pi/\ell)$ (red), $\kappa = 0.1(2\pi/\ell)$ (green), $\kappa = 0.14(2\pi/\ell)$ (purple), $\kappa = 0.18(2\pi/\ell)$ (orange), $\kappa = 0.22(2\pi/\ell)$ (pink), $\kappa = 0.26(2\pi/\ell)$ (Cyan), $\kappa = 0.3(2\pi/\ell)$ (brown), $\kappa = 0.34(2\pi/\ell)$ (magenta), $\kappa = 0.38(2\pi/\ell)$ (gray). The values are ordered from the topmost to the bottommost curve with respect to the origin $a_{\bar{p}}(a_{\bar{x}}) = 0$. In the case of K_z we choose the same widths for Δ multiplied by $\ell/2$ instead of $2\pi/\ell$.

function of $a_{\bar{x}}$, because (IV.36) and (IV.37) are independent with respect to the position of the Gaussian wave function in the modular position and momentum direction, $a_{\bar{x}}$ and $a_{\bar{p}}$, respectively. To see this, we recall that the functions $\zeta_x(\bar{x}, \bar{p}) = \cos(\bar{p}\ell/2)$ and $\zeta_z(\bar{x}, \bar{p}) = \cos(\bar{x}2\pi/\ell)$, which define the observables $\hat{\Gamma}_x$ and $\hat{\Gamma}_z$, are independent of the modular position \bar{x} and momentum \bar{p} , respectively, and thus the integration in Eqs. (IV.36) and (IV.37) factorizes. Furthermore, the behaviour of K_x and K_z as a function of $a_{\bar{p}}$ and $a_{\bar{x}}$, respectively, is identical because for the choice $\ell = 2\sqrt{\pi}$ we have $\ell/2 = 2\pi/\ell = \sqrt{\pi}$.

It is solely the behaviour of K_x and K_z which finally determines the expectation value (IV.35) and shows if the witness (IV.28) is capable to detect the logical GHZ states (IV.33). If we choose the Gaussian $f(\bar{x}, \bar{p})$ centered around the origin $(a_{\bar{x}}, a_{\bar{p}}) = (0, 0)$ we find that, for sufficiently squeezed modular wave functions (sufficiently small Δ and κ), K_x and K_z approach values near to 1 and thus the expectation value (IV.35) exceeds the separability bound of *one*. However, if we choose the Gaussian centered at one of the corners of the modular domain $(a_{\bar{x}}, a_{\bar{p}}) = (\pm\ell/2, \pm 2\pi/\ell)$, both K_x and K_z are near to zero and thus the GHZ state (IV.33) cannot be detected.

At this point we close our elaborations about the detection of entanglement in terms of modular-variable entanglement witnesses and turn to the study of Bell nonlocality. However, keep in mind that the above introduced techniques are not restricted to GHZ states and it will be a task of future work to find other interesting states that might be

detectable by such witnesses.

IV.2 Nonlocality

In this Section our aim is to study *Bell nonlocality* which we introduce in the following on the basis of a general treatment of nonlocal correlations in terms of discrete joint-probability distributions. We will see how Bell inequalities can be used to detect nonlocal correlations and discuss their relation to entanglement. As part of our results, we show how to adapt the CHSH inequality to more general measurements setups involving measurements of bounded continuous variables. Finally, we discuss examples of our considerations in terms of measurements of modular variables.

IV.2.1 Mathematical characterization of correlations

In order to introduce the concept of Bell nonlocality we consider the typical *Bell experiment* depicted in Fig. IV.2(a). A source (S) distributes two physical systems (for instance two particles) to two distant observers, usually referred to as Alice (A) and Bob (B). Each of the two observers then performs measurements of m different observables, labeled by A_i and B_j , respectively, with $i, j = 1, \dots, m$, each yielding n possible outcomes denoted by $a, b = 1, \dots, n$. For the following considerations the precise choice of Alice's and Bob's observables, A_i and B_i , is not of importance. We are only interested in recording the outcomes a and b of measurements corresponding to different measurement settings i and j , where the latter simply label different measurement possibilities without giving further details.

The outcomes of the experiment are distributed according to a joint-probability distribution $p(a, b|i, j)$ which can be experimentally estimated by repeating the measurements a sufficient number of times. We thus have n^2m^2 joint probabilities that completely characterize the Bell experiment. These probabilities are often expressed in a vector notation $\mathbf{p} = \{p(a, b|i, j)\}$ and referred to as *correlations* (or *behaviours*). Each experimental situation can thus be viewed as a point in a (n^2m^2) -dimensional vector space \mathcal{P} . By including the positivity and normalization condition of the joint probabilities $p(a, b|i, j)$ we are left with a $((n-1)^2m^2)$ -dimensional space.

However, the vector space \mathcal{P} of all normalized joint-probability distributions is still very large and, a given physical model used to calculate the probabilities $p(a, b|i, j)$, will in general impose constraints on the correlations \mathbf{p} which then live in a subspace of \mathcal{P} . The first constraints we want to discuss here are called the non-signalling constraints:

$$\sum_{b=1}^n p(a, b|i, j) = \sum_{b=1}^n p(a, b|i, j'), \quad \text{for all } a, i, j, j' \quad (\text{IV.38})$$

$$\sum_{a=1}^n p(a, b|i, j) = \sum_{a=1}^n p(a, b|i', j), \quad \text{for all } a, i, i', j \quad (\text{IV.39})$$

which imply that Alice's and Bob's marginal distributions $p(a|i, j) = p(a|i)$ and $p(a|i, j) = p(a|j)$ are independent of each others measurement settings hindering a direct and instantaneous communication between them. The latter would lead to a violation of relativity thus making the no-signalling constraints (IV.39) a reasonable physical assumption.

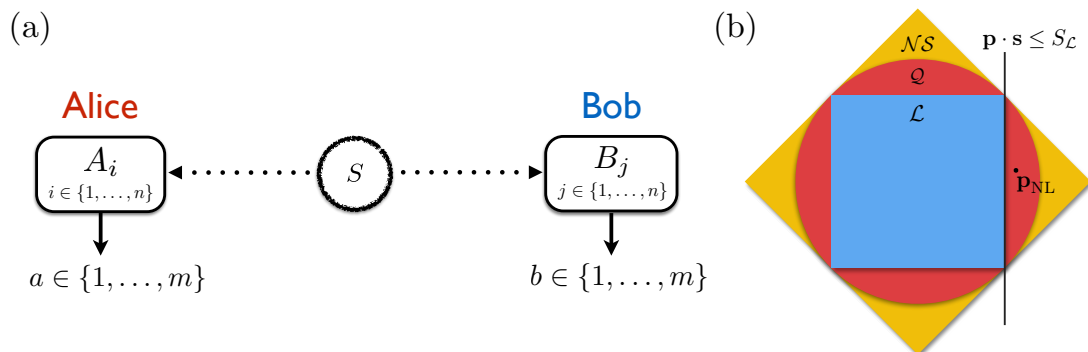


Figure IV.2: (a) Scheme of a Bell experiment. A source (S) creates two physical systems and distributes them to two distant observers, referred to as Alice (A) and Bob (B). Alice and Bob each perform n measurements on their subsystems with observables A_i and B_j , respectively. Each measurement can yield up to m different outcomes a and b . (b) Schematic representation of the three sets of correlations \mathcal{L} , \mathcal{Q} and \mathcal{NS} projected onto a two dimensional plane. The thick black line depicts a Bell inequality and the black point an element \mathbf{p}_{NL} of the quantum set \mathcal{Q} violating the Bell inequality $\mathbf{p} \cdot \mathbf{s} > S_{\mathcal{L}}$.

tion. The remaining correlations \mathbf{p} fulfilling the no-signalling constraints are elements in a subspace \mathcal{NS} of the whole space \mathcal{P} [Brunner et al., 2014].

Next, we want to consider the so-called locality constraint whose discovery is considered one of the main achievements of J. Bell [Bell, 1964]. The idea is to assume that the outcomes a and b of our Bell experiment are governed by some causal influence that is determined by a set of past factors described by the variable λ , referred to as *local hidden variable* (LHV). If the variable λ accounts for all past factors that might have caused correlations between the outcomes a and b , we can consequently factorize the joint probabilities as:

$$p(a, b|i, j, \lambda) = p(a|i, \lambda)p(b|j, \lambda). \quad (\text{IV.40})$$

Hence, the outcomes on Alice's and Bob's side depend solely on their local measurement settings i and j , respectively, and on the common hidden variable λ . Further on, in a more general description we have to assume that the hidden variable will, in general, not be constant during different runs of the experiment because its precise nature is unknown. The final joint probabilities are then given by an average over the hidden variable λ according to a probability distribution $q(\lambda)$. Taking all this into account, we thus arrive at the locality constraint:

$$p(a, b|i, j) = \int d\lambda q(\lambda)p(a|i, \lambda)p(b|j, \lambda), \quad (\text{IV.41})$$

which contains the additional assumption that the choice of the measurement settings i and j is made independently by Alice and Bob and thus is independent of λ . Equation (IV.41) represents a concise definition of locality imposed on the joint probabilities calculated within the context of local hidden variable theories (or local realistic theo-

ries). It is straightforward to see that the local joint probabilities always satisfy the no-signalling constraints (IV.39) making the set of local correlations \mathcal{L} a subset of the set of no-signalling correlations \mathcal{NS} .

Finally, we introduce the set of quantum correlations \mathcal{Q} which consists of all joint-probability distributions that can be expressed as a result of a quantum mechanical measurements (see Sec. II.1.4), as

$$p(a, b|i, j) = \text{tr} \left[\hat{E}_{a|i} \otimes \hat{E}_{b|j} \hat{\rho}_{AB} \right] \quad (\text{IV.42})$$

where $\hat{\rho}_{AB}$ is the joint density matrix on Alice's and Bob's tensor product space $\mathcal{H} = \mathcal{H}_A \otimes \mathcal{H}_B$, and $\{\hat{E}_{a|i}\}_{i=1, \dots, m}$ and $\{\hat{E}_{b|j}\}_{j=1, \dots, m}$ are sets of POVMs on \mathcal{H}_A and \mathcal{H}_B , respectively, characterizing their local measurement strategies. It is easy to show that all local correlations admit a representation according to Eq. (IV.42), thus making the local set \mathcal{L} a subset of the quantum set \mathcal{Q} [Pitowsky, 1986]. However, there are quantum correlations that fulfill the no-signalling constraint but do not belong to the local set \mathcal{L} [Rastall, 1985; Popescu and Rohrlich, 1994]. This implies the inclusion relation $\mathcal{L} \subset \mathcal{Q} \subset \mathcal{NS}$.

Furthermore, the three sets \mathcal{L} , \mathcal{Q} and \mathcal{NS} have the same dimensions $= 2(n-1)m + (d-1)^2 m^2$ [Pironio, 2005], they are bounded and convex [Pitowsky, 1986]. A simplified graphical representation of the discussed sets in two dimensions is presented in Fig. IV.2(b). To decide if a given \mathbf{p} belongs to one of the three sets \mathcal{L} , \mathcal{Q} or \mathcal{NS} one can make use of the hyperplane separation theorem, which states that for each \mathbf{p} , that does not belong to one of the three latter sets, one can find a hyperplane that separates this \mathbf{p} from the corresponding set (see Fig. IV.2(b)). Meaning, if $\mathbf{p} \notin \mathcal{L}, \mathcal{Q}, \mathcal{NS}$, then there exists an inequality:

$$\mathbf{p} \cdot \mathbf{s} = \sum_{a,b,i,j} s_{a,b;i,j} p(a, b|i, j) \leq S_{\mathcal{L}, \mathcal{Q}, \mathcal{NS}}, \quad (\text{IV.43})$$

which is violated if $\mathbf{p} \notin \mathcal{L}, \mathcal{Q}, \mathcal{NS}$. In the particular case of the local set \mathcal{L} , such inequalities are called Bell inequalities and the correlations \mathbf{p} which violate a Bell inequality are called nonlocal correlations. Therefore, in this context the term *nonlocality* refers specifically to the possibility of violating Bell inequalities. Furthermore, the bound on the inequalities which characterize the quantum set $S_{\mathcal{Q}}$ is called Tsirelson bound and $S_{\mathcal{NS}}$ no-signalling bound.

One specific example of the above Bell experiment is the one which considers $n = 2$ measurements on each subsystem yielding $m = 2$ different (binary) outcomes. In this case, the corresponding Bell inequality characterizing the set of local correlations \mathcal{L} is known as Clauser-Horne-Shimony-Holt (CHSH) inequality [Clauser et al., 1969] and mostly known in the form

$$-2 \leq \mathcal{B} = \langle A_1 B_1 \rangle + \langle A_1 B_2 \rangle + \langle A_2 B_1 \rangle - \langle A_2 B_2 \rangle \leq 2. \quad (\text{IV.44})$$

Further on, if we assume that the binary measurement outcomes are given by $a, b = \pm 1$, we can express the correlation functions contained in (IV.44) as $\langle A_i B_j \rangle = \sum_{a,b} ab p(a, b|i, j)$, allowing to express (IV.44) in the form (IV.43) with $S_{\mathcal{L}} = 2$. Correspondingly, the Tsirelson and no-signalling bound on the CHSH inequality read $S_{\mathcal{Q}} = 2\sqrt{2}$ and $S_{\mathcal{NS}} = 4$.

To show the violation of the CHSH inequality in quantum mechanics let's consider the entangled quantum state $|\psi\rangle = (|0\rangle_a|1\rangle_b - |1\rangle_a|0\rangle_b)/\sqrt{2}$. Further on, we consider the local measurements on Alice's side to be $A_1 = \hat{\sigma}_x$ and $A_2 = \hat{\sigma}_z$, and on Bob's side $B_1 = -(\hat{\sigma}_x + \hat{\sigma}_z)/\sqrt{2}$ and $B_2 = (\hat{\sigma}_z - \hat{\sigma}_x)/\sqrt{2}$. For Pauli operations it is easy to show that the correlation function in the above entangled state yields $\langle \hat{\sigma}_i \hat{\sigma}_j \rangle_{|\psi\rangle} = -\delta_{ij}$. Using this in the CHSH term (IV.44), we find that:

$$\langle A_1(B_1 + B_2) + A_2(B_1 - B_2) \rangle = -\sqrt{2}\langle \hat{\sigma}_x \hat{\sigma}_x \rangle - \sqrt{2}\langle \hat{\sigma}_z \hat{\sigma}_z \rangle = 2\sqrt{2} > 2. \quad (\text{IV.45})$$

Hence, the locality bound of *two* can be violated for a specific class of nonlocal states and appropriately chosen measurements. In the following, we will discuss more the relationship between such nonlocal states and entangled states.

IV.2.1.1 Entanglement vs. nonlocality

Entanglement is closely related to nonlocality. For instance, it is easy to see that every separable quantum state is local in the sense that it obeys a local joint-probability distribution (compare with Eq. (IV.41)):

$$\begin{aligned} P(a_1, a_2) &= \text{tr}[\hat{\rho}(\hat{E}_{a_1} \otimes \hat{E}_{a_2})] \\ &= \sum_{\lambda} p_{\lambda} \text{tr}[\hat{\rho}_1^{(\lambda)} \hat{E}_{a_1}] \text{tr}[\hat{\rho}_2^{(\lambda)} \hat{E}_{a_2}] \\ &= \sum_{\lambda} p_{\lambda} P(a_1, \lambda) P(a_2, \lambda). \end{aligned} \quad (\text{IV.46})$$

Hence, we can conclude that every quantum state which gives rise to nonlocal correlations, *i.e.* which violates a Bell inequality, will be also entangled. Entanglement is thus a necessary ingredient for the observation of nonlocal correlations in quantum mechanics. A natural question to ask is thus if entanglement is also sufficient for the observation of nonlocal correlations. In the case of pure states the answer is yes. For every pure quantum state it is possible to find local measurements such that the resulting measurement statistics violate a Bell inequality [Gisin, 1991; Home and Selleri, 2008].

Since entanglement is a necessary condition to violate any Bell inequality and thus the CHSH inequality (IV.44) can also be interpreted as entanglement witness. In particular, we can define the entanglement witness operator $\hat{W}_{\mathcal{B}} = 2\mathbb{1} - \hat{\mathcal{B}}$, with the CHSH operator $\hat{\mathcal{B}}$ defined as

$$\hat{\mathcal{B}} = \hat{A}_1 \otimes \hat{B}_1 + \hat{A}_1 \otimes \hat{B}_2 + \hat{A}_2 \otimes \hat{B}_1 - \hat{A}_2 \otimes \hat{B}_2. \quad (\text{IV.47})$$

However, one can improve the CHSH witness by assuming separability of the considered quantum states, instead of the stronger nonlocality condition (IV.41). This leads to a separability bound S_{sep} for the CHSH witness, which depends on the choice of the observables \hat{A}_i and \hat{B}_i and is in general lower than the nonlocality bound $S_{\mathcal{L}} = 2$ [Roy, 2005]. For instance, for the choice $\hat{A}_1 = \sigma_x$, $\hat{A}_2 = \sigma_z$, $\hat{B}_1 = (\sigma_x + \sigma_z)/\sqrt{2}$ and

$\hat{B}_2 = (\sigma_x - \sigma_z)/\sqrt{2}$, we find that the CHSH operator (IV.47) is given by:

$$\hat{\mathcal{B}} = \sqrt{2}\sigma_x \otimes \sigma_x + \sqrt{2}\sigma_z \otimes \sigma_z \quad (\text{IV.48})$$

whose expectation value for separable states is bounded by $S_{\text{sep}} = \sqrt{2}$ (as shown in Sec. IV.1.2). This highlights the difference between a device-independent test of nonlocality and a device-dependent entanglement test. While, in the former case, a violation of the bound $S_{\mathcal{L}}$ assures a violation of local-realism no matter if Alice and Bob trusted their measurement devices, in the latter case, a violation of S_{sep} implies the detection of entanglement only if the correct quantum measurements have been performed (see Eq. (IV.48)). Further on, the degree of violation of the CHSH value $\langle \hat{\mathcal{B}} \rangle$ is often also considered as a quantifier of entanglement since its maximal value, the Tsirelson bound $2\sqrt{2}$, is reached for maximally entangled states (see for example Eq. (IV.2)).

For mixed states the situation is a bit more subtle. It was first shown by Werner [Werner, 1989] that there exist mixed entangled quantum states which do not lead to nonlocality. Those so-called *Werner states* are given by all states that are invariant under the unitary transformation $\hat{U} \otimes \hat{U}$ with an arbitrary unitary operator \hat{U} . For two qubits the Werner states are all mixtures between the singlet Bell state $|\Psi_s\rangle$ and the white noise:

$$\hat{\rho}_p^W = p|\Psi_s\rangle\langle\Psi_s| + (1-p)\mathbb{1}/4. \quad (\text{IV.49})$$

In [Werner, 1989] it was shown that (IV.49) is separable if and only if $p \leq 1/3$, but they admit a local hidden variable model if $p \leq 5/12$ [Barrett, 2002]. Hence, there is a range of the parameter p in which $\hat{\rho}_p^W$ is entangled but not nonlocal. This discussion shows that there is a non-trivial relation between entanglement and nonlocality which is up to today not completely understood [Brunner et al., 2014].

One way to activate the nonlocality of mixed states is by using entanglement distillation. The latter transforms N copies of a mixed entangled state $\hat{\rho}$ into some smaller number of states which are almost maximally entangled. Thus, if one is able to distill pure entanglement from a finite number of copies of a mixed state one can reveal its nonlocality. However, not all mixed states are distillable. Peres even conjectured in 1999 that all non-distillable entangled states, referred to also as *bound entangled states*, do admit a local hidden variable model [Peres, 1999]. This conjecture was recently disproven by showing the violation of a Bell inequality with a specific bound entangled state [Vértesi and Brunner, 2014]. For multi-partite systems the situation becomes even more complicated and will not be further subject of this thesis [Chen et al., 2014; Cavalcanti et al., 2011; Ræisi et al., 2015].

IV.2.2 Experimental demonstration of Bell nonlocality

In the past 30 years there has been many demonstrations of Bell inequality violations in different types of physical system. Especially, the development of spontaneous parametric down-conversion techniques and the accompanied improvement of sources of entangled pairs of photons, has made Bell inequalities violations an almost trivial task. However, for many years, some stubborn realists have been refusing to accept these experiments as reliable demonstrations of Bell nonlocality due to the following experi-

mental loopholes.

First, the limited detection efficiency of single-photon detectors used in experiments opens the so called *detection loophole* and forces the experimenters to do the so called fair-sampling assumption. This means that the subset of all detected photons provides a fair sample of all photon pairs produced in the experiments and the measured data is representative of the data that would have been measured if the detectors had unit efficiency. The detection loophole can be closed if the efficiency of the detectors exceeds a certain threshold efficiency η^* .

In order to determine this threshold efficiency we assume a Bell test in terms of the above discussed CHSH scenario with measurements yielding binary outcomes ± 1 . Further on, we assume that Alice and Bob share a maximally entangled state and perform appropriate local measurements leading principally to a maximal violation of the CHSH inequality of $2\sqrt{2}$. However, Alice and Bob have a limited detection efficiency of η and assign to lost detection events the outcome $+1$. This leads to the following three cases. Either, with probability η^2 , both detectors click and the outcomes obtained by Alice and Bob are completely correlated ($\mathcal{B} = 2\sqrt{2}$), or, with probability $\eta(1 - \eta)$, only one detector clicks leading to completely uncorrelated measurement results ($\mathcal{B} = 0$), or, with probability $(1 - \eta)^2$, no detector clicks which yields always equal measurement outcomes for Alice and Bob ($\mathcal{B} = 2$).

The detection loophole can be closed if the CHSH value \mathcal{B} , after including all the aforementioned cases, is still larger than the local-realism bound [Mermin, 1986]:

$$2\sqrt{2}\eta^2 + 2(1 - \eta)^2 > 2, \quad (\text{IV.50})$$

leading to the following threshold efficiency

$$\eta^* = \frac{2}{1 + \sqrt{2}} \approx 82.8\%. \quad (\text{IV.51})$$

Other threshold efficiencies can be found for more complicated Bell experiments involving either more measurement settings, outcomes or parties [Brunner et al., 2014]. The detection loophole has been closed independently in experiments using entangled photon pairs [Giustina et al., 2013; Christensen et al., 2013]. A recent alternative approach that aims at demonstrating nonlocality, but avoids the necessity of closing the detection loophole, by doing the assumption of limited detection efficiencies, was discussed and realized in [Pütz et al., 2016].

Another important loophole, the so called locality loophole, is opened if one cannot exclude the possibility of Alice and Bob communicating over some hidden channel that transmits classical signals at the speed of light. In turn, such classical communication would allow in principle to explain the observed correlations, that lead to violations of Bell inequalities, by purely local mechanism. Hence, in order to close the locality loophole one has to assure that Alice and Bob are space-like separated making hidden classical communication between them impossible.

Furthermore, one has to be sure that the measurement setting of one of the two parties is not determined by an earlier event that might be causally related to the measurement setting on the respective other party. Thus, the measurement settings must be chosen randomly and freely with respect to the measurement settings on the other side. If this

is not the case one opens the so called *freedom of choices* or *measurement-independence loophole*.

Mathematically, the locality and the freedom of choice loophole can be expressed as:

$$p(a|i, j, b, \lambda) = p(a|i, \lambda), \quad p(b|i, j, a, \lambda) = p(b|j, \lambda), \quad (\text{IV.52})$$

and

$$q(\lambda|i, j) = q(\lambda), \quad (\text{IV.53})$$

respectively, leading together to the earlier introduced locality condition (IV.41). The first experiment which conclusively closed the locality loophole was the one by A. Aspect *et al.* in 1982 [Aspect *et al.*, 1982a]. They used high-speed electro-optic modulators, controlled by two independent quantum random number generators, to switch between two polarization measurement bases on each side and therefore excluded any classical communication between Alice and Bob which were separated by about 100 meters. Other experiments following the one by Aspect *et al.* were performed more than a decade later [Weihs *et al.*, 1998; Scheidl *et al.*, 2010]. The latter enforced a space-like separation also between the quantum random number generators and the source of the entangled photons.

Note that, strictly speaking, closing the locality loophole completely is not possible. Doing so requires a space-like separation between the moment determining the measurement settings on one side and the corresponding measurements on the other side. However, it is never possible to determine these moments exactly. How do we know that the choices of the measurement setting was determined at time $t = 0$ and not earlier? Or, how do we determine the exact moment of the measurement without doing assumptions of the measurement process itself [Kent, 2005]? Furthermore, the random choices of the measurement settings are taken according to random processes in quantum theory and we cannot be sure that these processes are also genuinely random according to some deeper, up to now unknown, theory. This aspect was discussed more deeply in [Vaidman, 2001]. In conclusion, since these last aspects have a rather philosophical touch, one usually refers to the reasonable locality loopholes as the ones mentioned in the previous paragraphs.

The first experiment that reported the closure of both the detection and the locality loophole was reported last year in [Hensen *et al.*, 2015]. Therein, the CHSH inequality was tested using entangled electron spins of nitrogen-vacancy defect centers in diamond that were entangled using an event-ready scheme originally proposed in [Żukowski *et al.*, 1993; Simon and Irvine, 2003]. The efficient readout of the electron spins thereby assured to avoid the fair-sampling assumption and the use of random basis selection together with fast spin readout of the 1.3km distant spins closed the locality loophole. Finally, they report a violation of the CHSH inequality of $\mathcal{B} = 2.42 \pm 0.20$, and conclude, by a null hypothesis test, that a local-realistic model of space-like separated parties describing their measured data can be excluded with a probability of at most 3.9%. This value was tightened considerably in two other loophole free Bell test using entangled photon pairs performed shortly after [Shalm *et al.*, 2015; Giustina *et al.*, 2015].

Having discussed some of the most important aspects concerning nonlocal correlations, their detection and experimental demonstration, in the case of measurements

with finitely many outcomes, we will turn now to the main question of this Section. Can we test the CHSH inequality with observables yielding infinitely many outcomes?

IV.2.3 Bell inequalities for bounded observables

In the remainder of this Section we will discuss the possibility of performing tests of local-realism in terms of measurements of bounded observables with possibly continuous outcomes. Examples of the latter are for instance measurements of modular variables, as discussed in Chapter III. In this respect, we need to derive a Bell inequality that can be applied to measurements of such observables. For the derivation of the CHSH inequality, and the Tsirelson bound, the assumption of binary measurement outcomes, *e.g.* ± 1 , was crucial. In the following, we will discuss to what extent Eq. (IV.44) can be applied also for more general measurements yielding non-binary outcomes [Ketterer et al., 2015].

IV.2.3.1 Bounded discrete measurement outcomes

One way of deriving a Bell inequality for measurements with bounded observables is by assuming discretized measurement scenario. In this respect, we consider pairs of observables, A_i and B_j , with $i, j = 1, 2$, on Alice and Bob's subsystem, respectively, each yielding d discrete outcomes: $a_1, a_2, b_1, b_2 = -(d-1)/2, \dots, (d-1)/2$, where we assumed d being even. The experimental average of a product of two such observables is thus given by:

$$\langle A_i B_j \rangle = \sum_{a,b} ab p(a, b|i, j), \quad (\text{IV.54})$$

with the joint-probabilities $p(a, b|i, j)$ for obtaining the outcomes a and b given the choice of the observables A_i and B_j . The joint-probabilities $p(a, b|i, j)$ are directly obtained from the experimental coincidence counts $N(a, b|i, j)$ through the simple formula:

$$p(a, b|i, j) = \frac{N(a, b|i, j)}{\sum_{a,b} N(a, b|i, j)}. \quad (\text{IV.55})$$

In the following, we want to derive a Bell inequality by assuming that the outcomes of the observables A_i and B_j are determined by a local hidden variable theory. In order to do so we follow the strategy presented in [Collins et al., 2002] and introduce d^4 probabilities $c_{\alpha_1, \alpha_2, \beta_1, \beta_2}$, where $\alpha_1, \alpha_2, \beta_1, \beta_2 = -(d-1)/2, \dots, (d-1)/2$ and $\sum_{\alpha_1, \alpha_2, \beta_1, \beta_2} c_{\alpha_1, \alpha_2, \beta_1, \beta_2} = 1$, which specify that on Alice's side the measurement of the observables A_1 and A_2 yield the outcomes α_1 and α_2 , respectively, and on Bob's side the measurement of the observables B_1 and B_2 yield the outcomes β_1 and β_2 , respectively. Note that this is a deterministic strategy because the measurement outcomes are completely determined by the value of the local variables α_1, α_2 and β_1, β_2 . Starting from a nondeterministic local hidden variable model is possible, however, one can rephrase every probabilistic hidden variable theory in the above way by incorporating the local randomness in the probabilities $c_{\alpha_1, \alpha_2, \beta_1, \beta_2}$ [Percival, 1998].

Further on, within the fixed local variable theory, the joint-probabilities for pair-measurements of observables on Alice's and Bob's side, respectively, read $p(A_1 =$

$\alpha_1, B_1 = \beta_1) = \sum_{\alpha_2, \beta_2} c_{\alpha_1, \alpha_2, \beta_1, \beta_2}$, and analogously for $p(A_1 = \alpha_1, B_2 = \beta_2)$, $p(A_2 = \alpha_2, B_1 = \beta_1)$ and $p(A_2 = \alpha_2, B_2 = \beta_2)$, and the expectation values of the products of the respective observables can be calculated as follows:

$$\langle A_1 B_1 \rangle = \sum_{\alpha_1, \alpha_2, \beta_1, \beta_2} \alpha_1 \beta_1 c_{\alpha_1, \alpha_2, \beta_1, \beta_2}, \quad \langle A_1 B_2 \rangle = \sum_{\alpha_1, \alpha_2, \beta_1, \beta_2} \alpha_1 \beta_2 c_{\alpha_1, \alpha_2, \beta_1, \beta_2}, \quad (\text{IV.56})$$

$$\langle A_2 B_1 \rangle = \sum_{\alpha_1, \alpha_2, \beta_1, \beta_2} \alpha_2 \beta_1 c_{\alpha_1, \alpha_2, \beta_1, \beta_2}, \quad \langle A_2 B_2 \rangle = \sum_{\alpha_1, \alpha_2, \beta_1, \beta_2} \alpha_2 \beta_2 c_{\alpha_1, \alpha_2, \beta_1, \beta_2}. \quad (\text{IV.57})$$

Now, by combining the different products in Eqs. (IV.56) and (IV.57) in a CHSH-like expression we find

$$\begin{aligned} \langle A_1 B_1 \rangle + \langle A_1 B_2 \rangle + \langle A_2 B_1 \rangle - \langle A_2 B_2 \rangle &= \sum_{\alpha_1, \alpha_2, \beta_1, \beta_2} [\alpha_1 \beta_1 + \alpha_1 \beta_2 + \alpha_2 \beta_1 - \alpha_2 \beta_2] c_{\alpha_1, \alpha_2, \beta_1, \beta_2} \\ &= \sum_{\alpha_1, \alpha_2, \beta_1, \beta_2} [\alpha_1 (\beta_1 + \beta_2) + \alpha_2 (\beta_1 - \beta_2)] c_{\alpha_1, \alpha_2, \beta_1, \beta_2}, \end{aligned} \quad (\text{IV.58})$$

whose absolute value is easily shown to be bounded by $2(d-1)^2/2^2 = (d-1)^2/2$, since the maximum outcomes of each individual observable are equal to $\pm(d-1)/2$. Hence, if we rescale the measurement outcomes such that they are within the interval $[-\mathcal{K}, +\mathcal{K}]$, by dividing the outcomes by $(d-1)/(2\mathcal{K})$, we find that Eq. (IV.58) is bounded by $2\mathcal{K}^2$. In the particular case $\mathcal{K} = 1$ we thus recover a CHSH-like inequality for discrete bounded observables:

$$\langle A_1 B_1 \rangle + \langle A_1 B_2 \rangle + \langle A_2 B_1 \rangle - \langle A_2 B_2 \rangle \leq 2. \quad (\text{IV.59})$$

Note that the bound of inequality (IV.59) does not depend on the number of outcomes d , thus holds particularly in the limit $d \rightarrow \infty$ of measurements with continuous outcomes. However, from an experimental point of view this is not of great importance because, due to the finite measurement precision for measurements of continuous variables, one ultimately has to rely on the discrete case. Nevertheless, in the following we will show an alternative way of proving Eq. (IV.59) by using directly observables with bounded continuous outcomes without going back to the discrete case.

IV.2.3.2 Bounded continuous measurement outcomes

Let's consider once again pairs of observables, A_i and B_j , with $i, j = 1, 2$, on Alice and Bob's subsystem, respectively, whereas each observable yields now bounded and continuous outcomes contained within the interval $[-\mathcal{K}, \mathcal{K}]$. Further on, if we assume that the outcomes of the above observables are predicted by a local and realistic theory, we know, from the discussion in Sec. IV.2.1, that the corresponding joint-probability density $p(a, b|i, j)$, for obtaining pairs of continuous outcomes $a, b \in [-\mathcal{K}, \mathcal{K}]$ given the measurement settings $i, j \in \{1, 2\}$, reads:

$$p(a, b|i, j) = \int_{\Lambda} d\lambda q(\lambda) p(a|i, \lambda) p(b|j, \lambda), \quad (\text{IV.60})$$

with the hidden-variable λ living on the hidden-parameter space Λ distributed according to the probability density $q(\lambda)$. Using Eq. (IV.60) we can calculate the expectation value of products between observables on Alice's and Bob's side, yielding:

$$\langle A_i B_j \rangle = \int_{-\mathcal{K}}^{\mathcal{K}} da \int_{-\mathcal{K}}^{\mathcal{K}} db a b p(a, b|i, j). \quad (\text{IV.61})$$

$$= \int_{\Lambda} d\lambda q(\lambda) \int_{-\mathcal{K}}^{\mathcal{K}} da \int_{-\mathcal{K}}^{\mathcal{K}} db ab p(a|i, \lambda)p(b|j, \lambda), \quad (\text{IV.62})$$

$$= \int_{\Lambda} d\lambda q(\lambda) \bar{a}_i(\lambda) \bar{b}_j(\lambda) \quad (\text{IV.63})$$

where $\bar{a}_i(\lambda) = \int_{-\mathcal{K}}^{\mathcal{K}} da a p(a|i, \lambda)$ ($\bar{b}_j(\lambda) = \int_{-\mathcal{K}}^{\mathcal{K}} db b p(b|j, \lambda)$) refers to the corresponding local expectation value on Alice's (Bob's) side. Note that, according to Fubini's theorem we are allowed to exchange the integrations over a , b and λ , since the function $f(a, b, \lambda) = ab q(\lambda)p(a|i, \lambda)p(b|j, \lambda)$ is integrable, meaning that the whole integral (IV.62) is bounded if one replaces the integrand with its absolute value $|f(a, b, \lambda)|$. Now, in order to derive a Bell inequality for bounded continuous measurements we combine the expectation values (IV.63) in a CHSH-like expression (compare with (IV.44)), to obtain

$$\begin{aligned} \mathcal{B} &= \langle A_1 B_1 \rangle + \langle A_1 B_2 \rangle + \langle A_2 B_1 \rangle - \langle A_2 B_2 \rangle \\ &= \int d\lambda q(\lambda) \underbrace{[\bar{a}_1(\lambda)(\bar{b}_1(\lambda) + \bar{b}_2(\lambda)) + \bar{a}_2(\lambda)(\bar{b}_1(\lambda) - \bar{b}_2(\lambda))]}_{=X(\lambda)}. \end{aligned} \quad (\text{IV.64})$$

The maximum of Eq. (IV.64) is directly related to the maximum of the quantity $X(\lambda)$ which is attained when the local expectation values $\bar{a}_i(\lambda)$ and $\bar{b}_j(\lambda)$ take their maximum values $\pm\mathcal{K}$. In this extremal case it is easy to see that $|X(\lambda)|$ can only be equal to $2\mathcal{K}^2$, and we find that:

$$|\mathcal{B}| \leq 2\mathcal{K}^2. \quad (\text{IV.65})$$

For observables that are bounded by $\mathcal{K} = 1$, we thus recover the same inequality as in Eq. (IV.59). Hence, for measurements of bounded observables, we can always apply the CHSH inequality with the generalized bound (IV.65) in order to test for nonlocal correlations.

An interesting feature of the generalized CHSH inequality (IV.65) is that, even though it involves measurements with continuous outcomes, it can be tested in terms of pure binary measurements only. If one considers, for instance, the observable A_x (the same reasoning will apply also to B_y) with $\mathcal{K} = 1$, we find that its expectation value is bounded by $\mathcal{K} = 1$ and can be expressed as $\langle \hat{A}_i \rangle = p_+ - p_-$, with probabilities p_{\pm} . Thereby, \pm refer to some binary property whose measurement outcomes reproduce the expectation value of the observable A_i . Hence, every Bell inequality that involves measurements of bounded observables can be tested by measuring an appropriately chosen binary observable. In the quantum realm, this refers to the discussion of Sec. II.1.4, where we showed that the expectation value of every quantum observable can be measured in terms of a two-valued POVM. Later on, when discussing possible experimental realizations of

measurements of bounded observables, we will make use of this fact (see Sec. III.4.3).

Finally, we would like to emphasize that the Bell inequality (IV.65) involves expectation values of products of the observables A_i and B_j and not normalized correlation functions, such as $E(A_i, B_j) = \langle A_i B_j \rangle / \sqrt{\langle A_i^2 \rangle \langle B_j^2 \rangle}$. This difference is important because in general we have $\langle A_i B_j \rangle \neq E(A_i, B_j)$. Only in the case of measurements of binary observables $A_i^{(bin)}$ and $B_j^{(bin)}$, yielding outcomes $\{\pm 1\}$, we have $(A_i^{(bin)})^2, (B_j^{(bin)})^2 = 1$ and thus $\langle A_i^{(bin)} B_j^{(bin)} \rangle = E(A_i^{(bin)}, B_j^{(bin)})$. This issue is also discussed in [Barut and Meystre, 1984], where the authors rightfully argue that a CHSH inequality involving correlations functions $E(A_i, B_j)$, with bounded continuous observables A_i and B_j , cannot exist. In particular, they find that the CHSH inequality, involving normalized correlation functions, can be violated also by measurements of a classical spin which yields bounded continuous outcomes. And indeed, the authors emphasize that in their case the violation of the local-realism bound of the CHSH inequality is due to the normalization of the correlation functions and not due to a violation of local-realism. In this sense the above derived Bell inequality (IV.65) is not in contradiction with the results presented in [Barut and Meystre, 1984].

IV.2.3.3 Nonlocality test with modular variables

In the following, we will use the generalized CHSH inequality (IV.65) to perform nonlocality tests in terms of measurements of modular variables. In Sec. III.1.1 we found that the most general quantum modular variables $F(\hat{x}, \hat{p})$ can be expressed as a superposition of displacement operators (see Eq. (III.9)) and thus has a phase-space Wigner representation (II.71) that is equal to a two-dimensional Fourier series in position and momentum $W_F(x, p) = F(x, p)/(2\pi)$ (see Eq. (III.7)). Hence, the modular variables $F(\hat{x}, \hat{p})$ have a clear classical analog which is given by the function $F(x, p)$. In order to make them admissible for the above nonlocality test we just have to choose a Fourier decomposition of $F(x, p)$ that is bounded. Examples are the modular variables $\hat{Q}_\varphi(\nu, \mu)$, discussed in Sec. III.1.2, which are bounded by *one*.

Further on, we choose the four observables \hat{A}_i and \hat{B}_j , for $i, j = 1, 2$, equal to bounded modular variables, with bound \mathcal{K} , and define the CHSH operator

$$\hat{\mathcal{B}} = \hat{A}_1 \hat{B}_1 + \hat{A}_1 \hat{B}_2 + \hat{A}_2 \hat{B}_1 - \hat{A}_2 \hat{B}_2, \quad (\text{IV.66})$$

whose phase-space distribution is given by

$$W_{\hat{\mathcal{B}}}(x, p) = W_{\hat{A}_1}(x, p) \left(W_{\hat{B}_1}(x, p) + W_{\hat{B}_2}(x, p) \right) + W_{\hat{A}_2}(x, p) \left(W_{\hat{B}_1}(x, p) - W_{\hat{B}_2}(x, p) \right), \quad (\text{IV.67})$$

where we made use the linearity of the Wigner function (see Eq. (II.72)). Due to the boundedness of the modular variables \hat{A}_i and \hat{B}_j , which implies $2\pi |W_{\hat{A}_i, \hat{B}_j}(x, p)| \leq \mathcal{K}$, we can also deduce a bound on the phase-space distribution (IV.67):

$$2\pi |W_{\hat{\mathcal{B}}}(x, p)| \leq 2\mathcal{K}^2. \quad (\text{IV.68})$$

Moreover, since the expectation value of $\hat{\mathcal{B}}$, with respect to an arbitrary quantum state

$\hat{\rho}$, can be calculated according to the identity (II.73):

$$\langle \hat{\mathcal{B}} \rangle = 2\pi \iint_{-\infty}^{\infty} dx dp W_{\hat{\mathcal{B}}}(x, p) W_{\hat{\rho}}(x, p) \quad (\text{IV.69})$$

we find that

$$|\langle \hat{\mathcal{B}} \rangle| \leq 2\mathcal{K}^2 \iint_{-\infty}^{\infty} dx dp W_{\hat{\rho}}(x, p) = 2\mathcal{K}^2, \quad (\text{IV.70})$$

which holds only if $W_{\hat{\rho}}(x, p)$ is a strictly non-negative function. Hence, a violation of local-realism in terms of measurements of modular variables is only possible if the corresponding quantum state has a Wigner distribution that is not strictly non-negative (in the next Section we will derive such states). This is in marked contrast to demonstrations of nonlocality in terms of measurements of observables having an unbounded Wigner distribution, such as the displaced parity operator, which can be achieved also with states that have a positive Wigner function [Banaszek and Wódkiewicz, 1998, 1999]. Similar conclusions were drawn independently in [Arora and Asadian, 2015].

In practice, we will have two possibilities to measure expectation values of the modular variables $F(\hat{x}, \hat{p})$ which, due to the Heisenberg uncertainty principle, cannot be accessed directly through measurements of \hat{x} and \hat{p} . Either, we find an appropriate binary measurement strategy (POVM) that allows us to determine the expectation value of $F(\hat{x}, \hat{p})$ indirectly (see discussion in Sec. II.1.4), or we are able to measure directly in the eigenbasis of the observable $F(\hat{x}, \hat{p})$, what allows us to calculate its expectation value through simple post processing. Both variants have been elaborated in detail in Sec. III.4.3, where we discussed possible experimental measurement strategies of modular variables.

IV.2.4 Violation of local-realism with modular variables

Following the discussion of the last Section we can test the CHSH inequality (IV.44) with all bounded modular variables according to Eq. (IV.65). Therefore, in particular, we can consider the set of observables $\text{Re}(\hat{X})$, $\text{Re}(\hat{Y})$ and $\text{Re}(\hat{Z})$, which in the modular representation read:

$$\hat{\Gamma}_x = \int_{-\ell/4}^{\ell/4} d\bar{x} \int_{-\pi/\ell}^{\pi/\ell} d\bar{p} \cos(i\bar{p}\ell/2) \hat{\sigma}_x(\bar{x}, \bar{p}), \quad (\text{IV.71})$$

$$\hat{\Gamma}_y = \int_{-\ell/4}^{\ell/4} d\bar{x} \int_{-\pi/\ell}^{\pi/\ell} d\bar{p} \cos(2\pi i\bar{x}/\ell - i\bar{p}\ell/2) \hat{\sigma}_y(\bar{x}, \bar{p}), \quad (\text{IV.72})$$

$$\hat{\Gamma}_z = \int_{-\ell/4}^{\ell/4} d\bar{x} \int_{-\pi/\ell}^{\pi/\ell} d\bar{p} \cos(2\pi i\bar{x}/\ell) \hat{\sigma}_z(\bar{x}, \bar{p}). \quad (\text{IV.73})$$

as we have seen in Sec. III.3.1. The observables (IV.71), (IV.72) and (IV.73), are examples of the modular variables discussed in Sec. III.1.2, and thus bounded by $\mathcal{K} = 1$. We emphasize once more that the above operators are non-commuting, as discussed in Sec. III.3.3.4, and thus are good candidates for the detection of nonlocality. We could have also chosen a different set of modular variables with similar commutation relations

that lead to another set of functions ζ_α in Eq. (IV.71)-(IV.73). Such novelly defined modular variables yield as well a local-realism threshold of *two* in the CHSH inequality (see also Eqs. (IV.44) and (IV.65)), as long as the individual observables are bounded by *one*.

IV.2.4.1 Approach 1: Using logical rotations

In analogy to nonlocality tests with qubits, we choose the observables on Alice's and Bob's side as $\hat{A}_i = e^{-i\hat{\Gamma}_z^1 \phi_i/2} \hat{\Gamma}_x e^{i\hat{\Gamma}_z^1 \phi_i/2}$ and $\hat{B}_j = e^{-i\hat{\Gamma}_z^1 \theta_j/2} \hat{\Gamma}_x e^{i\hat{\Gamma}_z^1 \theta_j/2}$, whereas the angles ϕ_i and θ_j , with $i, j = 0, 1$, define different measurement settings, respectively. The unitary transformations $e^{-i\hat{\Gamma}_z^1 \phi_i/2}$ and $e^{-i\hat{\Gamma}_z^1 \theta_j/2}$ can, as discussed in Sec. III.3.2, be considered as rotations around the z -axis of the Bloch sphere of the encoded logical qubits. Written in the modular representation, we thus have:

$$\hat{A}_i = \int_{-\ell/4}^{\ell/4} d\bar{x} \int_{-\pi/\ell}^{\pi/\ell} d\bar{p} \cos(i\bar{p}\ell/2) \hat{\sigma}_{\phi_i}(\bar{x}, \bar{p}), \quad (\text{IV.74})$$

$$\hat{B}_j = \int_{-\ell/4}^{\ell/4} d\bar{x} \int_{-\pi/\ell}^{\pi/\ell} d\bar{p} \cos(i\bar{p}\ell/2) \hat{\sigma}_{\theta_j}(\bar{x}, \bar{p}), \quad (\text{IV.75})$$

where $\hat{\sigma}_{\phi_i}(\bar{x}, \bar{p})$ and $\hat{\sigma}_{\theta_j}(\bar{x}, \bar{p})$ define, in analogy to Eqs. (III.84), (III.85) and (III.87), the corresponding (\bar{x}, \bar{p}) -dependent Pauli matrices in the directions \hat{n}_{ϕ_i} and \hat{n}_{θ_j} , respectively. Mathematically, we have $\hat{\sigma}_{\phi}(\bar{x}, \bar{p}) = \mathbf{n}_{\phi} \cdot \hat{\boldsymbol{\sigma}}(\bar{x}, \bar{p})$, where $\mathbf{n}_{\phi} = (n_x^{\phi}, n_y^{\phi}, n_z^{\phi})$ and $\hat{\boldsymbol{\sigma}}(\bar{x}, \bar{p}) = (\hat{\sigma}_x(\bar{x}, \bar{p}), \hat{\sigma}_y(\bar{x}, \bar{p}), \hat{\sigma}_z(\bar{x}, \bar{p}))$.

With quantum mechanical analogs of the observables A_i and B_j in hand we can write down the CHSH operator (IV.66) which, after inserting the observables (IV.74) and (IV.75), reads:

$$\hat{\mathcal{B}} = \iint_{-\ell/4}^{\ell/4} d\bar{x}_a d\bar{x}_b \iint_{-\pi/\ell}^{\pi/\ell} d\bar{p}_a d\bar{p}_b \cos(\bar{p}_a \ell/2) \cos(\bar{p}_b \ell/2) \hat{\mathcal{B}}(\bar{x}_a, \bar{p}_a; \bar{x}_b, \bar{p}_b), \quad (\text{IV.76})$$

where

$$\begin{aligned} \hat{\mathcal{B}}(\bar{x}_a, \bar{p}_a, \bar{x}_b, \bar{p}_b) &= \hat{\sigma}_{\phi_1}(\bar{x}_a, \bar{p}_a) \hat{\sigma}_{\theta_2}(\bar{x}_b, \bar{p}_b) + \hat{\sigma}_{\phi_1}(\bar{x}_a, \bar{p}_a) \hat{\sigma}_{\theta_2}(\bar{x}_b, \bar{p}_b) \\ &\quad + \hat{\sigma}_{\phi_2}(\bar{x}_a, \bar{p}_a) \hat{\sigma}_{\theta_2}(\bar{x}_b, \bar{p}_b) - \hat{\sigma}_{\phi_2}(\bar{x}_a, \bar{p}_a) \hat{\sigma}_{\theta_2}(\bar{x}_b, \bar{p}_b). \end{aligned} \quad (\text{IV.77})$$

Thereby, the operator (IV.77) has a phase-space Wigner representation that is equal to a sum of delta functions and therefore unbounded (see also the discussion about perfect GKP states at the end of Sec. III.2.1). Only after integration over \bar{x} and \bar{p} , with an appropriate weight function $\cos(\bar{p}_a \ell/2) \cos(\bar{p}_b \ell/2)$, it is possible to recover a proper Bell operator (IV.76) with a well-defined phase space distribution as in Eq. (IV.67).

Even though Eq. (IV.77) does not provide a proper Bell operator, we can take advantage of it in order to diagonalize the actual Bell operator (IV.76). Therefore, we consider Eq. (IV.77) as a matrix acting on the four-dimensional subspace spanned by the modular eigenstates $\{|\bar{x}_a, \bar{p}_a\rangle|\bar{x}_b, \bar{p}_b\rangle, |\bar{x}_a, \bar{p}_a\rangle|\bar{x}_b + \ell/2, \bar{p}_b\rangle, |\bar{x}_a + \ell/2, \bar{p}_a\rangle|\bar{x}_b, \bar{p}_b\rangle, |\bar{x}_a + \ell/2, \bar{p}_a\rangle|\bar{x}_b + \ell/2, \bar{p}_b\rangle\}$, which can be diagonalized easily. Further on, if we choose the angles which fix the measurement settings equal to $\phi_1 = 0$, $\phi_2 = \pi/2$, $\theta_1 = \pi/4$ and

$\phi_4 = -\pi/4$, this diagonalization yields two non-zero eigenvalues $\pm 2\sqrt{2}$ with the corresponding eigenvectors:

$$|\psi^{\pm 1}(\bar{x}_a, \bar{p}_a; \bar{x}_b, \bar{p}_b)\rangle = \frac{1}{\sqrt{2}} (|\bar{x}_a, \bar{p}_a\rangle |\bar{x}_b + \ell/2, \bar{p}_b\rangle \pm |\bar{x}_a + \ell/2, \bar{p}_a\rangle |\bar{x}_b, \bar{p}_b\rangle). \quad (\text{IV.78})$$

and the Bell operator (IV.76) can be expressed as

$$\begin{aligned} \hat{\mathcal{B}} = & 2\sqrt{2} \sum_{n=\pm 1} n \iint_{-\ell/4}^{\ell/4} d\bar{x}_a d\bar{x}_b \iint_{-\pi/\ell}^{\pi/\ell} d\bar{p}_a d\bar{p}_b \\ & \times \cos(\bar{p}_a \ell/2) \cos(\bar{p}_b \ell/2) |\psi^n(\bar{x}_a, \bar{p}_a; \bar{x}_b, \bar{p}_b)\rangle \langle \psi^n(\bar{x}_a, \bar{p}_a; \bar{x}_b, \bar{p}_b)|. \end{aligned} \quad (\text{IV.79})$$

We thus see that the entangled states (IV.78) violate the CHSH inequality maximally if we choose the modular momenta, \bar{p}_a and \bar{p}_b , equal to zero, while the modular positions, \bar{x}_a and \bar{x}_b , can take arbitrary values.

At this point we emphasize that the entangled states (IV.78) are modular eigenstates and thus nonnormalizable superpositions of position eigenstates (see also Eq. (III.34)). In order to obtain physically sound states we need to superpose them with an appropriate wave function. Remember that we have to choose the wave function only on the domain $[-\ell/4, \ell/4] \times [-\pi/\ell, \pi/\ell]$ on Alice and Bob system, respectively, yielding implicitly the wave function on the whole domain $[-\ell/4, 3\ell/4] \times [-\pi/\ell, \pi/\ell]$ through Eq. (IV.78). Furthermore, since we are interested in the entanglement with respect to our logical states $|0_L\rangle$ and $|1_L\rangle$, introduced in Sec. III.2.1, we choose the wave function to be separable within this subspace, namely: $f_{ab}(\bar{x}_a, \bar{p}_a; \bar{x}_b, \bar{p}_b) = f_a(\bar{x}_a, \bar{p}_a) f_b(\bar{x}_b, \bar{p}_b)$. With this choice we can construct the physically sound entangled state:

$$\begin{aligned} |\Psi_{ent}\rangle &= \iint_{-\ell/4}^{\ell/4} d\bar{x}_a d\bar{x}_b \iint_{-\pi/\ell}^{\pi/\ell} d\bar{p}_a d\bar{p}_b f_{ab}(\bar{x}_a, \bar{p}_a; \bar{x}_b, \bar{p}_b) |\psi^{\pm 1}(\bar{x}_a, \bar{p}_a; \bar{x}_b, \bar{p}_b)\rangle \\ &= \frac{1}{\sqrt{2}} (|0_L\rangle |1_L\rangle \pm |1_L\rangle |0_L\rangle), \end{aligned} \quad (\text{IV.80})$$

where $|0_L\rangle$ and $|1_L\rangle$ are defined according to Eqs. (III.75) and (III.76), respectively. The expectation value of the Bell operator (IV.79) with respect to the state (IV.80) then becomes:

$$\langle \hat{\mathcal{B}} \rangle = \pm K^{(a)} K^{(b)} 2\sqrt{2}, \quad (\text{IV.81})$$

with

$$K^{(a,b)} = \int_{-\ell/4}^{\ell/4} d\bar{x}_i \int_{-\pi/\ell}^{\pi/\ell} d\bar{p}_i \cos(\bar{p}_{a,b} \ell/2) |f_{a,b}(\bar{x}_{a,b}, \bar{p}_{a,b})|^2. \quad (\text{IV.82})$$

Equation (IV.81) shows that a violation of the CHSH inequality with the entangled logical state (IV.80) is possible if we choose the functions $f_{a,b}(\bar{x}_{a,b}, \bar{p}_{a,b})$ such that they have a large overlap (IV.82) with the corresponding function that defines the observables (III.94) (here $\cos(\bar{p}\ell/2)$).

In the following, in order to discuss the behaviour of (IV.81) numerically, we choose the wave function $f_{a,b}(\bar{x}_a, \bar{p}_a; \bar{x}_b, \bar{p}_b)$ equal to a Gaussian function with identical widths

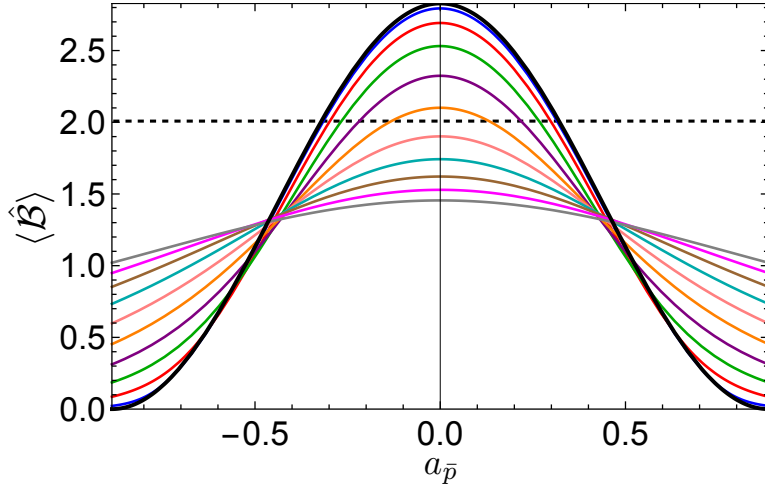


Figure IV.3: Plots of the expectation value of the Bell operator (IV.79) according to the state (IV.80) as a function of $a_{\bar{p}}$, for $\ell = 2\sqrt{\pi}$. Each curve corresponds to a different width in the modular position with increasing order from the uppermost to the lowest curve at the origin of the x -axis: $\kappa_i = 0.05(2\pi/\ell)$ (blue, uppermost), $\kappa_i = 0.1(2\pi/\ell)$ (red), $\kappa_i = 0.15(2\pi/\ell)$ (green), $\kappa_i = 0.2(2\pi/\ell)$ (purple), $\kappa_i = 0.25(2\pi/\ell)$ (orange), $\kappa_i = 0.3(2\pi/\ell)$ (pink), $\kappa_i = 0.35(2\pi/\ell)$ (cyan), $\kappa_i = 0.4(2\pi/\ell)$ (brown), $\kappa_i = 0.45(2\pi/\ell)$ (magenta, lowest) and $\kappa_i = 0.5(2\pi/\ell)$ (grey, lowest). All parameters are chosen equal for $i = a, b$. The black curve shows the function $2\sqrt{2} \cos^2(a_{\bar{p}}\ell/2)$ and the black dashed line indicates the local-realism threshold.

on Alice's and Bob's side, respectively. In particular, we set $f_{a,b}(\bar{x}_a, \bar{p}_a; \bar{x}_b, \bar{p}_b) = f(\bar{x}_a, \bar{p}_a)f(\bar{x}_b, \bar{p}_b)$, where $f(\bar{x}, \bar{p})$ is a two-dimensional Gaussian function with widths Δ and κ and with periodic boundary conditions on the domain $[-\ell/4, \ell/4] \times [-\pi/\ell, \pi/\ell[$ (for more details see also the discussion at the end of Sec. IV.1.3).

In Fig. IV.3, we present a plot of the expectation value of the CHSH operator (IV.79) with respect to the above defined wave function $f_{ab}(\bar{x}_a, \bar{p}_a; \bar{x}_b, \bar{p}_b)$ as a function of its location $a_{\bar{p}}$ in the interval $[-\pi/\ell, \pi/\ell[$ and for different modular momentum widths κ . The value $\langle \hat{\mathcal{B}} \rangle$ is invariant under the variation of $a_{\bar{x}}$ and Δ because for $\zeta_x(\bar{x}, \bar{p}) = \cos(\bar{p}\ell/2)$ the integrand in Eq. (IV.82) with respect to \bar{x} is a normalized Gaussian and thus its integral is independent of these parameters (see also Sec. IV.1.3). From Fig. IV.3 we deduce that a violation of the CHSH inequality is possible if the squeezing in the modular momentum is $\kappa \lesssim 0.27(2\pi/\ell)$, *i.e.* the width $1/\kappa$ of the envelope of the Gaussian comb in the position representation is large enough. If this condition is fulfilled a violation is found if the wave function $f_{a,b}(\bar{x}_{a,b}, \bar{p}_{a,b})$ is located in an interval centered around $a_{\bar{p}} = 0$. The behavior of the curves plotted in Fig. IV.3 reflects the characteristics of the precise choice of the function $\zeta_x(\bar{x}, \bar{p}) = \cos(\bar{p}\ell/2)$, thus of the measured modular variable $\hat{\Gamma}_x$. In particular, in the limit $\kappa \rightarrow 0$, we have $f_{a,b}(\bar{x}_{a,b}, \bar{p}_{a,b}) \propto \delta(\bar{p}_{a,b} - a_{\bar{p}})$ and thus $\langle \hat{\mathcal{B}} \rangle = 2\sqrt{2} \cos^2(a_{\bar{p}}\ell/2)$, as indicated by the black curve.

IV.2.4.2 Approach 2: Using the shear operation

In the last Section we have demonstrated the violation of the CHSH inequality in terms of measurements of the modular variable $\hat{\Gamma}_x$ in combination with the rotation operations (III.108). Further on, we want to present one more way to perform such a nonlocality test that avoids the use of the rotations defined in Sec. III.3.2, but rather uses one of the single mode Clifford operations introduced in Sec. III.2.2.2. The reason for this is that the experimental implementation of the rotations (III.108) in terms of the transverse degrees of freedom of photons requires the use of a specific optical element, *e.g.* a spatial light modulator, while here we show that it is possible to restrict ourselves to the free-propagation of the photons only (see also Sec. II.3.1).

Let's consider the operator $\hat{\Gamma}_z = \text{Re}(\hat{Z})$ in the modular representation:

$$\hat{\Gamma}_z = \int_{-\ell/4}^{\ell/4} d\bar{x} \int_{-\pi/\ell}^{\pi/\ell} d\bar{p} \cos(\bar{x}2\pi/\ell) \hat{\sigma}_z(\bar{x}, \bar{p}), \quad (\text{IV.83})$$

as in Eq. (IV.73). Furthermore, to specify different measurement settings we define the transformed operator $\hat{\Gamma}'_\phi = \hat{U}^\dagger(\phi_a) \hat{A}_{s_a} \hat{U}(\phi_a)$, using the the Fourier transformed shear operation $\hat{U}(\phi_a) = e^{i\hat{p}^2 \ell^2 \phi / (2\pi)^2}$, introduced in Sec. III.2.2.2. Specifically, by choosing $\phi = \pi/2$, we get:

$$\hat{\Gamma}'_{\frac{\pi}{2}} = \int_0^{\ell/2} d\bar{x} \int_0^{h/\ell} d\bar{p} \cos(\bar{x}2\pi/\ell - \bar{p}\ell/(2\hbar)) \hat{\sigma}_y(\bar{x}, \bar{p}), \quad (\text{IV.84})$$

what is equal to $\hat{\Gamma}_y = \text{Re}(\hat{Y})$. Using the operators (IV.83) and (IV.84) we can define the following Bell operator:

$$\hat{\mathcal{B}} = \hat{\Gamma}_z^{(1)} \hat{\Gamma}_z^{(2)} + \hat{\Gamma}_z^{(1)} \hat{\Gamma}_y^{(2)} + \hat{\Gamma}_y^{(1)} \hat{\Gamma}_z^{(2)} - \hat{\Gamma}_y^{(1)} \hat{\Gamma}_y^{(2)}. \quad (\text{IV.85})$$

In contrast to the Bell operator (IV.76) found in the last Section, Eq. (IV.85) can not be written as an integral over a (\bar{x}, \bar{p}) -dependent Bell operator (IV.77), due to the different functions under the integral in Eq. (IV.83) and (IV.84). Nevertheless, candidates of entangled states that lead to a violation of local-realism can be found by diagonalizing the operator

$$\begin{aligned} \hat{\mathcal{B}}(\bar{x}_a, \bar{p}_a, \bar{x}_b, \bar{p}_b) &= \hat{\sigma}_z(\bar{x}_a, \bar{p}_a) \hat{\sigma}_z(\bar{x}_b, \bar{p}_b) + \hat{\sigma}_z(\bar{x}_a, \bar{p}_a) \hat{\sigma}_y(\bar{x}_b, \bar{p}_b) \\ &\quad + \hat{\sigma}_y(\bar{x}_a, \bar{p}_a) \hat{\sigma}_z(\bar{x}_b, \bar{p}_b) - \hat{\sigma}_y(\bar{x}_a, \bar{p}_a) \hat{\sigma}_y(\bar{x}_b, \bar{p}_b), \end{aligned} \quad (\text{IV.86})$$

expressed in the basis $\{|\{\bar{x}_a + i\ell/2, \bar{p}_a\}\rangle|\{\bar{x}_b + j\ell/2, \bar{p}_b\}\rangle\}$, with $i, j = 0, 1$. This yields two nonzero eigenvalues $\pm 2\sqrt{2}$ and the corresponding eigenvectors:

$$\begin{aligned} |\psi_\pm(\bar{x}_a, \bar{p}_a; \bar{x}_b, \bar{p}_b)\rangle &= \frac{1}{N_\pm} [|\bar{x}_a, \bar{p}_a\rangle|\bar{x}_b, \bar{p}_b\rangle + |\bar{x}_a + \ell/2, \bar{p}_a\rangle|\bar{x}_a + \ell/2, \bar{p}_a\rangle \\ &\quad \pm i(\sqrt{2} \mp 1) (|\bar{x}_a, \bar{p}_a\rangle|\bar{x}_a + \ell/2, \bar{p}_a\rangle + |\bar{x}_a + \ell/2, \bar{p}_a\rangle|\bar{x}_a, \bar{p}_a\rangle)], \end{aligned} \quad (\text{IV.87})$$

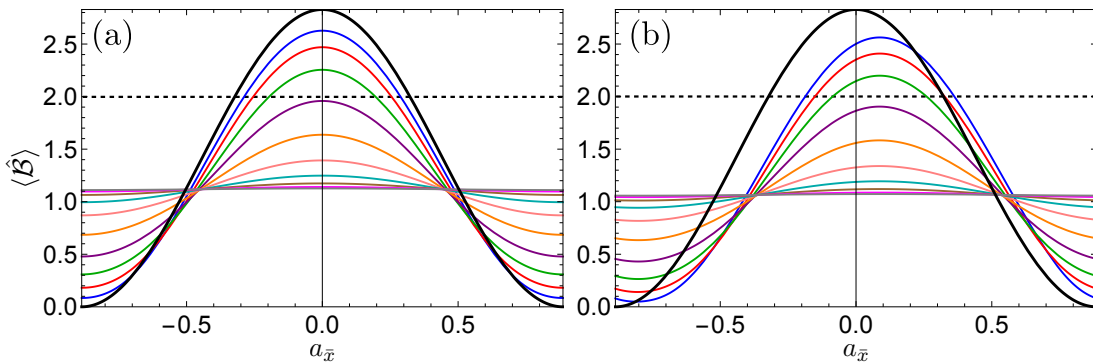


Figure IV.4: Plots of the expectation value of the Bell operator (IV.85) in terms of the state (IV.87) with a Gaussian wave function as a function of $a_{\bar{x}}$, for $\ell = 2\sqrt{\pi}$, $\kappa_i = 0.1(2\pi/\ell)$, $a_{\bar{p}} = 0$ (left) and $a_{\bar{p}} = 0.1(2\pi/\ell)$ (right). Each curve corresponds to a different width in the modular position with increasing order from the uppermost to the lowest curve at the origin of the x -axis: $\Delta_i = 0.05\ell$ (blue, uppermost), $\Delta_i = 0.075\ell$ (red), $\Delta_i = 0.1\ell$ (green), $\Delta_i = 0.125\ell$ (purple), $\Delta_i = 0.15\ell$ (orange), $\Delta_i = 0.175\ell$ (pink), $\Delta_i = 0.2\ell$ (cyan), $\Delta_i = 0.225\ell$ (brown), $\Delta_i = 0.25\ell$ (magenta) and $\Delta_i = 0.275\ell$ (grey, lowest). All parameters are chosen equal for $i = a, b$. The black curve shows the function $2\sqrt{2}\cos^2(a_{\bar{x}}\ell/2)$ and the black dashed line indicates the local-realism threshold.

where $N_{\pm} = 2(2 \mp \sqrt{2})^{1/2}$. These nonnormalizable states violate the CHSH inequality maximally for the choice $\bar{x}_{a/b} = 0$ and $\bar{p}_{a/b} = 0$, yielding $\langle \hat{\mathcal{B}} \rangle = \pm 2\sqrt{2}$. Furthermore, we can construct physically sound states by continuously superposing the states (IV.87) with Gaussian wave packets, as discussed in the last Section.

In Fig. IV.4, we present numerical results of $\langle \hat{\mathcal{B}} \rangle$ according to Eq. (IV.85) as a function of a_x , for different values of the parameters Δ , κ and $a_{\bar{p}}$, showing a violation of the CHSH inequality for the entangled state (IV.87) superposed with a Gaussian wave packet. In contrast to the last section, the expectation value $\langle \hat{\mathcal{B}} \rangle$ is not invariant under one of the parameters $a_{\bar{x}}$, $a_{\bar{p}}$, Δ and κ , because the function $\zeta_y(\bar{x}, \bar{p}) = \cos(\bar{x}2\pi/\ell - \bar{p}\ell/2)$ depends on both the modular position and momentum. In Fig. IV.4(a), where we set $a_{\bar{p}} = 0$ and $\kappa = 0.1(2\pi/\ell)$, all curves are symmetric with respect to the origin $a_{\bar{x}} = 0$ and a violation occurs for a modular position width of $\Delta \lesssim 0.12\ell$. The finite value of κ results in an overall decrease of the expectation value $\langle \hat{\mathcal{B}} \rangle$, as compared to Fig. IV.3. Also here the curves have a \cos^2 -shape for small values of the modular position and momentum widths Δ and κ , respectively. In Fig. IV.4(b), we set $a_{\bar{p}} = 0.1(2\pi/\ell)$ leading to an asymmetric curve shape and a slight decrease of the values of $\langle \hat{\mathcal{B}} \rangle$.

Having shown the theoretical violation of the CHSH inequality we will move on now and discuss the use of measurements of modular variables in the context of contextuality tests of quantum mechanics.

IV.3 Contextuality

This Section is devoted to the study of contextuality as yet another fundamental property of quantum mechanics which, in contrast to entanglement and Bell nonlocality, is

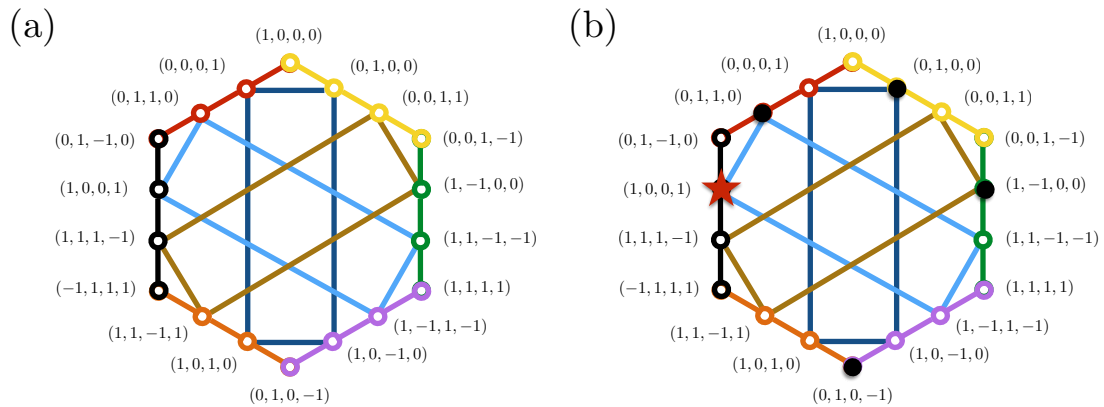


Figure IV.5: (a) Graph representing nine observables each consisting of four vertices that are connected by colored edges. (b) The same graph including black dots representing pre-determined outcomes to each of the nine observables. At least one of the observables cannot assign a unique pre-determined value (red star).

not based on correlations between two or more spatially separated subsystem. In this respect, we will first give an introduction in order to explain the terms (non)contextuality and discuss the Peres-Mermin square as a possible approach for its detection. Following this we will turn to the main subject of this Section and discuss the generalization of the Peres-Mermin scenario to Hilbert spaces of arbitrary dimension and demonstrate our findings at examples, including the case of modular variables.

IV.3.1 Contextuality and the Peres-Mermin square

The question of whether physical systems have intrinsic non-contextual properties is a long standing debate that was turned upside down with the advent of quantum physics. The measurement outcome dependence upon previously made measurements is at the heart of the Einstein-Podolsky-Rosen (EPR) paradox [Einstein et al., 1935], that evidences the conflict between classical and quantum views of realism. The contextuality of quantum theory, contrary to its classical analog, is ensured by the Kochen-Specker theorem [Kochen and Specker, 1967].

In a non-contextual theory, the result of a measurement of an observable A depends only on the state of the system and the observable A being measured. Additionally, measurement outcomes can depend on some (possibly hidden) variable λ describing the state of the system. If one knows λ then one can predict the outcome of any measurement: we say thus that measurement outcomes are pre-determined. This corresponds to the classical view in which every system is in a well defined state. In particular, in a non-contextual theory, measurement outcomes do not depend on the compatible observables that are measured together with A .

The initial argument by Kochen-Specker to show the contextuality of quantum mechanics used a set of 117 vectors in a 3-dimensional space [Kochen and Specker, 1967]. To give a simpler, more intuitive explanation of why quantum mechanics is contextual we consider a *four*-dimensional Hilbert space and on it, eight observables, each defined

by four orthonormal eigenvectors. In Fig. IV.5, we present these observables and their corresponding eigenvectors in a graph. Each vertex of the graph depicts one of the 16 eigenvectors and the vertices are connected by colored edges forming *nine* observables. It is evident that a measurement of one of the nine observables can lead to results whose corresponding eigenvectors are shared by other observables in the graph. In a non-contextual theory one has to assign predetermined outcomes to each of the observables. Examples of such predetermined values are depicted in Fig. IV.5(b) by black dots covering one vertex of the corresponding measured observables. If we now try to assign predetermined outcomes to all the observables depicted in the graph, we see that this is not possible. Either one of the observables cannot yield a single determined outcome or the measurement outcomes cannot be predefined. This contradiction demonstrates that the measurement outcomes in quantum mechanics cannot be reproduced by a classical theory, in which measurement results are predetermined by some hidden variables.

Since Kochen-Specker many attempts have been made to refine the definition of the contextuality argument in order to turn it into an experimentally testable property. The contextuality of quantum mechanics was proven for a particular state and a Hilbert space of dimension 4 by Peres [Peres, 1990]. Mermin showed that this argument could be recast to find a state independent proof of contextuality [Mermin, 1990]. Mermin's arguments were also used later on to derive state independent non-contextuality inequalities, *i.e.* inequalities that can be violated by any state if contextuality holds [Cabello, 2008; Kleinmann et al., 2012; Yu and Oh, 2012]. One way to obtain such inequalities is by using the so-called Peres Mermin square (PMS) which is particularly attractive from an experimental perspective. Indeed there have been experimental demonstrations of contextuality based on the PMS with trapped ions [Kirchmair et al., 2009], nuclear spin ensembles [Moussa et al., 2010] and photons [Amselem et al., 2009, 2012; D'Ambrosio et al., 2013]. In addition, it has been proven that contextuality is a critical resource for quantum computing [Veitch et al., 2012; Raussendorf, 2013; Howard et al., 2014; Delfosse et al., 2015; Raussendorf et al., 2015].

In order to recall the principles of the PMS let us consider a set of nine dichotomic observables $\{A_{jk}\}$, $i, j = 1, 2, 3$, and present them in a table as depicted in Fig. IV.6(left). The observables are chosen such that they are mutually commuting whenever they share a common subscript. Thus, products of observables occupying the same row or column in the table (see Fig. IV.6(left)) can be measured simultaneously and we can construct the following measurable quantity:

$$\langle X \rangle = \langle A_{11}A_{12}A_{13} \rangle + \langle A_{21}A_{22}A_{23} \rangle + \langle A_{31}A_{32}A_{33} \rangle \quad (\text{IV.88})$$

$$+ \langle A_{11}A_{21}A_{31} \rangle + \langle A_{12}A_{22}A_{32} \rangle - \langle A_{13}A_{23}A_{33} \rangle. \quad (\text{IV.89})$$

In a non-contextual theory, where observables assign pre-determined values -1 or 1 , one can show that the maximum value of $\langle X \rangle$ is equal to 4, simply by testing all possible combination of outcomes of the observables $\{A_{jk}\}$ [Cabello, 2008].

In contrast, if one considers quantum theory the observables $\{A_{ij}\}$ are given by hermitian operators with a binary spectrum, for instance by products of Pauli operators (see Eqs. (II.3)-(II.5)), as depicted in Fig. IV.6(right). In this case one can easily check that the observables in the same row or column are mutually commuting. However, because the product of operators along each row and column is equal to $\mathbb{1}$ and for the

Classical:				Quantum:			
A_{jk}	$k = 1$	$k = 2$	$k = 3$	A_{jk}	$k = 1$	$k = 2$	$k = 3$
$j = 1$	A_{11}	A_{12}	A_{13}	$j = 1$	$\hat{\sigma}_x \otimes \mathbb{1}$	$\mathbb{1} \otimes \hat{\sigma}_x$	$\hat{\sigma}_x \otimes \hat{\sigma}_x$
$j = 2$	A_{21}	A_{22}	A_{23}	$j = 2$	$\mathbb{1} \otimes \hat{\sigma}_z$	$\hat{\sigma}_z \otimes \mathbb{1}$	$\hat{\sigma}_z \otimes \hat{\sigma}_z$
$j = 3$	A_{31}	A_{32}	A_{33}	$j = 3$	$\hat{\sigma}_x \otimes \hat{\sigma}_z$	$\hat{\sigma}_z \otimes \hat{\sigma}_x$	$\hat{\sigma}_y \otimes \hat{\sigma}_y$

Figure IV.6: The Peres-Mermin square for measurements of classical binary observables $A_{ij} \in \{\pm 1\}$ (left) and for measurements of tensor products of Pauli operators (II.7), $\hat{\sigma}_{x,y,z}$ (right).

last column equal to -1 , one finds that the maximum value of the quantity (IV.89) is given by $\langle X \rangle_{QM} = 6$ and thus violates the classical bound of *four*. This proves that measurement outcomes predicted by quantum mechanics can not be reproduced by a non-contextual theory. Moreover, the latter holds independently of which state the system is prepared in.

Even though the study of contextuality was originally focused on discrete variable system, such as qubits and qudits, it is also possible to find state independent non-contextual inequalities for continuous variables in the PMS [Plastino and Cabello, 2010; Asadian et al., 2015]. In this case, one notes that the operators used to derive the inequalities have a bounded spectrum. This last property ensures that their expectation values can be expressed as the ones of dichotomic observables defined in an extended space [Horodecki, 2003]. The bounded observables used in [Plastino and Cabello, 2010; Asadian et al., 2015] can be obtained by measuring bounded functions of observables with an arbitrary spectrum. Similar techniques were used in [Ketterer et al., 2015; Arora and Asadian, 2015] to test Bell inequalities [Einstein et al., 1935; Bell, 1964; Clauser et al., 1969], a particular case of non-contextual inequalities (see Sec. IV.2). Nevertheless, ruling out local realism in experiments requires to satisfy more stringent constraints as those necessary to prove the contextuality of quantum mechanics. The contextuality of quantum mechanics can be proven, in principle, by measuring well chosen observables, independently of the system's particular state [Badziąg et al., 2009]. It is thus of interest to characterize which properties observables must have in order to reveal contextuality and to maximally violate non-contextuality inequalities.

So far, the contextuality of quantum mechanics has been shown for specific observables defined by continuous or discrete variables. In addition, according to the considered case, the border between contextual and non-contextual theories varies. It is natural to seek to identify the common features of the existing results and try to formalize the general conditions quantum observables must fulfill in order to demonstrate state independent contextuality irrespectively of their dimensionality. Such understanding would potentially enable state-independent tests of this fundamental property of quantum mechanics in quantum system of various dimensions. In other words, what are the common/distinctive properties and features of non-contextual inequalities? How can one build a suitable inequality from arbitrary observables permitting the demonstration of state-independent contextuality?

IV.3.2 Peres-Mermin square for arbitrary unitary operators

After having introduced the reader to the topic of contextuality we will seek now to formulate tests of contextuality in Hilbert spaces of arbitrary dimensions. As discussed in Sec. IV.3.1, contextuality is another fundamental property of quantum mechanics which, in contrast to entanglement and nonlocality, does not rely on correlations between two spatially separated parties. Using the Peres-Mermin square (see Table IV.6) one can construct inequalities (see Eq. (IV.89)), involving measurements of binary observables, that allow to demonstrate the contextuality through its violation. Let's reproduce this inequality here:

$$\begin{aligned} \langle X \rangle = & \langle A_{11}A_{12}A_{13} \rangle + \langle A_{21}A_{22}A_{23} \rangle + \langle A_{31}A_{32}A_{33} \rangle \\ & + \langle A_{11}A_{21}A_{31} \rangle + \langle A_{12}A_{22}A_{32} \rangle - \langle A_{13}A_{23}A_{33} \rangle < 4, \end{aligned} \quad (\text{IV.90})$$

where each term $A_{ij}A_{kl}A_{st}$ is a commuting product of binary observables contained in the same row or column of the Peres-Mermin square (see Fig. IV.6). As explained in Sec. IV.3.1, in the quantum case one can choose the observables A_{ij} equal to tensor products of Pauli operators (II.7) leading to a state-independent violation of inequality (IV.90). This state-independence constitutes a particularly interesting aspect of the contextuality of quantum mechanics which will be at the heart of our following considerations.

In the following we show that a generalized version of the Peres-Mermin square approach can be formulated using complex functions (continuous or discrete) with absolute values equal to 1, instead of the above real binary observables A_{ij} . This leads to inequalities involving measurements of the real and imaginary parts of such functions which both are bounded within the interval $[-1, 1]$ and thus can represent, for instance, bounded modular variables $F(x, p)$. Enlightening results that will help us here as guidelines were obtained by Asadian *et al.* [Asadian et al., 2015], where the particular case of contextuality tests in terms of phase space displacement operators was studied. In this work, several interesting conditions for testing contextuality in phase space were obtained that can be understood further in the light of the framework that we devise here.

Non-contextual inequalities involving complex functions can be derived by choosing the A_{jk} 's appearing in the PMS as $U_{jk} = A_{jk}^R + iA_{jk}^I$, with $|A_{jk}^R|^2 + |A_{jk}^I|^2 = 1$, as shown by the left table in Fig. IV.7. In quantum mechanics in turn, the complex functions U_{jk} become unitary operators which we can choose to be defined on a bipartite system, as shown in Fig. IV.7, with three unitary operations \hat{U}_j , with $j = 1, 2, 3$, defined on one of the two subsystems, respectively. A similar notation was used in [Asadian et al., 2015], with the important difference that in the mentioned reference the authors focused on the specific case of displacement operators, while here we consider arbitrary unitary operators \hat{U}_j defined in a Hilbert space of arbitrary dimension. By doing so, we can identify the original Peres-Mermin square (see Fig. IV.6) as a particular case of the generalized Peres-Mermin square with arbitrary complex function or unitary operators (see Fig. IV.7).

If we multiply rows and columns of the classical Peres-Mermin square in Fig. IV.7, we arrive at a quantity that involves complex functions as well. In order to transform it into a real quantity we have to take its real or imaginary part. For instance, taking

Classical:				Quantum:			
U_{jk}	$k = 1$	$k = 2$	$k = 3$	\hat{U}_{jk}	$k = 1$	$k = 2$	$k = 3$
$j = 1$	U_{11}	U_{12}	U_{13}	$j = 1$	$\hat{U}_1^\dagger \otimes \mathbb{1}$	$\mathbb{1} \otimes \hat{U}_1^\dagger$	$\hat{U}_1 \otimes \hat{U}_1$
$j = 2$	U_{21}	U_{22}	U_{23}	$j = 2$	$\mathbb{1} \otimes \hat{U}_2^\dagger$	$\hat{U}_2^\dagger \otimes \mathbb{1}$	$\hat{U}_2 \otimes \hat{U}_2$
$j = 3$	U_{31}	U_{32}	U_{33}	$j = 3$	$\hat{U}_1 \otimes \hat{U}_2$	$\hat{U}_2 \otimes \hat{U}_1$	$\hat{U}_3 \otimes \hat{U}_3$

Figure IV.7: The Peres-Mermin square for measurements of classical complex observables U_{ij} (left) with absolute value 1 and for measurements of tensor products of arbitrary unitary operators \hat{U}_j , with $j = 1, 2, 3$ (right).

the real part leads to

$$\langle \text{Re}(X) \rangle = \langle R_1 \rangle + \langle R_2 \rangle + \langle R_3 \rangle + \langle C_1 \rangle + \langle C_2 \rangle - \langle C_3 \rangle, \quad (\text{IV.91})$$

where R_j and C_k denote the real parts of a product of operators contained in a row or a column, respectively, which can be expressed in terms of the real and imaginary parts of the complex functions U_{ij} , yielding:

$$R_j = (A_{j1}^R A_{j2}^R - A_{j1}^I A_{j2}^I) A_{j3}^R - (A_{j1}^I A_{j2}^R + A_{j1}^R A_{j2}^I) A_{j3}^I, \quad (\text{IV.92})$$

$$C_k = (A_{1k}^R A_{2k}^R - A_{1k}^I A_{2k}^I) A_{3k}^R - (A_{1k}^I A_{2k}^R + A_{1k}^R A_{2k}^I) A_{3k}^I. \quad (\text{IV.93})$$

In order to derive a classical bound on the quantity (IV.91) we assign deterministic outcomes to the quantities A_{ij}^R and A_{kl}^I that take values in the interval $[-1, 1]$. If we further assume that they take only the maximal values ± 1 we find that the classical bound on the quantity (IV.91) is given by 12. However, by extending the results of [Asadian et al., 2015] to arbitrary complex functions we can lower the non-contextual bound and arrive at: $\langle \text{Re}(X) \rangle \leq 3\sqrt{3}$. To show this one has to exploit the fact that the complex functions U_{ij} have absolute values equal to 1 which is a condition that is always true also for unitary operators \hat{U}_{ij} . Enforcing this constraint while maximizing $\langle \text{Re}(X) \rangle$ allows us to arrive at a new classical bound. The maximization can be performed by employing the theory of Lagrange multipliers. In this respect, we introduce an auxiliary function:

$$\langle \text{Re}(X) \rangle^{(\text{aux})} = \langle \text{Re}(X) \rangle - \lambda \sum_{ij} |(A_{ij}^R)^2 + (A_{ij}^I)^2 - 1|, \quad (\text{IV.94})$$

which, through the condition $\nabla \langle \text{Re}(X) \rangle^{(\text{aux})} = 0$, can be used to calculate the maximum of $\langle \text{Re}(X) \rangle$ under the constraint $|U_{ij}| = 1$, and with the A_{ij}^R 's and A_{kl}^I 's being classical random variables taking values in the interval $[-1, 1]$. Eventually one finds that, for $\lambda \geq 2$, this maximum is given by $3\sqrt{3}$ defining a new noncontextual bound on the quantity (IV.91). We note that constraints, such as $|U_{ij}| = 1$, impose additional assumptions on the observables contained in Eq. (IV.91) which might open a loophole that can be exploited to fake the violation of the bound $3\sqrt{3}$. However, in order to circumvent this problem we can use directly the expression $\langle \text{Re}(X) \rangle^{(\text{aux})}$, whose classical bound is also given by $3\sqrt{3}$, without doing any assumptions on the observables being measured.

Finally, we can recover the known Peres-Mermin square for qubits, shown in Fig. IV.6, by assuming that the real or imaginary part of the complex functions U_{ij} is equal to zero and the other yields binary outcomes. In this case, the above maximization of (IV.91) recovers the known noncontextual bound of 4.

We now move to the quantum description of the PMS using unitary operators (see Fig. IV.7(right)). Unitary operators are in general not observables but can be measured in terms of their real and imaginary parts, \hat{A}_{jk}^R and \hat{A}_{jk}^I , which themselves are observables. In order to maximally violate the non-contextual inequality $\langle \text{Re}(X) \rangle \leq 3\sqrt{3}$ we have to enforce that products of operators in each row and column of the Peres-Mermin square (see Fig. IV.7(right)) are equal to $\mathbb{1}$, with the exception of the last column that must yield $-\mathbb{1}$. Furthermore, unitaries in the same row or column must be compatible which leads to the constraints $[\hat{U}_1, \hat{U}_3] = 0$ or $\{\hat{U}_1, \hat{U}_3\} = 0$, and similarly for \hat{U}_2 and \hat{U}_3 . These conditions cannot be verified all at the same time, and the only possibility to obtain a state independent maximal violation of the considered noncontextuality inequality is to enforce $\{\hat{U}_1, \hat{U}_3\} = 0$ and $\{\hat{U}_2, \hat{U}_3\} = 0$. Combining the above ingredients leads to the following conditions for maximal violation of noncontextuality inequalities derived from the Peres-Mermin square: $\hat{U}_1\hat{U}_2\hat{U}_3 = \pm i\mathbb{1}$ and $\hat{U}_2\hat{U}_1\hat{U}_3 = \mp i\mathbb{1}$, which can be expressed in a more compact way as:

$$\{\hat{U}_1, \hat{U}_2\} = 0, \quad (\text{IV.95})$$

$$\hat{U}_3 = \pm i\hat{U}_2^\dagger\hat{U}_1^\dagger. \quad (\text{IV.96})$$

From the conditions (IV.95) and (IV.96) we see that a state independent maximal violation of the Peres-Mermin inequality requires that the unitary operators U_1 and U_2 are anti-commuting and that they completely determine the operator U_3 through the relation (IV.96). Hence, if the unitary operators in the Peres-Mermin square (see Fig. IV.7(right)) fulfill the commutation relations:

$$\{\hat{U}_i, \hat{U}_j\} = 2\delta_{ij}\hat{U}_i^2, \quad (\text{IV.97})$$

$$[\hat{U}_i, \hat{U}_j] = \pm 2i\epsilon_{ijk}\hat{U}_k^\dagger, \quad (\text{IV.98})$$

the expectation (IV.91) maximally violates the noncontextuality inequality with $\langle \text{Re}(X) \rangle = 6$, no matter in which state $|\Psi\rangle$ the system is in. Conditions (IV.95) and (IV.96) are general, and to our knowledge, have not been established so far. Previous results showing the possibility of violation of the non-contextual inequalities are particular cases obeying these conditions. Examples are state independent contextuality using two-level systems [Cabello, 2008] and displacement operators [Plastino and Cabello, 2010; Asadian et al., 2015].

Now, we make a step further beyond the relations (IV.95) and (IV.96), and answer to the following question: given a unitary operator \hat{U}_1 , what are the necessary and sufficient conditions for finding two other operators \hat{U}_2 and \hat{U}_3 such that (IV.95) and (IV.96) are satisfied and thus lead to a maximal violation of noncontextuality inequalities derived from the Peres-Mermin square? To answer this question we show first that a given unitary operator \hat{U} , acting on a Hilbert space \mathcal{H} , admits an anti-commuting partner if and only if for each eigenvalue λ_i of \hat{U} , we find a corresponding eigenvalue $-\lambda_i$ whose eigenspace has the same dimension K_i as the one of λ_i . Once we have found an operator

that fulfills this statement we can express it in some basis as a direct sum:

$$\hat{U} = \bigoplus_{i=1}^N \lambda_i \sigma_z^{(i)}, \quad (\text{IV.99})$$

where $\pm\lambda_i$ are the eigenvalues of \hat{U} , $\hat{\sigma}_z^{(i)} = \bigoplus_{j=1}^{K_i} \hat{\sigma}_z$ is a direct sum of Pauli matrices (II.5) acting on the eigenspace associated to the eigenvalue $\pm\lambda_i$ with degeneracy K_i , and N is an arbitrary, possibly infinite, integer value that is smaller than the Hilbert space dimension. In the particular case of a nondegenerate spectrum $\hat{\sigma}_z^{(i)} = \hat{\sigma}_z$ acts on a two dimensional subspace.

To prove the above statement we assume first that \hat{U} fulfills the above condition on the spectrum and prove that it admits an anti-commuting partner. We restrict ourselves here to the finite dimensional case. Let's define the set of eigenvalues of \hat{U} as $\{\lambda_1, \dots, \lambda_N, -\lambda_1, \dots, -\lambda_N\}$, and the set of eigenvectors associated to each of the eigenvalues $\pm\lambda_i$ as $\{|e_{i,j}^\pm\rangle\}$, with possible degeneracy $j \in \{1, \dots, K_i\}$. Since \hat{U} is a unitary operator, we know that the set of eigenvectors $\{|e_{i,j}^\pm\rangle\}$ represents an orthonormal basis of the Hilbert space. Further on, we define an operator \hat{U}' through: $\hat{U}'|e_{i,j}^\pm\rangle = \lambda'_i|e_{i,j}^\mp\rangle$, where λ'_i are arbitrary complex numbers with absolute value 1, which maps an orthonormal basis to another orthonormal basis thus providing a unitary operator. A simple calculation yields:

$$\begin{aligned} (\hat{U}\hat{U}' + \hat{U}'\hat{U})|e_{i,j}^\pm\rangle &= \lambda'_i\hat{U}|e_{i,j}^\mp\rangle \pm \lambda_i\hat{U}'|e_{i,j}^\pm\rangle \\ &= \mp\lambda_i\lambda'_i|e_{i,j}^\mp\rangle \pm \lambda_i\lambda'_i|e_{i,j}^\mp\rangle = 0. \end{aligned} \quad (\text{IV.100})$$

showing that \hat{U} and \hat{U}' are anti-commuting. Hence, we have found an anti-commuting partner to \hat{U} defined through the condition $\hat{U}'|e_{i,j}^\pm\rangle = \lambda'_i|e_{i,j}^\mp\rangle$, leading to the expression:

$$\hat{U}' = \bigoplus_{i=1}^N \lambda'_i \sigma_x^{(i)}, \quad (\text{IV.101})$$

where $\sigma_x^{(i)} = \bigoplus_{j=1}^{K_i} \sigma_x$. Diagonalization of Eq. (IV.101) yields for \hat{U}_2 the same form as in (IV.99).

To prove the converse statement let's assume that we have two unitary operators \hat{U} and \hat{U}' satisfying $\{\hat{U}, \hat{U}'\} = 0$. We denote by λ an eigenvalue of \hat{U} with the corresponding eigenvectors $\{|e_i\rangle\}$, where $i = 1 \dots K$. Using the anti-commutation relation we can prove that $\hat{U}'|e_i\rangle$ is an eigenvector of \hat{U} with eigenvalue $-\lambda$:

$$(\hat{U}\hat{U}' + \hat{U}'\hat{U})|e_i\rangle = \hat{U}\hat{U}'|e_i\rangle + \hat{U}'\lambda|e_i\rangle \quad (\text{IV.102})$$

$$\Rightarrow \hat{U}\hat{U}'|e_i\rangle = -\lambda\hat{U}'|e_i\rangle. \quad (\text{IV.103})$$

Since $\{|e_i\rangle\}$ is an orthonormal set and \hat{U}' is a unitary operator, $\{\hat{U}'|e_i\rangle\}$ is also an orthonormal set, which proves that $-\lambda$ is an eigenvalue of \hat{U} of dimension larger or equal than K . The same reasoning can be applied to the set of eigenvectors of \hat{U} with eigenvalue $-\lambda$ to show that the dimension of the eigenspace associated to λ is higher or

equal than the dimension of the eigenspace associated to $-\lambda$ and thus equal.

With respect to testing noncontextuality inequalities, the above statement allows us to decide whether a unitary operator \hat{U}_1 admits anti-commuting partners \hat{U}_2 and \hat{U}_3 , such that the three of them can be used to demonstrate a state-independent maximal violation of the Peres-Mermin inequality. Furthermore, if \hat{U}_1 has an anti-commuting partner \hat{U}_2 , it follows that, in some basis, they can be expressed in the form (IV.99) and (IV.101), respectively. Once \hat{U}_1 and \hat{U}_2 are found, the third unitary operator \hat{U}_3 is directly determined by Eq. (IV.96), yielding:

$$\hat{U}_3 = \pm \bigoplus_{i=1}^N (\lambda_i \lambda'_i)^* \sigma_y^{(i)}. \quad (\text{IV.104})$$

This shows that maximal state-independent contextuality in the PMS is a very peculiar property related to binary spectrum of operators whose spectral decomposition, continuous or discrete, can be written in terms of finite or infinite direct sums of Pauli matrices.

We will now continue and study examples of operators satisfying the above introduced conditions and show how they relate to the particular cases that were discussed in previous works.

IV.3.3 Contextuality in finite dimensional Hilbert spaces

The decompositions (IV.99), (IV.101) and (IV.104) reveal the binary structure of the spectrum of the unitary operators \hat{U}_i , with $i = 1, 2, 3$, which is at the heart of a maximal violation of the Peres-Mermin non-contextuality inequality for finite N . Thus, state independent maximal violation of contextuality in a Peres-Mermin scenario is only possible in a Hilbert space of even dimension and formed by two parties which are themselves also of even dimension. In [Asadian et al., 2015], the authors reached a similar conclusion for the case of discrete displacements in phase space. Thanks to the generality of the conditions obtained here, we can analyze in more detail a scenario containing measurements of finite discrete dimensional quantum systems, so-called qudits (see Sec. II.1.2 for an introduction).

To begin let's consider the simplest case of qubit measurements, corresponding to $N = 1$ in Eq. (IV.99), (IV.101) and (IV.104), for which we recover the Peres-Mermin scenario discussed in Sec. IV.3.1 with the Peres-Mermin squares depicted in Fig. IV.6. When moving to higher dimensional systems, for instance, a pair of spin S particles, contextuality can be demonstrated using the following rotation operators:

$$\hat{R}_1 = e^{i\hat{S}_x t_1}, \quad \hat{R}_2 = e^{i\hat{S}_y t_2}, \quad \hat{R}_3 = e^{i\hat{S}_z t_3}, \quad (\text{IV.105})$$

where \hat{S}_x , \hat{S}_y and \hat{S}_z are the three vector components of the spin S operator $\hat{\mathbf{S}}$ (recall Eqs. (II.22)-(II.24)), generating the group $\text{SU}(2)$ of all unitary rotations in a $d = 2S + 1$ dimensional Hilbert space. In order to build a Peres-Mermin square, one must choose t_1 , t_2 and t_3 such that R_1 , R_2 and R_3 verify (IV.95) and (IV.96). The matrix elements of the z -component of $\hat{\mathbf{S}}$ read $(S_z)_{ab} = (S + 1 - b)\delta_{a,b}$, and the eigenvalues of R_1 are $\exp(i(S + 1 - b)t_1)$, for $b = 0, \dots, d - 1$. Hence, condition (IV.95) and (IV.96) are only satisfied if $t_3 = \pi$ and, since S_x and S_y are unitarily equivalent to S_z , if $t_1 = t_2 = \pi$. In

this case, R_1 , R_2 and R_3 lead to a maximal violation of the Peres-Mermin inequality in terms of rotations of half-integer spins, generalizing the qubit case presented in Sec. IV.3.

IV.3.4 Contextuality in infinite dimensional Hilbert spaces

We can also study observables which are defined in infinite dimensional Hilbert spaces. For instance, if one considers the Hilbert space of a single mode of the electromagnetic field (see Sec. II.2) spanned by single mode Fock basis $\{|n\rangle|n = 0, 1, \dots, \infty\}$, we can define the photon number parity operator as $\hat{P} = (-1)^{\hat{n}}$, where \hat{n} is the photon number operator fulfilling $\hat{n}|n\rangle = n|n\rangle$. The parity operator has two eigenvalues ± 1 which are both infinitely degenerate and thus can be expressed as in Eq. (IV.99) with $N = 1$, $\lambda_1 = 1$ and $K_1 = \infty$. To see this, we write in the Fock basis $\hat{P} = \sum_{n=0}^{\infty} |2n\rangle\langle 2n| - |2n+1\rangle\langle 2n+1|$ which is equivalent to $\bigoplus_{j=1}^{\infty} \hat{\sigma}_z$ and thus to Eq. (IV.99). According to Eqs. (IV.101) and (IV.104) we can define two anti-commuting partners of the parity operator $\hat{P} = \hat{P}_x \hat{P}_y$ which read:

$$\hat{P}_x = \bigoplus_{j=1}^{\infty} \hat{\sigma}_x, \quad \hat{P}_y = \bigoplus_{j=1}^{\infty} \hat{\sigma}_y. \quad (\text{IV.106})$$

These kind of pseudospin operators were also used to show that the EPR state (II.146) can lead to a maximal violation of nonlocality in terms of the CHSH inequality [Chen et al., 2002].

IV.3.5 Contextuality with modular variables

Our results can also be used to demonstrate state independent contextuality for measurements of observables with continuous spectrum. In particular, we want to formulate a contextuality test that involves measurements of modular variables, as introduced in Sec. III.3. To do so we consider the logical Pauli operations (III.83), (III.86) and (III.82) which are equal to three displacement operators (the three displacements are illustrated in Fig. III.7) and in the modular representation read:

$$\hat{Z} = \int_{-\ell/4}^{\ell/4} d\bar{x} \int_{-\pi/\ell}^{\pi/\ell} d\bar{p} e^{2\pi i \bar{x}/\ell} \hat{\sigma}_z(\bar{x}, \bar{p}), \quad (\text{IV.107})$$

$$\hat{X} = \int_{-\ell/4}^{\ell/4} d\bar{x} \int_{-\pi/\ell}^{\pi/\ell} d\bar{p} e^{-i\bar{p}\ell/2} \hat{\sigma}_x(\bar{x}, \bar{p}), \quad (\text{IV.108})$$

$$\hat{Y} = \int_{-\ell/4}^{\ell/4} d\bar{x} \int_{-\pi/\ell}^{\pi/\ell} d\bar{p} e^{i\bar{p}\ell/2 - 2\pi i \bar{x}/\ell} \hat{\sigma}_y(\bar{x}, \bar{p}), \quad (\text{IV.109})$$

These logical operators fulfill by definition the relations (IV.97) and (IV.98), as discussed in Sec. III.2.2.1, and thus lead to a maximal violation of the Peres-Mermin inequality. Thereby, the corresponding real and imaginary parts contained in Eqs. (IV.92) and (IV.93) correspond to measurements of a particular set of modular variables, namely of the hermitian components of the displacement operators (IV.107), (IV.108) and (IV.109) (see Sec. III.1.2).

A similar result has been obtained in [Asadian et al., 2015], where it was shown that

for a phase space displacement operator $\mathcal{D}(\alpha_1) = e^{\alpha_1 \hat{a}^\dagger - \alpha_1^* \hat{a}}$, one can always find other displacement operators $\mathcal{D}(\alpha_2)$ and $\mathcal{D}(\alpha_3)$, such that they satisfy the relations (IV.95) and (IV.96).¹ The condition for this to hold is that α_1 , α_2 and α_3 fulfill the relations $\text{Im}(\alpha_i \alpha_j^*) = \pm\pi/2$ and $\alpha_1 + \alpha_2 + \alpha_3 = 0$. However, it is the modular representation which allows us to write the displacements (IV.108), (IV.109) and (IV.107), namely those displacements that form a rectangular triangle in phase space (see Fig. III.7), as a continuous superposition of Pauli operators $\hat{\sigma}_\beta(\bar{x}, \bar{p})$, with $\beta = x, y, z$ (see Eqs. (III.84), (III.85) and (III.87)). Hence, we find that Eqs. (IV.107)-(IV.109) are equivalent to the general unitary operators \hat{U}_i , with $i = 1, 2, 3$, defined in Eqs. (IV.99), (IV.101) and (IV.104), with eigenvalues $\lambda(\bar{x}, \bar{p}) = e^{2\pi i \bar{x}/\ell}$ of \hat{U}_1 , $\lambda'(\bar{x}, \bar{p}) = e^{i\bar{p}\ell/2}$ of \hat{U}_2 and $(\lambda(\bar{x}, \bar{p})\lambda'(\bar{x}, \bar{p}))^* = e^{i\bar{p}\ell/2 - 2\pi i \bar{x}/\ell}$ of \hat{U}_3 . Remember that according to our remarks in Sec. IV.3.2 also $-\lambda(\bar{x}, \bar{p})$, $-\lambda'(\bar{x}, \bar{p})$ and $-(\lambda(\bar{x}, \bar{p})\lambda'(\bar{x}, \bar{p}))^*$ are eigenvalues of the three unitary operators, respectively. Hence, we find that the three unitary operators \hat{U}_1 , \hat{U}_2 and \hat{U}_3 are completely determined by the functions $\lambda(\bar{x}, \bar{p})$ and $\lambda'(\bar{x}, \bar{p})$. In contrast to the case of the parity operator, here all eigenvalues are nondegenerate, *i.e.* $K(\bar{x}, \bar{p}) = 1$, and we can read the integrals in Eqs. (IV.107)-(IV.109) equivalently as a continuous direct sum over Pauli matrices $\hat{\sigma}_\beta$, with $\beta = x, y, z$, weighted by the functions $\lambda(\bar{x}, \bar{p})$, $\lambda'(\bar{x}, \bar{p})$ and $(\lambda(\bar{x}, \bar{p})\lambda'(\bar{x}, \bar{p}))^*$, respectively.

In conclusion, we have derived general conditions for unitary operators in order to lead to a maximal violation of noncontextuality inequalities derived from the Peres-Mermin square irrespectively of the dimension of the system used to test it. In particular, we find a characterization of these operators that allows us to naturally decompose them into direct sums of Pauli matrices thereby revealing a relation between the binary properties of their spectrum and the ability to lead to maximal state independent contextuality. A consequence of our results is that it is not possible to maximally violate such inequalities state independently with bipartite systems if one of them is described by an odd dimensional Hilbert space. Nevertheless, we show how contextuality can be demonstrated with infinite dimensional systems characterized by either discrete or continuous variables.

IV.4 Discussion

In this Chapter we have studied tests of fundamental properties of quantum mechanics, namely entanglement, nonlocality and contextuality, in Hilbert spaces of various dimensions. Thereby, one of our central concerns was to find appropriate tools to test for these properties in terms of measurements of judiciously chosen modular variables. Finally, with these tools in hand we were able to demonstrate the applicability of our quantum information framework, developed in Chapter III. However, some considerations made in the previous Sections proved themselves useful regardless of the specific application to measurements of modular variables.

First, after a short introduction to some basics methods of entanglement detection, we showed how to use the stabilizer formalism for continuous-variable systems to derive entanglement witnesses involving measurements of modular variables. The derived witnesses are capable of detecting entanglement of multipartite states defined with re-

¹A definition of the displacement operator as function of $\alpha = (\nu + i\mu)/\sqrt{2}$ was given in Eq. (II.136).

spect to the logical basis $\{|0_L\rangle, |1_L\rangle\}$, defined in Sec. III.2.1, and thus demonstrate the usefulness of measurements of modular variables for the detection of a certain class of continuous-variable entangled states.

The second part of this Chapter was devoted to the study of Bell nonlocality. In this respect, we first gave a mathematical characterization of different types of correlations in terms of joint-probability distribution and showed how to detect nonlocal correlations in terms of Bell inequalities involving measurements with finitely many outcomes. Then, we turned to the question of how to test for nonlocality with observables yielding bounded but possibly infinite many outcomes. Our special attention was thereby on the use of the CHSH inequality in the context of such, more general measurement setups. Our results help creating a general environment for CHSH inequality tests without the need of binning procedures or prior knowledge of the physical properties of the system, rendering CHSH inequalities tests accessible to a broader class of experimental systems. Finally, we discussed numerical examples of CHSH inequality tests using measurements of modular variables and show how to violate it in terms of entangled states defined in the logical basis $\{|0_L\rangle, |1_L\rangle\}$.

Finally, we studied the contextuality of quantum mechanics as a fundamental property that does not rely on correlations between two spatially separated subsystems but rather on the incompatibility of measurements in general. Also here, we first gave a short introduction to contextuality itself and reviewed one of the most famous approaches to detect contextuality in a state-independent fashion using the Peres-Mermin square. Further on, we derived general conditions for operators to maximally violate non-contextuality inequalities in the Peres-Mermin scenario. A consequence of our results is that it is not possible to maximally violate such inequalities for any state using bipartite systems where one of the systems is described by an odd dimensional Hilbert space. Nevertheless, we show how contextuality can be demonstrated using systems of arbitrarily high dimensional subsystems and with continuous-variable measurements. In both the discrete and continuous case we find a characterization in terms of the spectrum of the observables that can be used to maximally violate the non-contextual bound in the Peres-Mermin inequality. This characterization allow us to find a natural decomposition of the observables in terms of direct sums of Pauli matrices.

Perspectives of our results are the implementation of the discussed methods in a wide range of physical systems which are characterized either by discrete- or by continuous-variable degrees of freedom. Examples of which are the transverse degrees of freedom of single photons, the quadratures of the electromagnetic field, or the motional degrees of freedom of trapped ions or micro-mechanical oscillators (see Chapter I for appropriate references). Since such tests are the basis of many quantum information protocols, that use fundamental properties of quantum mechanics as a resource, they might prove themselves useful for hybrid technologies making use of both discrete- and continuous-variable encodings simultaneously. Especially applications with macroscopic systems seem feasible due to the clear classical correspondence of the modular variables measurements and by their accesibility in terms of positive operator valued measurements.

Future work could involve improvements of the developed techniques in order to make the detection of a larger class of entangled or nonlocal states in terms of modular variables measurements possible. This might render our methods more attractive in systems for which the above logical basis is a rather unnatural choice. Moreover, we

might think of applying our ideas also to detect other interesting properties, such as steering or quantum coherence.

V Quantum information processing by means of the Talbot-Effect

While in the last two Chapters our focus was rather on devising and applying a general theoretical framework for quantum information processing in phase space, we turn now to a more specific experimentally motivated situation and show how the Talbot effect can be exploited to process discrete quantum information encoded in the spatial degrees of freedom of single photons. The Talbot effect occurs when plane waves are diffracted by periodic gratings leading to replications of the wavefront's structure after multiples of a characteristic propagation distance, referred to as the Talbot length. We will see that this effect, in combination with one additional linear optical element, is sufficient to perform universal single mode operations of d -dimensional quantum systems. Furthermore, entangling operations based on a novel beam-splitter device and on spontaneous parametric down-conversion are discussed. The latter permits to create deterministically d -dimensional entangled photon pairs which can be used as a resource for quantum information processing with photons besides the commonly used polarization or orbital angular momentum degrees of freedom. Finally, we demonstrate the produced entanglement by violating d -dimensional Bell inequalities and discuss potential implementations with entangled matter waves apart from single photons.

V.1 Near-field interference behind diffraction gratings

In this first Section we aim at providing the most important basics of near-field interference after periodic diffraction gratings and introduce the above mentioned *Talbot effect*. First, we will derive the expression of the scattered spatial wave function of the light field as a function of its propagation distance after the grating. Further on, we analyze the particular structure of this so-called *Talbot carpet* and emphasize characteristic propagation distances for which the spatial wave front depicts different periodicities. For this introduction we will stay close to the lines of the article [Case et al., 2009].

Now, we consider the following experimental setup, depicted in Fig. V.1(a). A plane wave with wave number $k = 2\pi/\lambda$ (wavelength λ) is propagating in the z -direction and impinging onto a periodic diffraction grating, placed at position $z = 0$ in the (x, y) -plane, with periodic modulation in the x -direction and periodicity ℓ . The size of the slits in the y -direction is assumed to be very large compared to the wavelength λ of the incoming plane wave such that no diffraction occurs in this direction and we can restrict ourselves to the interference in the (x, z) -plane. Directly after the grating at position $z = 0$ the wave takes the same form as the transmission function of the grating:

$$\Psi(x, 0) = \psi_0(x) = \sum_m A_m e^{imxk\ell} \quad (\text{V.1})$$

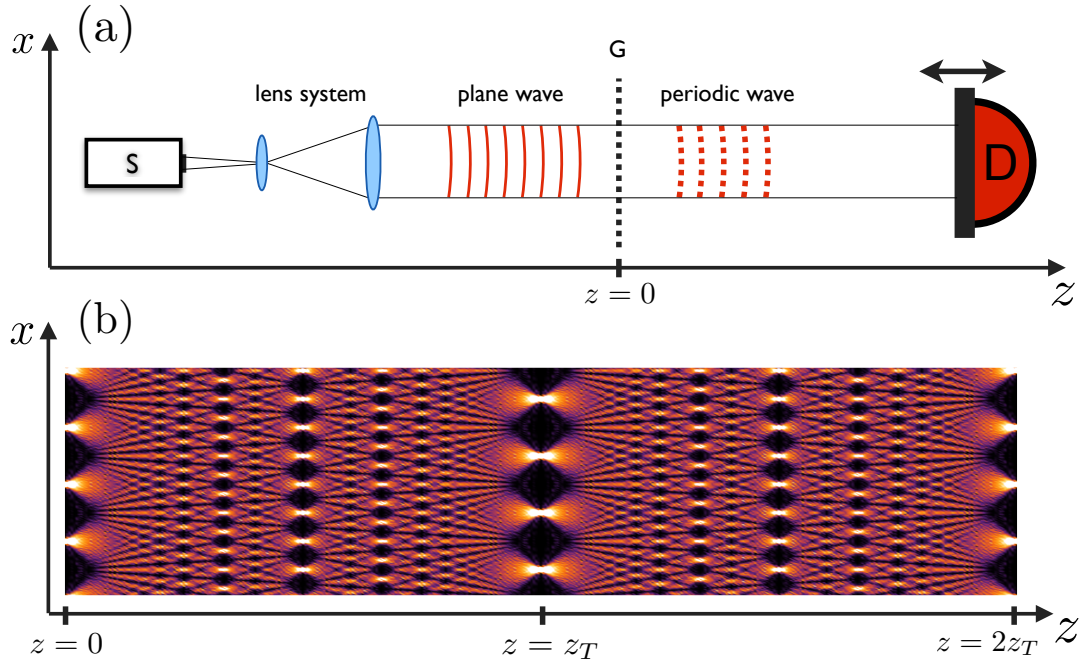


Figure V.1: (a) Schematic representation of an experimental setup used to measure the Talbot effect. A light field emitted by a source (S) is sent through a lens system that spatially filters and expands the beam in order to create parallel plane waves. The plane wave then falls at position $z = 0$ onto a grating (G) and creates a periodic diffraction pattern that is recorded with an appropriate detector, for instance, a CCD camera, at different positions z . (b) Density plot of the absolute value of the wave function (V.2) for rectangular slits with distance ℓ and width $a = 0.1\ell$. For propagation distances $z = z_T$ and $z = 2z_T$ the wave function produces an image of the grating transmission function.

which imprints multiples of the phase $k_\ell = 2\pi/\ell$ into the transverse momentum of the outgoing field. The Fourier coefficients A_m determine the precise shape of the outgoing periodic wave function and, in the case of rectangular slits with width a , reads: $A_m = (a/\ell)e^{-im\pi a/\ell}\text{sinc}(2m\pi a/\ell)$. Another possibility is to choose a grating whose transmission function is given by a comb of Gaussians with width Δ : $A_m = e^{-(2\pi m\Delta)^2/(2\ell^2)}$ (for an example see Fig. III.5 in the last Chapter).

Further on, as discussed in Sec. II.3.1.1, the free-space propagation of the transverse light field is determined by the paraxial Helmholtz (II.154) equation and, according to Eq. (II.155), simply imprints an additional phase e^{izk_z} on the transverse wave function. Remember that in the paraxial approximation (see Sec. II.2.3) the transverse wave vector component k_x is small compared to the total wave vector $k = \sqrt{k_x^2 + k_z^2}$, leading to $k_z \approx k - (mk_\ell)^2/2k$ and thus to the wave function:

$$\Psi(x, z) = \sum_m A_m e^{imxk_\ell} e^{izk_z} \approx \sum_m A_m e^{imxk_\ell} e^{-i\pi m^2 z/z_T} \quad (\text{V.2})$$

where we defined a new characteristic length $z_T = \ell^2/\lambda$, the so-called *Talbot length*. We note that Equation (V.2) aims at describing the near-field interference after the diffraction grating and will not predict accurately the transition to the far-field regime in which the condition $\ell \sin \theta = n\lambda$ determines the position of interference minima and maxima. Reasons for this are the assumptions of an infinitely extended grating that is illuminated by a plane wave. For more realistic descriptions, that account also for the transition between near- and far-field, one has to assume either a finitely extended grating that is illuminated by a plane wave or a infinitely extended grating and a finitely extended incoming wave packet.

To investigate the behavior of the wave function (V.2) let's consider the following specific propagation distances:

$$z = (s + q/r)2z_T, \quad (\text{V.3})$$

where s , q and r are integers, and q and r are relative primes. In this case, Eq. (V.2) becomes

$$\Psi(x, z) = \sum_{j=0}^{r-1} a_j \psi_0 \left(x - \frac{j}{r} \ell \right), \quad (\text{V.4})$$

where

$$a_j = \frac{1}{r} \sum_{n=0}^{r-1} e^{-2\pi i(n^2 - jn)q/r}. \quad (\text{V.5})$$

showing that the transverse wave-function is a linear combination of r replicas of the initial state $\psi_0(x)$ each displaced in the x direction by integer multiples of ℓ/r . Thereby, the coefficients a_j define the weight and phase of the corresponding linear combinations, which depend on p and r . One can see that the wave function (V.4) is $2z_T$ periodic and for the propagation distance $z = z_T$ it reproduces the grid transmission profile shifted in x -direction by half of the slit distance ℓ . Both situations can be observed in Fig. V.1(b), which presents a density plot of the wave function (V.4), also referred to as Talbot carpet. This self replication effect was observed first by Talbot in 1936 and explained theoretically by Rayleigh in 1881. A measurement of the whole Talbot carpet $|\Psi(x, z)|^2$ can be found in [Case et al., 2009]. The Talbot effect has also been observed experimentally with atomic matter waves [Nowak et al., 1997], and Bose-Einstein condensates [Mark et al., 2011].

For other propagation distances, apart from those in Eq. (V.3), the Talbot carpet displays a more complicated fractal behavior, referred to as irrational Talbot effect [Berry and Klein, 1996]. In the following, we will solely restrict ourselves to the rational Talbot effect, corresponding to propagation distances given by Eq. (V.3), and show it can be used to process discrete quantum information encoded in the transverse wave function (V.4).

V.2 Processing information by weaving Talbot carpets

V.2.1 Definition of logical states

After this short introduction to near-field interference and the Talbot effect we proceed now and use the Talbot effect in order to process D -dimensional quantum system encoded in the transverse wave function (V.4). To do so, we consider a discrete set of basis states $\{|j_d\rangle|j = 0, \dots, d-1\}$ defined in terms of the spatial wave functions

$$\langle x|j_d\rangle = \psi_0(x - \frac{j}{d}\ell). \quad (\text{V.6})$$

Hence, each basis state corresponds to a periodic wave function $\psi_0(x)$, defined by the Fourier coefficients A_m and the periodicity ℓ , that is displaced by the factor $\frac{d}{D}\ell$. Experimental means that allow for a production of such Talbot qudits are very close to those discussed in Sec. III.4.1. One can, for instance, send single photons through diffraction gratings and post-select only those photons that pass through the grating. Or, for a deterministic production, one can use pump-engineering techniques for the spatial degrees of freedom of photon pairs produced by spontaneous parametric down-conversion [Monken et al., 1998; Walborn et al., 2010], and produce heralded single-photons prepared in one of the above logical states. For instance, by pumping the non-linear crystal with a laser field that has a spatial distribution $\psi_0(x_p)$ we produce two entangled photons and the detection of one of them prepares the other photon in the state $\psi_0(x)$.

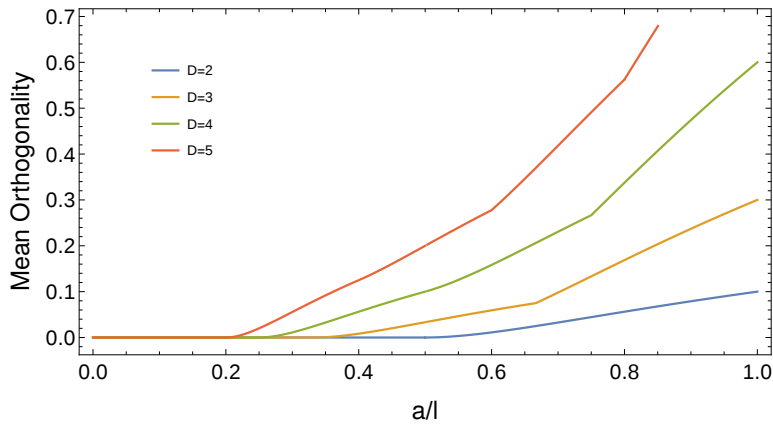


Figure V.2: Plot of the mean orthogonality $2 \sum_{j>j'} |\langle j_d|j'_d\rangle|^2/d(d-1)$ for the Talbot qudit logical basis states as function of a/ℓ . For higher dimensions d (or D inside the caption of the figure) the inter-slits distance ℓ has to be much greater than the slit size a , in order to assure orthogonality among the basis states. This figure was taken from the publication [Farías et al., 2015].

Since the overlap among the different wave functions (V.6) is in general nonzero, the Talbot basis state $|j_d\rangle$ are not perfectly orthogonal. For example, for a rectangular transmission function this overlap depends on the ratio between the slit width a and their distance ℓ . To understand for which ratios a/ℓ our Talbot basis states are still

sufficiently orthogonal we present in Fig. V.2 a plot of their mean orthogonality, which is defined as $2 \sum_{j>j'} |\langle j_d | j'_d \rangle|^2 / d(d-1)$, between all the states of the computational basis, for a given dimension d , as a function of a/ℓ [Fariás et al., 2015]. Figure V.2 shows numerically that for small encoded qudits, namely $d \leq 5$, perfect orthogonality is achieved for $\frac{a}{\ell} \in \{0, \frac{1}{d}\}$. If we interpolate this rule to higher dimensions we find that the number of orthogonal states that one can encode is given by $d = \ell/a$.

Another limitation that one has to consider for a realistic experimental implementation is the finite initial extension of the transverse photon wave packet and the resulting illumination of only a finite number of slits in the grating. This issue was discussed already previously in Sec. III.4.1, where we presented the fidelity of an one element of the logical basis, *e.g.* $|0_d\rangle$, with respect to itself after multiples of the free-propagation distance $2z_T$ for different values of the initial envelope of the single photon wave packet σ and the corresponding number of illuminated slits l (see Fig. III.11). While the fidelity decays rapidly for small values of σ , it is well preserved for larger values of the number of illuminated slits, as also reported experimentally in [Case et al., 2009].

V.2.2 Logical operations

In [Fariás et al., 2015], it was shown that, on this logical qudit space, one can define a complete set of single mode operations that are realized in terms of two optical primitives: the near-field propagation of the optical field after the grating, namely the Talbot effect, and one additional optical element that allows to imprint a position dependent phase on the field, called spatial light modulator (SLM). Adding a single two-mode operation, implemented by a position dependent beam splitter, proposed in the same paper, allows us to complete the set of operations on the encoded qudit space for universal quantum computation. In the following we summarize these logical operations, following Ref. [Fariás et al., 2015].

V.2.2.1 The Talbot gate

The main advantage of processing quantum information encoded in perfectly periodic wave functions, as defined in Eq. (V.6), is that their free-propagation itself implements a specific classes of single qudit logical operations. The aim of this Section is to show what kind of transformations can be realized in this way depending on the specific choice of the propagation distance $z = (s + q/r)2z_T$. For this purpose, we introduce the gate $\hat{T}_{q/r}$ which represents the unitary transformation that can be associated to a given propagation distances q/r with respect to the length $2z_T$ (see also Eq. (V.3)):

$$\Psi(x, q/r) = \langle x | \hat{T}_{q/r} | j_d \rangle. \quad (\text{V.7})$$

In the following we will distinguish between the cases of even and odd dimensions d .

First, for even dimensions d , we consider the propagation distances $1/r$, where r is an integer. In particular, for propagation distances given by $r = 2d$ we find that, according to Eq. (V.4), the wave function of one of the m 'th qudit basis states is given by:

$$\Psi\left(x - \frac{m}{D}\ell, z = 1/(2d)\right) = \sum_{j=0}^{d-1} a_{2j} \psi_0\left(x - \frac{m+j}{d}\ell\right). \quad (\text{V.8})$$

with

$$a_{2j} = \frac{1}{\sqrt{d}} e^{-i\frac{\pi}{4}} e^{i\frac{\pi j^2}{d}}. \quad (\text{V.9})$$

Hence, the free-propagation transforms each state $|m_d\rangle$ of the Talbot computational basis (V.6) into an equally weighted superposition:

$$\hat{T}_{1/(2d)}|m_d\rangle = \sum_{j=0}^{d-1} a_{2j}|(j+m)_d\rangle, \quad (\text{V.10})$$

where we introduced the modulo d summation $(j+m)_d = (j+m) \bmod d$, with relative phase factors a_{2j} given by Eq. (V.9). In terms of the generalized Pauli operator $\hat{\sigma}_x^{(d)}$ (see Eq. (II.17)), the action of the *Talbot gate* $\hat{T}_{1/2d}$ can be expressed as follows:

$$\hat{T}_{1/(2d)}|m_d\rangle = \sum_{j=0}^{d-1} a_{2j}(\hat{\sigma}_x^{(d)})^j|m_d\rangle. \quad (\text{V.11})$$

For odd dimensions d , we define the Talbot gate analogously for propagation distances $1/d$. In this case, the free-propagation transforms the Talbot basis states according to the operation

$$\hat{U}_{1/d} = \sum_{j=0}^{d-1} a_j(\hat{\sigma}_x^{(d)})^j. \quad (\text{V.12})$$

where

$$a_j = \frac{1}{\sqrt{d}} \left(\frac{2}{d}\right) e^{i\frac{\pi}{4}(j-1)} e^{i\frac{\pi(d+1)^2 j^2}{d}} \quad (\text{V.13})$$

with the Jacobi symbol $\left(\frac{a}{b}\right)$ defined for odd integers b , which, depending on the dimension, takes values ± 1 . Hence, as in the even case, the Talbot gate takes the computational basis states and transforms them into equally weighted superpositions with relative phases given by Eq. (V.13). Note, that for even and odd dimension the Talbot gate is associated to different propagation distances, $1/(2d)$ and $1/d$, respectively, and thus depends on the parity of the dimension of the system that is encoded into the periodic wave function (V.4). For a discussion of the mathematical properties of the gate $\hat{T}_{1/r}$ and its relation to the discrete Fourier transform we refer the reader to the publication [Farías et al., 2015].

V.2.2.2 Diagonal gates

Even though the free-propagation of the encoded Talbot qudit states implements a whole family of interesting single qudit operations, it is not sufficient to perform universal single qudit operations. To achieve the latter we introduce one additional operation that relies on the application of a spatial light modulator (see also the discussion at the end of Sec. II.3.1.1) and allows to implement a position dependent phase to the

transverse optical field:

$$\Psi(x) \longrightarrow e^{i\phi(x)}\Psi(x). \quad (\text{V.14})$$

This operation allows us to apply constant phases ϕ_j to the periodic regions on which the wave function of a computational basis state $|j_d\rangle$ is nonzero, and thus enables the realization of diagonal phase gates, defined as:

$$\hat{Z}_{\vec{\phi}} = \sum_{j=0}^{d-1} e^{i\phi_j} |j_d\rangle\langle j_d|, \quad (\text{V.15})$$

where $\vec{\phi} = (\phi_0, \dots, \phi_{D-1})$, which transform an arbitrary qudit state $|\Psi\rangle = \sum_{j=0}^{d-1} c_j |j_d\rangle$ as

$$|\Psi\rangle \longrightarrow \sum_{j=0}^{d-1} \lambda_d e^{i\phi_j} |j_d\rangle. \quad (\text{V.16})$$

The above defined diagonal phase gate $\hat{Z}_{\vec{\phi}}$, with a fixed phase vector $\vec{\phi}$, together with the previously defined Talbot gate $\hat{T}_{1/(2d)}$, generate all single qudit Clifford operations (see discussion about the Clifford group in Sec. II.1.1 and II.1.2). In particular, in [Fariás et al., 2015] it was shown how to implement the quantum Fourier transform. In order to make the above set of gates universal we need to supplement it with a non-Clifford gate which can be trivially realized using the diagonal gate $\hat{Z}_{\vec{\phi}}$ and an appropriate phase vector $\vec{\phi}'$ [Howard and Vala, 2012]

V.2.2.3 The Talbot qubit

In order to strengthen our intuition of the above introduced gates, we demonstrate their action in the simplest case, for $d = 2$. The Talbot gate $\hat{T}_{1/(2d)}$ reads in this case:

$$\hat{T}_{1/4} = \frac{e^{-i\frac{\pi}{4}}}{\sqrt{2}} (\mathbb{1} + i\hat{\sigma}_x) = e^{-i\frac{\pi}{4}} e^{i\frac{\pi}{4}\hat{\sigma}_x}, \quad (\text{V.17})$$

which leads to $\hat{T}_{1/2} = (\hat{T}_{1/4})^2 = \hat{\sigma}_x^{(d)}$. In combination with the diagonal phase gate $\hat{Z}_{\vec{\phi}}$ and the identity $e^{-i\frac{\pi}{2}} e^{i\frac{\pi}{4}\hat{\sigma}_x} e^{i\frac{\pi}{4}\hat{\sigma}_z} e^{i\frac{\pi}{4}\hat{\sigma}_x} = \hat{H}$ this leads us to the implementation of the Hadamard gate:

$$\hat{H} = \hat{T}_{1/4} \hat{Z}_{\pi/4} \hat{T}_{1/4}, \quad (\text{V.18})$$

where $\hat{Z}_{\pi/4} = e^{i\pi/4}|0_2\rangle\langle 0_2| + e^{-i\pi/4}|1_2\rangle\langle 1_2|$. Now, we can exploit the Hadamard gate to prepare arbitrary single qubit unitary operations, using the identity [Nielsen and Chuang, 2000]:

$$\hat{R}_z \left(\frac{\pi}{2} + \phi \right) \hat{H} \hat{R}_z(\theta) \hat{H} |0\rangle = \cos(\theta)|0\rangle + e^{i\phi} \sin(\theta)|1\rangle. \quad (\text{V.19})$$

where $\hat{R}_z(\theta)$ denotes a rotation around the z -axis of the Bloch sphere and thus simply a diagonal phase gate $\hat{Z}_\theta = e^{i\theta}|0_2\rangle\langle 0_2| + e^{-i\theta}|1_2\rangle\langle 1_2|$. In Fig. V.3, we illustrate the preparation of an arbitrary qubit state, according to Eq. (V.19), using only free-propagation and diagonal gates.

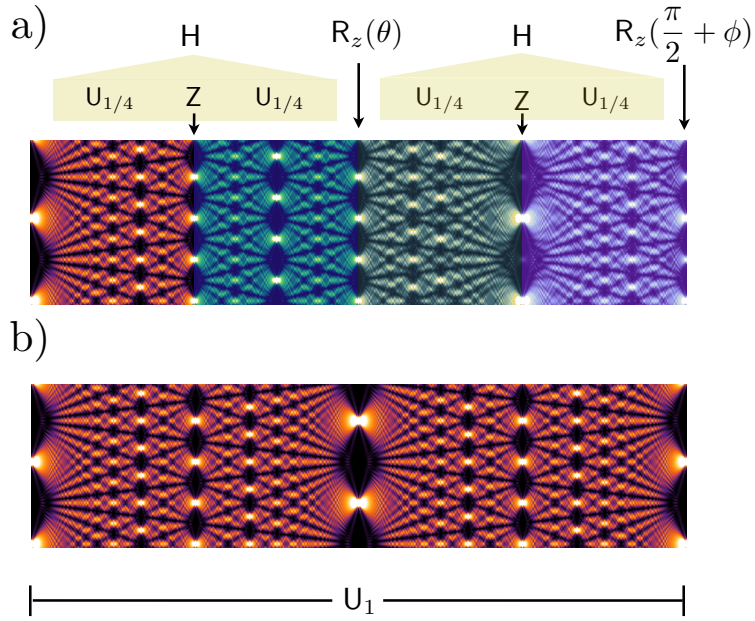


Figure V.3: This Figure, which was taken from [Farías et al., 2015], shows in (a) a circuit consisting of Hadamard gates and rotations around the z -axis that prepares an arbitrary single qubit states. The colors illustrate the application of a phase gate at the beginning of the corresponding region. This circuit requires a free-propagation of $2z_T$. For comparison, (b) shows the Talbot carpet for the same propagation distance $2z_T$ without the application of intermediate phase gates.

V.2.3 Spatially Dependent Beam Splitter

For completeness, we want to elaborate now on the possibility to render our Talbot quantum information processing framework universal using a novel optical beam splitter device introduced in [Farías et al., 2015]. This device will enable us to entangle probabilistically two individual Talbot qudits and thus can be used to define an appropriate two qudit gate. In comparison to the usual symmetric beam splitter (see Sec. II.3.2) with reflection and transmission coefficients t and r , we consider here a spatially-dependent beam splitter, denoted as SDBS, whose transmission and reflection coefficients depend on the coordinate x . We restrict ourselves to only one spatial dimension x leading to transmission and reflection coefficients $t(x)$ and $r(x)$, respectively, with $|t(x)|^2 + |r(x)|^2 = 1 \forall x$. The SDBS device can be applied to our Talbot qudits with piecewise constant coefficients t_d and r_d corresponding to each periodic region of the computational basis wave functions $\langle x|j_d\rangle$. For an illustration of such a spatially dependent beam-splitter see Fig. V.4. The SDBS transforms the Talbot qudit basis states as

$$|j_d\rangle_a \longrightarrow t_d|j_d\rangle_a + ir_d|j_d\rangle_b \quad (\text{V.20a})$$

$$|j_d\rangle_b \longrightarrow t_d|j_d\rangle_b + ir_d|j_d\rangle_a. \quad (\text{V.20b})$$

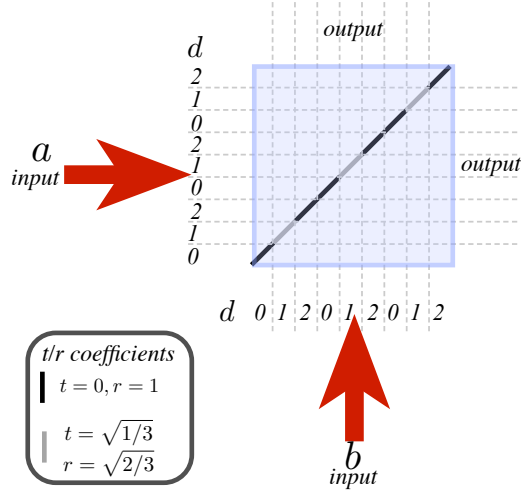


Figure V.4: Example of a spatially dependent beam splitter (SDBS) for spatial quDits. Shown is an example for $D = 3$. The colored regions represent parts of the beam splitter with different transmission coefficients t_d and reflection coefficients r_d . The Figure was taken from [Farías et al., 2015].

Further on, we show how one can perform a two-photon phase gate for spatial Talbot qudits via post-selection using SPBSs, as shown in Figure V.5. A two-photon interference on a first SDBS device with $t_k = 1/\sqrt{3}$, $r_k = \sqrt{2/3}$ for a fixed basis state k , and $t_d = 0$, $r_d = 1$ for all other values of $d \in \{0, \dots, k-1, k+1, \dots, D-1\}$, is followed by additional SDBSs with coefficients $t_k = 1$, $r_k = 0$ for fixed basis state k , and $t_d = 1/\sqrt{3}$, $r_d = \sqrt{2/3}$ for $d \in \{0, \dots, k-1, k+1, \dots, D-1\}$ in modes a and b , respectively. If we consider only events where one photon leaves the outputs of each of the final SDBSs, all different combinations of computational basis states result in one of the following:

$$|k_D\rangle_a |k_D\rangle_b \longrightarrow -\frac{1}{3} |k_D\rangle_a |k_D\rangle_b \longrightarrow -\frac{1}{3} |k_D\rangle_a |k_D\rangle_b, \quad (\text{V.21})$$

$$|k_D\rangle_a |d_D\rangle_b \longrightarrow \frac{1}{\sqrt{3}} |k_D\rangle_a |d_D\rangle_b \longrightarrow \frac{1}{3} |k_D\rangle_a |d_D\rangle_b, \quad (\text{V.22})$$

$$|d_D\rangle_a |k_D\rangle_b \longrightarrow \frac{1}{\sqrt{3}} |d_D\rangle_a |k_D\rangle_b \longrightarrow \frac{1}{3} |d_D\rangle_a |k_D\rangle_b, \quad (\text{V.23})$$

$$|d_D\rangle_a |d_D\rangle_b \longrightarrow |d_D\rangle_a |d_D\rangle_b \longrightarrow \frac{1}{3} |d_D\rangle_a |d_D\rangle_b, \quad (\text{V.24})$$

with the input state in the first column, the state after the two-photon interference at the first SDBS in the second column and the state after the last two SDBS in the third column. This transformation results in a π phase shift if the two photons are in state k , and no phase shift for all other possibilities. For $d = 2$, we thus find the controlled-phase gate, \hat{C}_Z (see Sec. II.1.1). Due to the post-selection of the photons this gate has a success probability of $1/9$ and is thus not very efficient. A discussion how the above gate could be applied for a scalable implementation can be found in [Farías et al., 2015].

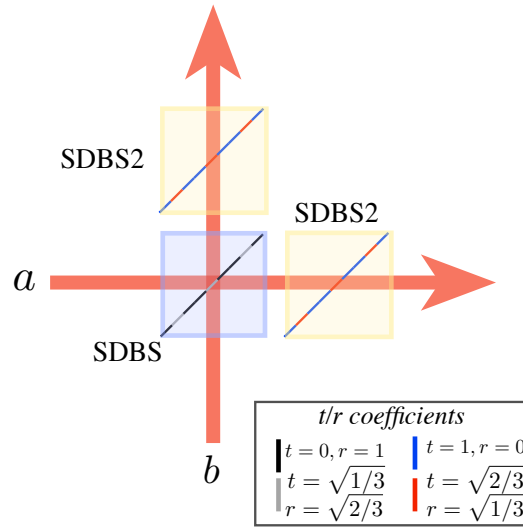


Figure V.5: Realization of a controlled gate between Talbot Qudits. SDBSs are spatially dependent beam splitters with different transmission and reflection coefficients. The Figure was taken from [Fariás et al., 2015].

In the next Section we will introduce a novel scheme to create deterministically d -dimensional entangled Talbot photon pairs from spontaneous parametric down-conversion and linear optical elements only.

V.3 Creation of entangled Talbot carpets

In this Section we introduce a method which enables us to create deterministically D -dimensional entangled Talbot states, such as

$$|\text{ET}_d\rangle = \frac{1}{\sqrt{D}} \sum_{d=0}^{D-1} |d_D\rangle |d_D\rangle. \quad (\text{V.25})$$

from spontaneous parametric down-conversion in combination with linear optical operations. The latter have been both discussed independently in Sec. II.3.1.1 and II.3.1.3, respectively. At the heart of our method presented in the following is a scheme that allow us to produce arbitrary single mode Talbot qudits. We will introduce this scheme first and show later on how it can be used to produced entangled Talbot qudits (V.25).

V.3.1 Talbot carpet synthesizer

Now we will present a device that converts a monochromatic single-photon field into an arbitrary superposition of Talbot basis states (V.6). The scheme is illustrated in Fig. V.6. An almost plane wave is incident on a d -slit Young aperture with slit width a and distance s . Assuming that the incident wave function $\mathcal{E}_{in}(x)$ is approximately

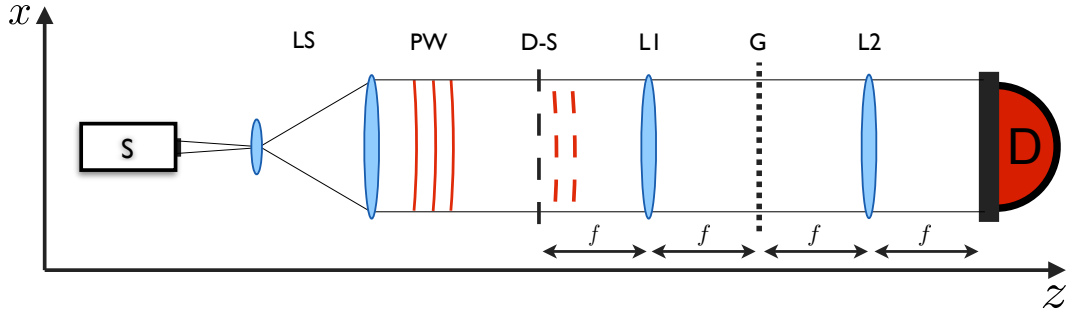


Figure V.6: Schematic representation of the proposed scheme to produce arbitrary Talbot states. A lens system (LS) prepares a nearly plane wave (PW) which is incident on a D -slit aperture (D-S) creating the state $\psi_D(x)$, followed by the transformation shown in Eq. (V.27). Lenses (L1,L2) of focal length f implement two Fourier transforms and the grating (G) is placed in the Fourier plane in between (L1) and (L2). (D) denotes the detector.

constant over each slit, directly after the aperture the outgoing wave function is given by

$$S_d(x) = \sum_{j=0}^{d-1} c_j S(x - js), \quad (\text{V.26})$$

where $S(x)$ defines the transmission profile of each of the identical slits, and the complex amplitudes are given by $c_j \propto \mathcal{E}_{in}(ds)$ and $\sum_{j=0}^{d-1} |c_j|^2 = 1$. The state (V.26) is an arbitrary superposition state of the D states describing the passage through each one of the d slits. In principle, one can control the amplitudes c_d by controlling the amplitude and phase of the input field before the slit aperture. In order to transform Eq. (V.26) into a D -dimensional Talbot state, we apply a lens (L1) to implement a Fourier transform, and place a grating G at the Fourier plane of the lens. A second lens (L2) performs a second Fourier transform. For simplicity we assume that each lens has focal length f . The wave function of the state resulting from this transformation is given by:

$$\psi_{out}(x) = \mathcal{F}\{G(x) \cdot \mathcal{F}\{S_d(x)\}\} = (\mathcal{F}\{G\} * S_d)(x), \quad (\text{V.27})$$

where \mathcal{F} is the Fourier transform and $*$ denotes the convolution. In the second equality in Eq. (V.27) we used the convolution theorem for Fourier transforms. We see that the output field at the Fourier plane of lens L2 is the convolution of the Fourier transform of the grating G with the original d -slit state S_d . Writing the grating transmission function as $G(x) = \sum_m A_m e^{2\pi i m x / \ell_g}$, the Fourier transform of $G(x)$ is given by

$$\mathcal{F}\{G\}(x') = \sum_{m=-\infty}^{+\infty} A_m \delta\left(\frac{m}{\ell_g} - \frac{x'}{f\lambda}\right). \quad (\text{V.28})$$

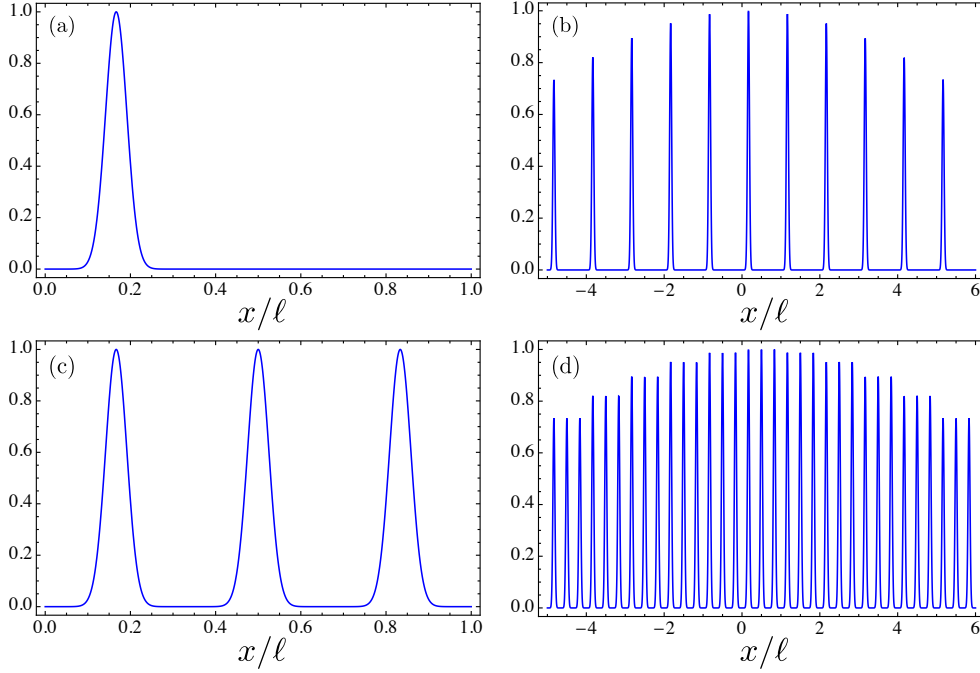


Figure V.7: Plots of the wave function $\psi_{d=3}(x)$ (left column) and its transformed version $\tilde{\psi}_{d=3}(x)$ (right column), with a Gaussian slit transmission profile $S(x)$ with width $\Delta = 0.025s$, a Gaussian grating transmission function $G(x)$ with width $\kappa = 0.025s$ and slit distance $\ell_g = s$. Shown are two examples: amplitudes $c_0 = 1$, $c_1 = 0$, $c_2 = 0$ in (a,b) and $c_j = 1/\sqrt{d}$ in (c,d).

Using equations (V.26) and (V.28) in (V.27), we have

$$\psi_{out}(x) = \sum_{j=0}^{d-1} c_j T_j(x), \quad (\text{V.29})$$

where

$$T_j(x) = \sum_{m=-\infty}^{m=+\infty} A_m S\left(x - js - \frac{mf\lambda}{\ell_g}\right) \quad (\text{V.30})$$

describes the transmission function of an *effective grating* consisting of an infinite periodic comb of slit functions S , each centered at $ds - mf\lambda/\ell_g$. The period of the effective grating is $\ell = mf\lambda/\ell_g$. The function $T_j(x)$ can then be chosen as the wave function of the Talbot basis states: $T_j(x) = \langle x|j_d\rangle$. The state at the output plane (V.29) is thus an arbitrary superposition of Talbot states, controlled by the amplitudes c_j .

As example, we treat the case where the transmission profile $S(x)$ of the slits in the d -slits aperture is Gaussian function with width Δ , and the grating transmission function is given by a Gaussian comb with Fourier coefficients $A_m = e^{-(2\pi m\sigma)^2/(2\ell_g^2)}$, where σ is the width of the Gaussian spikes and ℓ_g the distance between them. In Fig. V.7, we plot examples of the wave functions $S(x)$ and $\tilde{\psi}_d(x)$ for this case with $d = 3$. We chose Gaussian functions for computational simplicity, however any function can be used.

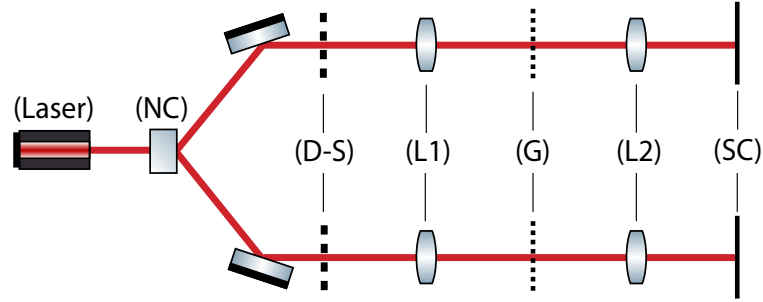


Figure V.8: Experimental proposal: A laser is incident on a non-linear crystal (NC) producing two down-converted photons in the state $|\psi\rangle_{12}$ and subsequently pass through individual D -slits apertures (D-S) creating the state $|\psi\rangle_{12,g}$. The following elements implement on each photon the same transformation as in Fig. V.6. (SC) denotes the detection screen.

V.3.2 Entangled Talbot qudits

We now turn to the question of how to produce a D -dimensional entangled Talbot state from spontaneous parametric down-conversion. The corresponding experimental scheme for this task is depicted in Fig. V.8. The basic idea is to use the Talbot state synthesizer from last section, one for each photon, and engineer the spatial correlations to control the entanglement in the Talbot basis. We start by recalling that the transverse state of two photons produced in SPDC can be expressed as follows [Walborn et al., 2010]:

$$|\psi\rangle_{12} = \iint dx_1 dx_2 \psi_{12}(x_1, x_2) |x_1\rangle |x_2\rangle, \quad (\text{V.31})$$

where

$$\psi_{12}(x_1, x_2) = \vartheta(x_1 + x_2) \gamma(x_1 - x_2), \quad (\text{V.32})$$

is the transverse wave function of the twin photons and $|x_1\rangle |x_2\rangle$ a two mode Fock state describing a single transverse mode of each photon (see also Sec. II.3.1.3). The functions $\vartheta(x_1 + x_2)$ and $\gamma(x_1 - x_2)$ are determined by the pump field profile and the phase matching function of the down-conversion process, respectively. In typical down-conversion experiments, one can employ the *double gaussian approximation* [Walborn et al., 2010] in which both ϑ and γ are described by Gaussian functions with widths κ_1 and κ_2 , respectively. The ratio $R = \kappa_1/\kappa_2$ describes the amount of spatial entanglement between the photons. Plots of the wave function (III.134) are presented in Fig. V.9 for different values of R . As shown in the Fig. V.8, we send the down-converted photons through the same optical elements as in Fig. V.6. First, after the identical D -slit apertures the wave function (III.134) becomes:

$$\psi_{12}^{(d)}(x_1, x_2) = S_d(x_1) S_d(x_2) \vartheta(x_1 + x_2) \gamma(x_1 - x_2), \quad (\text{V.33})$$

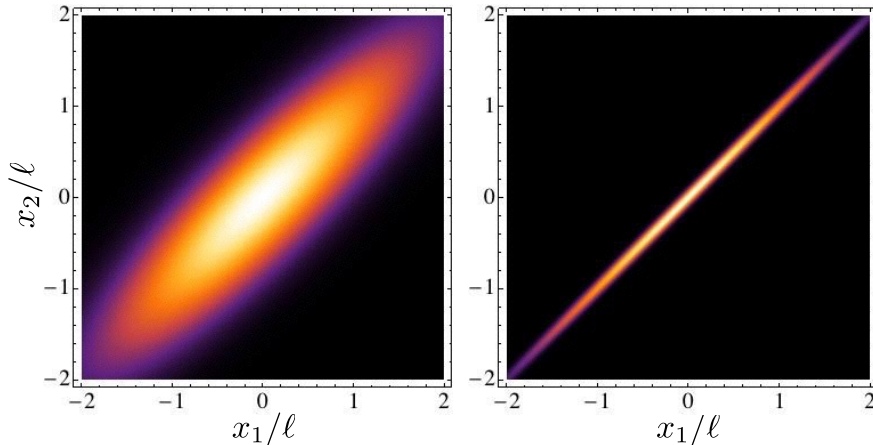


Figure V.9: (color online) Density plots of the wave function $\psi_{12}(x_1, x_2)$ with $\vartheta(x)$ and $\gamma(x)$ chosen as Gaussians with widths $\kappa_1 = 2\ell$ and $\kappa_2 = 1/2\ell$ (left), $1/18\ell$ (right). The fact that the two plotted probability densities are reduced with respect to the variable $x_1 - x_2$, as compared to the variable $x_1 + x_2$, clearly shows that the transverse position of photons are correlated (see also the discussion in Sec. II.3.1.3).

where S_d is the transmission functions of the d -slit apertures given in Eq. (V.26). It is well known that under proper conditions the two-photon wave function (V.33) describes entangled *Young qudits* [Neves et al., 2005; Carvalho et al., 2012]. In particular, when the ratio R is sufficiently large, the photons can be made to always pass through the same slit. To illustrate this, plots of the wave function (V.33) with $S(x)$ given by a Gaussian, are presented in Fig. V.10 for different amounts of spatial entanglement R .

After the d -slits we apply to both photons the same sequence of operations: a Fourier transform, a grating operation and another Fourier transform (see Eq. (V.27)), giving:

$$\Psi(x_1, x_2) = [\mathcal{F}\{G\}(x_1)\mathcal{F}\{G\}(x_2)] * \psi_{12}^{(d)}(x_1, x_2). \quad (\text{V.34})$$

Using Eqs. (V.28) and (V.33), we arrive at

$$\begin{aligned} \Psi(x_1, x_2) &= \sum_{j_1, j_2} \sum_{m_1=-\infty}^{\infty} \sum_{m_2=-\infty}^{\infty} A_{1, m_1} A_{2, m_2} \psi_{12} \left(x_1 - \frac{m_1 f \lambda}{\ell_g}, x_2 - \frac{m_2 f \lambda}{\ell_g} \right) \\ &\times S \left(x_1 - \frac{m_1 f \lambda}{\ell_g} - j_1 s \right) S \left(x_2 - \frac{m_2 f \lambda}{\ell_g} - j_2 s \right). \end{aligned} \quad (\text{V.35})$$

If the width a of the slit functions S is small compared to κ_{\pm} , we can approximate

$$\psi_{12} \left(x_1 - \frac{m_1 f \lambda}{\ell_g}, x_2 - \frac{m_2 f \lambda}{\ell_g} \right) \approx \vartheta(j_1 s + j_2 s) \gamma(j_1 s - j_2 s). \quad (\text{V.36})$$

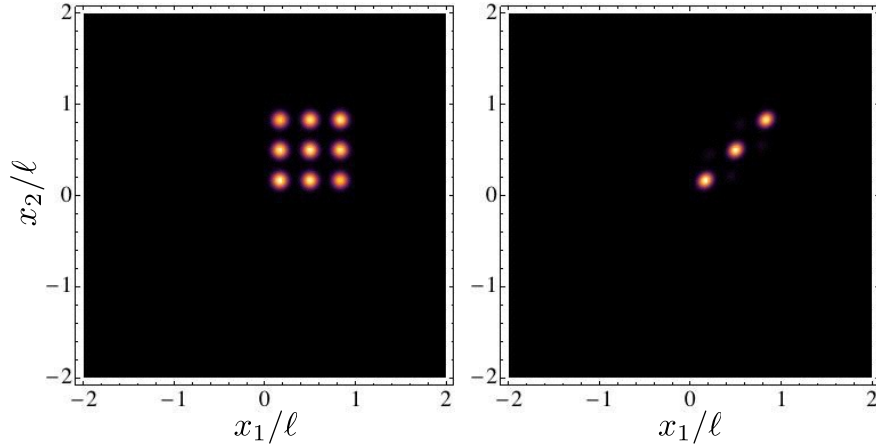


Figure V.10: (color online) Density plots of the wave function $\psi_{12}^{(d)}(x_1, x_2)$ with $\kappa_1 = 2\ell$ and $\kappa_2 = 1/2\ell$ (left), $1/18\ell$ (right) and a Gaussian transmission profile $\psi_0(x)$ with width $\delta = 0.05\ell$ for $d = 3$.

Using Eq. (V.30) we can rewrite this equation as

$$\Psi(x_1, x_2) = \sum_{j_1, j_2} C_{j_1, j_2} T_{j_1}(x_1) T_{j_2}(x_2) \quad (\text{V.37})$$

where

$$\begin{aligned} C_{j_1, j_2} &= \vartheta(j_1 s + j_2 s) \gamma(j_1 s - j_2 s) \\ &= A \exp\left(-\frac{s^2}{4\Delta_+^2} \left(j_1^2 + \frac{2\Delta_+^2}{\Delta_-^2} j_1 j_2 + j_2^2\right)\right), \end{aligned} \quad (\text{V.38})$$

and A is a normalization factor, such that $\sum_{j_1, j_2} |C_{j_1, j_2}|^2 = 1$. Here $1/\Delta_{\pm}^2 = 1/\kappa_{\pm}^2 \pm 1/\kappa_{\mp}^2$.

The final state (V.37) is a superposition of effective grating states for photons 1 and 2. The entanglement depends explicitly on the coefficients C_{d_1, d_2} . In the coefficient of the cross term Δ_+^2/Δ_-^2 in (V.38) we identify the spatial correlation coefficient of the photon pair defined above: $\Delta_+^2/\Delta_-^2 = -R$. When the spatial correlation is large so that $\kappa_- \ll \kappa_+$ and $R \approx 1$, we have $C_{d_1, d_2} \approx \exp[-s^2(d_1 - d_2)^2/4\Delta_+^2]$. To ensure a large amount of entanglement in the $D \times D$ dimensional two photon Talbot state requires $s^2/4\Delta_+^2 \gg 1$, resulting in $\kappa_-^2 \ll s^2$. In other words, to produce entangled Talbot states we need a transverse correlation length at the spontaneous parametric down-conversion source that is smaller than the distance between slits in the D -slit apparatus.

As example, we plot the wave function $\Psi(x_1, x_2)$ in the case of a $D = 2$ and $D = 3$ slit apertures in Fig. V.11 using the same Gaussian slit profile and grating transmission functions as in previous examples.

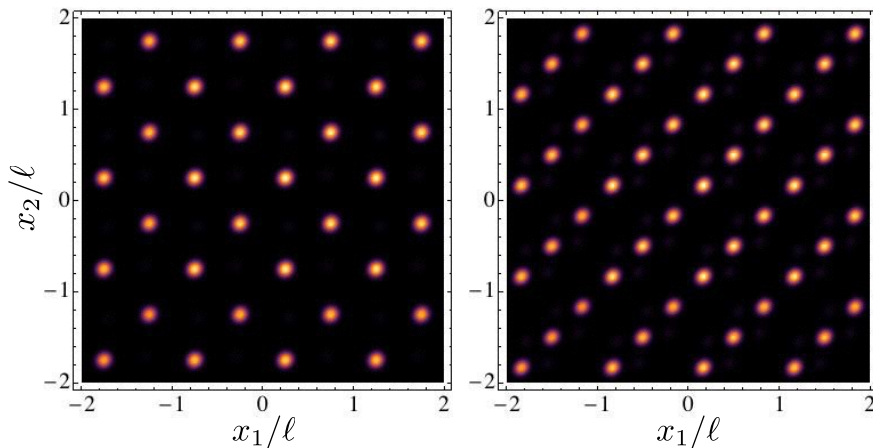


Figure V.11: (color online) Density plots of the wave function $\Psi(x_1, x_2)$ with $\kappa_1 = 2\ell$, $\kappa_2 = 1/18\ell$, a Gaussian transmission profile $\psi_0(x)$ with width $\delta = 0.05\ell$ and a Gaussian grating transmission function with slit width $\sigma = 0.05\ell$ and distance $\ell_g = \ell$ for $d = 2$ (left) and $d = 3$ (right). Note that the photons are correlated with respect to the definition of the logical Talbot states. This is in contrast to Fig. V.9, where the photons are correlated with respect to the position x_1 and x_2 .

V.4 Nonlocality test with entangled Talbot carpets

The possibility to produce deterministically d -dimensional entangled Talbot states makes our Talbot quantum information processing framework an interesting alternative to other schemes that encode discrete information into the transverse degrees of freedom of single photons, *e.g.* using the orbital angular momentum. In order to further underline the usefulness of our framework we will show in the following Section how to violate d -dimensional Bell inequalities with entangled Talbot states. We will first focus on the pedagogically valuable case of the CHSH inequality (see Eq. (IV.44)) and then turn to Bell inequalities that rely on measurements with more than two outcomes.

V.4.1 CHSH scenario

First, we focus on the well-known CHSH inequality (see Eq. IV.44) that involves only measurements of observables with binary outcomes ($d = 2$). We consider a bipartite system consisting of subsystems that are referred to Alice and Bob who each carry out two possible measurements, A_1, A_2 and B_1, B_2 , respectively. The CHSH inequality was discussed in detail in Sec. IV.2 and, for convenience, we reproduce its expression here:

$$|\langle A_1 B_1 \rangle + \langle A_1 B_2 \rangle + \langle A_2 B_1 \rangle - \langle A_2 B_2 \rangle| \leq 2. \quad (\text{V.39})$$

For each measurement setting $i = 1, 2$ and $j = 1, 2$, the correlation function $\langle A_i B_j \rangle = \sum_{a,b=\pm 1} ab p(a, b|i, j)$, between outcomes a and b of measurements A_i and B_j , respectively, is determined by the corresponding joint-probability distribution $p(a, b|i, j)$.

In a quantum mechanical description of the above measurement scenario the sets of observables A_i and B_j become hermitian operators \hat{A}_i and \hat{B}_j , and the joint probability

distributions $p(a, b|i, j)$ are equal to expectation values of some measurement operators $\hat{\Pi}_{a|i}$ and $\hat{\Pi}_{b|j}$, according to

$$p(a, b|i, j) = \text{tr}[\hat{\Pi}_{a|i} \otimes \hat{\Pi}_{b|j} \hat{\rho}]. \quad (\text{V.40})$$

with the bipartite quantum state $\rho \in \mathcal{H}_1 \otimes \mathcal{H}_2$ living in the tensor product space of two Hilbert spaces with dimension $d = 2$. As discussed in Sec. IV.2.1, a maximum value violation $2\sqrt{2}$ of Eq. (V.39) can be obtained with a maximally entangled state $|\phi_+\rangle = \frac{1}{\sqrt{2}}(|00\rangle + |11\rangle)$ if Alice choses to measure the observables $\hat{A}_1 = \hat{X}$ and $\hat{A}_2 \hat{Z}$, while Bob measures $\hat{B}_1 = (\hat{X} + \hat{Z})/\sqrt{2}$ and $\hat{B}_2 = (\hat{X} - \hat{Z})/\sqrt{2}$.

For what will come after it is convenient to assume that both Alice and Bob perform their measurements in the computational basis $\{|0\rangle, |1\rangle\}$, and different measurement setting are chosen in terms of appropriate unitary transformations \hat{U}_{A_i} and \hat{U}_{B_j} that map the eigenbasis of the corresponding observables \hat{A}_i and \hat{B}_j onto the computational basis. In particular, in order to achieve a maximal violation of the CHSH inequality with the above Bell state $|\phi_+\rangle$, Alice needs to apply the unitary transformations $\hat{U}_{A_1} = \hat{R}_y(\pi/2)$ and $\hat{U}_{A_2} = \mathbb{1}$, before the measurement in the computational basis (see Eq. (II.8) for the definition of the single qubit rotation operator $\hat{R}_y(\pi/2)$). On Bob's side, the corresponding unitaries read: $\hat{U}_{B_1} = \hat{R}_y(\pi/4)$ and $\hat{U}_{B_2} = \hat{R}_y(3\pi/4)$.

After some algebraic manipulations one finds that all of Alice's and Bob's measurement settings can be realized by the composition of two basic gates, introduced in Sec. V.2.2:

$$\hat{U}_\gamma = \hat{T}_{1/4} \hat{Z}_\gamma \hat{T}_{1/4} = \begin{pmatrix} \sin(\gamma) & \cos(\gamma) \\ \cos(\gamma) & -\sin(\gamma) \end{pmatrix}, \quad (\text{V.41})$$

the qubit Talbot gate $\hat{T}_{1/4} = e^{-i\pi/4}(\mathbb{1} + i\hat{\sigma}_x)/\sqrt{2}$ (see Eq. (V.11) and (V.17)) and the diagonal phase gate $\hat{Z}_\gamma = e^{i\gamma}|0\rangle\langle 0| + e^{-i\gamma}|1\rangle\langle 1|$ (see Eq. (V.15)). The respective parameters in Eq. (V.41) are $\gamma = \pi/4$ on Alice's side and $\gamma = -5\pi/8$ and $\gamma = \pi/8$ on Bob's side.

Hence, using the free-propagation of single photons plus one spatial light modulator and position measurements of the spatial photon distribution, we can violate the CHSH inequality (V.39) with an entangled Talbot state $|\text{ET}_2\rangle$ (see Sec. V.3).

V.4.2 Measurements with more outcomes

A generalization of the CHSH inequality for measurements with arbitrary many finite outcomes was developed by Collins *et al.* in [Collins et al., 2002]. Assume that Alice and Bob carry out two possible measurements A_1 or A_2 and B_1 or B_2 , respectively, which can have d possible outcomes: $0, \dots, d-1$. Further on, in a local realistic theory, one can show that the following inequality holds

$$I_D = \sum_{k=0}^{[d/2]-1} \left(1 - \frac{2k}{d-1}\right) J_k \leq 2, \quad (\text{V.42})$$

where

$$\begin{aligned}
J_k = & P(A_1 = B_1 + k) - P(A_1 = B_1 - k - 1) \\
& + P(B_2 = A_1 + k) - P(B_2 = A_1 - k - 1) \\
& + P(B_1 = A_2 + k + 1) - P(B_1 = A_2 - k) \\
& + P(A_2 = B_2 + k) - P(A_2 = B_2 - k - 1),
\end{aligned} \tag{V.43}$$

and

$$P(a = b + k) = \sum_{j=0}^{d-1} P(a = j, b = j + k \bmod d), \tag{V.44}$$

yield the joint-probabilities that the outcomes a and b , of $A_{1/2}$ and $B_{1/2}$, differ by $k \bmod d$. For $d = 2$, Eq. (V.42) recovers the CHSH inequality (V.39).

Maximal violation of the inequality (V.42) is reached for maximally entangled qudit states of the form

$$|\phi_d\rangle = \frac{1}{\sqrt{d}} \sum_{j=0}^{d-1} |j_d\rangle |j_d\rangle, \tag{V.45}$$

and projective measurements by Alice and Bob in the bases [Collins et al., 2002]:

$$|f_\alpha\rangle = \frac{1}{\sqrt{d}} \sum_{j=0}^{d-1} e^{2\pi i j(f+\alpha)/d} |j_d\rangle, \tag{V.46}$$

$$|f'_\beta\rangle = \frac{1}{\sqrt{d}} \sum_{j=0}^{d-1} e^{2\pi i j(-f'+\beta)/d} |j_d\rangle, \tag{V.47}$$

where $f, f' = 0, \dots, d-1$, and with $\alpha_1 = 0$, $\alpha_2 = 1/2$, $\beta_1 = 1/4$ and $\beta_2 = -1/4$, respectively. Interestingly, the inequalities (V.42) provide an increase in the quantum mechanical violation with increasing of d . The maximal violation according to the state (V.45) and the measurements in the bases (V.46) and (V.47) reads:

$$I_d^{(\text{QM})} = 4d \sum_{k=0}^{\lfloor d/2 \rfloor - 1} \left(1 - \frac{2k}{d-1}\right) (q_k - q_{-(k+1)}) \tag{V.48}$$

where $q_c = 1/(2d^3 \sin^2(\pi(c+1/4)/d))$. Hence, for $d = 2$ we obtain the Tsirelson bound $I_2^{(\text{QM})} = 2\sqrt{2}$, and, for $d \rightarrow \infty$ the quantum mechanical bound of Eq. (V.42) yields $I_\infty^{(\text{QM})} \approx 2.96981$ [Collins et al., 2002].

As in the CHSH case we assume that Alice and Bob are able to measure in the computational basis $\{|j_d\rangle | j = 0, \dots, d-1\}$, and different measurement settings, according to the bases (V.46) and (V.47), are chosen in terms of appropriate unitary transformations \hat{U}_A and \hat{U}_B before the measurement. These unitaries have to map the corresponding

measurement bases onto the computational basis, according to:

$$\hat{U}_A |f_\alpha\rangle = e^{if(f)} |j_d\rangle \quad (\text{V.49})$$

$$\hat{U}_B |f'_\beta\rangle = e^{ig(f')} |j_d\rangle, \quad (\text{V.50})$$

where $f(k)$ and $g(l)$ define arbitrary phases. It is easy to see that the unitary operations which perform these mappings are given by:

$$\hat{U}_A = |j_d\rangle \langle f_\alpha| = \frac{1}{\sqrt{d}} \sum_{j'=0}^{d-1} e^{-\frac{2\pi i j'(f+\alpha)}{d}} |j_d\rangle \langle j'_d| \quad (\text{V.51})$$

$$\hat{U}_B = |j_d\rangle \langle f'_\beta| = \frac{1}{\sqrt{d}} \sum_{j'=0}^{d-1} e^{\frac{2\pi i j'(f'-\beta)}{d}} |j_d\rangle \langle j'_d|. \quad (\text{V.52})$$

To achieve these operators with the Talbot effect a combination of Talbot gates and general phase gates can be used (see Eq. (V.11) and (V.15)). Let us define the diagonal operation through

$$\theta_j = \frac{\pi}{4} - \frac{2\pi\gamma j}{d} - \frac{\pi j^2}{d}, \quad (\text{V.53})$$

where $\gamma = \alpha, \beta$. Considering $\hat{U}_A = T_{1/(2d)} Z_\theta$, where one can show that

$$\hat{T}_{1/(2d)} Z_\theta = \sum_{j=0}^{d-1} e^{-i\pi d^2/D} |j_d\rangle \langle j_\gamma|, \quad (\text{V.54})$$

which is the required form for the operators \hat{U}_A, \hat{U}_B . Thus, through application of the phase gate and the Talbot gate, it is possible to project the bases (V.46) and (V.47) into the computational basis, allowing to test the d -dimensional Bell inequalities (V.42) in terms of the the Talbot effect.

In the next Section we will discuss as perspective the implementation of the above discussed Bell experiment using material particles and matter waves.

V.4.3 Perspectives: Bell test with material particles and matter waves

The observation of interference effects with material particles is one of the clearest demonstrations of the wave-like behaviour of matter in quantum mechanics. In a Young's D -slit experiment interference can be revealed if the width a of the slits in the D -slit aperture and the de Broglie wavelength $\lambda_B = h/(mv)$, where m is the mass and v the velocity of the particles, are of the same order of magnitude. Consequently, an observation of the Talbot effect with matter waves in the near-field after a D -slits aperture is not only possible, but in the last few decades scientists have been successfully observing matter wave interference effects with atoms and molecules with increasingly big masses [Arndt et al., 2014]. In this Section, we discuss briefly the possibility of performing a Bell inequality test with entangled material particles using the Talbot effect.

First, we need to create a spatially entangled pair material particles in an EPR state, which then can be used as starting point for implementing the scheme introduced in Sec.

V.3. However, while the wave-like behavior of atoms and large molecules is routinely observed in state-of-the-art experiments, the creation of entanglement between such material particles is rather difficult. Here, we comment on two experimental proposals that allow for the creation of pairs of entangled atoms originating from Bose-Einstein condensates (BECs). The first one is based on a four-wave mixing process of two colliding BECs induced by a stimulated Raman transitions. If the collision strength is sufficiently weak, the production of entangled EPR pairs of metastable helium atoms becomes feasible [Perrin et al., 2007; Kofler et al., 2012; Bonneau et al., 2013]. The second proposal is based on controlled molecular Feshbach dissociation of molecules in a dilute BEC by applying weak dissociation pulses [Kheruntsyan et al., 2005; Kheruntsyan, 2006; Köhler et al., 2006]. In both proposals the atoms can be further processed while falling in free space.

Once a spatially entangled EPR pair of two atoms has been produced, the entanglement creation scheme in Sec. V.3 can be applied in order to transform the EPR state into an entangled Talbot state. Thus, we need to find analogs of the optical elements used to implement the D -slits, the gratings and the Fourier transform. D -slits and gratings with an appropriate slit width and distance can be implemented using either nano-fabricated material gratings, or optical phase gratings which themselves are realized by laser fields [Arndt et al., 2014]. Furthermore, free propagating particles will independently undergo a Fourier transform via propagation from the near-field to the far-field region after the respective optical elements.

At this stage we have in hand an entangled Talbot state of material particles that can in principle be used to perform a test of the Bell inequalities discussed in Sec. V.4. Thereby, the most challenging part will be to implement the phase gate (V.11) with propagating atoms. One possibility might be to manipulate the matter wave with light pulses that themselves are controlled via a SLM in a similar manner as discussed in [Carrat et al., 2014].

V.5 Discussion

This Chapter was specifically devoted to the development of means that allow to process discrete d -dimensional quantum information encoded in the transverse degrees of freedom of single photons via the optical Talbot effect. While many aspects of the developments in this Chapter seemed conceptually similar to the more general considerations made in Chapter III, here, our main concern was to focus on a very specific experimental platform. We found that single mode encoded qudit states can be processed using solely the free-propagation of the single photons in combination with one additional linear optical element, a spatial light modulator. Entanglement operations can be either performed probabilistically using a novel spatially dependent beam-splitter device or by, by employing spontaneous parametric down-conversion in combination with linear optical operations. The latter allowed us to show, for the first time, how to prepare deterministically d -dimensional spatially entangled photons pairs without the need of post-selection. Finally, we showed how to violate d -dimensional Bell inequalities using the produced states and outline a possible macroscopic Bell test in terms of entangled material particles.

VI Nonlocality of hybrid entangled states

The following Chapter is devoted to an investigation of the nonlocal properties of hybrid entangled states between particle-like single photon Fock states and wave-like optical coherent states. Both of the latter classes of states allow to encode discrete quantum states by exploiting their even and odd parity subspaces, but have completely different properties what concerns state preparation, manipulation and detection. Hybrid entangled states offer the possibility to combine these two strategies and thus might lead to protocols that profit from the advantages of both, particle- and wave-like optical qubits. In this respect, we develop a hybrid scheme to test the CHSH inequality with discrete- and continuous-variable measurements enabling the demonstration of the nonlocal properties of the considered hybrid entanglement. Finally, accounting for realistic experimental losses allows us to assess the feasibility of an experimental demonstration of hybrid nonlocality in quantum optics experiments. Our elaborations are strongly motivated by the recent experimental demonstration of such hybrid entanglement in the group of J. Laurat at Laboratoire Kastler Brossel in Paris. Many of the subsequent elaborations and calculations were inspired and performed in close collaboration with experimentalists from this group.

VI.1 Hybrid entanglement

As mentioned in Chapter I the term hybrid systems refers to many different experimental contexts. In this Section we are particularly interested in the study of hybrid entangled states of the electromagnetic field. To introduce the reader to this concept we will first discuss the class of hybrid entangled states we are dealing with in the following and show how they can be produced in a quantum optics experiment. Afterwards we will turn to the question of how to test such states for nonlocal correlations.

VI.1.1 Hybrid entanglement between particle- and wave-like states

Processing quantum information in continuous variables often relies on a specific encoding allowing to define logical subspaces corresponding to the eigenspaces of some dichotomic observable. One way of doing so was discussed in Chapter III, where we dichotomized the Hilbert space with respect to the modular position. Here, we want to focus on another dichotomic observable enabling the definition of discrete logical states: the photon-number parity $\hat{P} = (-1)^{\hat{n}}$, where \hat{n} is the photon number operator (see also Sec. IV.3.4). The parity operator thus has two eigenvalues ± 1 and its eigenstates fulfill the relation $\hat{P}|\text{even,odd}\rangle = \pm|\text{even,odd}\rangle$. It is this even and odd parity subspaces that we will use in the following to encode information.

One of the most famous parity encodings is the one that exploits the presence and the absence of single photons in order to encode logical qubits. This scheme attracted much attention because it is at the heart of the first demonstration that efficient universal quantum computation, using only linear optical operations and single photon sources, is possible [Knill et al., 2001; Kok et al., 2007].

An alternative encoding involves using even and odd cat states to define logical qubits. Cat states are superposition of coherent states with opposite phases, *e.g.* $|\text{cat}^\pm\rangle \propto |\alpha\rangle \pm |-\alpha\rangle$, referred to as even or odd depending on their relative phase. It is easy to see that the cat states $|\text{cat}^\pm\rangle$ also belong to the even and odd parity subspaces, respectively. Such types of cat state encodings, as well as the related coherent state encoding $|\pm\alpha\rangle$, have attracted considerable attention during the last decade leading to proposals for realizing universal quantum computation [Jeong and Kim, 2002; Ralph et al., 2003; Lund et al., 2008; Albert et al., 2016], but also quantum communication protocols can profit from such wave-like optical qubits [Sangouard et al., 2010; Brask et al., 2010].

The two aforementioned parity encodings have very different properties in what concerns state manipulations and measurements. The cat state encoding usually benefits from the experimental toolbox used to process continuous quadrature amplitudes of electromagnetic fields. This includes, for instance, the deterministic state production through nonlinear processes, their manipulation via linear optical elements and the efficient measurement via homodyne detection (see Sec. II.3.2). However, such states usually suffer from decoherence effects, such as photon loss and dephasing. Moreover, due to technical reasons continuous-variable states can never be produced with unit fidelity leading to intrinsic inaccuracies. The same toolbox is principally also available for the processing of qubits encoded in single photon states, though supplemented with the additional complication that many operations can only be realized probabilistically. Furthermore, the efficiency of single-photon detections, which for this encoding are sometimes more desirable, is usually not as high as that of homodyne detections (see Sec. II.3.2.3).

A possibility to combine the advantages of both encodings is by using an hybrid approach of single photon and cat state encoded qubits [van Loock, 2011]. For instance, in [Lee and Jeong, 2013] it was shown how to perform near-deterministic quantum teleportation in terms of all-optical hybrid entanglement or, in [Rigas et al., 2006; Wittmann et al., 2010], its usefulness for quantum key distribution was exploited. Hybrid entangled states are also used in quantum bus approaches which interactions of single photon states are avoided and mediated by a common optical mode [van Loock et al., 2008]. Such hybrid entangled states might be of the form:

$$|\Psi_\gamma\rangle = \frac{1}{\sqrt{2}} [|0\rangle|\text{cat}^- \rangle + |1\rangle|\text{cat}^+ \rangle] \quad (\text{VI.1})$$

where $|\text{cat}^\pm\rangle = 1/N_\pm (|\gamma\rangle \pm |-\gamma\rangle)$ with normalization factor $N_\pm = \sqrt{2 \pm 2e^{-2|\gamma|^2}}$. The states $|0\rangle$ and $|1\rangle$ represent vacuum and single photon states, respectively, and $|\gamma\rangle$ is a coherent state with complex amplitude γ . A plot of the two-mode Wigner function $W(x_a, p_a; x_b, p_b)$ is presented in Fig. VI.1. In the limit of large $|\gamma|$ we can

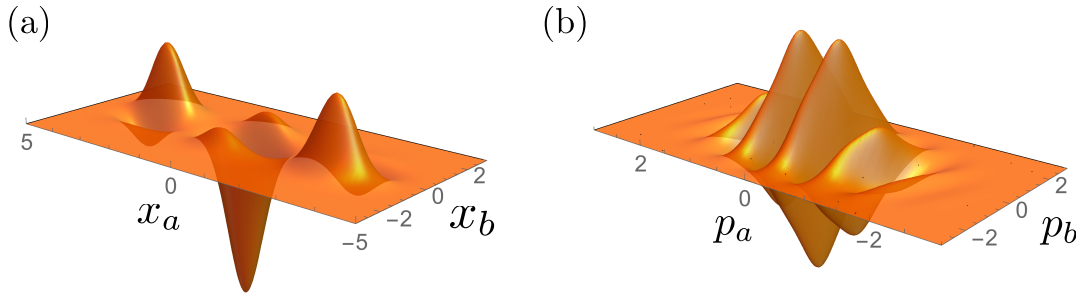


Figure VI.1: Plot of the two-mode Wigner function $W(x_a, p_a; x_b, p_b)$ of the hybrid entangled state (VI.1) for $\gamma = 3$ in the planes (a) $p_a = p_b = 0$ and (b) $x_a = x_b = 0$.

replace $N_{\pm} \rightarrow \sqrt{2}$ and approximate the state (VI.1) as:

$$|\Psi_{\gamma}\rangle \approx \frac{1}{\sqrt{2}} [|+\rangle |\gamma\rangle - |-\rangle |-\gamma\rangle], \quad (\text{VI.2})$$

where $|\pm\rangle = 1/\sqrt{2}(|0\rangle \pm |1\rangle)$.

An optical measurement induced creation of hybrid entangled states at a distance of the form (VI.1) was proposed and implemented recently in [Morin et al., 2014]. In the following, we will briefly review the preparation of such states and then turn to the study of their nonlocal properties.

VI.1.2 Experimental production of hybrid entangled states

The optical circuit which allows for the generation of the hybrid entangled state (VI.1) is illustrated in Fig. VI.2. Two spatially separated parties, referred to as Alice and Bob, use the single-photon and the cat state qubit encoding, respectively, in order to process information. In order to establish hybrid entanglement between each other Alice and Bob first produce locally and independently a nonclassical state of light. Alice prepares, on her side, a two-mode squeezed state $|\psi_{in}\rangle = |0\rangle_s |0\rangle_i + \lambda |1\rangle_s |1\rangle_i + \mathcal{O}(\lambda^2)$ by pumping an optical parametric oscillator, as outlined in Sec. II.3.2.2. On the second subsystem, Bob produces locally an even cat state $|\text{cat}^+\rangle$ by exploiting one of the well established methods presented in [Ourjoumtsev et al., 2006, 2007]. One possibility is, for instance, to subtract a single photon from a squeezed vacuum state generating an even cat state with amplitude $|\gamma| \lesssim 1$ which depends on the squeezing factor of the initial state [Ourjoumtsev et al., 2006].

Next, the even cat state $|\text{cat}^+\rangle_a$ on Alice side is sent through a beam-splitter with small reflection coefficient r_a , where the subscript a refers to mode- a . In the limit of small reflectivity $r_a = \sin \theta \approx \theta \ll 1$, the beam-splitter operation can be approximated as $\hat{B}(\theta) = e^{\theta(\hat{a}\hat{b}^\dagger - \hat{a}^\dagger\hat{b})} \approx \mathbb{1} + \theta(\hat{a}\hat{b}^\dagger - \hat{a}^\dagger\hat{b})$. Together with the two-mode squeezed state on Bob's side the initial state on all four modes reads:

$$|\Psi_{in}\rangle = (\mathbb{1} + \theta(\hat{b}'^\dagger\hat{a}'))(\mathbb{1} + \lambda\hat{c}^\dagger\hat{d}^\dagger)|\text{cat}^+\rangle_a |0\rangle_{b'} |0\rangle_c |0\rangle_d \quad (\text{VI.3})$$

where a' and b' denote the output modes of the beam-splitter on Alice's side. Further,

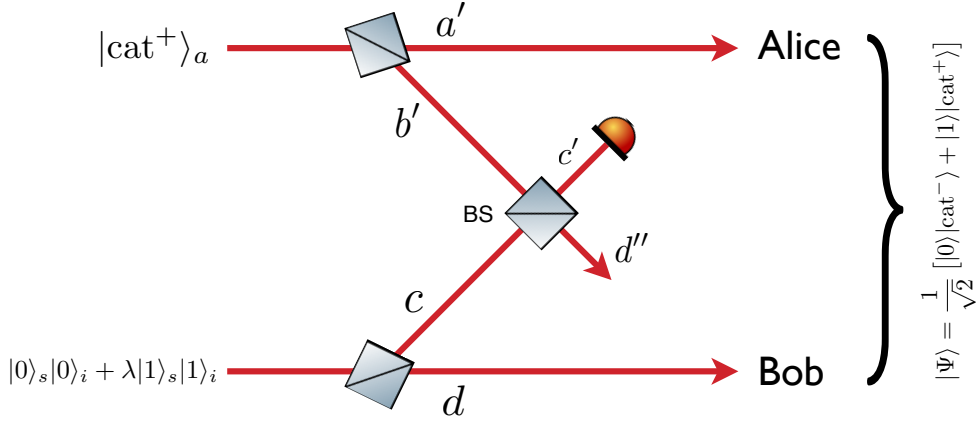


Figure VI.2: Experimental setup showing the generation of the hybrid entangled state (VI.1). Mode a is prepared in an even cat state and sent through a beam-splitter (BS) with high transmissivity such that a single photon is subtracted. Simultaneously, the two modes of the two-mode squeezed state $|0\rangle_s|0\rangle_i + \lambda|1\rangle_s|1\rangle_i$ are split into two spatial modes, denoted by c and d . Further on, mode b' and c are sent through another beam-splitter and detected in the output mode c' . The latter detection heralds the generation of the hybrid state in the modes a' and d .

the modes b' and c are sent to a router in order to herald the production of the hybrid entanglement. Once arrived at the router mode b' and c are mixed by another beam-splitter with transmission t and reflection r . According to the relations (II.177) and (II.178) we then arrive at the state:

$$|\Psi'\rangle = \left[\mathbb{1} + \theta \hat{a}'^\dagger (t(\hat{b}'^\dagger)^\dagger + r(\hat{c}'^\dagger)^\dagger) + \lambda \hat{d}'^\dagger (t(\hat{c}'^\dagger)^\dagger - r(\hat{b}'^\dagger)^\dagger) \right] |\text{cat}^+\rangle_a |0\rangle_{b'} |0\rangle_c |0\rangle_d \quad (\text{VI.4})$$

where we neglected the second-order term proportional to $\lambda\theta$. A detection of a single photon in mode c' then heralds the production of the state:

$$|\Psi''\rangle = \theta r |0\rangle_d (\hat{a}'^\dagger)^\dagger |\text{cat}^+\rangle_{a'} + \lambda t |1\rangle_d |\text{cat}^+\rangle_{a'}. \quad (\text{VI.5})$$

Hence, since the subtraction of a single photon from an even cat state produces an odd cat state $\hat{a}^\dagger |\text{cat}^+\rangle = \gamma |\text{cat}^-\rangle$, the heralded state can be written as:

$$|\Psi_{out}\rangle = \theta r \gamma |0\rangle_d |\text{cat}^-\rangle_{a'} + \lambda t |1\rangle_d |\text{cat}^+\rangle_{a'}, \quad (\text{VI.6})$$

An equal superposition can be obtained by adjusting the reflection/transmission rates of the beam-splitter as $r/t = \lambda/(\theta\gamma)$. Once the weights are balanced we can write the state (VI.6) with proper normalizations as:

$$|\Psi_{out}\rangle = \frac{1}{\sqrt{2}} \left[|0\rangle_d \frac{1}{\mathcal{N}^-} (|\gamma\rangle_{a'} - |-\gamma\rangle_{a'}) + |1\rangle_d \frac{1}{\mathcal{N}^+} (|\gamma\rangle_{a'} + |-\gamma\rangle_{a'}) \right]. \quad (\text{VI.7})$$

with the normalization factors $\mathcal{N}^\pm = \sqrt{2 \pm 2e^{-2|\gamma|^2}}$. To express (VI.7) in a rotated

basis we can write:

$$|\Psi_{out}\rangle = \frac{1}{\sqrt{2}} \left[\left(\frac{1}{\mathcal{N}^-} |0\rangle_d + \frac{1}{\mathcal{N}^+} |1\rangle_d \right) |\gamma\rangle_{a'} - \left(\frac{1}{\mathcal{N}^-} |0\rangle_d - \frac{1}{\mathcal{N}^+} |1\rangle_d \right) |-\gamma\rangle_{a'} \right]. \quad (\text{VI.8})$$

which in the limit of approximately orthogonal coherent states $\langle \gamma | -\gamma \rangle \ll 1$ yields Eq. (VI.2).

VI.1.3 Measurement and experimental losses

The two-mode hybrid state is then characterized by high efficiency homodyne detection (see Sec. II.3.2.3) that is taking datapoints on each mode for different choices of quadratures. Note that using homodyne detection is rather an experimentally motivated choice. Other measurements, *i.e.* photon number resolving detections, can be envisioned but are technically not as well developed as homodyne detections. The subsequent post-processing of the measured data depends on the specific protocol one wants to implement. In the following, we shortly discuss some possible strategies allowing to perform nonlocality and entanglement tests.

For a nonlocality test we have to take data points for random choices of quadratures yielding the corresponding joint-probability distribution $p(a, b; \theta, \phi)$, where a (b) denotes the outcome of a measurement of the quadrature x_θ (x_ϕ) on Alice's (Bob's) side. The joint-probabilities $p(a, b; \theta, \phi)$ can then be used to test, for instance, the continuous-variable Bell inequality derived by E. G. Cavalcanti et al. which involves first and second moments of the measured quadratures [Cavalcanti et al., 2007]. Another possibility to perform a nonlocality test is to use a binning procedure where one assigns binary values (for instance ± 1) to the outcomes of the quadrature measurements depending on, *i.e.* their sign [Wenger et al., 2003; García-Patrón et al., 2004]. The binned outcomes can then be used to test the CHSH inequality (IV.44). Similarly, one can also test the CHSH inequality in terms of modular variables measurements whose expectation values can be calculated from the joint-probability distribution $p(a, b; \theta, \phi)$ of the performed quadrature measurements [Ketterer et al., 2015]. However, with none of the mentioned methods, we were able to theoretically demonstrate the nonlocality of the hybrid entangled states (VI.1).

Another, slightly different approach for testing the CHSH inequality is by using photon number parity measurements which also yield binary measurement outcomes. In [Banaszek and Wódkiewicz, 1998, 1999; Chen et al., 2002], it was shown that in this way one can demonstrate the nonlocality also for states having a strictly positive Wigner function. However, the parity has the disadvantage that it is inaccessible for homodyne measurements and thus requires photon number resolving detectors. Nevertheless, in Sec. VI.3 we will show that it is still possible to demonstrate the nonlocality of the hybrid entangled state (VI.1) by violating the CHSH inequality in terms of parity measurements.

In turn, if one aims at demonstrating hybrid entanglement instead of nonlocality one can follow a more straightforward approach. Homodyne measurements for an equally distributed choice of quadratures allow one to reconstruct the full two-mode density matrix using a maximum likelihood algorithm [Lvovsky and Raymer, 2009]. Having available the experimentally reconstructed density matrix of the produced hybrid en-

tangled state we can then straightforwardly calculate entanglement criteria including the two-mode correlation functions contained in the CHSH inequality. In this case, the violation of the CHSH inequality can, however, only be regarded as a demonstration of entanglement and not of nonlocality. This is due to the fact that the process of reconstructing the density matrix does already imply the validity of quantum mechanics and thus cannot be considered as device-independent (see Sec. IV.2).

In the following, we will summarize some losses occurring in different steps of the experiment outlined in the last Section. The mentioned numerical values are rough estimates of the real transmission and loss rates present in the experiment discussed in [Morin et al., 2014]. During the process of generating the states two main kinds of losses are of importance:

1. The losses in the crystal of the OPO, where the two-mode squeezed states are generated, leading to a transmission of about 96%. These losses are fixed and can only be improved by changing the crystal or the coatings inside the cavity.
2. The losses due to the imperfect detection are about 15%. For instance, the finite efficiency of the photodiodes used to perform the homodyne detection, the phase-matching of the analyzed beam with the local oscillator, optical isolators and beam splitters. The latter are very well known and do not occur before the produced state under consideration is measured.

The overall transmission taking into account these losses is about 81% leading to 66% for two modes, but 92% if corrected for detection losses. On top of these losses one has to take into account the finite fidelity of the generated states with the real state (VI.1) which is about 94%. Hence, by combining the experimental losses with the imperfect fidelity of the states we get an overall transmission of about 86%.

VI.2 Qubit, parity and hybrid CHSH inequality

As discussed in previous Chapters, the CHSH inequality (IV.44) was first derived under the condition that the measured observables have binary outcomes. In the quantum realm such observables are given by superpositions of Pauli operators (II.3)-(II.5), which physically correspond, for instance, to polarization or spin measurements and can violate the classical bound 2 of the CHSH inequality:

$$\mathcal{B} = \langle \hat{\sigma}_{\mathbf{v}_a} \hat{\sigma}_{\mathbf{v}_b} \rangle + \langle \hat{\sigma}_{\mathbf{v}_a} \hat{\sigma}_{\mathbf{v}_{b'}} \rangle + \langle \hat{\sigma}_{\mathbf{v}_{a'}} \hat{\sigma}_{\mathbf{v}_b} \rangle - \langle \hat{\sigma}_{\mathbf{v}_{a'}} \hat{\sigma}_{\mathbf{v}_{b'}} \rangle \leq 2\sqrt{2}, \quad (\text{VI.9})$$

for some entangled state $|\Psi_{\text{ent}}\rangle$, where $\hat{\sigma}_{\mathbf{v}} = \mathbf{v} \cdot \hat{\boldsymbol{\sigma}}$ with $\mathbf{v} = (v_x, v_y, v_z)$, $|\mathbf{v}| = 1$ and the Pauli operator $\hat{\boldsymbol{\sigma}} = (\hat{\sigma}_x, \hat{\sigma}_y, \hat{\sigma}_z)$. In spherical coordinates we can write $\mathbf{v} = (\sin(\theta) \cos(\phi), \sin(\theta) \sin(\phi), \cos(\theta))$ and thus get

$$\begin{aligned} \hat{\sigma}_{\mathbf{v}} &= \sin(\theta) \cos(\phi) \hat{\sigma}_x + \sin(\theta) \sin(\phi) \hat{\sigma}_y + \cos(\theta) \hat{\sigma}_z \\ &= \begin{pmatrix} \cos \theta & e^{-i\phi} \sin \theta \\ e^{i\phi} \sin \theta & -\cos \theta \end{pmatrix} \end{aligned} \quad (\text{VI.10})$$

The maximum value of \mathcal{B} that can be obtained according to the laws of quantum mechanics is $2\sqrt{2}$ and referred to as Tsirelson bound (see Sec. IV.2). Given a set of

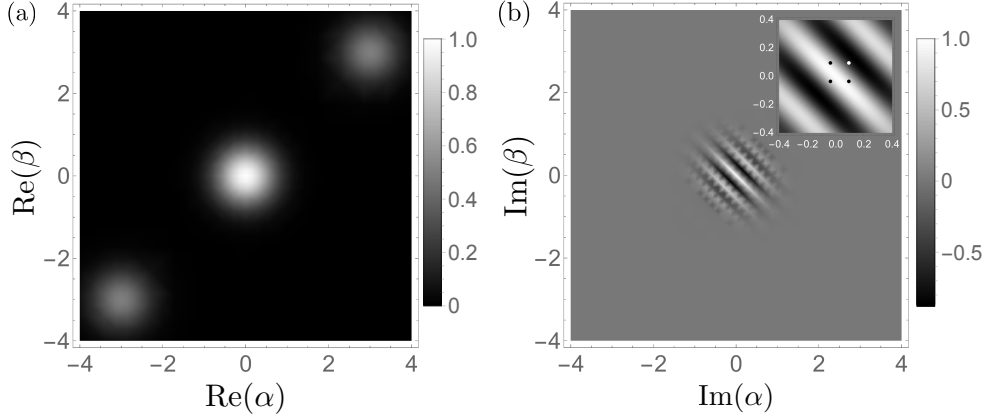


Figure VI.3: Density plot of the Wigner function of the two-mode entangled cat state $|\Phi\rangle$, for $\gamma = 3$, in the planes (a) $\text{Im}(\alpha) = \text{Im}(\beta) = 0$ and (b) $\text{Re}(\alpha) = \text{Re}(\beta) = 0$. The inset shows an enlargement of the interference fringes for smaller values of $\text{Im}(\alpha)$ and $\text{Im}(\beta)$ including the sampling points that lead to a violation of the CHSH inequality.

measurement settings a, b, a', b' , maximum violation of the inequality (IV.44) occurs for some maximally entangled states $|\psi\rangle$, e.g. $|\psi\rangle = 1/\sqrt{2}(|0\rangle|0\rangle + |1\rangle|1\rangle)$ (see Sec. IV.2 for an example).

In general, the CHSH inequality can also be tested with states living in higher than two-dimensional Hilbert spaces provided the observables under consideration have a binary spectrum. In the following, we will test the CHSH-inequality using measurements of the photon number parity operator $\hat{P} = e^{i\pi\hat{a}^\dagger\hat{a}}$, where $\hat{n} = \hat{a}^\dagger\hat{a}$ is the photon number operator and \hat{a} (\hat{a}^\dagger) is the photon annihilation (creation) operator of the corresponding optical mode. The eigenspaces corresponding to the two eigenvalues of the parity operator are infinite dimensional and spanned by the Fock states containing either even $2n$ or odd $2n + 1$ photons. Further on, we consider measurements of the displaced parity operator

$$\hat{\Pi}(\alpha) = \hat{D}(\alpha)\hat{P}\hat{D}(-\alpha), \quad (\text{VI.11})$$

where $\hat{D}(\alpha) = \hat{D}(\nu, \mu)$ is the phase space displacement operator with $\alpha = (\nu + i\mu)/\sqrt{2}$ (see also Sec. II.2.4.2), in order to mimic different measurement settings a, b, a' and b' . Note, that the expectation value of the displaced parity operator is directly related to the Wigner function $W(x, p) = W(\alpha = (x + ip)/\sqrt{2})$ of the state under consideration, through $\langle \hat{\Pi}(\alpha) \rangle = \frac{\pi}{2}W(\alpha)$ [Lutterbach and Davidovich, 1997; Banaszek and Wódkiewicz, 1998; Banaszek et al., 1999].

This leads to the following representation of the CHSH-inequality in terms of parity measurements:

$$\mathcal{B}_{\text{par}} = \langle \hat{\Pi}(\alpha)\hat{\Pi}(\beta) \rangle + \langle \hat{\Pi}(\alpha)\hat{\Pi}(\beta') \rangle + \langle \hat{\Pi}(\alpha')\hat{\Pi}(\beta) \rangle - \langle \hat{\Pi}(\alpha')\hat{\Pi}(\beta') \rangle \leq 2\sqrt{2}. \quad (\text{VI.12})$$

The parity CHSH value \mathcal{B}_{par} violates the local-realism threshold of *two*, for instance, with a two-mode squeezed state $|r\rangle_{\text{TMSV}} = \sqrt{1 - \lambda^2} \sum_{n=0}^{\infty} (-\lambda)^n |n\rangle_a |n\rangle_b$, for which we

get:

$$\mathcal{B}_{\text{TMSS}} = \exp[-2 \cosh(2r)(|\alpha|^2 + |\beta|^2) + 2 \sinh(2r)(\alpha\beta + \alpha^*\beta^*)] \quad (\text{VI.13})$$

and in the infinite squeezing limit yields $\mathcal{B}_{\text{TMSS}} \rightarrow 8/3^{(\frac{9}{8})} \approx 2.32$, for $\alpha = -\alpha' = \beta'/2 = \sqrt{\ln(3)/(16 \cosh 2r)}$ and $\beta = 0$ [Jeong et al., 2003]. Almost maximal violation of Equation (VI.12) can be reached with a two-mode entangled cat state $|\Phi\rangle = (|\gamma\rangle|\gamma\rangle + |-\gamma\rangle|-\gamma\rangle)/\mathcal{N}_\gamma$, where $\mathcal{N}_\gamma = \sqrt{2(1 + e^{-4\gamma\gamma^*})}$. If we set $\gamma = 3$, and the measurement settings equal to $\alpha = \beta = -0.035$ and $\alpha' = \beta' = 0.095$, as shown in [Milman et al., 2005], we find that $\mathcal{B}_{\gamma=3} = 2.77$. In order to obtain maximal violation we have to take the limit $\gamma \rightarrow \infty$ of very large cat states, yielding $\mathcal{B}_{\gamma \rightarrow \infty} \rightarrow 2\sqrt{2}$, if the sampling points α, β, α' and β' at the same time go to zero as $1/\gamma$. In Fig. VI.3, we present a density plot of the two-mode Wigner function $W(\alpha, \beta) = \frac{4}{\pi^2} \langle \hat{\Pi}(\alpha) \hat{\Pi}(\beta) \rangle$ of the entangled cat state $|\Phi\rangle$ in the planes $\text{Im}(\alpha) = \text{Im}(\beta) = 0$ and $\text{Re}(\alpha) = \text{Re}(\beta) = 0$. The sampling points leading to a violation of the CHSH inequality are indicated inside the plot. In the case of the two-mode entangled cat state one has to choose imaginary sampling points near to the interference fringes at the origin otherwise no violation can be observed.

Finally, we can also consider a combination of the CHSH inequality (VI.9) and its parity version (VI.12) in order to test Hybrid systems for nonlocal correlations (see Sec. VI.1). More precisely, we perform Pauli measurements $\hat{\sigma}_{\mathbf{v}}$ on first subsystem and displaced parity measurements $\hat{\Pi}(\beta)$ on the second subsystem. In this case, the corresponding CHSH value reads:

$$\mathcal{B}_{\text{hyb}} = \langle \hat{\sigma}_{\mathbf{v}} \hat{\Pi}(\beta) \rangle + \langle \hat{\sigma}_{\mathbf{v}'} \hat{\Pi}(\beta') \rangle + \langle \hat{\sigma}_{\mathbf{v}} \hat{\Pi}(\beta) \rangle - \langle \hat{\sigma}_{\mathbf{v}'} \hat{\Pi}(\beta') \rangle \leq 2\sqrt{2}. \quad (\text{VI.14})$$

where $\sigma_{\mathbf{v}^{(l)}}$ and $\hat{\Pi}(\beta^{(l)})$ defined according to Eq. (VI.10) and Eq. (VI.11), respectively. In the next Section we will discuss how to demonstrate the nonlocality of the hybrid entangled state (VI.1) using the inequality (VI.14).

VI.3 Nonlocality of hybrid entanglement

VI.3.1 Theoretical violation of the CHSH inequality

In this Section we will use the methods discussed in Sec. VI.2 to test the CHSH inequality with the hybrid entangled state

$$|\Psi_\gamma\rangle = \frac{1}{\sqrt{2}} [|0\rangle|\text{cat}^- \rangle + |1\rangle|\text{cat}^+ \rangle], \quad (\text{VI.15})$$

where we will restrict ourselves to cat state sizes $\gamma \leq 3$. This choice is motivated by the fact that the experimental techniques discussed in Sec. VI.1.2 allow for the production of cat states with $\gamma \lesssim 2$, and thus values $\gamma > 3$ are experimentally out of reach. Even for cavity quantum electro-dynamics (QED) or circuit QED techniques the production of cat states with $g > 3$ is very challenging [Deleglise et al., 2008; Vlastakis et al., 2015].

First, we will use the parity CHSH inequality (VI.12) to test the hybrid entangled state (VI.15). Further on, since the expectation value of the tensor product of two displaced parity operators $\hat{\Pi}(\alpha)\hat{\Pi}(\beta)$ is related to the two-mode Wigner function $W(\alpha, \beta)$, where $\alpha = (x_a + ip_a)/\sqrt{2}$ ($\beta = (x_b + ip_b)/\sqrt{2}$), we simply have to find an appropriate

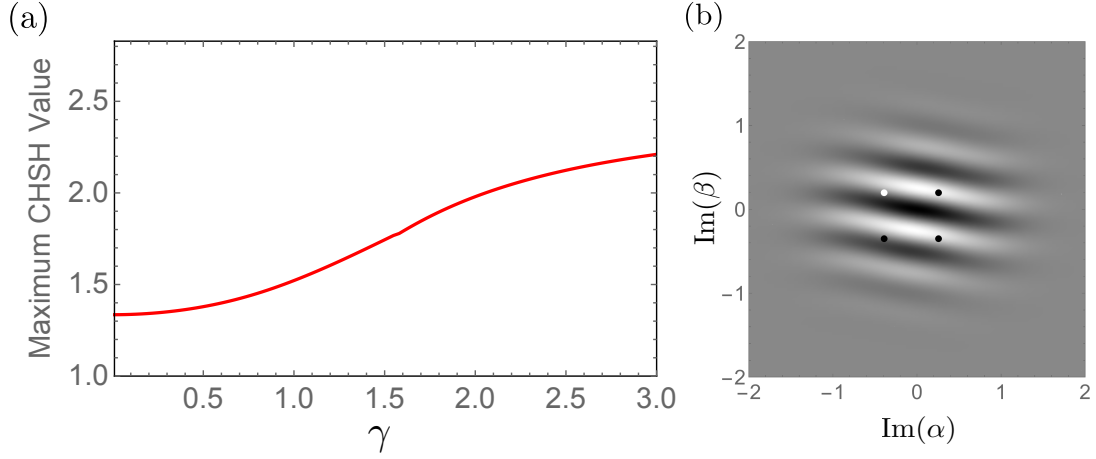


Figure VI.4: (a) Plot of the maximized CHSH value $\mathcal{B}_{\text{par}}^{(\text{max})}$ as a function of $g = \gamma$. (b) Density plot of the Wigner function $W(\alpha, \beta)$ in the plane $\text{Re}(\alpha) = \text{Re}(\beta) = 0$ including the sampling points α, α', β and β' .

set of points α, α', β and β' of the Wigner function that maximizes the CHSH value (see Fig. VI.1):

$$\mathcal{B}_{\text{par}} = \langle \hat{\Pi}(\alpha)\hat{\Pi}(\beta) \rangle + \langle \hat{\Pi}(\alpha)\hat{\Pi}(\beta') \rangle + \langle \hat{\Pi}(\alpha')\hat{\Pi}(\beta) \rangle - \langle \hat{\Pi}(\alpha')\hat{\Pi}(\beta') \rangle \leq 2\sqrt{2}. \quad (\text{VI.16})$$

In Fig. VI.4(a) we present a plot of the $\mathcal{B}_{\text{par}}^{(\text{max})}$, maximized over the values α, β, α' and β' , as a function of the size of the cat states γ . We see that for small values of γ the local-realism bound of *two* is not violated and only for cat state sizes $\gamma \gtrsim 2$ a demonstration of Bell nonlocality can be achieved. For $\gamma = 3$ we find the largest CHSH value $\mathcal{B}_{\text{par}}^{(\text{max})} \approx 2.21$ in the interval $\gamma \in [0, 3]$, for $\alpha = i0.35$, $\alpha' = -i0.55$, $\beta = -i0.49$ and $\beta' = i0.28$. These values form a square in phase space as we can see in Fig. VI.4(b), where we present a density plot of the Wigner function $W(\alpha, \beta)$ in the plane $\text{Re}(\alpha) = \text{Re}(\beta) = 0$.

Next, we want to compare the violation achieved with displaced parity measurements on Alice's and Bob's side using Eq. (VI.16) with a hybrid measurement strategy which employs Pauli measurements on Alice's and displaced parity measurements on Bob's side (see Eq. (VI.14)). In order to do so we first have to evaluate the hybrid correlation functions contained in Eq. (VI.14), yielding:

$$\begin{aligned} \langle \hat{\sigma}_{\mathbf{v}} \hat{\Pi}(\alpha) \rangle_{\Psi_{\gamma}} &= \frac{1}{2} \left[\langle 0 | \hat{\sigma}_{\mathbf{v}} | 0 \rangle \langle \gamma | \hat{\Pi}(\alpha) | \gamma \rangle + \langle 0 | \hat{\sigma}_{\mathbf{v}} | 1 \rangle \langle \gamma | \hat{\Pi}(\alpha) | -\gamma \rangle \right. \\ &\quad \left. + \langle 1 | \hat{\sigma}_{\mathbf{v}} | 0 \rangle \langle -\gamma | \hat{\Pi}(\alpha) | \gamma \rangle + \langle 1 | \hat{\sigma}_{\mathbf{v}} | 1 \rangle \langle -\gamma | \hat{\Pi}(\alpha) | -\gamma \rangle \right]. \quad (\text{VI.17}) \end{aligned}$$

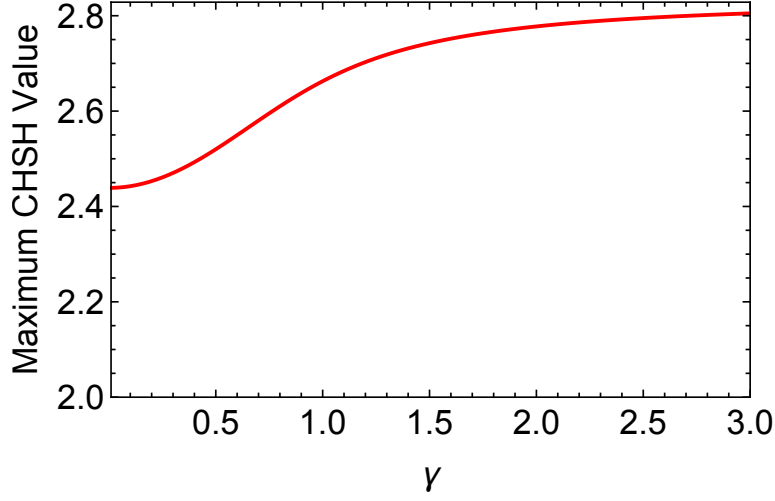


Figure VI.5: Plot of the maximal CHSH value $\mathcal{B}_{\text{hyb}}^{(\text{max})}$ as a function of the size γ of the Hybrid Cat State $|\Psi_\gamma\rangle$.

where

$$\begin{aligned}
 \langle \gamma | \hat{\Pi}(\alpha) | \delta \rangle &= \langle \gamma | \hat{D}(\alpha) \hat{P} \hat{D}^\dagger(\alpha) | \delta \rangle = \langle \gamma | \hat{D}(\alpha) \hat{P} | \delta - \alpha \rangle e^{-i\text{Im}(\alpha\delta^*)} \\
 &= \langle \gamma | \hat{D}(\alpha) | \alpha - \delta \rangle e^{-i\text{Im}(\alpha\delta^*)} \\
 &= \langle \gamma | 2\alpha - \delta \rangle e^{-i\text{Im}(\alpha\delta^*)} e^{i\text{Im}(-\alpha\delta^*)} \\
 &= \langle \gamma | 2\alpha - \delta \rangle e^{i\text{Im}[2\alpha\delta^*]}. \tag{VI.18}
 \end{aligned}$$

To evaluate the Eq. (VI.18) we used the relations $\hat{D}(\gamma + \delta) = \hat{D}(\gamma)\hat{D}(\delta)e^{-i\text{Im}[\gamma\delta^]}$ for the product of two displacement operators and that $\langle \gamma | \delta \rangle = e^{-\frac{1}{2}(|\gamma|^2 + |\delta|^2 - 2\delta\gamma^*)}$. Further on, we insert the terms (VI.17) into Eq. (VI.14) and numerically maximize \mathcal{B}_{hyb} over all free parameters $\theta, \phi, \theta', \phi', \beta$ and β' . In Fig.VI.5 we present a plot the maximum value $\mathcal{B}_{\text{hyb}}^{(\text{max})}$ as a function of the cat state size γ .

We find that the hybrid cat state $|\Psi_\gamma\rangle$ violates the hybrid CHSH inequality (VI.14) for all values of the cat state size $\gamma \in [0, 3[$. In particular, in the limit $\gamma \rightarrow 0$ the CHSH value converges to the finite value 2.44, and in the limit of large γ , $\mathcal{B}_{\text{hyb}}^{(\text{max})}$ converges towards the upper quantum bound $2\sqrt{2}$. In the former case, this is due to the fact that the odd cat state $|\text{cat}^- \rangle$ converges towards a single photon state $|1\rangle$ in the limit of small γ , and the even cat state $|\text{cat}^+ \rangle$ towards a vacuum state. Thus, in the limit $\gamma \rightarrow 0$ the hybrid state (VI.15) becomes a single photon entangled state $|\Psi_{\gamma \rightarrow 0}\rangle = (|0\rangle|1\rangle + |1\rangle|0\rangle)/\sqrt{2}$. In contrast, in the opposite limit of large γ , the two cat states $|\text{cat}\rangle^\pm$ become orthogonal and we end up in a maximally entangled state with respect to the single photon encoding $|0_L(1_L)\rangle = |0(1)\rangle$ on Alice's side and the cat state encoding $|0_L(1_L)\rangle = |\text{cat}^\pm\rangle$ on Bob's side. In both cases the limiting state is entangled with respect to parity measurements and thus yields a violation of the CHSH inequality.

Figure VI.5 also confirms that the hybrid measurement strategy leads to an improved violation of the CHSH inequality, as compared to the previously discussed case with

parity measurements on both Alice's and Bob's side (see Fig. VI.4(a)). This is due to the fact that arbitrary Pauli measurements (VI.10) on the first subsystem have a larger flexibility in choosing different measurement bases in the single photon logical space, compared to displaced parity measurements. The dependency of the observed violation on the specific basis choice on Alice's system is further illustrated in Fig. VI.6, where we plot for $\gamma = 1$ and $\theta = \phi = 0$ the maximized value $\mathcal{B}_{\text{hyb}}^{(\text{max})}$ (maximized with respect to β and β') as a function of θ' and ϕ' . Hence, for further investigations which include the influence of losses on the observed violation of the CHSH inequality we will restrict ourselves to the hybrid measurement strategy (see Eq. (VI.14)).

In the next Section we will study the influence of losses on the observed violation of the CHSH inequality. In particular, we will give a threshold on the amount of losses that can be tolerated in each mode without jeopardizing the violation of local-realism.

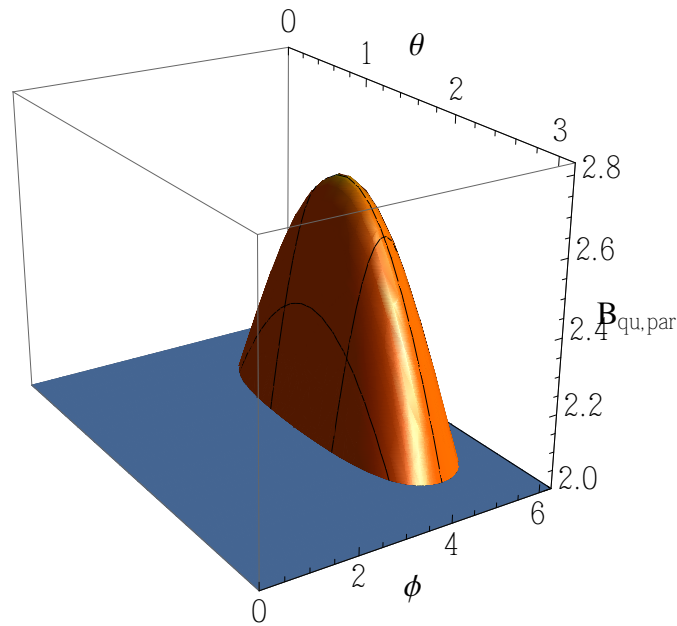


Figure VI.6: Plot of the CHSH value $\mathcal{B}_{\text{qu,par}}$ as a function of the angle θ' and ϕ' for $\gamma = 1$, $\beta = 0.156$ and $\beta' = -0.156$.

VI.3.2 Nonlocality under the influence of losses

An important question concerning the experimental demonstration of nonlocality in terms of the hybrid inequality (VI.14) is to what extent the observed violation is resilient with respect to optical losses. Possible experimental losses in an optical implementation were discussed in Sec. VI.1.3. Theoretically we can model them by applying beam-splitter operations with transmission η on each mode of the ideal hybrid state (VI.15), and subsequently tracing out the two reflected output modes of the beam splitters. The state resulting from this procedure depends on the parameter η which mimics the efficiency of the experiment. Maximizing \mathcal{B} for different values of η thus allows us to study the violation of the CHSH inequality under the influence of different amounts of

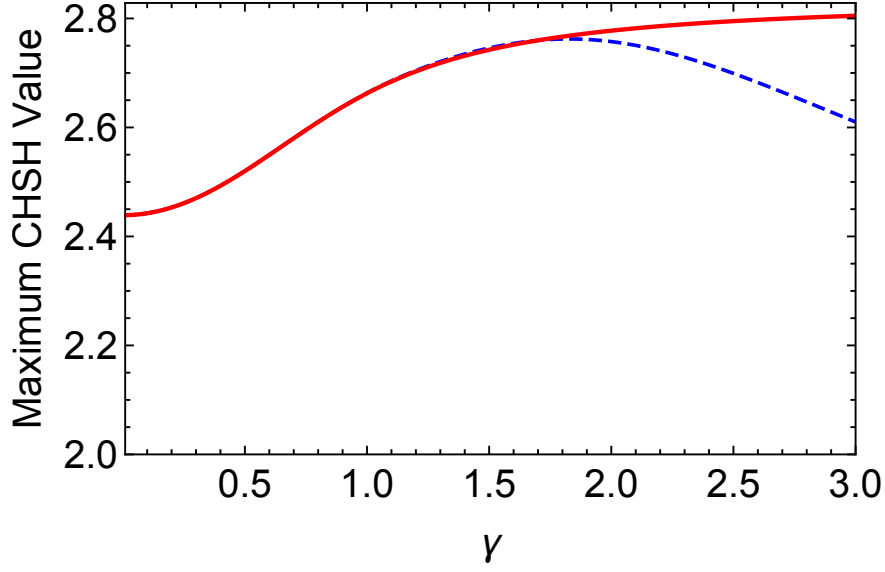


Figure VI.7: Plot of the maximized CHSH value $\mathcal{B}_{\text{hyb}}^{(\text{max})}$ as a function of γ for $\eta = 1$ calculated using the analytical expression (VI.17) (red line) and the approximate expression by truncating the Fock space for photon numbers $n > 6$ (blue dashed line). It is apparent that the latter approximation breaks down for sizes $\gamma \gtrsim 1.5$ of the hybrid entangled state $|\Psi_\gamma\rangle$.

losses (keep in mind that the total transmission on both modes is given by η^2).

To start we calculate the action of the beam splitter operations on the hybrid state (VI.15). The beam-splitter with transmission η was discussed in Sec. II.3.2.1 and is easily summarized by the following transformations of the annihilation (creation) operators of the corresponding input modes: $a^{(\dagger)} \rightarrow \sqrt{\eta}a^{(\dagger)} + \sqrt{1-\eta}b^{(\dagger)}$ and $b^{(\dagger)} \rightarrow \sqrt{\eta}b^{(\dagger)} - \sqrt{1-\eta}a^{(\dagger)}$. Applying them to each mode of the hybrid state (VI.15) together with an additional third and fourth vacuum mode leads to the expression:

$$\begin{aligned}
|\Psi_\gamma\rangle_{\text{noise}} = & \frac{1}{\sqrt{2}\mathcal{N}_-} \left[|\sqrt{\eta}\alpha\rangle|\sqrt{1-\eta}\alpha\rangle|0\rangle|0\rangle - |-\sqrt{\eta}\alpha\rangle|-\sqrt{1-\eta}\alpha\rangle|0\rangle|0\rangle \right] \\
& + \frac{1}{\sqrt{2}\mathcal{N}_+} \left[\sqrt{\eta}|\sqrt{\eta}\alpha\rangle|\sqrt{1-\eta}\alpha\rangle|1\rangle|0\rangle + \sqrt{1-\eta}|\sqrt{\eta}\alpha\rangle|\sqrt{1-\eta}\alpha\rangle|0\rangle|1\rangle \right. \\
& \left. + \sqrt{\eta}|-\sqrt{\eta}\alpha\rangle|-\sqrt{1-\eta}\alpha\rangle|1\rangle|0\rangle + \sqrt{1-\eta}|-\sqrt{\eta}\alpha\rangle|-\sqrt{1-\eta}\alpha\rangle|0\rangle|1\rangle \right].
\end{aligned} \tag{VI.19}$$

Next, we calculated the density matrix belonging to the state (VI.19) and trace over the modes a' and b' . In order to be able to calculate the partial trace we replace the coherent states in Eq. (VI.19) by their Fock state representation, truncate terms in the expansion that are of the order $n > 6$ ¹ and use the resulting approximate state to calculate the reduced density matrix numerically. The expectation values contained in

¹The justification of the choice $n > 6$ is discussed shortly after.

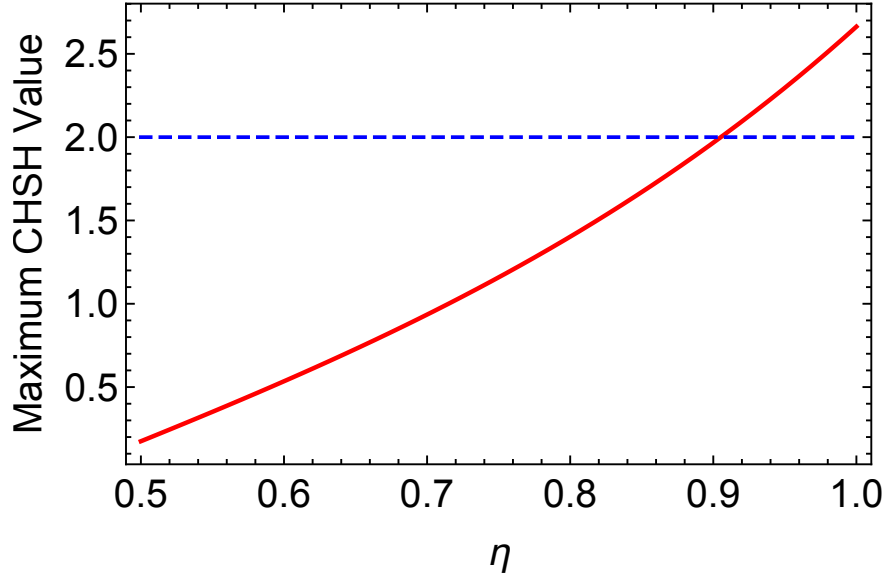


Figure VI.8: Plot of the maximized CHSH value $\mathcal{B}_{\text{hyb}}^{(\max)}$ as a function of the transmission parameter η for $\gamma = 1$, $\theta_1 = 0$, $\phi_1 = 0$, $\theta_2 = 1.57$, $\phi_2 = -1.57$, $\beta = i0.156$ and $\beta' = -i0.156$. The blue dashed horizontal line indicates the local realism threshold given by the CHSH inequality.

the CHSH inequality (VI.14) can then be calculated using Eq. (VI.10) and the Laguerre polynomial expansion of the displaced parity operator:

$$\hat{\Pi}(\alpha) = \sum_n |2n, \alpha\rangle \langle 2n, \alpha| - |2n+1, \alpha\rangle \langle 2n+1, \alpha|, \quad (\text{VI.20})$$

where

$$|n, \alpha\rangle = e^{-\frac{|\alpha|^2}{2}} \sum_m (\alpha^*)^{n-m} \sqrt{\frac{m!}{n!}} L_m^{n-m}(|\alpha|^2) |m\rangle, \quad (\text{VI.21})$$

with the generalized Laguerre polynomials L_p^ℓ (see Appendix A for a definition of $L_p^\ell(x)$). Equation (VI.20) and (VI.21) can be combined to get the simpler expression:

$$\hat{\Pi}(\alpha) = \frac{2}{\pi} e^{-|\alpha|^2/2} \sum_{k,l} (-1)^k \sqrt{\frac{l!}{k!}} (2\alpha^*)^{k-l} L_l^{k-l}(4|\alpha|^2) |k\rangle \langle l|, \quad (\text{VI.22})$$

for $k \geq l$ and

$$\hat{\Pi}(\alpha) = \frac{2}{\pi} e^{-|\alpha|^2/2} \sum_{k,l} (-1)^l \sqrt{\frac{k!}{l!}} (2\alpha)^{l-k} L_k^{l-k}(4|\alpha|^2) |k\rangle \langle l|, \quad (\text{VI.23})$$

for $k < l$.

Before we proceed the calculations with transmission rates $\eta < 1$, we have to verify

for which sizes of the entangled hybrid state (VI.15) our numerical method, using a truncated Fock basis, yields a valid approximation of the exact results. Therefore, we plot in Fig. VI.7 the maximum value of the CHSH inequality as a function of γ with the transmission rate $\eta = 1$, calculated using the truncated Fock state method and using the exact method discussed in Sec. VI.1. We see that, for a Fock state dimension of $n = 6$ on each mode, our numerical method yields a good approximation if $|\gamma| \leq 1.5$, and thus can be used to predict the experimental results for $|\gamma| \lesssim 1$.

Further on, we investigate the dependency of the violation of the CHSH inequality on different values of the optical transmission η . If the minimal transmission η , which still yields a violation of the CHSH inequality, is below the transmission η_{exp} that is present in the experiment [Morin et al., 2014], an experimental observation of nonlocality is within reach. To find out if this is the case, we choose the parameters in the CHSH inequality equal to those values that resulted in a maximum for $\gamma = 1$ and $\eta = 1$, in Fig. VI.7, and plot the corresponding CHSH value as a function of the transmission rate η , as presented in Fig. VI.8. We find that the CHSH value decays with decreasing transmission η making a violation of the CHSH inequality impossible for $\eta < 0.9$. Hence, the total optical transmission in the experiment has to be not less than of the order of $\eta^2 = 0.81$, in order to witness trustworthily the nonlocality of the entangled hybrid state (VI.15).

VI.4 Discussion

In conclusion we have shown how to demonstrate the nonlocality of hybrid entangled states between particle-like and wave-like optical qubits of the form

$$|\Psi_\gamma\rangle = \frac{1}{\sqrt{2}} [|0\rangle|\text{cat}^-\rangle + |1\rangle|\text{cat}^+\rangle], \quad (\text{VI.24})$$

realized by single photon ($|0_L(1_L)\rangle = |0(1)\rangle$) and cat state ($|0_L(1_L)\rangle = |\text{cat}^\pm\rangle$) encodings, on Alice's and Bob's subsystem, respectively. After a short introduction of interesting properties and the experimental production of such hybrid entangled states in quantum optics experiments, we reviewed known approaches allowing to test the CHSH inequality using arbitrary Pauli and displaced parity measurements. Using the latter we found that the nonlocality of the considered hybrid states can be revealed with displaced parity measurements on Alice's and Bob's subsystem, respectively. Further on, by combining Pauli measurements and displaced parity measurements in a hybrid measurement setup we were able to find an improved violation of the CHSH inequality. In particular, the state $|\Psi_\gamma\rangle$ violates the defined hybrid Bell inequality for all values of the cat state size γ and thus might be especially of interest for hybrid protocols exploiting different qubit encodings simultaneously. Finally, we also included possible experimental losses in our theoretical consideration showing that a demonstration of hybrid nonlocality, with γ of the order of unity, is possible if the overall experimental transmission in each mode is not less than 90%.

Possible future investigations could include the search for other appropriate device independent strategies for the detection of entanglement or Bell nonlocality of hybrid entangled states in terms of homodyne measurements. This would be desirable because

the discussed parity measurements require the use of photon resolving detectors which are not as well developed as standard homodyne detections. One possibility of doing so might be to derive novel entanglement witnesses involving measurements of modular variables, similar to those discussed in Sec. IV.1.3, that allow to detect hybrid entanglement. The latter can be assessed by homodyne detection and simple post processing of the measurement outcomes.

VII Summary and conclusions

In this thesis we developed theoretical means that allow to process discrete quantum information encoded into system characterized by degrees of freedom described by continuous variables. Thereby, we specifically focused on the use of modular variables as helpful technique for revealing discrete structures of continuous-variable states, operations and observables. Further on, we derived tests of fundamental properties of quantum mechanics in Hilbert spaces of various dimensions and showed how to apply them within our modular variables quantum information processing framework. Our developments were strongly guided by the potential of future experimental implementations using the transverse degrees of freedom of single photons.

In the first part of this manuscript we devised a framework for quantum information processing in phase space based on the technique of modular variables. Using the latter we dichotomized the Hilbert space of a single mode of continuous variables with respect to the modular position in order to define appropriate logical states, operations and readout observables. These three ingredients thus provided us with a solid framework for handling discrete quantum information encoded into continuous variables. Moreover, with our judiciously chosen modular variables readout observables we established an interesting and yet unexplored connection between specific classes of modular variables and their associated sets of logical wave functions. This connection was shown to be useful later on in order to find violations of modular variables entanglement witnesses and Bell inequalities. The appeal of such modular variables as readout observables is that they can be assessed via POVM measurements in different physical systems. Here, we focused on implementations using the transverse degrees of freedom of single photons, but also cold atoms or micro-mechanical oscillators are suitable platforms for manipulating and measuring modular variables. In the former case we showed that linear optical elements are sufficient to manipulate the spatial distribution of single photons and we worked out two schemes to measure the corresponding readout observables, using direct photon position measurements, on the one hand, and an indirect interferometric scheme, on the other hand.

A second big theme of this thesis was the study of test of fundamental properties of quantum mechanics with measurements of observables living in Hilbert spaces of various dimensions. In particular, we focused on entanglement, Bell nonlocality and contextuality. For each of these properties we derived appropriate entanglement witnesses, Bell inequalities and contextuality tests. The developed techniques have a rather general character but can be seen as a natural application of the previously introduced modular variables phase space framework. First, we used a continuous-variable stabilizer formalism to derive entanglement witnesses which involve measurements of modular variables and are capable of detecting entanglement among the previously introduced modular variables logical states. Further on, we showed how to test discrete-variable Bell inequalities, such as the CHSH inequality, in terms of arbitrary bounded observables.

These Bell inequalities turn out to be closely related to the aforementioned entanglement witnesses for modular-variable measurements. Finally, we found conditions on sets of observables in order to yield maximal state-independent violations of contextuality inequalities in discrete and continuous variables. These conditions highlight common features of observables that lead to maximal violations of contextuality inequalities in Hilbert spaces of different dimensions.

After having devised a rather theoretically oriented framework for quantum information processing in phase space we turned to a more experimentally motivated scheme allowing to process discrete quantum information encoded in the transverse degrees of freedom of single photons. Specifically, we exploited the optical Talbot effect in order to manipulate d -dimensional quantum systems encoded in the periodic near-field interference pattern of plane waves after having passed through periodic diffraction gratings. In particular, we saw that the free-propagation of the single photons in combination with a single optical element, a spatial light modulator, allows to implement universal single qudit operations. Furthermore, we discussed means to perform two-mode operations of photons carrying such an encoding and we showed how to produce deterministically d -dimensional entangled photon pairs using spontaneous parametric down-conversion and linear optical elements only. Finally, we demonstrated the applicability of this quantum information processing scheme by showing how to violate d -dimensional Bell inequalities with the corresponding entangled states. An outlook on possible realization of such a Bell test in terms of material particles was given at the end of the corresponding Chapter, as well.

Finally, we changed gears a little bit and investigated the nonlocal properties of so-called hybrid entanglement between particle-like and wave-like optical qubits. The latter might bear potential improvements for hybrid quantum information protocols, such as quantum teleportation or quantum key distribution. We first reviewed different strategies that can be followed to test for the nonlocality of such states using homodyne measurements and photon resolving detections. Further on, we showed that a hybrid measurement strategy, that makes use of Pauli measurements and displaced parity measurements on the two subsystems of the hybrid entangled state, respectively, yields a violation of the CHSH inequality for all parameters of the hybrid entangled state. The latter also holds after accounting for optical losses in the calculations of the corresponding terms in the CHSH inequality. Hence, theoretically a demonstration of the nonlocality of the considered hybrid entangled states is possible while its experimental implementation remains a challenging task.

In conclusion, we have discussed a whole range of concepts that are of potential interest for future developments of hybrid techniques. The latter include, on the one hand, the formulation of new quantum information protocols that profit from the simultaneous use of discrete- and continuous-variable encodings. Since such protocols make use of fundamental properties of quantum mechanics as resources they might benefit from our considerations about entanglement, nonlocality and contextuality detection in terms of modular-variable measurements. On the other hand, we contributed to the development of experimental hybrid techniques which exploit different degrees of freedom of a single quantum systems, *e.g.* the polarization and spatial degrees of freedom of photons, by providing new ways to encode discrete quantum information in continuous variables. But also hybrid networks, that consist of various physical systems, *e.g.* trapped ions

and atoms or micro- and nano-mechanical oscillators, depend on the formulation such theoretical means since their vibrational degrees of freedom often require a treatment in a continuous variable representation.

At last, the work presented in this dissertation can be seen as a starting point of many new interesting investigations to be carried out in the future. One big issue that was touched only slightly during our elaborations about modular variables is their important role for fault-tolerant implementations of universal quantum computations in continuous-variable systems. An interesting question to explore deeper is why up to today the only way of achieving fault-tolerance in continuous variables is by using a modular variables logical encoding. Furthermore, might quantum computation algorithms also profit from a state readout in terms of modular variables measurements as do the presently introduced test of fundamental properties of quantum mechanics? The formulation of specific modular-variable quantum computation algorithms could be an interesting task for future work. In particular, the model of measurement based quantum computation is thereby of great importance due to the existing experimental capabilities of producing large continuous-variable cluster states.

Another route of research consists of generalizations of the presented modular-variable techniques. For instance, a desirable goal is to formulate novel modular-variables criteria that allow to test for entanglement or nonlocality of a broader class of continuous-variable states, *e.g.* the hybrid entangled states discussed in the previous Chapter or more general classes of entangled cat states. One way of doing so might be to find appropriate phase space operations that stabilize such states approximately such that the resulting entanglement witnesses can detect their correlations at least partially. However, also other mathematical techniques, such as the use of matrices of moments, have previously proved to be useful to derive entanglement witnesses for different classes of states and could be helpful for our considerations. In the case of contextuality, future studies of other contextuality inequalities and their conditions for maximal state-independent violations can be envisioned in order to clarify the generality of our conditions.

Furthermore, modular-variable techniques might be of interest also for the detection of other quantum mechanical resources, such as steering or quantum coherence. The latter are properties for which the use of such techniques is rather unexplored but might be of interest due to the accessibility of modular variables through POVM measurements. Moreover, the investigation of such resources in macroscopic systems consisting of a large number of degrees of freedom, is an active research topic that might profit from techniques involving the manipulation and measurement of modular variables.

Concerning the presented Talbot quantum information processing scheme one of the main perspectives for future work will be its application to systems of material particles. Even though, we have already elaborated briefly on the possibility of experimentally implementing such a scheme with atoms, our considerations are up to now not mature enough and require further investigations. Thereby, one of the main issues is the realization of a position phase gate on the transverse field of a propagating matter wave, which with light fields is straightforwardly implemented using a spatial light modulator. Also, the question how to produce spatially entangled material particles, with the size of an atom or larger, is worth to be further investigated. Finally, other interesting test of quantum mechanical properties, *e.g.* contextuality, in terms of photons or material particles could be envisioned.

A Laguerre- and Hermite polynomials

A.1 Laguerre polynomials

The Laguerre polynomials are defined as the solutions of the Laguerre differential equation [Messiah, 1979, 1991]:

$$x y''(x) + (1 - x) y'(x) + n y(x) = 0 \quad n = 0, 1, \dots, \quad (\text{A.1})$$

and can be expressed as follows:

$$L_n(x) = \frac{e^x}{n!} \frac{d^n}{dx^n} (x^n e^{-x}) = \sum_{j=1}^n \frac{(-1)^j}{j!} \binom{n}{j} x^j. \quad (\text{A.2})$$

Examples are:

$$L_0(x) = 1, \quad (\text{A.3})$$

$$L_1(x) = -x + 1, \quad (\text{A.4})$$

$$L_2(x) = \frac{1}{2} (x^2 - 4x + 2), \quad (\text{A.5})$$

and higher orders can be calculated using the following recursion relations:

$$(n + 1) L_{n+1}(x) = (2n + 1 - x) L_n(x) - n L_{n-1}(x), \quad (\text{A.6})$$

$$x L'_n(x) = n L_n(x) - n L_{n-1}(x). \quad (\text{A.7})$$

The associated Laguerre polynomials are then defined as:

$$L_n^k(x) = (-1)^k \frac{d^k}{dx^k} L_{n+k}(x) = \sum_{j=1}^n \frac{(-1)^j}{j!} \binom{n+k}{n-j} x^j. \quad (\text{A.8})$$

which fulfill the associated Laguerre differential equation:

$$x y''(x) + (k + 1 - x) y'(x) + n y(x) = 0, \quad n = 0, 1, \dots, \quad k \leq n. \quad (\text{A.9})$$

Corresponding examples are:

$$L_0^k(x) = 1, \quad (\text{A.10})$$

$$L_1^k(x) = -x + k + 1, \quad (\text{A.11})$$

$$L_2^k(x) = \frac{1}{2} [x^2 - 2(k + 2)x + (k + 1)(k + 2)], \quad (\text{A.12})$$

and higher orders can be calculated with:

$$L_n^k(x) = \frac{k+1-x}{n} L_{n-1}^{k+1}(x) - \frac{x}{n} L_{n-1}^{k+2}(x), \quad (\text{A.13})$$

$$L_k^{n-k}(x) = \frac{n-k+1-x}{k} L_{k-1}^{n-(k-1)}(x) - \frac{x}{k} L_{k-2}^{n-(k-2)}(x). \quad (\text{A.14})$$

A.2 Hermite polynomials

The Hermite polynomials are defined as the solutions of the Hermite differential equation [Messiah, 1979, 1991]:

$$H_n''(x) - 2x \cdot H_n'(x) + 2n \cdot H_n(x) = 0 \quad (n = 0, 1, 2, \dots), \quad (\text{A.15})$$

and can be expressed as follows:

$$H_n(x) = (-1)^n e^{x^2} \frac{d^n}{dx^n} e^{-x^2} = e^{x^2/2} \left(x - \frac{d}{dx} \right)^n e^{-x^2/2} \quad (\text{A.16})$$

or explicitly

$$H_n(x) = (-1)^n \sum_{k_1+2k_2=n} \frac{n!}{k_1!k_2!} (-1)^{k_1+k_2} (2x)^{k_1}. \quad (\text{A.17})$$

Examples are:

$$H_0(x) = 1, \quad (\text{A.18})$$

$$H_1(x) = 2x, \quad (\text{A.19})$$

$$H_2(x) = 4x^2 - 2, \quad (\text{A.20})$$

and higher orders can be calculated using the following recursion relations:

$$H_{n+1}(x) = 2x H_n(x) - 2n H_{n-1}(x), \quad (\text{A.21})$$

$$H_n'(x) = 2n H_{n-1}(x). \quad (\text{A.22})$$

B Modular variables: explicit calculations

B.1 Commutators of modular and integer operators

In this Appendix we will give explicit derivations of the commutators (III.18) and (III.19), given in Sec. III.1.3. For convenience we reproduce these expressions here:

$$[\hat{x}, \hat{M}] = i \frac{\ell}{2\pi} \left(\mathbb{1} - \ell \int_{-\pi/\ell}^{\pi/\ell} d\bar{p} |\ell/2, \bar{p}\rangle \langle \ell/2, \bar{p}| \right), \quad (\text{B.1})$$

$$[\hat{N}, \hat{p}] = \frac{i}{\ell} \left(\mathbb{1} - \frac{2\pi}{\ell} \int_{-\ell/2}^{\ell/2} d\bar{x} |\bar{x}, \pi/\ell\rangle \langle \bar{x}, \pi/\ell| \right). \quad (\text{B.2})$$

We will begin with Eq. (B.1) and note first that the modular position and momentum operators read in the modular representation (see Sec. III.1.4), as follows:

$$\hat{x} = \int_{-\ell/2}^{\ell/2} \int_{-\pi/\ell}^{\pi/\ell} d\bar{x} d\bar{p} \bar{x} |\bar{x}, \bar{p}\rangle \langle \bar{x}, \bar{p}|, \quad (\text{B.3})$$

$$\hat{p} = \int_{-\ell/2}^{\ell/2} \int_{-\pi/\ell}^{\pi/\ell} d\bar{x} d\bar{p} \bar{p} |\bar{x}, \bar{p}\rangle \langle \bar{x}, \bar{p}|. \quad (\text{B.4})$$

In order to express the integer operator $\hat{M} = (\hat{p} - \hat{p})\ell/(2\pi)$ in the modular representation we first have to find the modular representation of the momentum operator \hat{p} . The latter can be obtained using the decomposition of the identity (III.35), as follows:

$$\begin{aligned} \hat{p} &= \iint_{-\ell/2}^{\ell/2} d\bar{x}_{1/2} \iint_{-\pi/\ell}^{\pi/\ell} d\bar{p}_{1/2} \int_{-\infty}^{\infty} dp p \langle \bar{x}_1, \bar{p}_1 | p \rangle \langle p | \bar{x}_2, \bar{p}_2 \rangle |\bar{x}_1, \bar{p}_1\rangle \langle \bar{x}_2, \bar{p}_2| \\ &= \frac{1}{\ell} \iint_{-\ell/2}^{\ell/2} d\bar{x}_{1/2} \int_{-\pi/\ell}^{\pi/\ell} d\bar{p} \sum_{m \in \mathbb{Z}} (\bar{p} + 2\pi m/\ell) e^{i\bar{x}_1(\bar{p} + m2\pi/\ell)} e^{-i\bar{x}_2(\bar{p} + 2\pi m/\ell)} |\bar{x}_1, \bar{p}\rangle \langle \bar{x}_2, \bar{p}| \\ &= \frac{1}{\ell} \iint_{-\ell/2}^{\ell/2} d\bar{x}_{1/2} \int_{-\pi/\ell}^{\pi/\ell} d\bar{p} \bar{p} \underbrace{\sum_{m \in \mathbb{Z}} e^{i2\pi m(\bar{x}_1 - \bar{x}_2)/\ell} e^{i\bar{p}(\bar{x}_1 - \bar{x}_2)}}_{=\ell\delta(\bar{x}_1 - \bar{x}_2)} |\bar{x}_1, \bar{p}\rangle \langle \bar{x}_2, \bar{p}| \\ &+ \frac{1}{\ell} \iint_{-\ell/2}^{\ell/2} d\bar{x}_{1/2} \int_{-\pi/\ell}^{\pi/\ell} d\bar{p} \sum_{m \in \mathbb{Z}} \underbrace{2\pi m/\ell e^{i2\pi m(\bar{x}_1 - \bar{x}_2)/\ell} e^{i\bar{p}(\bar{x}_1 - \bar{x}_2)}}_{=i \frac{d}{d\bar{x}_2} (\ell\delta(\bar{x}_1 - \bar{x}_2))} |\bar{x}_1, \bar{p}\rangle \langle \bar{x}_2, \bar{p}| \end{aligned} \quad (\text{B.5})$$

where we used the relation (III.37) and that $p = \bar{p} + 2\pi m/\ell$. By further simplifying Eq. (B.5) we obtain:

$$\hat{p} = \hat{p} + \frac{i\ell}{2\pi} \iint_{-\ell/2}^{\ell/2} d\bar{x}_1 d\bar{x}_2 \int_{-\pi/\ell}^{\pi/\ell} d\bar{p} e^{i\bar{p}(\bar{x}_1 - \bar{x}_2)} \left. \frac{d\delta(\bar{x}_1 - \bar{x})}{d\bar{x}} \right|_{\bar{x}=\bar{x}_2} |\bar{x}_1, \bar{p}\rangle \langle \bar{x}_2, \bar{p}| \quad (\text{B.6})$$

and thus have

$$\hat{M} = \frac{i\ell}{2\pi} \iint_{-\ell/2}^{\ell/2} d\bar{x}_1 d\bar{x}_2 \int_{-\pi/\ell}^{\pi/\ell} d\bar{p} e^{i\bar{p}(\bar{x}_1 - \bar{x}_2)} \left. \frac{d\delta(\bar{x}_1 - \bar{x})}{d\bar{x}} \right|_{\bar{x}=\bar{x}_2} |\bar{x}_1, \bar{p}\rangle \langle \bar{x}_2, \bar{p}|, \quad (\text{B.7})$$

and a similar calculation leads to the integer position operator \hat{N} . If we now multiply \hat{x} with \hat{M} we obtain

$$\hat{x}\hat{M} = \frac{i\ell}{2\pi} \iint_{-\ell/2}^{\ell/2} d\bar{x}_1 d\bar{x}_2 \int_{-\pi/\ell}^{\pi/\ell} d\bar{p} \bar{x}_1 e^{i\bar{p}(\bar{x}_1 - \bar{x}_2)} \left. \frac{d\delta(\bar{x}_1 - \bar{x})}{d\bar{x}} \right|_{\bar{x}=\bar{x}_2} |\bar{x}_1, \bar{p}\rangle \langle \bar{x}_2, \bar{p}|. \quad (\text{B.8})$$

Further on, in order to derive the commutator relation (B.1) we calculate the action of $\hat{x}\hat{M}$ on an arbitrary state $|\Psi\rangle = \int_{-\ell/2}^{\ell/2} d\bar{x} \int_{-\pi/\ell}^{\pi/\ell} d\bar{p} \Psi(\bar{x}, \bar{p}) |\bar{x}, \bar{p}\rangle$, yielding:

$$\hat{x}\hat{M}|\Psi\rangle = \int_{-\ell/2}^{\ell/2} d\bar{x}_1 \int_{-\pi/\ell}^{\pi/\ell} d\bar{p} \left[\frac{i\ell}{2\pi} \bar{x}_1 \int_{-\ell/2}^{\ell/2} d\bar{x}_2 e^{i\bar{p}(\bar{x}_1 - \bar{x}_2)} \left. \frac{d\delta(\bar{x}_1 - \bar{x})}{d\bar{x}} \right|_{\bar{x}=\bar{x}_2} \Psi(\bar{x}_2, \bar{p}) \right] |\bar{x}_1, \bar{p}\rangle \quad (\text{B.9})$$

and the corresponding modular wave function reads:

$$\begin{aligned} \langle \bar{x}_1, \bar{p} | \hat{x}\hat{M} | \Psi \rangle &= \frac{i\ell}{2\pi} \bar{x}_1 \int_{-\ell/2}^{\ell/2} d\bar{x}_2 e^{i\bar{p}(\bar{x}_1 - \bar{x}_2)} \left. \frac{d\delta(\bar{x}_1 - \bar{x})}{d\bar{x}} \right|_{\bar{x}=\bar{x}_2} \Psi(\bar{x}_2, \bar{p}) \\ &= \frac{i\ell}{2\pi} \bar{x}_1 \underbrace{\left[e^{i\bar{p}(\bar{x}_1 - \frac{\ell}{2})} \Psi\left(\frac{\ell}{2}, \bar{p}\right) \delta\left(\bar{x}_1 - \frac{\ell}{2}\right) - e^{i\bar{p}(\bar{x}_1 + \frac{\ell}{2})} \Psi\left(-\frac{\ell}{2}, \bar{p}\right) \delta\left(\bar{x}_1 + \frac{\ell}{2}\right) \right]}_{=0} \\ &\quad - \frac{i\ell}{2\pi} \bar{x}_1 \left[(-i)\bar{p}\Psi(\bar{x}_1, \bar{p}) + \left. \frac{d\Psi(\bar{x}, \bar{p})}{d\bar{x}} \right|_{\bar{x}=\bar{x}_1} \right] \\ &= -\frac{\ell}{2\pi} \bar{x}_1 \bar{p} \Psi(\bar{x}_1, \bar{p}) - \frac{i\ell}{2\pi} \bar{x}_1 \left. \frac{d\Psi(\bar{x}, \bar{p})}{d\bar{x}} \right|_{\bar{x}=\bar{x}_1}, \end{aligned} \quad (\text{B.10})$$

where in the first step we used partial integration and in the second step the quasi-periodicity condition (III.42). Equivalently, the second term of the commutator becomes

$$\begin{aligned} \langle \bar{x}_1, \bar{p} | \hat{M}\hat{x} | \Psi \rangle &= \frac{i\ell^2}{2\pi} \delta\left(\bar{x}_1 - \frac{\ell}{2}\right) \Psi\left(\frac{\ell}{2}, \bar{p}\right) + \Psi(\bar{x}_1, \bar{p}) \\ &\quad - \frac{\ell}{2\pi} \bar{x}_1 \bar{p} \Psi(\bar{x}_1, \bar{p}) - \frac{i\ell}{2\pi} \bar{x}_1 \left. \frac{d\Psi(\bar{x}, \bar{p})}{d\bar{x}} \right|_{\bar{x}=\bar{x}_1}, \end{aligned} \quad (\text{B.11})$$

and together with Eq. (B.10) we obtain

$$\langle \bar{x}_1, \bar{p} | [\hat{x}, \hat{M}] | \Psi \rangle = \frac{i\ell}{2\pi} \left[\Psi(\bar{x}_1, \bar{p}) - \ell \delta(\bar{x}_1 - \frac{\ell}{2}) \Psi(\frac{\ell}{2}, \bar{p}) \right], \quad (\text{B.12})$$

what yields the commutator relation (B.1). The second relation (B.2) can be shown with an analogous calculation.

B.2 Bound on expectation values of readout observables

In this Appendix we will summarize some more details of mathematical derivations made in Sec. III.3. Let us start by reproducing the definition of our modular readout observables:

$$\hat{\Gamma}_\beta = \int_{-\ell/4}^{\ell/4} d\bar{x} \int_{-\pi/\ell}^{\pi/\ell} d\bar{p} \zeta_\beta(\bar{x}, \bar{p}) \hat{\sigma}_\beta(\bar{x}, \bar{p}), \quad \beta = x, y, z \quad (\text{B.13})$$

where $\zeta_\beta(\bar{x}, \bar{p})$ are arbitrary real functions with domain $[-\ell/4, \ell/4] \times [-\pi/\ell, \pi/\ell]$, and the operators $\hat{\sigma}_\beta(\bar{x}, \bar{p})$ are defined as in Eqs. (III.84), (III.85) and (III.87). Next, the matrix elements of the operators (III.84), (III.85) and (III.87) in the modular basis read:

$$\begin{aligned} \langle \bar{x}', \bar{p}' | \hat{\sigma}_z(\bar{x}_0, \bar{p}_0) | \bar{x}, \bar{p} \rangle &= \delta(\bar{p} - \bar{p}_0) \delta(\bar{p}' - \bar{p}_0) \\ &\times \left[\delta(\bar{x} - \bar{x}_0) \delta(\bar{x}' - \bar{x}_0) \pm \delta(\bar{x} - \frac{\ell}{2} - \bar{x}_0) \delta(\bar{x}' - \frac{\ell}{2} - \bar{x}_0) \right], \end{aligned} \quad (\text{B.14})$$

$$\begin{aligned} \langle \bar{x}', \bar{p}' | \hat{\sigma}_x(\bar{x}_0, \bar{p}_0) | \bar{x}, \bar{p} \rangle &= \delta(\bar{p} - \bar{p}_0) \delta(\bar{p}' - \bar{p}_0) \\ &\times \left[\delta(\bar{x}' - \bar{x}_0) \delta(\bar{x} - \frac{\ell}{2} - \bar{x}_0) e^{-i\bar{p}\ell/2} + \delta(\bar{x}' - \frac{\ell}{2} - \bar{x}_0) \delta(\bar{x} - \bar{x}_0) e^{i\bar{p}\ell/2} \right], \end{aligned} \quad (\text{B.15})$$

$$\begin{aligned} \langle \bar{x}', \bar{p}' | \hat{\sigma}_y(\bar{x}_0, \bar{p}_0) | \bar{x}, \bar{p} \rangle &= -i \delta(\bar{p} - \bar{p}_0) \delta(\bar{p}' - \bar{p}_0) \\ &\times \left[\delta(\bar{x}' - \bar{x}_0) \delta(\bar{x} - \frac{\ell}{2} - \bar{x}_0) e^{-i\bar{p}\ell/2} - \delta(\bar{x}' - \frac{\ell}{2} - \bar{x}_0) \delta(\bar{x} - \bar{x}_0) e^{i\bar{p}\ell/2} \right]. \end{aligned} \quad (\text{B.16})$$

Now, using Eqs. (III.95)-(III.98), we can show that the (\bar{x}, \bar{p}) -dependent Pauli matrices $\sigma_\alpha(\bar{x}, \bar{p})$, with $\alpha = x, y, z$, fulfill the relation:

$$\hat{\sigma}_\alpha(\bar{x}, \bar{p}) \hat{\sigma}_\beta(\bar{x}', \bar{p}') = \delta(\bar{x}' - \bar{x}) \delta(\bar{p}' - \bar{p}) \left[i \sum_{\gamma=x,y,z} \varepsilon_{\alpha\beta\gamma} \hat{\sigma}_\gamma(\bar{x}, \bar{p}) + \delta_{\alpha,\beta} \mathbb{1}(\bar{x}, \bar{p}) \right] \quad (\text{B.17})$$

where $\alpha, \beta = x, y, z$ and $\mathbb{1}(\bar{x}, \bar{p}) = \|\bar{x}, \bar{p}\| \langle \bar{x}, \bar{p} | + \|\bar{x} + \ell/2, \bar{p}\| \langle \bar{x} + \ell/2, \bar{p} |$. The relation (III.95) resembles the one of a real Pauli algebra, which was given in Eq. (II.6), with additional delta functions ensuring that the products of Pauli operators corresponding to different subspaces, labeled by (\bar{x}, \bar{p}) and (\bar{x}', \bar{p}') , respectively, vanish. Further on, we can calculate the expectation value of the observables (III.94) with respect to an

arbitrary CV state expressed in the modular representation (III.72), yielding:

$$\begin{aligned}
\langle \hat{\Gamma}_x \rangle &= \iiint_{-\ell/4}^{\ell/4} d\bar{x} d\bar{x}_1 d\bar{x}_2 \iint_{-\pi/\ell}^{\pi/\ell} d\bar{p} d\bar{p}_1 d\bar{p}_2 \zeta_x(\bar{x}, \bar{p}) f^*(\bar{x}_1, \bar{p}_1) f(\bar{x}_2, \bar{p}_2) \\
&\quad \times \langle \Psi(\bar{x}_1, \bar{p}_1) | \hat{\sigma}_x(\bar{x}, \bar{p}) | \Psi(\bar{x}_2, \bar{p}_2) \rangle \\
&= \iiint_{-\ell/4}^{\ell/4} d\bar{x} d\bar{x}_1 d\bar{x}_2 \iint_{-\pi/\ell}^{\pi/\ell} d\bar{p} d\bar{p}_1 d\bar{p}_2 \zeta_x(\bar{x}, \bar{p}) f^*(\bar{x}_1, \bar{p}_1) f(\bar{x}_2, \bar{p}_2) \\
&\quad \times \left[\cos\left(\frac{\theta(\bar{x}_1, \bar{p}_1)}{2}\right) \sin\left(\frac{\theta(\bar{x}_2, \bar{p}_2)}{2}\right) e^{\phi(\bar{x}_2, \bar{p}_2)} + \cos\left(\frac{\theta(\bar{x}_2, \bar{p}_2)}{2}\right) \sin\left(\frac{\theta(\bar{x}_1, \bar{p}_1)}{2}\right) e^{\phi(\bar{x}_1, \bar{p}_1)} \right] \\
&\quad \times \delta(\bar{x}_1 - \bar{x}) \delta(\bar{x} - \bar{x}_2) \delta(\bar{p}_1 - \bar{p}) \delta(\bar{p} - \bar{p}_2) \\
&= \int_{-\ell/4}^{\ell/4} d\bar{x} \int_{-\pi/\ell}^{\pi/\ell} d\bar{p} \zeta_x(\bar{x}, \bar{p}) |f(\bar{x}, \bar{p})|^2 2 \cos\left(\frac{\theta(\bar{x}, \bar{p})}{2}\right) \sin\left(\frac{\theta(\bar{x}, \bar{p})}{2}\right) \cos(\phi(\bar{x}, \bar{p})) \\
&= \int_{-\ell/4}^{\ell/4} d\bar{x} \int_{-\pi/\ell}^{\pi/\ell} d\bar{p} \zeta_x(\bar{x}, \bar{p}) |f(\bar{x}, \bar{p})|^2 \sin(\theta(\bar{x}, \bar{p})) \cos(\phi(\bar{x}, \bar{p})), \tag{B.18}
\end{aligned}$$

In the second step of the computation (III.99) we dropped cross terms that are proportional to products of delta functions, such as $\delta(\bar{x}_1 + \ell/2 - \bar{x})\delta(\bar{x} - \bar{x}_2)$. The latter are nonzero only in a single point (set of measure zero) and thus vanish upon integration of \bar{x}_1 and \bar{x}_2 over the interval $[-\ell/4, \ell/4]$. Equivalently, the expectation values of the observables $\hat{\Gamma}_y$ and $\hat{\Gamma}_z$ read:

$$\langle \hat{\Gamma}_y \rangle = \int_{-\ell/4}^{\ell/4} d\bar{x} \int_{-\pi/\ell}^{\pi/\ell} d\bar{p} \zeta_y(\bar{x}, \bar{p}) |f(\bar{x}, \bar{p})|^2 \sin(\theta(\bar{x}, \bar{p})) \sin(\phi(\bar{x}, \bar{p})), \tag{B.19}$$

$$\langle \hat{\Gamma}_z \rangle = \int_{-\ell/4}^{\ell/4} d\bar{x} \int_{-\pi/\ell}^{\pi/\ell} d\bar{p} \beta_z(\bar{x}, \bar{p}) |f(\bar{x}, \bar{p})|^2 \cos(\theta(\bar{x}, \bar{p})). \tag{B.20}$$

Or, we can write:

$$\langle \hat{\Gamma} \rangle = \int_{-\ell/4}^{\ell/4} d\bar{x} \int_{-\pi/\ell}^{\pi/\ell} d\bar{p} |f(\bar{x}, \bar{p})|^2 (\zeta(\bar{x}, \bar{p}) \cdot \mathbf{v}(\bar{x}, \bar{p})), \tag{B.21}$$

where $\zeta(\bar{x}, \bar{p}) = (\zeta_x(\bar{x}, \bar{p}), \zeta_y(\bar{x}, \bar{p}), \zeta_z(\bar{x}, \bar{p}))^T$, and

$$\begin{aligned}
\mathbf{v}(\bar{x}, \bar{p}) &= (v_x(\bar{x}, \bar{p}), v_y(\bar{x}, \bar{p}), v_z(\bar{x}, \bar{p}))^T \\
&= (\sin(\theta(\bar{x}, \bar{p})) \cos(\phi(\bar{x}, \bar{p})), \sin(\theta(\bar{x}, \bar{p})) \sin(\phi(\bar{x}, \bar{p})), \cos(\theta(\bar{x}, \bar{p})))^T. \tag{B.22}
\end{aligned}$$

Further on, we show that the sum over the squares of the expectation values (III.99),

Bibliography

- Abouraddy, A. F., Yarnall, T., Saleh, B. E. A., and Teich, M. C. *Violation of Bell's inequality with continuous spatial variables*. Physical Review A **75**, 052114 (2007).
- Abouraddy, A. F., Yarnall, T. M., Di Giuseppe, G., Teich, M. C., and Saleh, B. E. A. *Encoding arbitrary four-qubit states in the spatial parity of a photon pair*. Physical Review A **85**, 062317 (2012).
- Adesso, G. and Illuminati, F. *Entanglement in continuous-variable systems: recent advances and current perspectives*. Journal of Physics A: Mathematical and Theoretical **40**, 7821 (2007).
- Aharonov, Y., Pendleton, H., and Petersen, A. *Modular variables in quantum theory* **2**, 213 (1969).
- Albert, V. V., Shu, C., Krastanov, S., Shen, C., Liu, R.-B., Yang, Z.-B., Schoelkopf, R. J., Mirrahimi, M., Devoret, M. H., and Jiang, L. *Holonomic Quantum Control with Continuous Variable Systems*. Physical Review Letters **116**, 140502 (2016).
- Ali-Khan, I., Broadbent, C. J., and Howell, J. C. *Large-Alphabet Quantum Key Distribution Using Energy-Time Entangled Bipartite States*. Physical Review Letters **98**, 060503 (2007).
- Alicki, R. and Lendi, K. *Quantum dynamical semigroups and applications*. Lectures Notes in Physics (Springer, Berlin, 2007).
- Allen, L., Barnett, S., and Padgett, M. *Optical Angular Momentum*. Optics & Optoelectronics (Taylor & Francis, 2003).
- Amselem, E., Danielsen, L. E., López-Tarrida, A. J., Portillo, J. R., Bourennane, M., and Cabello, A. *Experimental Fully Contextual Correlations*. Physical Review Letters **108**, 200405 (2012).
- Amselem, E., Rådmark, M., Bourennane, M., and Cabello, A. *State-Independent Quantum Contextuality with Single Photons*. Physical Review Letters **103**, 160405 (2009).
- Arndt, M., Dörre, N., Eibenberger, S., Haslinger, P., Rodewald, J., Hornberger, K., Nimmrichter, S., and Mayor, M. *Matter wave interferometry with composite quantum objects*. In G. M. Tino and M. A. Kasevich, editors, *Atom Interferometry*, volume 188, 89 – 141 (IOS Press, 2014).
- Arora, A. S. and Asadian, A. *Proposal for a macroscopic test of local realism with phase-space measurements*. Physical Review A **92**, 062107 (2015).

- Asadian, A., Brukner, C., and Rabl, P. *Probing Macroscopic Realism via Ramsey Correlation Measurements*. Physical Review Letters **112**, 190402 (2014).
- Asadian, A., Budroni, C., Steinhoff, F. E. S., Rabl, P., and Gühne, O. *Contextuality in Phase Space*. Physical Review Letters **114**, 250403 (2015).
- Aspden, R. S., Tasca, D. S., Boyd, R. W., and Padgett, M. J. *EPR-based ghost imaging using a single-photon-sensitive camera*. New Journal of Physics **15**, 073032 (2013).
- Aspect, A., Dalibard, J., and Roger, G. *Experimental Test of Bell's Inequalities Using Time-Varying Analyzers*. Physical Review Letters **49**, 1804 (1982a).
- Aspect, A., Grangier, P., and Roger, G. *Experimental Tests of Realistic Local Theories via Bell's Theorem*. Physical Review Letters **47**, 460 (1981).
- Aspect, A., Grangier, P., and Roger, G. *Experimental Realization of Einstein-Podolsky-Rosen-Bohm Gedankenexperiment: A New Violation of Bell's Inequalities*. Physical Review Letters **49**, 91 (1982b).
- Badziąg, P., Bengtsson, I., Cabello, A., and Pitowsky, I. *Universality of State-Independent Violation of Correlation Inequalities for Noncontextual Theories*. Physical Review Letters **103**, 050401 (2009).
- Banaszek, K., Radzewicz, C., Wódkiewicz, K., and Krasiński, J. S. *Direct measurement of the Wigner function by photon counting*. Physical Review A **60**, 674 (1999).
- Banaszek, K. and Wódkiewicz, K. *Nonlocality of the Einstein-Podolsky-Rosen state in the Wigner representation*. Physical Review A **58**, 4345 (1998).
- Banaszek, K. and Wódkiewicz, K. *Testing Quantum Nonlocality in Phase Space*. Physical Review Letters **82**, 2009 (1999).
- Barrett, J. *Nonsequential positive-operator-valued measurements on entangled mixed states do not always violate a Bell inequality*. Physical Review A **65**, 042302 (2002).
- Barros, M. R., Ketterer, A., Fariás, O. J., de Melo, F., Milman, P., and Walborn, S. P. *Violating D -dimensional Bell Inequalities with Entangled Quantum Carpets*. in preparation (2016).
- Barut, A. O. and Meystre, P. *A classical model of EPR experiment with quantum mechanical correlations and bell inequalities*. Physics Letters A **105**, 458 (1984).
- Bell, J. S. *On the Einstein-Podolsky-Rosen paradox*. Physics **1**, 195 (1964).
- Bell, J. S. *On the Problem of Hidden Variables in Quantum Mechanics*. Reviews of Modern Physics **38**, 447 (1966).
- Berry, M. V. and Klein, S. *Integer, fractional and fractal Talbot effects*. Journal of Modern Optics **43**, 2139 (1996).
- Blais, A., Huang, R.-S., Wallraff, A., Girvin, S. M., and Schoelkopf, R. J. *Cavity quantum electrodynamics for superconducting electrical circuits: An architecture for quantum computation*. Physical Review A **69**, 062320 (2004).

- Bonneau, M., Ruaudel, J., Lopes, R., Jaskula, J.-C., Aspect, A., Boiron, D., and Westbrook, C. I. *Tunable source of correlated atom beams*. Physical Review A **87**, 061603 (2013).
- Brask, J. B., Rigas, I., Polzik, E. S., Andersen, U. L., and Sørensen, A. S. *Hybrid Long-Distance Entanglement Distribution Protocol*. Physical Review Letters **105**, 160501 (2010).
- Braunstein, S. L. *Squeezing as an irreducible resource*. Physical Review A **71**, 055801 (2005).
- Braunstein, S. L. and Kimble, H. J. *Teleportation of Continuous Quantum Variables*. Physical Review Letters **80**, 869 (1998).
- Braunstein, S. L. and van Loock, P. *Quantum information with continuous variables*. Reviews of Modern Physics **77**, 513 (2005).
- Breuer, H. and Petruccione, F. *The Theory of Open Quantum Systems* (Oxford University Press, 2007).
- Brukner, Č., Żukowski, M., Pan, J.-W., and Zeilinger, A. *Bell's Inequalities and Quantum Communication Complexity*. Physical Review Letters **92**, 127901 (2004).
- Brunner, N., Cavalcanti, D., Pironio, S., Scarani, V., and Wehner, S. *Bell nonlocality*. Reviews of Modern Physics **86**, 419 (2014).
- Buhrman, H., Cleve, R., Massar, S., and de Wolf, R. *Nonlocality and communication complexity*. Reviews of Modern Physics **82**, 665 (2010).
- Busch, P. and Lahti, P. J. *To what extent do position and momentum commute?* Physics Letters A **115**, 259 (1986).
- Busch, P., Schonbek, T. P., and Schroeck, F. E. *Quantum observables: Compatibility versus commutativity and maximal information*. Journal of Mathematical Physics **28**, 2866 (1987).
- Cabello, A. *Experimentally Testable State-Independent Quantum Contextuality*. Physical Review Letters **101**, 210401 (2008).
- Carrat, V., Cabrera-Gutiérrez, C., Jacquy, M., Tabosa, J. W., de Lesegno, B. V., and Pruvost, L. *Long-distance channeling of cold atoms exiting a 2D magneto-optical trap by a Laguerre-Gaussian laser beam*. Opt. Lett. **39**, 719 (2014).
- Carvalho, M. A. D., Ferraz, J., Borges, G. F., de Assis, P. L., Pádua, S., and Walborn, S. P. *Experimental observation of quantum correlations in modular variables*. Physical Review A **86**, 032332 (2012).
- Case, W. B., Tomandl, M., Deachapunya, S., and Arndt, M. *Realization of optical carpets in the Talbot and Talbot-Lau configurations*. Optics Express **17**, 20966 (2009).
- Cavalcanti, D. and Skrzypczyk, P. *Quantum steering: a short review with focus on semidefinite programming*. ArXiv e-prints arXiv:1604.00501 (2016).

- Cavalcanti, E. G., Foster, C. J., Reid, M. D., and Drummond, P. D. *Bell Inequalities for Continuous-Variable Correlations*. Physical Review Letters **99**, 210405 (2007).
- Cavalcanti, E. G., He, Q. Y., Reid, M. D., and Wiseman, H. M. *Unified criteria for multipartite quantum nonlocality*. Physical Review A **84**, 032115 (2011).
- Chen, Y., Neill, C., Roushan, P., Leung, N., Fang, M., Barends, R., Kelly, J., Campbell, B., Chen, Z., Chiaro, B., Dunsworth, A., Jeffrey, E., Megrant, A., Mutus, J. Y., O'Malley, P. J. J., Quintana, C. M., Sank, D., Vainsencher, A., Wenner, J., White, T. C., Geller, M. R., Cleland, A. N., and Martinis, J. M. *Qubit Architecture with High Coherence and Fast Tunable Coupling*. Physical Review Letters **113**, 220502 (2014).
- Chen, Z.-B., Pan, J.-W., Hou, G., and Zhang, Y.-D. *Maximal Violation of Bell's Inequalities for Continuous Variable Systems*. Physical Review Letters **88**, 040406 (2002).
- Christensen, B. G., McCusker, K. T., Altepeter, J. B., Calkins, B., Gerrits, T., Lita, A. E., Miller, A., Shalm, L. K., Zhang, Y., Nam, S. W., Brunner, N., Lim, C. C. W., Gisin, N., and Kwiat, P. G. *Detection-Loophole-Free Test of Quantum Nonlocality, and Applications*. Physical Review Letters **111**, 130406 (2013).
- Clauser, J. F., Horne, M. A., Shimony, A., and Holt, R. A. *Proposed Experiment to Test Local Hidden-Variable Theories*. Physical Review Letters **23**, 880 (1969).
- Cohen-Tannoudji, C., Diu, B., and Laloë, F. *Mécanique quantique I*. Collection Enseignement des sciences (Hermann, 1998).
- Collins, D., Gisin, N., Linden, N., Massar, S., and Popescu, S. *Bell Inequalities for Arbitrarily High-Dimensional Systems*. Physical Review Letters **88**, 040404 (2002).
- Curtright, T. L., Fairlie, D. B., and Zachos, C. K. *A Compact Formula for Rotations as Spin Matrix Polynomials* **10**, 084 (2014).
- D'Ambrosio, V., Herbauts, I., Amselem, E., Nagali, E., Bourennane, M., Sciarrino, F., and Cabello, A. *Experimental Implementation of a Kochen-Specker Set of Quantum Tests*. Physical Review X **3**, 011012 (2013).
- D'Angelo, M., Kim, Y.-H., Kulik, S. P., and Shih, Y. *Identifying Entanglement Using Quantum Ghost Interference and Imaging*. Physical Review Letters **92**, 233601 (2004).
- Deleglise, S., Dotsenko, I., Sayrin, C., Bernu, J., Brune, M., Raimond, J.-M., and Haroche, S. *Reconstruction of non-classical cavity field states with snapshots of their decoherence*. Nature **455**, 510 (2008).
- Delfosse, N., Allard Guerin, P., Bian, J., and Raussendorf, R. *Wigner Function Negativity and Contextuality in Quantum Computation on Rebits*. Physical Review X **5**, 021003 (2015).
- Devoret, M. H. and Schoelkopf, R. J. *Superconducting Circuits for Quantum Information: An Outlook*. Science **339**, 1169 (2013).

- Duan, L.-M., Giedke, G., Cirac, J. I., and Zoller, P. *Inseparability Criterion for Continuous Variable Systems*. Physical Review Letters **84**, 2722 (2000).
- Einstein, A., Podolsky, B., and Rosen, N. *Can Quantum-Mechanical Description of Physical Reality Be Considered Complete?* Physical Review **47**, 777 (1935).
- Eisert, J. and Plenio, M. B. *Introduction to the basics of entanglement theory in continuous-variable systems*. International Journal of Quantum Information **01**, 479 (2003).
- Ekert, A. K. *Quantum cryptography based on Bell's theorem*. Physical Review Letters **67**, 661 (1991).
- Englert, B.-G., Lee, K. L., Mann, A., and Revzen, M. *Periodic and discrete Zak bases*. Journal of Physics A: Mathematical and General **39**, 1669 (2006).
- Erhard, M., Qassim, H., Mand, H., Karimi, E., and Boyd, R. W. *Real-time imaging of spin-to-orbital angular momentum hybrid remote state preparation*. Physical Review A **92**, 022321 (2015).
- Fariás, O. J., de Melo, F., Milman, P., and Walborn, S. P. *Quantum information processing by weaving quantum Talbot carpets*. Physical Review A **91**, 062328 (2015).
- Freedman, S. J. and Clauser, J. F. *Experimental Test of Local Hidden-Variable Theories*. Physical Review Letters **28**, 938 (1972).
- Furusawa, A., Sørensen, J. L., Braunstein, S. L., Fuchs, C. A., Kimble, H. J., and Polzik, E. S. *Unconditional Quantum Teleportation*. Science **282**, 706 (1998).
- García-Patrón, R., Fiurášek, J., Cerf, N. J., Wenger, J., Tualle-Brouiri, R., and Grangier, P. *Proposal for a Loophole-Free Bell Test Using Homodyne Detection*. Physical Review Letters **93**, 130409 (2004).
- Gisin, N. *Bell's inequality holds for all non-product states*. Physics Letters A **154**, 201 (1991).
- Gittsovich, O., Moroder, T., Asadian, A., Gühne, O., and Rabl, P. *Nonclassicality tests and entanglement witnesses for macroscopic mechanical superposition states*. Physical Review A **91**, 022114 (2015).
- Giustina, M., Mech, A., Ramelow, S., Wittmann, B., Kofler, J., Beyer, J., Lita, A., Calkins, B., Gerrits, T., Nam, S. W., Ursin, R., and Zeilinger, A. *Bell violation using entangled photons without the fair-sampling assumption*. Nature **497**, 227 (2013).
- Giustina, M., Versteegh, M. A. M., Wengerowsky, S., Handsteiner, J., Hochrainer, A., Phelan, K., Steinlechner, F., Kofler, J., Larsson, J.-Å., Abellán, C., Amaya, W., Pruneri, V., Mitchell, M. W., Beyer, J., Gerrits, T., Lita, A. E., Shalm, L. K., Nam, S. W., Scheidl, T., Ursin, R., Wittmann, B., and Zeilinger, A. *Significant-Loophole-Free Test of Bell's Theorem with Entangled Photons*. Physical Review Letters **115**, 250401 (2015).

- Glancy, S. and Knill, E. *Error analysis for encoding a qubit in an oscillator*. Physical Review A **73**, 012325 (2006).
- Gneiting, C. and Hornberger, K. *Detecting Entanglement in Spatial Interference*. Physical Review Letters **106**, 210501 (2011).
- Gneiting, C. and Hornberger, K. *Nonlocal Young tests with Einstein-Podolsky-Rosen-correlated particle pairs*. Physical Review A **88**, 013610 (2013).
- Gomes, R. M., Salles, A., Toscano, F., Souto Ribeiro, P. H., and Walborn, S. P. *Quantum entanglement beyond Gaussian criteria*. Proceedings of the National Academy of Sciences of the United States of America **106**, 21517 (2009).
- Gottesman, D. *Class of quantum error-correcting codes saturating the quantum Hamming bound*. Physical Review A **54**, 1862 (1996).
- Gottesman, D. *Stabilizer codes and quantum error correction*. Phd thesis, California Institute of Technology (1997).
- Gottesman, D. *The Heisenberg representation of quantum computers*. In *International Conference on Group Theoretic Methods in Physics*, 9807006 (1998).
- Gottesman, D. and Chuang, I. L. *Demonstrating the viability of universal quantum computation using teleportation and single-qubit operations*. Nature **402**, 390 (1999).
- Gottesman, D., Kitaev, A., and Preskill, J. *Encoding a qubit in an oscillator*. Physical Review A **64**, 012310 (2001).
- Grosshans, F. and Grangier, P. *Continuous Variable Quantum Cryptography Using Coherent States*. Physical Review Letters **88**, 057902 (2002).
- Grosshans, F., Van Assche, G., Wenger, J., Brouri, R., Cerf, N. J., and Grangier, P. *Quantum key distribution using gaussian-modulated coherent states*. Nature **421**, 238 (2003).
- Gu, M., Weedbrook, C., Menicucci, N. C., Ralph, T. C., and van Loock, P. *Quantum computing with continuous-variable clusters*. Physical Review A **79**, 062318 (2009).
- Gühne, O., Budroni, C., Cabello, A., Kleinmann, M., and Larsson, J.-A. *Bounding the quantum dimension with contextuality*. Physical Review A **89**, 062107 (2014).
- Gühne, O. and Tóth, G. *Entanglement detection*. Physics Reports **474**, 1 (2009).
- Gunter, G., Anappara, A. A., Hees, J., Sell, A., Biasiol, G., Sorba, L., De Liberato, S., Ciuti, C., Tredicucci, A., Leitenstorfer, A., and Huber, R. *Sub-cycle switch-on of ultrastrong light-matter interaction*. Nature **458**, 178 (2009).
- Haroche, S., Brune, M., and Raimond, J. M. *Measuring the photon number parity in a cavity: from light quantum jumps to the tomography of non-classical field states*. Journal of Modern Optics **54**, 2101 (2007).

- Hensen, B., Bernien, H., Dreau, A. E., Reiserer, A., Kalb, N., Blok, M. S., Ruitenber, J., Vermeulen, R. F. L., Schouten, R. N., Abellan, C., Amaya, W., Pruneri, V., Mitchell, M. W., Markham, M., Twitchen, D. J., Elkouss, D., Wehner, S., Taminiau, T. H., and Hanson, R. *Loophole-free Bell inequality violation using electron spins separated by 1.3 kilometres*. *Nature* **526**, 682 (2015).
- Hioe, F. T. and Eberly, J. H. *N -Level Coherence Vector and Higher Conservation Laws in Quantum Optics and Quantum Mechanics*. *Physical Review Letters* **47**, 838 (1981).
- Home, D. and Selleri, F. *Bell's theorem and the EPR paradox*. *La Rivista del Nuovo Cimento* (1978-1999) **14**, 1 (2008).
- Hor-Meyll, M., de Almeida, J. O., Lemos, G. B., Ribeiro, P. H. S., and Walborn, S. P. *Ancilla-Assisted Measurement of Photonic Spatial Correlations and Entanglement*. *Physical Review Letters* **112**, 053602 (2014).
- Horodecki, K., Horodecki, M., Horodecki, P., Horodecki, R., Pawłowski, M., and Bourennane, M. *Contextuality offers device-independent security*. *ArXiv e-prints* 1006.0468 (2010).
- Horodecki, M., Horodecki, P., and Horodecki, R. *Separability of mixed states: necessary and sufficient conditions*. *Physics Letters A* **223**, 1 (1996).
- Horodecki, P. *Mean of continuous variables observable via measurement on a single qubit*. *Physical Review A* **67**, 060101 (2003).
- Horodecki, R., Horodecki, P., Horodecki, M., and Horodecki, K. *Quantum entanglement*. *Reviews of Modern Physics* **81**, 865 (2009).
- Howard, M. and Vala, J. *Qudit versions of the qubit $\pi/8$ gate*. *Physical Review A* **86**, 022316 (2012).
- Howard, M., Wallman, J., Veitch, V., and Emerson, J. *Contextuality supplies the 'magic' for quantum computation*. *Nature* **510**, 351 (2014).
- Howell, J. C., Bennink, R. S., Bentley, S. J., and Boyd, R. W. *Realization of the Einstein-Podolsky-Rosen Paradox Using Momentum- and Position-Entangled Photons from Spontaneous Parametric Down Conversion*. *Physical Review Letters* **92**, 210403 (2004).
- Hudson, R. L. *When is the wigner quasi-probability density non-negative?* *Reports on Mathematical Physics* **6**, 249 (1974).
- Ioannou, L. M. and Travaglione, B. C. *Quantum separability and entanglement detection via entanglement-witness search and global optimization*. *Physical Review A* **73**, 052314 (2006).
- Jackson, J. *Classical Electrodynamics* (Wiley-VCH, Weinheim, 1998).
- Jeong, H. and Kim, M. S. *Efficient quantum computation using coherent states*. *Physical Review A* **65**, 042305 (2002).

- Jeong, H., Son, W., Kim, M. S., Ahn, D., and Brukner, Č. *Quantum nonlocality test for continuous-variable states with dichotomic observables*. Physical Review A **67**, 012106 (2003).
- Karimi, E., Leach, J., Slussarenko, S., Piccirillo, B., Marrucci, L., Chen, L., She, W., Franke-Arnold, S., Padgett, M. J., and Santamato, E. *Spin-orbit hybrid entanglement of photons and quantum contextuality*. Physical Review A **82**, 022115 (2010).
- Kent, A. *Causal quantum theory and the collapse locality loophole*. Physical Review A **72**, 012107 (2005).
- Ketterer, A., Keller, A., Coudreau, T., and Milman, P. *Testing the Clauser-Horne-Shimony-Holt inequality using observables with arbitrary spectrum*. Physical Review A **91**, 012106 (2015).
- Ketterer, A., Keller, A., Walborn, S. P., Coudreau, T., and Milman, P. *Quantum information processing in phase space: A modular variables approach*. Physical Review A **94**, 022325 (2016).
- Kheruntsyan, K. V. *Quantum Atom Optics with Fermions from Molecular Dissociation*. Physical Review Letters **96**, 110401 (2006).
- Kheruntsyan, K. V., Olsen, M. K., and Drummond, P. D. *Einstein-Podolsky-Rosen Correlations via Dissociation of a Molecular Bose-Einstein Condensate*. Physical Review Letters **95**, 150405 (2005).
- Kiesel, N., Schmid, C., Weber, U., Ursin, R., and Weinfurter, H. *Linear Optics Controlled-Phase Gate Made Simple*. Physical Review Letters **95**, 210505 (2005).
- Kimble, H. J. *The quantum internet*. Nature **453**, 1023 (2008).
- Kirchmair, G., Zahringer, F., Gerritsma, R., Kleinmann, M., Gühne, O., Cabello, A., Blatt, R., and Roos, C. F. *State-independent experimental test of quantum contextuality*. Nature **460**, 494 (2009).
- Kleinmann, M., Budroni, C., Larsson, J.-A., Gühne, O., and Cabello, A. *Optimal Inequalities for State-Independent Contextuality*. Physical Review Letters **109**, 250402 (2012).
- Knill, E., Laflamme, R., and Milburn, G. J. *A scheme for efficient quantum computation with linear optics*. Nature **409**, 46 (2001).
- Kochen, S. and Specker, E. P. *The Problem of Hidden Variables in Quantum Mechanics*. Journal of Mathematics and Mechanics **17**, 59 (1967).
- Kofler, J., Singh, M., Ebner, M., Keller, M., Kotyrba, M., and Zeilinger, A. *Einstein-Podolsky-Rosen correlations from colliding Bose-Einstein condensates*. Physical Review A **86**, 032115 (2012).
- Köhler, T., Góral, K., and Julienne, P. S. *Production of cold molecules via magnetically tunable Feshbach resonances*. Reviews of Modern Physics **78**, 1311 (2006).

- Kok, P., Munro, W. J., Nemoto, K., Ralph, T. C., Dowling, J. P., and Milburn, G. J. *Linear optical quantum computing with photonic qubits*. *Reviews of Modern Physics* **79**, 135 (2007).
- Kurizki, G., Bertet, P., Kubo, Y., Mølmer, K., Petrosyan, D., Rabl, P., and Schmiedmayer, J. *Quantum technologies with hybrid systems*. *Proceedings of the National Academy of Sciences* **112**, 3866 (2015).
- Lake, K., Weidt, S., Randall, J., Standing, E. D., Webster, S. C., and Hensinger, W. K. *Generation of spin-motion entanglement in a trapped ion using long-wavelength radiation*. *Physical Review A* **91**, 012319 (2015).
- Lambert, N., Johansson, R., and Nori, F. *Macrorealism inequality for optoelectromechanical systems*. *Physical Review B* **84**, 245421 (2011).
- Langford, N. K., Weinhold, T. J., Prevedel, R., Resch, K. J., Gilchrist, A., O'Brien, J. L., Pryde, G. J., and White, A. G. *Demonstration of a Simple Entangling Optical Gate and Its Use in Bell-State Analysis*. *Physical Review Letters* **95**, 210504 (2005).
- Lanyon, B. P., Barbieri, M., Almeida, M. P., Jennewein, T., Ralph, T. C., Resch, K. J., Pryde, G. J., O'Brien, J. L., Gilchrist, A., and White, A. G. *Simplifying quantum logic using higher-dimensional Hilbert spaces*. *Nat Phys* **5**, 134 (2009).
- Laversanne-Finot, A., Ketterer, A., Barros, M. R., Walborn, S. P., Coudreau, T., Keller, A., and Milman, P. *General conditions for maximal violation of non-contextuality in discrete and continuous variables*. *ArXiv e-prints arXiv:1512.03334* (2015).
- Laversanne-Finot, A., Ketterer, A., Barros, M. R., Walborn, S. P., Coudreau, T., Keller, A., and Milman, P. *Contextuality in a Peres—Mermin square using arbitrary operators*. *Journal of Physics: Conference Series* **701**, 012026 (2016).
- Lee, S.-W. and Jeong, H. *Near-deterministic quantum teleportation and resource-efficient quantum computation using linear optics and hybrid qubits*. *Physical Review A* **87**, 022326 (2013).
- Leibfried, D., Blatt, R., Monroe, C., and Wineland, D. *Quantum dynamics of single trapped ions*. *Reviews of Modern Physics* **75**, 281 (2003).
- Leonhardt, U. *Measuring the Quantum State of Light*. *Cambridge Studies in Modern Optics* (Cambridge University Press, 1997).
- Lloyd, S. *Almost Any Quantum Logic Gate is Universal*. *Physical Review Letters* **75**, 346 (1995).
- Lloyd, S. and Braunstein, S. L. *Quantum Computation over Continuous Variables*. *Physical Review Letters* **82**, 1784 (1999).
- van Loock, P. *Optical hybrid approaches to quantum information*. *Laser & Photonics Reviews* **5**, 167 (2011).

- van Loock, P., Munro, W. J., Nemoto, K., Spiller, T. P., Ladd, T. D., Braunstein, S. L., and Milburn, G. J. *Hybrid quantum computation in quantum optics*. Physical Review A **78**, 022303 (2008).
- van Loock, P., Weedbrook, C., and Gu, M. *Building Gaussian cluster states by linear optics*. Physical Review A **76**, 032321 (2007).
- Loudon, R. *The Quantum Theory of Light*. Oxford Science Publications (Oxford University Press, 2000).
- Lund, A. P., Ralph, T. C., and Haselgrove, H. L. *Fault-Tolerant Linear Optical Quantum Computing with Small-Amplitude Coherent States*. Physical Review Letters **100**, 030503 (2008).
- Lutterbach, L. and Davidovich, L. *Method for Direct Measurement of the Wigner Function in Cavity QED and Ion Traps*. Physical Review Letters **78**, 2547 (1997).
- Lvovsky, A. I. and Raymer, M. G. *Continuous-variable optical quantum-state tomography*. Reviews of Modern Physics **81**, 299 (2009).
- Machado, S., Milman, P., and Walborn, S. P. *Interferometric scheme for direct measurement of moments of transverse spatial variables of photons*. Physical Review A **87**, 053834 (2013).
- Mancini, S., Giovannetti, V., Vitali, D., and Tombesi, P. *Entangling Macroscopic Oscillators Exploiting Radiation Pressure*. Physical Review Letters **88**, 120401 (2002).
- Mandel, L. and Wolf, E. *Optical Coherence and Quantum Optics* (Cambridge University Press, 1995).
- Mark, M. J., Haller, E., Danzl, J. G., Lauber, K., Gustavsson, M., and Nägerl, H.-C. *Demonstration of the temporal matter-wave Talbot effect for trapped matter waves*. New Journal of Physics **13**, 085008 (2011).
- Marshall, K., Pooser, R., Siopsis, G., and Weedbrook, C. *Repeat-until-success cubic phase gate for universal continuous-variable quantum computation*. Physical Review A **91**, 032321 (2015).
- Menicucci, N. C. *Fault-Tolerant Measurement-Based Quantum Computing with Continuous-Variable Cluster States*. Physical Review Letters **112**, 120504 (2014).
- Menicucci, N. C., van Loock, P., Gu, M., Weedbrook, C., Ralph, T. C., and Nielsen, M. A. *Universal Quantum Computation with Continuous-Variable Cluster States*. Physical Review Letters **97**, 110501 (2006).
- Mermin, N. D. *The EPR Experiment—Thoughts about the “Loophole”a*. Annals of the New York Academy of Sciences **480**, 422 (1986).
- Mermin, N. D. *Simple unified form for the major no-hidden-variables theorems*. Physical Review Letters **65**, 3373 (1990).
- Messiah, A. *Quantenmechanik 2* (De Gruyter, Berlin, 1979).

- Messiah, A. *Quantenmechanik* (de Gruyter, Berlin, 1991).
- Milburn, G. J. *Quantum optical Fredkin gate*. Physical Review Letters **62**, 2124 (1989).
- Milman, P., Auffeves, A., Yamaguchi, F., Brune, M., Raimond, J. M., and Haroche, S. *A proposal to test Bell's inequalities with mesoscopic non-local states in cavity QED*. Eur. Phys. J. D **32**, 233 (2005).
- Monken, C. H., Ribeiro, P. H. S., and Pádua, S. *Transfer of angular spectrum and image formation in spontaneous parametric down-conversion*. Physical Review A **57**, 3123 (1998).
- Monroe, C., Meekhof, D. M., King, B. E., and Wineland, D. J. *A "Schrödinger Cat" Superposition State of an Atom*. Science **272**, 1131 (1996).
- Moreau, P.-A., Devaux, F., and Lantz, E. *Einstein-Podolsky-Rosen Paradox in Twin Images*. Physical Review Letters **113**, 160401 (2014).
- Moreira, S. V., Keller, A., Coudreau, T., and Milman, P. *Modeling Leggett-Garg-inequality violation*. Physical Review A **92**, 062132 (2015).
- Morin, O., Bancal, J.-D., Ho, M., Sekatski, P., D'Auria, V., Gisin, N., Laurat, J., and Sangouard, N. *Witnessing Trustworthy Single-Photon Entanglement with Local Homodyne Measurements*. Physical Review Letters **110**, 130401 (2013).
- Morin, O., Huang, K., Liu, J., Le Jeannic, H., Fabre, C., and Laurat, J. *Remote creation of hybrid entanglement between particle-like and wave-like optical qubits*. Nat Photon **8**, 570 (2014).
- Moussa, O., Ryan, C. A., Cory, D. G., and Laflamme, R. *Testing Contextuality on Quantum Ensembles with One Clean Qubit*. Physical Review Letters **104**, 160501 (2010).
- Muthukrishnan, A. and Stroud, C. R. *Multivalued logic gates for quantum computation*. Physical Review A **62**, 052309 (2000).
- Nagali, E., Sciarrino, F., De Martini, F., Marrucci, L., Piccirillo, B., Karimi, E., and Santamato, E. *Quantum Information Transfer from Spin to Orbital Angular Momentum of Photons*. Physical Review Letters **103**, 013601 (2009).
- Neves, L., Lima, G., Aguirre Gómez, J. G., Monken, C. H., Saavedra, C., and Pádua, S. *Generation of Entangled States of Qudits using Twin Photons*. Physical Review Letters **94**, 100501 (2005).
- Neves, L., Lima, G., Delgado, A., and Saavedra, C. *Hybrid photonic entanglement: Realization, characterization, and applications*. Physical Review A **80**, 042322 (2009).
- Nielsen, M. and Chuang, I. *Quantum Computation and Quantum Information* (Cambridge University Press, New York, 2000).
- Nowak, S., Kurtsiefer, C., Pfau, T., and David, C. *High-order Talbot fringes for atomic matter waves*. Opt. Lett. **22**, 1430 (1997).

- O'Brien, J. L., Pryde, G. J., White, A. G., Ralph, T. C., and Branning, D. *Demonstration of an all-optical quantum controlled-NOT gate*. *Nature* **426**, 264 (2003).
- Okamoto, R., Hofmann, H. F., Takeuchi, S., and Sasaki, K. *Demonstration of an Optical Quantum Controlled-NOT Gate without Path Interference*. *Physical Review Letters* **95**, 210506 (2005).
- Ourjoumtsev, A., Jeong, H., Tualle-Brouiri, R., and Grangier, P. *Generation of optical /'Schrodinger cats/' from photon number states*. *Nature* **448**, 784 (2007).
- Ourjoumtsev, A., Tualle-Brouiri, R., Laurat, J., and Grangier, P. *Generating Optical Schrödinger Kittens for Quantum Information Processing*. *Science* **312**, 83 (2006).
- Ozaktas, H., Kutay, M., and Zalevsky, Z. *The Fractional Fourier Transform: With Applications in Optics and Signal Processing*. Wiley Series in Pure and Applied Optics (Wiley, 2001).
- Paris, M. G. A. *Displacement operator by beam splitter*. *Physics Letters A* **217**, 78 (1996).
- Percival, I. C. *Quantum transfer functions, weak nonlocality and relativity*. *Physics Letters A* **244**, 495 (1998).
- Peres, A. *Incompatible results of quantum measurements*. *Physics Letters A* **151**, 107 (1990).
- Peres, A. *All the Bell Inequalities*. *Foundations of Physics* **29**, 589 (1999).
- Perrin, A., Chang, H., Krachmalnicoff, V., Schellekens, M., Boiron, D., Aspect, A., and Westbrook, C. I. *Observation of Atom Pairs in Spontaneous Four-Wave Mixing of Two Colliding Bose-Einstein Condensates*. *Physical Review Letters* **99**, 150405 (2007).
- Pironio, S. *Lifting Bell inequalities*. *Journal of Mathematical Physics* **46**, 062112 (2005).
- Pitowsky, I. *The range of quantum probability*. *Journal of Mathematical Physics* **27**, 1556 (1986).
- Plastino, Á. R. and Cabello, A. *State-independent quantum contextuality for continuous variables*. *Physical Review A* **82**, 022114 (2010).
- Popescu, S. and Rohrlich, D. *Quantum nonlocality as an axiom*. *Foundations of Physics* **24**, 379 (1994).
- Pütz, G., Martin, A., Gisin, N., Aktas, D., Fedrici, B., and Tanzilli, S. *Quantum Nonlocality with Arbitrary Limited Detection Efficiency*. *Physical Review Letters* **116**, 010401 (2016).
- Rabl, P., Cappellaro, P., Dutt, M. V. G., Jiang, L., Maze, J. R., and Lukin, M. D. *Strong magnetic coupling between an electronic spin qubit and a mechanical resonator*. *Physical Review B* **79**, 041302 (2009).

- Raeisi, S., Kurzyński, P., and Kaszlikowski, D. *Entropic Tests of Multipartite Nonlocality and State-Independent Contextuality*. Physical Review Letters **114**, 200401 (2015).
- Ralph, T. C., Gilchrist, A., Milburn, G. J., Munro, W. J., and Glancy, S. *Quantum computation with optical coherent states*. Physical Review A **68**, 042319 (2003).
- Rastall, P. *Locality, Bell's theorem, and quantum mechanics*. Foundations of Physics **15**, 963 (1985).
- Raussendorf, R. *Contextuality in measurement-based quantum computation*. Physical Review A **88**, 022322 (2013).
- Raussendorf, R. and Briegel, H. J. *A One-Way Quantum Computer*. Physical Review Letters **86**, 5188 (2001).
- Raussendorf, R., Browne, D. E., Delfosse, N., Okay, C., and Bermejo-Vega, J. *Contextuality as a resource for qubit quantum computation*. ArXiv e-prints arXiv:1511.08506 (2015).
- Rayleigh, L. XXV. *On copying diffraction-gratings, and on some phenomena connected therewith*. Philosophical Magazine Series 5 **11**, 196 (1881).
- Reid, M. D., Drummond, P. D., Bowen, W. P., Cavalcanti, E. G., Lam, P. K., Bachor, H. A., Andersen, U. L., and Leuchs, G. *Colloquium: The Einstein-Podolsky-Rosen paradox: From concepts to applications*. Reviews of Modern Physics **81**, 1727 (2009).
- de Riedmatten, H., Marcikic, I., Scarani, V., Tittel, W., Zbinden, H., and Gisin, N. *Tailoring photonic entanglement in high-dimensional Hilbert spaces*. Physical Review A **69**, 050304 (2004).
- Rigas, J., Gühne, O., and Lütkenhaus, N. *Entanglement verification for quantum-key-distribution systems with an underlying bipartite qubit-mode structure*. Physical Review A **73**, 012341 (2006).
- Roy, S. M. *Multipartite Separability Inequalities Exponentially Stronger than Local Reality Inequalities*. Physical Review Letters **94**, 010402 (2005).
- Sangouard, N., Simon, C., Gisin, N., Laurat, J., Tualle-Brouri, R., and Grangier, P. *Quantum repeaters with entangled coherent states*. J. Opt. Soc. Am. B **27**, A137 (2010).
- Scarani, V., Bechmann-Pasquinucci, H., Cerf, N. J., Dušek, M., Lütkenhaus, N., and Peev, M. *The security of practical quantum key distribution*. Reviews of Modern Physics **81**, 1301 (2009).
- Scheidl, T., Ursin, R., Kofler, J., Ramelow, S., Ma, X.-S., Herbst, T., Ratschbacher, L., Fedrizzi, A., Langford, N. K., Jennewein, T., and Zeilinger, A. *Violation of local realism with freedom of choice*. Proceedings of the National Academy of Sciences **107**, 19708 (2010).

- Shalm, L. K., Meyer-Scott, E., Christensen, B. G., Bierhorst, P., Wayne, M. A., Stevens, M. J., Gerrits, T., Glancy, S., Hamel, D. R., Allman, M. S., Coakley, K. J., Dyer, S. D., Hodge, C., Lita, A. E., Verma, V. B., Lambrocco, C., Tortorici, E., Migdall, A. L., Zhang, Y., Kumor, D. R., Farr, W. H., Marsili, F., Shaw, M. D., Stern, J. A., Abellán, C., Amaya, W., Pruneri, V., Jennewein, T., Mitchell, M. W., Kwiatt, P. G., Bienfang, J. C., Mirin, R. P., Knill, E., and Nam, S. W. *Strong Loophole-Free Test of Local Realism**. Physical Review Letters **115**, 250402 (2015).
- Simon, C. and Irvine, W. T. M. *Robust Long-Distance Entanglement and a Loophole-Free Bell Test with Ions and Photons*. Physical Review Letters **91**, 110405 (2003).
- Simon, R. *Peres-Horodecki Separability Criterion for Continuous Variable Systems*. Physical Review Letters **84**, 2726 (2000).
- Stoler, D. *Operator methods in physical optics*. J. Opt. Soc. Am. **71**, 334 (1981).
- Tasca, D. S., Gomes, R. M., Toscano, F., Souto Ribeiro, P. H., and Walborn, S. P. *Continuous-variable quantum computation with spatial degrees of freedom of photons*. Physical Review A **83**, 052325 (2011).
- Tasca, D. S., Walborn, S. P., Souto Ribeiro, P. H., and Toscano, F. *Detection of transverse entanglement in phase space*. Physical Review A **78**, 010304 (2008).
- Tasca, D. S., Walborn, S. P., Souto Ribeiro, P. H., Toscano, F., and Pellat-Finiet, P. *Propagation of transverse intensity correlations of a two-photon state*. Physical Review A **79**, 033801 (2009).
- Terhal, B. M. *Natural Computing Detecting quantum entanglement*. Theoretical Computer Science **287**, 313 (2002).
- Tollaksen, J., Aharonov, Y., Casher, A., Kaufherr, T., and Nussinov, S. *Quantum interference experiments, modular variables and weak measurements*. New Journal of Physics **12**, 013023 (2010).
- Tóth, G. and Gühne, O. *Entanglement detection in the stabilizer formalism*. Physical Review A **72**, 022340 (2005).
- Vaidman, L. *Tests of Bell inequalities*. Physics Letters A **286**, 241 (2001).
- Veitch, V., Ferrie, C., Gross, D., and Emerson, J. *Negative quasi-probability as a resource for quantum computation*. New Journal of Physics **14**, 113011 (2012).
- Vernaz-Gris, P., Ketterer, A., Keller, A., Walborn, S. P., Coudreau, T., and Milman, P. *Continuous discretization of infinite-dimensional Hilbert spaces*. Physical Review A **89**, 052311 (2014).
- Vértesi, T. and Brunner, N. *Disproving the Peres conjecture by showing Bell nonlocality from bound entanglement*. Nat Commun **5** (2014).
- Vlastakis, B., Kirchmair, G., Leghtas, Z., Nigg, S. E., Frunzio, L., Girvin, S. M., Mirrahimi, M., Devoret, M. H., and Schoelkopf, R. J. *Deterministically Encoding Quantum Information Using 100-Photon Schrödinger Cat States*. Science **342**, 607 (2013).

- Vlastakis, B., Petrenko, A., Ofek, N., Sun, L., Leghtas, Z., Sliwa, K., Liu, Y., Hatridge, M., Blumoff, J., Frunzio, L., Mirrahimi, M., Jiang, L., Devoret, M. H., and Schoelkopf, R. J. *Characterizing entanglement of an artificial atom and a cavity cat state with Bell's inequality*. Nat Commun **6** (2015).
- Walborn, S. P., Monken, C. H., Pádua, S., and Souto Ribeiro, P. H. *Spatial correlations in parametric down-conversion*. Physics Reports **495**, 87 (2010).
- Walborn, S. P., Salles, A., Gomes, R. M., Toscano, F., and Souto Ribeiro, P. H. *Revealing Hidden Einstein-Podolsky-Rosen Nonlocality*. Physical Review Letters **106**, 130402 (2011).
- Weedbrook, C., Pirandola, S., García-Patrón, R., Cerf, N. J., Ralph, T. C., Shapiro, J. H., and Lloyd, S. *Gaussian quantum information*. Reviews of Modern Physics **84**, 621 (2012).
- Weihs, G., Jennewein, T., Simon, C., Weinfurter, H., and Zeilinger, A. *Violation of Bell's Inequality under Strict Einstein Locality Conditions*. Physical Review Letters **81**, 5039 (1998).
- Wenger, J., Hafezi, M., Grosshans, F., Tualle-Brouiri, R., and Grangier, P. *Maximal violation of Bell inequalities using continuous-variable measurements*. Physical Review A **67**, 012105 (2003).
- Werner, R. F. *Quantum states with Einstein-Podolsky-Rosen correlations admitting a hidden-variable model*. Physical Review A **40**, 4277 (1989).
- Weyl, H. *The Theory of Groups and Quantum Mechanics*. Dover Books on Mathematics (Dover Publications, 1950).
- Wittmann, C., Fürst, J., Wiechers, C., Elser, D., Häsel, H., Lütkenhaus, N., and Leuchs, G. *Witnessing effective entanglement over a 2 km fiber channel*. Optics Express **18**, 4499 (2010).
- Yu, S. and Oh, C. H. *State-Independent Proof of Kochen-Specker Theorem with 13 Rays*. Physical Review Letters **108**, 030402 (2012).
- Zak, J. *Finite Translations in Solid-State Physics*. Physical Review Letters **19**, 1385 (1967).
- Zhang, J. and Braunstein, S. L. *Continuous-variable Gaussian analog of cluster states*. Physical Review A **73**, 032318 (2006).
- Żukowski, M., Zeilinger, A., Horne, M. A., and Ekert, A. K. *"Event-ready-detectors" Bell experiment via entanglement swapping*. Physical Review Letters **71**, 4287 (1993).